OPTIMUM DESIGN OF GRID STRUCTURES OF REVOLUTION USING HOMOGENISED MODEL

D. Slinchenko

Submitted in fulfilment of the academic requirements for the degree of Doctor of Philosophy in the Department of Mechanical Engineering at the University of Natal.

Durban, South Africa
November 2000

Abstract

The present study involves analysis and design optimisation of lattice composite structures using symbolic computation. The concept of a homogenised model is used to represent heterogeneous composite isogrid structure as a homogeneous structure with the stiffness equivalent to the original grid structure. A new homogenisation technique is developed and used in the present study.

The configuration of a unit cell and the geometrical parameters of the ribs of a composite isogrid cylinder are optimised subject to a strength criterion in order to maximise externally applied loading to provide maximum strength and stiffness of the structure as a whole. The effects of tension and torsion on the optimum design are investigated.

Special purpose computation routines are developed using the symbolic computation package *Mathematica* for the calculation of equivalent stiffness of a structure, failure analysis and calculation of optimum design parameters. The equivalent stiffness homogenisation approach, in conjunction with optimum search routines, is used to determine the optimal values of the design variables. The numerical approach employed in the present study was necessitated by the computational inefficiency and conventional difficulties of linking the optimiser and the FEM analysis package for calculating the stress resultants used in the optimisation process. These drawbacks were successfully overcome by developing special purpose symbolic computation routines to compute stress resultants directly in the program using a new homogenisation approach for the model with equivalent stiffness.

In the design optimisation of cylindrical isogrids the computational efficiency of the optimisation algorithm is improved and good accuracy of the results has been achieved. The investigation on the basis of failure analysis shows that the difference in the value of the maximum load applied to the optimal and non-optimal isogrid structure can be quite substantial, emphasising the importance of optimisation for the composite isogrid structures. The computational efficiency of optimisation algorithms is critical and therefore special purpose symbolic computation routines are developed for its improvement.

A number of optimal design problems for isogrid structures are solved for the case of maximum applied load design.

Declaration

I declare that this dissertation is my own unaided work except where due acknowledgement is made to others. This dissertation is being submitted for the Degree of Doctor of Philosophy to the University of Natal, Durban, and has not been submitted previously for any other degree examination.

Denys Slinchenko November 2000.

Acknowledgements

I express my gratitude to my supervisors, Professors Viktor Verijenko and Sarp Adali, for their guidance and encouragement; to my colleague Dr. Pavel Tabakov and fellow postgrads for their support and help.

Financial assistance from National Research Foundation of South Africa is gratefully acknowledged.

Nomenclature

Equivalent Stiffness Model

x, y, z	Co-ordinate directions.
u_x, u_y, u_z	Components of displacement in the x, y, and z directions.
u_x^0, u_y^0, u_z^0	Components of displacement of a midsurface.
β_x, β_y	Rotations of a midsurface about x and y axes.
$\varepsilon_{xx}, \varepsilon_{yy}, \varepsilon_{xy}$	Strain components.
$\varepsilon_{xx}^0, \varepsilon_{yy}^0, \varepsilon_{xy}^0$	Midsurface (or membrane) strains.
k_{xx}, k_{yy}, k_{xy}	Curvatures of a shell.
N_{xx}, N_{yy}, N_{xy}	Shell resultant forces.
M_{xx}, M_{yy}, M_{xy}	Shell resultant moments.
Q_x, Q_y	Shell transverse shear forces.
N_i^*, Q_i^*, S_i^*	Axial, transverse shear (in the normal direction and tangential to a median surface) forces in the ribs.
M_i^*, G_i^*, H_i^*	Bending, transverse shear (in the plane normal and tangential to a median surface) and torsion moments in the ribs.
$\sigma_{xx}, \sigma_{yy}, \sigma_{xy}, \sigma_{xz}, \sigma_{yz}$	Stress components.
A_{ij}	Extensional stiffness components.
B_{ij}	Extensional-bending coupling stiffness components.
D_{ij}	Bending stiffness components.
A_{kl}	Transverse shear stiffness.
$\varepsilon_{xz}^0, \varepsilon_{yz}^0$	Transverse shear strains on a midsurface.
N_{ij}^T, M_{ij}^T	Resultant thermal forces and moments.
C_{kl}	Non-reduced stiffness of a material.
K_4, K_5	Shear correction coefficients.
$\alpha_{xx}, \alpha_{yy}, \alpha_{xy}$	Coefficients of thermal expansion.

ΔT	Change in temperature from the stress-free state.
$N_{xx}^{*}, N_{yy}^{*}, N_{xy}^{*}, M_{xx}^{*}, M_{yy}^{*}, M_{xy}^{*}$	Shell resultant thermal coefficients.
ρ_0	Mass per unit area.
ρ	Density of the material.
ρ_2	Rotary inertia per unit area.
$[N],[M],[V]$	In-plane stress resultant vector, bending moment resultant vector and out-of-plane shear resultant vector.
$\{\varepsilon\},\{k\}$	In-plane strain vector and curvature vector.
$[A]$, $[B]$, $[D]$, $[H]$	Extension, coupling, flexural and transverse shear stiffness matrices.
E_x, E_s	Longitudinal and shear module.
d	Spacing for each set of ribs.
J, A, I	Torsion constant, area and second moment of inertia of the ribs.
χ	Shear correction factor.
ν_{ij}, G_{ij}	Poison's ratio and shear modulus.
Q_{ij}	Stiffness matrix members.
X_t, X_c	Tensile and compressive strength of a composite in the first material direction.
Y_t, Y_c	Tensile and compressive strength of a composite in the second material direction.
S	Shear strength of a composite.

Developed Homogenised Model

α, β	Curvilinear orthogonal co-ordinates of the points on a median surface.
u, v, w	Outer normal to the surface of a shell.
ε_1, ε_2, ω, χ_1, χ_2, τ	Components of deformation of the median surface.
$'X^{*}, Y^{*}, Z^{*}$	Projections of the vector of load intensity to the directions of the unit co-ordinate vectors and the outer normal to a median surface of a shell.

m_α^*, m_β^*	Intensities of the distributed moments.
A, B	Coefficients of the first quadratic form for a median surface.
k_1, k_2	Curvatures of the normal sections of a median surface along the co-ordinate lines.
k_{12}	Torsion of the co-ordinate lines.
ε_1, ε_2, ω, χ_1, χ_2, τ	Components of tangential and bending deformation of a median surface of a shell.
n	Number of the families ribs.
F_i, J_{1i}, J_{2i}, J_{3i}	Area, main central moments of inertia and torsion moment of inertia of the rib's cross-section.
E_i, G_i	Young's and shear moduli of the ribs.
a_i	Distance between the axes of the ribs that belong to the *i*-th family.
a	Notation in the case when $a_1 = a_2$.
K_i, I_i, I_i^0, C_i	Parameters which show the relationship between the corresponding stiffness characteristics of the ribs and the distance between their axes.
K	Notation in the case when $K_1 = K_2$.
M_{1s}, M_{1s}	Additional bending moments acting in the plane tangential to a median surface.
φ_i	Angle between the axes α and an axes of the first family of ribs.
φ	Notation in the case when $\varphi_1 = \varphi_2$.
$k(\alpha)$	Function of rigidity of an elastic constraint.
ψ_i	Angles of rotation about the normal to a median surface of the axes of two adjacent members of two different families of ribs.
∇_i	Operator that denotes differentiation towards the tangent to the axis of a rib, which belongs to the *i*-th family.
L_{ij}	Linear differential operators.
ρ	Radius of inertia of the rib's cross-section for the case of

	in-plane bending of a grid plate.
θ_1, θ_2	Angles of rotation of the normal to a median surface of a plate in the planes x=const, y=const.
r_{1i}	Non-dimensional section radius of inertia of a rib, which belongs to the i-th family.
X, Y, Z	Load components.
X_*, Y_*, Z_*	Surface loading components.
Φ	Resolving function.
R_1, R_2	Main radii of curvature of the surface of a shell.
r	Equation of the median surface of a shell.
ψ	Angle between the normal to a median surface of a cylindrical shell and it axis of revolution.
R_0	Radius of a median surface of a cylindrical shell.
g	Distributed surface load.
y_i	Components of the vector of unknown functions.
f_i	Vector of loading conditions.
P_i	Components of the square matrix of the stiffness properties and geometric characteristics of a shell.
B_0, B_1	Rectangular matrices of boundary conditions.
C	Rigid body displacement of a shell in the direction of an outer normal to the median surface.

Optimum Search Algorithm

X	Vector of design variables.
$\vec{X}^0$	Initial vector of design variables.
$\vec{S}^1$	Search vector.
α^*	Value that yields the optimal design in the direction defined by $\vec{S}$.
J	Set of constraints.

$F(\vec{X})$	Objective function.
$g_j(X)$	Active constraints.
q	Iteration number.
α^*	Scalar move parameter.
$X_i^l,\ X_i^u$	Low and upper side constraints.
λ_j	Lagrange multipliers.
B	Positive definite identity matrix.
Φ	Pseudo-objective function.

Maximum Applied Load Design

q	Maximum applied load.
$q_{ten},\ q_{tor}$	Tension and torsion components of a load.
b, h	Width and height of a rectangular cross-section of a rib.
w_s	Load scaling factor.
P_{cr}	Critical load.
$\sigma_i,\ \tau_{ij}$	Normal and shear stresses components.
N_i	Axial force in the rib in the i-th direction.
A	Cross-sectional area.
Q_i	Shear forces.

List of Figures

List of Tables

Contents

Main Project Objectives

The objective of the project is to develop an efficient and inexpensive technique for design and analysis of composite lattice structures. The technique must be capable of predicting the optimum lattice parameters and cell configuration for the particular type of load/constraint combination.

1 Introduction

1.1 Overview

In this chapter different types of grid structures used in a wide variety of applications, primarily in the aerospace and civil engineering fields, are being surveyed. A variety techniques of manufacturing of grid structures is also briefly covered. The chapter concludes with a review of the methods and techniques used in the analysis of lattice structures.

Structures for different engineering applications must satisfy a variety of functional parameters and properties depending on their usage. Composite isogrid structures (Figure 1.1) provide a great potential to replace conventional metal structures by offering a higher strength to weight ratio, flexibility in design, custom tailoring of desired properties and the ability to sustain different environments.

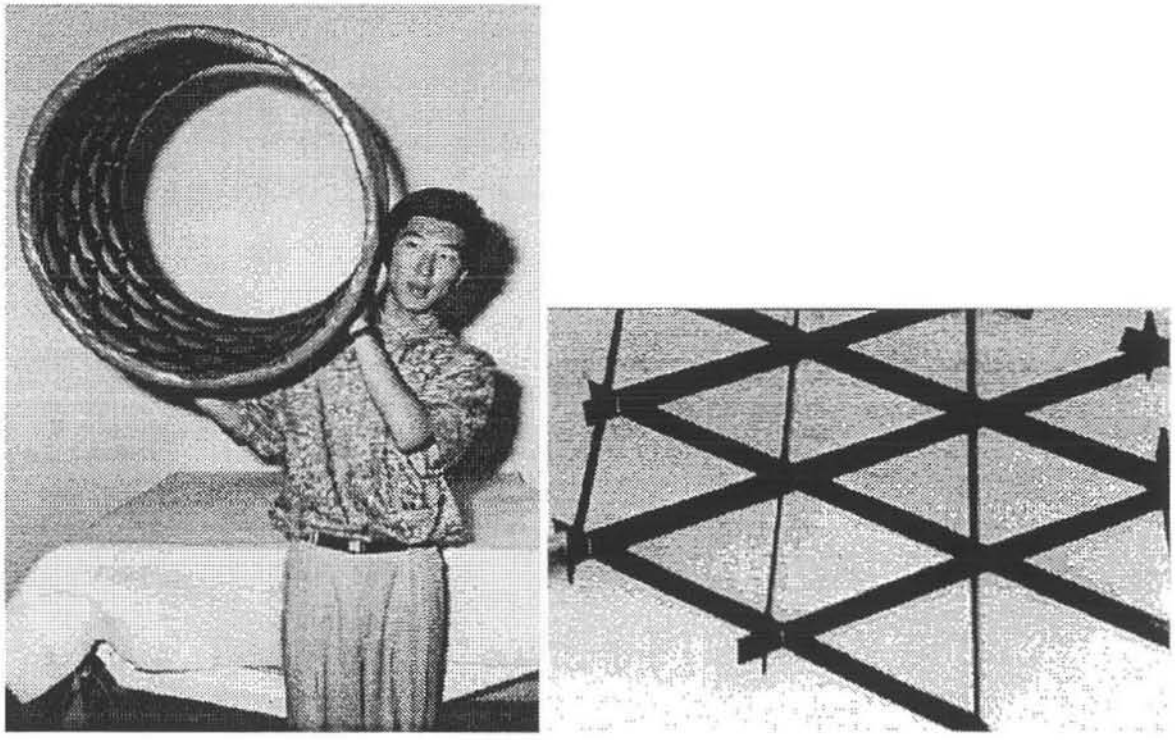

Figure 1.1 Isogrid structure

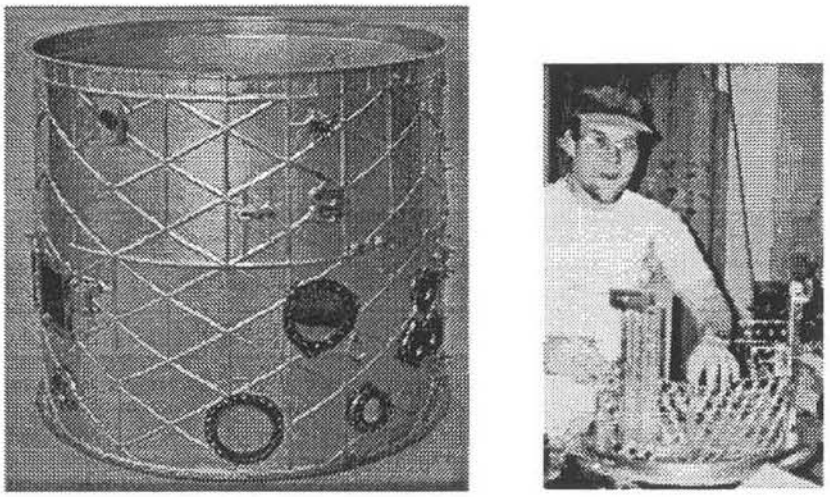

Figure 1.2 Isogrid tanks

Shells supported by a grid lattice of the stiffeners have been considered as a possible replacement to monocoque, skin-stringer, and honeycomb sandwich structures [52], [88]. The concept of isogrid represents the lattice of interconnected ribs made from continuous very strong, stiff and tough fibres. The ribs that comprise the structure are arranged in three families in a way that creates a repetitive pattern of a triangular cells (Figure 1.3).

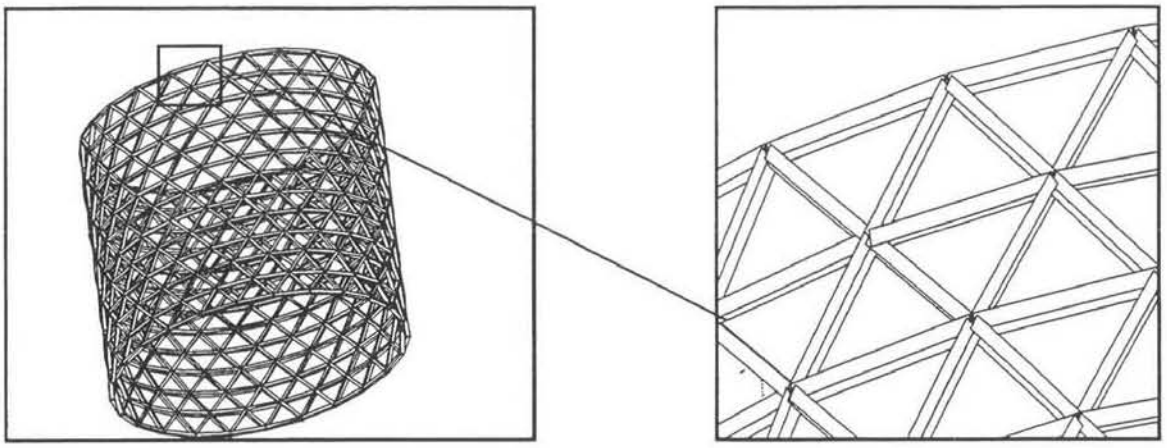

Figure 1.3 Isogrid cylindrical structure

A unidirectional arrangement of the ribs possesses good impact damage tolerance, resistance to delamination and crack propagation across the grid. The first generation of isogrid structures were metal isogrids, which were essentially the integral equilateral triangular stiffening ribs machined onto a metallic skin surface. Manufacturing of such metal isogrids was very laborious task and subsequently required up to two years of lead time. Besides it was an expensive procedure and obtained components came out excessively heavy. Significant reduction of weight and

subsequently manufacturing costs was achieved by replacing the aluminium shrouds structure with those made of composite materials.

Composite materials gained their popularity and became widely used in various areas such as aerospace industry, civil engineering, sporting goods, etc. relatively recently. This is due to a number of advantages these materials possess. A composite is a material having two or more distinct constituents which are usually referred as fibre reinforcement and matrix. Unlike conventional isotropic materials, fibre-matrix composites exhibit very high specific strength and stiffness in the direction of fibre reinforcement. With incorporation of this phenomenon arises a great opportunity to create a material with the custom tailored properties by combining several composite layers with certain mutual orientations to provide strength and stiffness in many directions. Incorporation of composite materials provides structures with a lighter weight, dimensional stability, increased stiffness, minimum outgassing and low cost.

However, composite structures, which are traditionally made from multidimensional laminates, suffer from a major deficiency: they are predisposed to microcracking and delimitation due to material mismatch between the layers which limits their performance. In contrast to the laminates, grid structures posses multidirectional stiffness by running the ribs in several directions, which can avoid material mismatch associated with laminates. The lack of material mismatch provides composite grid structures with much better resistance to delamination, crack propagation and superior impact damage tolerance (the latter is usually occurs at the interface between different material layers in laminates).

The ribs comprising a grid structure are usually loaded in their axial direction so that in a composite grid structure fibres are usually oriented along the rib's axial direction to provide their maximum axial strength and stiffness. As long as the composite ribs are orthotropic their transverse stiffness is much less than the axial. In order to compensate for the loss of transverse (bending) stiffness the ribs are usually of a high aspect ratio in that direction (from 3 to 5). Inplane stiffness of grid structures can also be altered subject to the number of families of ribs incorporated and their mutual orientation which will subsequently define a repetitive cell pattern. There are several cell patterns conventionally used in grid structures (Figure 1.4).

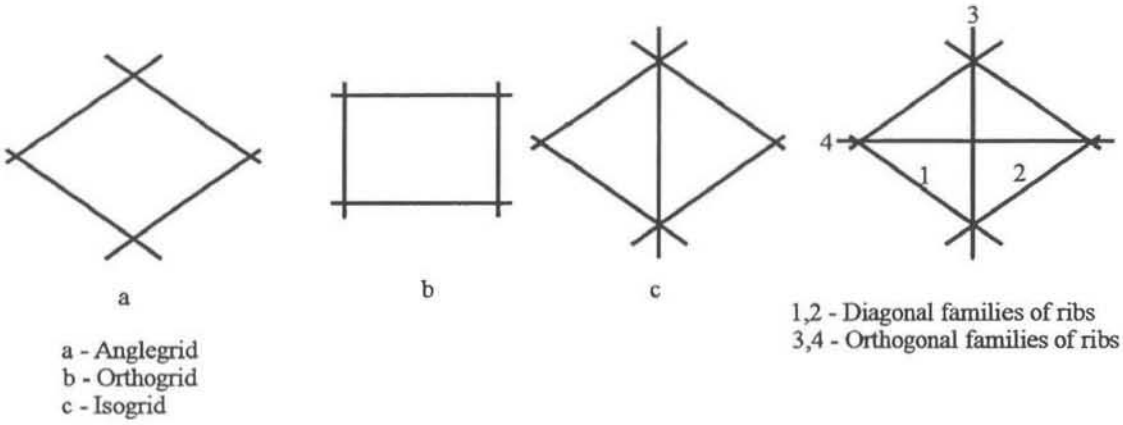

Figure 1.4 Cell configurations

The use of one or other pattern usually depends on the way the structure is loaded. The behaviour of different types of grid structures has been analysed by S. Huybrechts [36]. This analysis shows that:

- Grid structures with diagonal ribs (Figure 1.4) have much higher strength when the applied in-plane biaxial load has the same sign (either tension or compression) than when loads of both signs presented.
- Adding extra circumferential family of ribs to the tri-directional structure (isogrid) reduces the first failure strength of a grid structure. Failure in this case is a material failure.
- The major contribution to the grid structure's shear strength comes from the diagonal families of ribs. The steeper diagonal ribs go - the higher shear strength the structure obtains.

Based on these conclusions and series of test performed the general comparison of three major types of grid structures can be made:

1. **Anglegrid** (Figure 1.4 (a)) exhibits high shear strength, but low axial strength because of the lack of axial ribs.
2. **Orthogrid** (Figure 1.4 (b)) in contrast to the anglegrid shows much higher axial strength, but tremendous decrease in the shear strength. With the angle ribs removed the interaction between the orthogonal ribs becomes much smaller. This

explains the reduced shear strength of the structure due to the absence of coupling between orthogonal families of ribs.

3. **Isogrid** (Figure 1.4 (c)) exhibits high strength for both normal and shear loading. However, despite its name, the isogrid is not isotropic and shows much higher strength in the direction coincident with axial ribs than in the direction transverse to it. When the aspect ratio of the rib's cross-section increases (they become taller and thinner) and the buckling of the ribs becomes an important factor, isogrid structures exhibit significantly higher strength to tensile loads than to compressive loads. Isogrids are often become weaker and tend to buckling of the axial rib when subjected to the combined load: compressive along the axial ribs and tensile transverse to the axial ribs. A composite isogrid significantly outperforms an aluminium one due to the ability to run composite fibres exclusively axially along the ribs, which tremendously increases their strength.

The technology of fabrication of stiffened composite structural members was developed in late seventies in the US by the McDonnell Douglas Corporation [39]. In this method a composite isogrid structure with an outer skin was produced by moulding a stiffened member with an equilateral triangular cell arrangement of ribs made of carbon fibre/polymer based composition to a partially cured condition. A suitable elastomer was then injected into the open spaces of the isogrid rib stiffener to stabilise partially cured composite for subsequent forming and curing operations. The resulting stiffening member was heat-formed to the required contour. Cylindrical structure for instance was manufactured by assembling four initial contours shaped as 90 degrees arch-shaped isogrid panels. The outer skin which represented a composite laminate was manufactured separately by laying up a plurality of layers of preimpregnated tape within a mould (cylindrical mould for a cylindrical structure). The assembly process was performed by installing four heat formed isogrid stiffeners into the interior of the skin to form the final shape of the structure. Isogrid stiffeners and the skins were then co-cured to achieve their unity and the final isogrid shell structure was obtained by removing the mould and subsequent removing elastomer from the spaces between the isogrid rib stiffeners.

Many distinct areas of application for composite isogrid structures have emerged. These are payload shrouds, solar array substrates and civil engineering structures.

This structural concept also has a great potential for automation of the manufacturing process including continuous filament winding and resin transfer moulding. Only recently the concept of the grid made of unidirectional continuous fibres was introduced and it is predominantly applied in the aerospace industry [71], [75], [72].

The advanced grid structures have been manufactured in several countries. In the United States a number of companies and research institution were involved in the development of advanced grid structures: Boeing Company, US Air Force Research Lab, McDonnell-Douglas, Alliant Tech Systems, Stanford University, and others. In the early 1990s, the Air Force Phillips Laboratory was involved in an effort that finally achieved high quality, light weight composite isogrid structures [37], [38]. These structures were manufactured using tooling made of silicon rubber and proved to have extremely high strength-weight ratios. Advanced composite grid structures have been manufactured also in the leading Russian Composite Centre, the Central Research Institute of Special Machine Building (CRISMB) [106]. High-performance lattice structures from carbon and aramid epoxy composites were manufactured using continuous filament winding. These structural elements are used in aeroplane frames and space launch vehicles (Figure 1.6, Figure 1.7).

Companies such as Chemgrate, Inc were able to fabricate large quantities of low cost, low fibre content grid structures for use as non-corrosive flooring for commercial property and factories. Significant research at Stanford University, Ohio State University and Georgia Tech has lead to several new analysis techniques [73], [51] and [47] that were verified using the grid structure floor grating.

Presently composite grid structures are extensively used by the aerospace industry. The US Air Force MightySat I satellite, launched off the US space shuttle in December, 1998, had a grid structure for its upper payload deck, fabricated using the SnapSat™ concept developed by Composite Optics International. Delta II interstage replacement was built using Russian manufacturing process. The Boeing Company is developing a grid stiffened fairing for the Minotaur Launch Vehicle, expected to fly in the year 2000.

Another advantage of grid structures that they have significantly higher damage tolerance than their main competitor, the honeycomb sandwich. Grid structures also

have an ability to limit spread of damage and subsequently resistant to catastrophic failures. This phenomenon is due to limiting delamination resulting from the impact damage to the area within the cell. Composite grid structures have also higher in-plane (but lower out-of-plane) stiffness than the equivalent honeycomb structures which defines the area of their application. The other advantage of the isogrid compared to the honeycomb sandwich is resistance to water absorption which can further lead to the degradation of the core.

Composite grid structures are also attractive because of the low cost of the manufacturing which can be significantly automated. This feature is particularly beneficial for grid structures of revolution.

1.2 Manufacturing Methods for Grid Structures

The following manufacturing methods of grid structures are presently known:

Manufacturing techniques developed in the former Soviet Union [106]:

1. *Wet Winding Around Pins.*
2. *Free Winding.* Free forming of the ribs using the traditional filament winding process. The tows are placed with the offset from each other on the top of the tows of the previous layer. This process results in the ribs of poor quality, but is the cheapest of all.
3. *Winding into a light weight core.* This technology includes: winding of the inner skin; machining of the core sprayed on the mandrel surface; machining the grooves in the core; winding the ribs into the grooves; winding the outer skin.
4. *Winding into the grooves formed in an elastic coating.* The coating is then pulled out of the lattice.
5. *Winding into the grooves formed in the metal liner.* This process is used for manufacturing tanks and pressure vessels and yields a hybrid metal-composite structure.

Manufacturing techniques developed in United States:

1. *Wet winding in hard tooling with e-beam cure.* This technology was developed at Boeing Co.
2. *Nodal spreading.* Developed at Stanford University.
3. *Winding into solid rubber tooling.* Developed at Phillips Lab.
4. *The hybrid tooling method.* Developed at Air Force Research Laboratory [54].
5. *Fibre placement with hybrid tooling.* Developed at Boeing Co.
6. *Fibre placement with expansion inserts.* Developed at Alliant Tech Systems.
7. *The located expansion tooling method.* Developed at Air Force Research Laboratory and Boeing Co.
8. *Wet winding.* The Brute Force approach.
9. *The SnapSat ™method.* Developed at Composite Optics, Inc.
10. *The TRIG Method.* Developed at Stanford University.

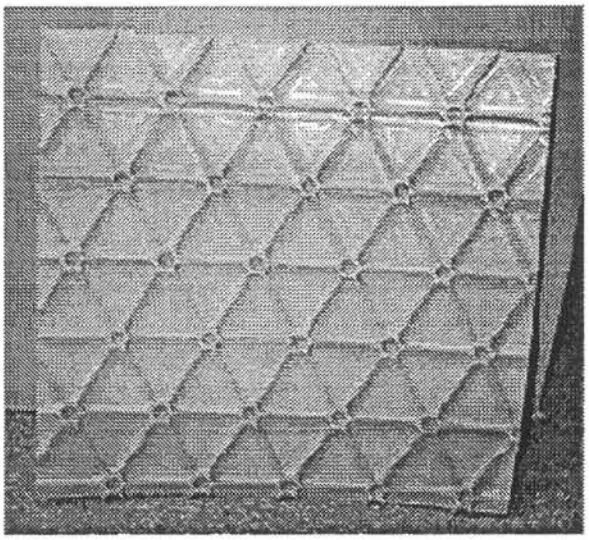

Figure 1.5 Aluminum Isogrid.

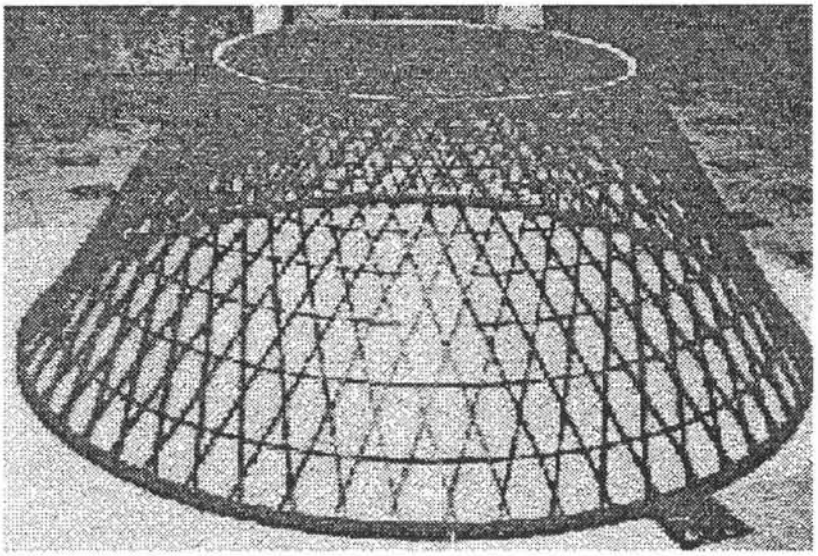

Figure 1.6 Lattice composite spacecraft attachment fitting-adapter.

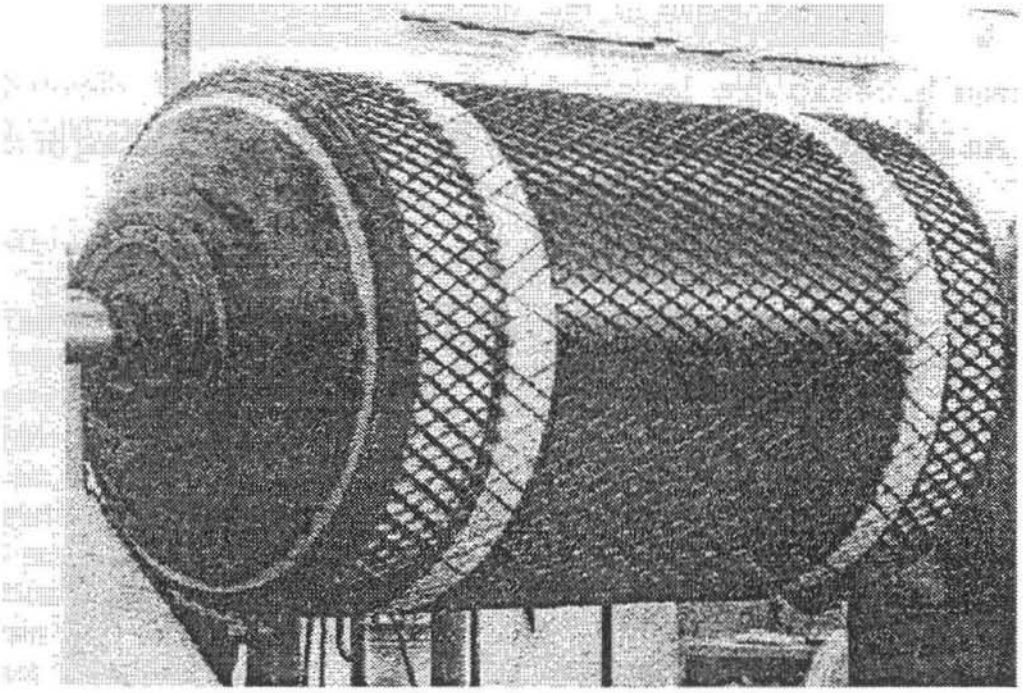

Figure 1.7 Composite wound grid structure.

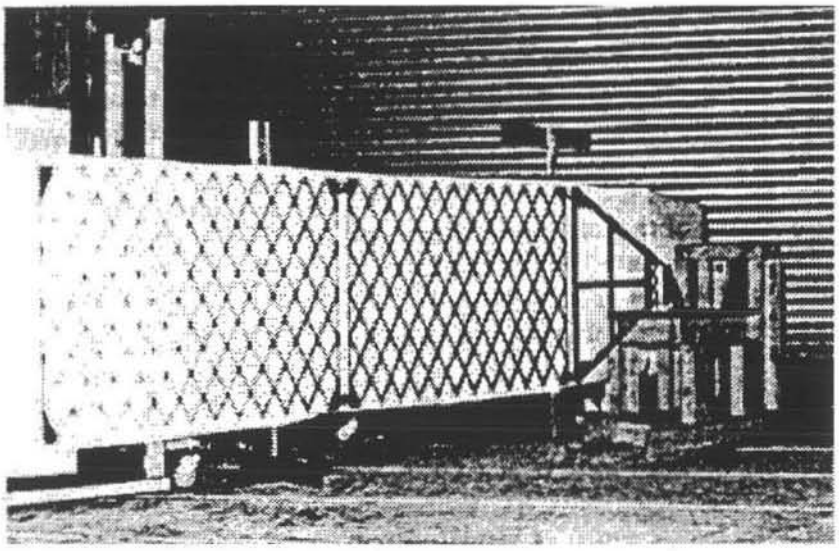

Figure 1.8 Open isogrid structure

1.3 Survey of Analysis Techniques

Grid stiffened structures have been studied quite extensively for the last two decades. The following techniques are currently known to be used for their modelling and analysis:

1. In the US early analytical analysis for grid structures was developed by L. W. Rahfield [73] and at the Air Force Phillips Lab. A relatively simple set of equations was developed to predict rib buckling. Grid structures that were fabricated had tall, thin ribs, and the buckling of the ribs was a major failure factor for the structures at a time.
2. Significant analytical work was done on grid structures in the former Soviet Union by Tarnopol'skii [91], [92]. Structural behaviour was analysed on the basis of 'smearing' stiffeners.
3. The analysis of lattice structures with a regular and dense system of ribs was performed by the research group of the Central Research Institute of Special Machine Building [106] on the basis of continuum models with ribs smeared over the structure surface. Constitutive equations of the continuum model were used to construct a structural stiffness matrix for the finite element analysis, which was subsequently used for the investigation of structural behaviour and stress concentration in the vicinity of structural discontinuities (doors, joints, etc.). The constitutive equations were also used to solve the problem of local buckling induced by local stresses. The discrete models were used to analyse grid structures without skins due to the possible local buckling of the ribs. The finite element method was used to overcome the complexity of high order general equations of shell theory. The ribs of the FEM structure were modelled with beam elements working in tension, compression, bending and torsion.
4. The equivalent stiffness approach was developed by H. Chen [13] for analysis of grid stiffened structures on the basis of 'smeared' grid stiffeners to a solid plate of equivalent properties.
5. S. Huybrechts [36] were developed failure envelope analysis and made a series of finite element derivations for grid structures with discontinuities.
6. Rib buckling predictions developed at Ohio State University and the Air Force Research Lab [53].

7. The general homogenisation approach was used by A. Kalamkarov [42], [43], [44] for analysis of composite and reinforced systems of irregular structure. The modelling is based on the calculation of effective stiffness and strength and solutions for the effective module and local stresses in composites are obtained by means of homogenisation.

2 Modelling on the Basis of Equivalent Stiffness

2.1 Abstract

In this chapter the Equivalent Stiffness technique is used for modelling and analysis of lattice structures. The approach taken to crate the Equivalent Stiffness Model (ESM) is described in details. The advantages and disadvantages of ESM are discussed. Verification of the analysis on the basis of the ESM and the finite element method is also presented.

2.2 Homogenisation Approach

2.2.1 Preface

In this section the term "exact" modelling refers to the modelling based on finite element method. The term "exact model" is used as an opposite to "homogenised (or continuous) model". The latter has only the smeared stiffness equivalent to the real structure, but the structural members (ribs and skins) are not "exactly" presented in the model.

Exact modelling and the subsequent analysis of composite grid structures using the finite element method is quite laborious. Lattice structure models that use beam elements to represent interconnected shrouds require finite element mesh to coincide with the actual geometry of the structure to adequately describe the given cell pattern. This will result in an excessively large model, which will subsequently require more effort for performing calculations. Moreover, recreation of the model on each optimisation iteration will be complicated if the geometry is to be represented exactly. One of the solutions will be to incorporate a rather simplified model with the stiffness equivalent to the original. The transition from the exact model to the equivalent stiffness model is shown in Figure 2.1:

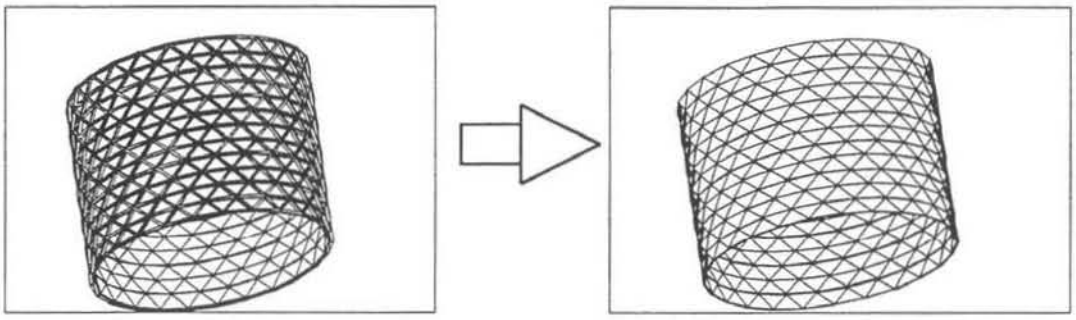

Exact Model Equivalent Stiffness Model

Figure 2.1 Transition from exact model to equivalent stiffness model

Several attempts were made to represent the complex non-uniform structure as a uniform homogeneous structure with the same stiffness properties as the original one. Some of the approaches that were undertaken for the creation of the Equivalent Stiffness Model (ESM) used specially designed "stiffened elements" [19], [57], [62], [70], [71], [75], [72], special macroelements that have the combined stiffness of the rib and both outer and inner skins. ESM was created for orthogrid structures by incorporating the additional stiffness of the shell elements in the direction of the diagonal families of ribs in [19], [57], [62]. The above mentioned methods of "smearing" the grid were suitable for the particular applications, i.e. certain types of loading conditions, orientation of ribs, etc. In these models assumptions were made regarding stress distribution and in some models in-plane bending and shear of ribs are not taken into account. The most complete transition from the exact model to the equivalent stiffness model has been performed by H. Chen and S. Tsai [13] for an arbitrary rib configuration that can be unsymmetrical, subjected to general loads and multiple failure mechanisms. In this approach an integrated equivalent stiffness model is developed to describe a grid structure with or without laminated skins. The model includes all the important effects such as torsion, in-plane bending and shear of ribs and has the form of a Mindlin plate. The model also gives an opportunity to perform refined stress analysis incorporating exact FEM modelling in certain regions of ESM where high accuracy is required or stress concentration occurs [36].

2.3 Lamination Theory

The finite element analysis package *MSC/NASTRAN*, which was chosen for modelling an isogrid structure, uses the assumptions of classical lamination theory in formulating shell behaviour for non-uniform and composite laminate element properties [56]. The CQUAD4, CQUAD8, CTRIA3 and CTRIA6 elements are available the modelling composite and non-uniform materials. This approach allows one to model plates with coupled membrane and bending elastic behaviour. This behaviour can be simulated directly by inputting membrane, bending, membrane-bending coupling and transverse shear constitutive relationships.

The following assumptions regarding the behaviour of the laminae are made in classical lamination theory [14]:

- The laminae are perfectly bonded together.
- The bonds are infinitesimally thin and no lamina can slip relative to another.
- A linear variation of strain through the laminate thickness is assumed.

The displacement of a shell can be described by the displacement and rotation of its midsurface, the straining of a shell can be described by the straining and curvature changes of its midsurface, and the equilibrium of a shell can be described by the equilibrium of stresses integrated through the thickness of the shell.

The figure below shows a flat rectangular shell, the edges of which are aligned with the X and Y axes of a Cartesian co-ordinate system. The XY plane of this co-ordinate system is halfway between the top and bottom surfaces of the shell; that is, the midsurface of the shell is at z=0. The shell has thickness t, so that the top surface is at z=t/2 and the bottom surface is at z=-t/2, as the following figure illustrates:

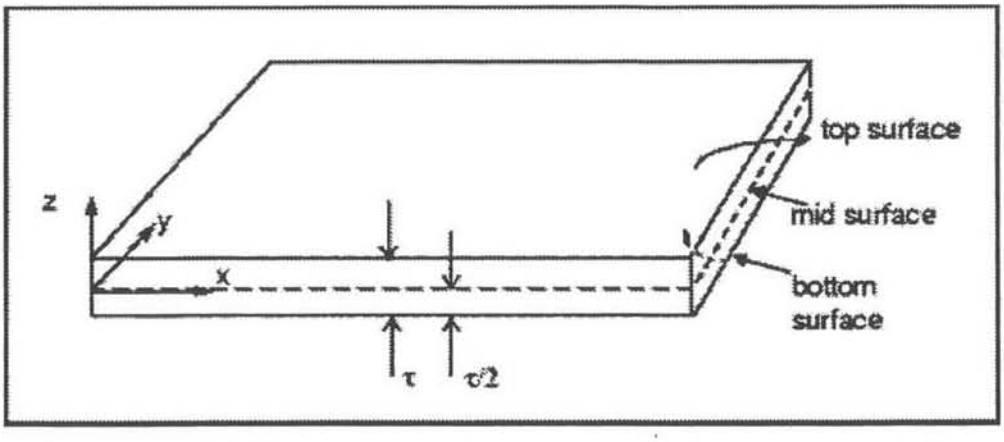

Figure 2.2 Rectangular shell element

As mentioned above, it is assumed that the displacement of any point (x, y, z) in a shell can be expressed in terms of the displacement and rotation of the point (x, y, 0) on the midsurface of the shell. The deformation in the X-Y plane of the shell at any point at a distance z in the normal direction to plate middle surface is

$$\begin{aligned} u_x(x,y,z) &= u_x^0(x,y) + z\beta_y(x,y), \\ u_y(x,y,z) &= u_y^0(x,y) - z\beta_x(x,y), \\ u_z(x,y,z) &= u_z^0(x,y), \end{aligned} \tag{2.1}$$

where u_x, u_y, u_z are the components of displacement in the x, y, and z directions, respectively; u_x^0, u_y^0, u_z^0 are the components of displacement of the midsurface; β_x, β_y are the (small) rotations of the midsurface about the x and y axes, respectively.

Similarly, the strain components ε_{xx}, ε_{yy} and ε_{xy} of any point (x, y, z) can be expressed in terms of the midsurface (or membrane) strains ε_{xx}^0, ε_{yy}^0, ε_{xy}^0 and curvature changes k_{xx}, k_{yy}, k_{xy} as:

$$\begin{aligned} \varepsilon_{xx}(x,y,z) &= \varepsilon_{xx}^0(x,y) + zk_{xx}(x,y), \\ \varepsilon_{yy}(x,y,z) &= \varepsilon_{yy}^0(x,y) + zk_{yy}(x,y), \\ \varepsilon_{xy}(x,y,z) &= \varepsilon_{xy}^0(x,y) + zk_{xy}(x,y). \end{aligned} \tag{2.2}$$

For flat shells, the tensor shear strain components are:

$$\begin{Bmatrix} \varepsilon_{xx}^0 \\ \varepsilon_{yy}^0 \\ \varepsilon_{xy}^0 \end{Bmatrix} = \begin{Bmatrix} \dfrac{\partial u_x^0}{\partial x} \\ \dfrac{\partial u_y^0}{\partial y} \\ \dfrac{1}{2}\left(\dfrac{\partial u_x^0}{\partial y} + \dfrac{\partial u_y^0}{\partial x} \right) \end{Bmatrix}, \tag{2.3}$$

$$\begin{Bmatrix} k_{xx} \\ k_{yy} \\ k_{xy} \end{Bmatrix} = \begin{Bmatrix} \dfrac{\partial \beta_x^0}{\partial x} \\ -\dfrac{\partial \beta_y^0}{\partial y} \\ \dfrac{1}{2}\left(\dfrac{\partial \beta_y^0}{\partial y} - \dfrac{\partial \beta_x^0}{\partial x} \right) \end{Bmatrix}. \tag{2.4}$$

The shell resultant forces $\left(N_{xx}, N_{yy}, N_{xy}\right)$, the shell resultant moments $\left(M_{xx}, M_{yy}, M_{xy}\right)$, and the shell transverse shear forces $\left(Q_x, Q_y\right)$ are obtained by integrating the stress components $\left(\sigma_{xx}, \sigma_{yy}, \sigma_{xy}, \sigma_{xz}, \sigma_{yz}\right)$ through the thickness of the shell. The shell resultant forces are given by:

$$\begin{Bmatrix} N_{xx} \\ N_{yy} \\ N_{xy} \end{Bmatrix} = \int_{-½}^{½} \begin{Bmatrix} \sigma_{xx} \\ \sigma_{yy} \\ \sigma_{xy} \end{Bmatrix} dz. \tag{2.5}$$

The shell resultant moments are given by:

$$\begin{Bmatrix} M_{xx} \\ M_{yy} \\ M_{xy} \end{Bmatrix} = \int_{-½}^{½} \begin{Bmatrix} \sigma_{xx} \\ \sigma_{yy} \\ \sigma_{xy} \end{Bmatrix} z dz. \tag{2.6}$$

The shell transverse shear forces are given by:

$$\begin{Bmatrix} Q_x \\ Q_y \end{Bmatrix} = \int_{-½}^{½} \begin{Bmatrix} \sigma_{xz} \\ \sigma_{yz} \end{Bmatrix} dz. \tag{2.7}$$

The following figure illustrates the sign conventions employed for the resultant forces and moments, and transverse shear forces. Note that a positive moment, M_{xx}, induces positive strain, ε_{xx}, in the top half of the shell ($z > 0$) and negative strain in the bottom half of the shell ($z < 0$).

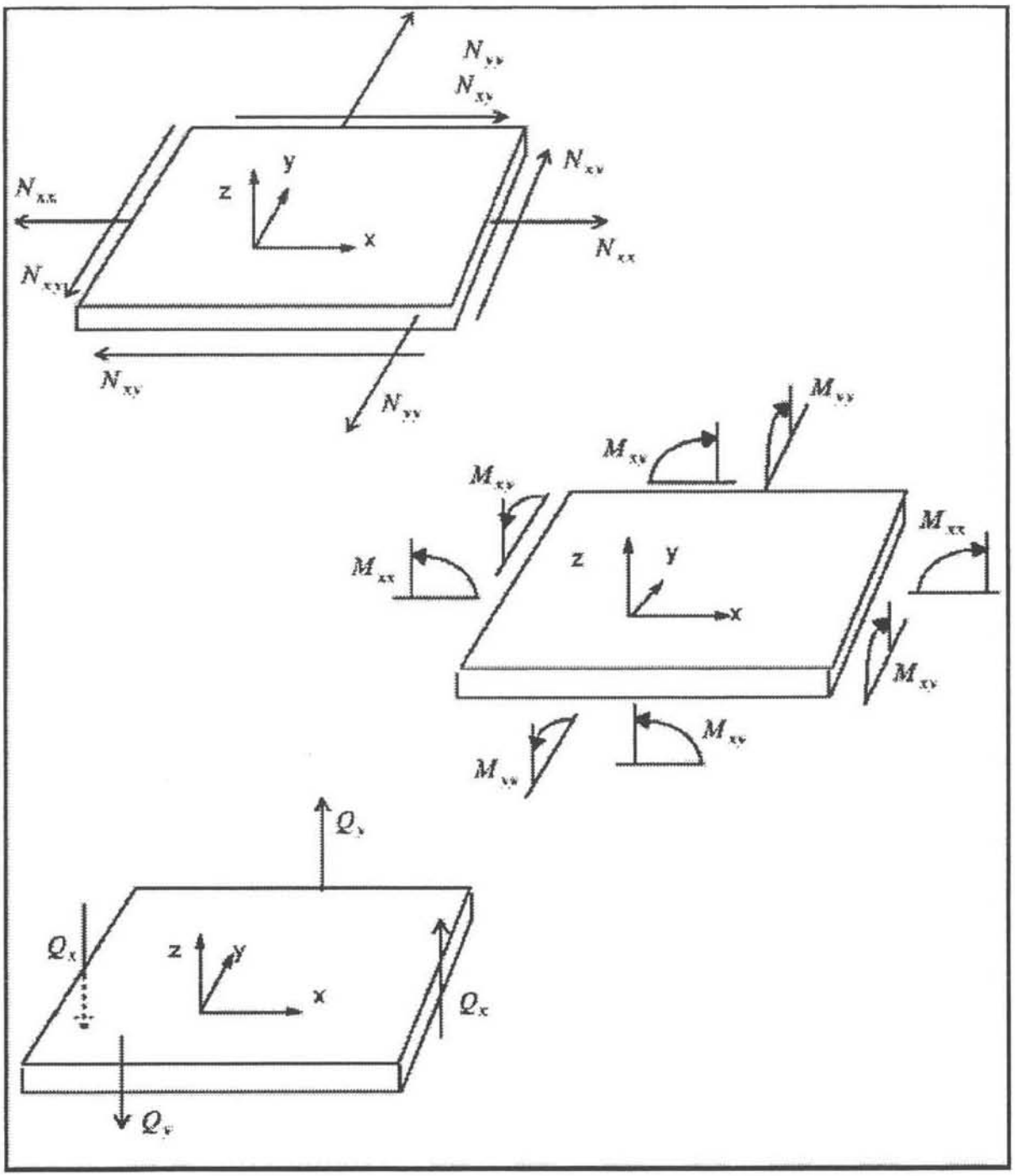

Figure 2.3 Sign conventions for the stress resultants

The relationship between the shell resultants, and the midsurface strains and curvature changes from the classical shell theory [59] are given as:

$$\begin{Bmatrix} N_{xx} \\ N_{yy} \\ N_{xy} \\ \cdots \\ M_{xx} \\ M_{yy} \\ M_{xy} \end{Bmatrix} = \begin{bmatrix} A_{11} & A_{12} & A_{16} & \vdots & B_{11} & B_{12} & B_{16} \\ A_{12} & A_{22} & A_{26} & \vdots & B_{12} & B_{22} & B_{26} \\ A_{16} & A_{26} & A_{66} & \vdots & B_{16} & B_{26} & B_{66} \\ \cdots & \cdots & \cdots & \vdots & \cdots & \cdots & \cdots \\ B_{11} & B_{12} & B_{16} & \vdots & D_{11} & D_{12} & D_{16} \\ B_{12} & B_{22} & B_{26} & \vdots & D_{12} & D_{22} & D_{26} \\ B_{16} & B_{26} & B_{66} & \vdots & D_{16} & D_{26} & D_{66} \end{bmatrix} \begin{Bmatrix} \varepsilon_{xx}^0 \\ \varepsilon_{yy}^0 \\ 2\varepsilon_{xy}^0 \\ \cdots \\ k_{xx} \\ k_{yy} \\ 2k_{xy} \end{Bmatrix} + \begin{Bmatrix} N_{xx}^T \\ N_{yy}^T \\ N_{xy}^T \\ \cdots \\ M_{xx}^T \\ M_{yy}^T \\ M_{xy}^T \end{Bmatrix}, \tag{2.8}$$

$$\begin{Bmatrix} Q_x \\ Q_y \end{Bmatrix} = \begin{bmatrix} A_{55} & A_{45} \\ A_{45} & A_{44} \end{bmatrix} \begin{Bmatrix} 2\varepsilon_{xz}^0 \\ 2\varepsilon_{yz}^0 \end{Bmatrix}. \tag{2.9}$$

In equation (2.8), the quantities A_{ij} (where *i, j = 1, 2, 6*) are the shell extensional stiffnesses, the quantities D_{ij} are the bending stiffnesses, the quantities B_{ij} are the extensional-bending coupling stiffnesses, and the quantities A_{kl} (where *k,l = 4,5*) are the transverse shear stiffnesses. The quantities ε_{xz}^0 and ε_{yz}^0 are the transverse shear strains on the midsurface. The quantities N_{ij}^T and M_{ij}^T are the resultant thermal forces and moments respectively.

The shell stiffness and thermal resultants introduced in equations (2.8) and (2.9) are defined by integrating the material properties of the shell through the thickness of a shell. The extensional, bending, and extensional-bending stiffnesses are given by:

$$A_{ij} = \int_{-½}^{½} Q_{ij}\,dz \qquad i,j = 1,2,6. \tag{2.10}$$

$$B_{ij} = \int_{-½}^{½} Q_{ij}\,z\,dz \qquad i,j = 1,2,6. \tag{2.11}$$

$$D_{ij} = \int_{-½}^{½} Q_{ij}\,z^2\,dz \qquad i,j = 1,2,6. \tag{2.12}$$

where Q_{ij} are the reduced stiffness of the material.

The transverse shear stiffness is given by:

$$A_{ij} = K_k K_l \int_{-½}^{½} C_{kl}\,dz \qquad k,l = 4,5, \tag{2.13}$$

where: C_{kl} is (non-reduced) is the stiffness of the material, and K_4, K_5 are the shear correction coefficients, which for a homogeneous shell are often taken to be $K_4 = K_5 = \sqrt{5/6}$ [59].

If the material of a shell is distributed symmetrically about the midsurface, then the integral in equation (2.11) vanishes and the extensional-bending coupling stiffnesses B_{ij} are identically equal to zero.

The resultant thermal forces and moments are given by:

$$\begin{Bmatrix} N_{xx}^T \\ N_{yy}^T \\ N_{xy}^T \end{Bmatrix} = -\int_{-½}^{½} \begin{bmatrix} Q_{11} & Q_{12} & Q_{16} \\ Q_{12} & Q_{22} & Q_{26} \\ Q_{16} & Q_{26} & Q_{66} \end{bmatrix} \begin{Bmatrix} \alpha_{xx} \\ \alpha_{yy} \\ 2\alpha_{xy} \end{Bmatrix} \Delta T dz, \tag{2.14}$$

$$\begin{Bmatrix} M_{xx}^T \\ M_{yy}^T \\ M_{xy}^T \end{Bmatrix} = -\int_{-½}^{½} \begin{bmatrix} Q_{11} & Q_{12} & Q_{16} \\ Q_{12} & Q_{22} & Q_{26} \\ Q_{16} & Q_{26} & Q_{66} \end{bmatrix} \begin{Bmatrix} \alpha_{xx} \\ \alpha_{yy} \\ 2\alpha_{xy} \end{Bmatrix} \Delta T z dz, \tag{2.15}$$

where α_{xx}, α_{yy}, α_{xy} are the coefficients of thermal expansion of the material, and ΔT is the change in temperature from the stress-free state.

If the change in temperature is uniform through the thickness of the shell, then equations (2.14) and (2.15) may be removed from the integral, resulting in equations (2.16) and (2.17):

$$\begin{Bmatrix} N_{xx}^T \\ N_{yy}^T \\ N_{xy}^T \end{Bmatrix} = \begin{Bmatrix} N_{xx}^* \\ N_{yy}^* \\ N_{xy}^* \end{Bmatrix} \Delta T, \tag{2.16}$$

$$\begin{Bmatrix} M_{xx}^T \\ M_{yy}^T \\ M_{xy}^T \end{Bmatrix} = \begin{Bmatrix} M_{xx}^* \\ M_{yy}^* \\ M_{xy}^* \end{Bmatrix} \Delta T, \tag{2.17}$$

where N_{xx}^*, N_{yy}^*, N_{xy}^*, M_{xx}^*, M_{yy}^*, M_{xy}^* are the shell resultant thermal coefficients, which are given by:

$$\begin{Bmatrix} N_{xx}^* \\ N_{yy}^* \\ N_{xy}^* \end{Bmatrix} = -\int_{-½}^{½} \begin{bmatrix} Q_{11} & Q_{12} & Q_{16} \\ Q_{12} & Q_{22} & Q_{26} \\ Q_{16} & Q_{26} & Q_{66} \end{bmatrix} \begin{Bmatrix} \alpha_{xx} \\ \alpha_{yy} \\ 2\alpha_{xy} \end{Bmatrix} dz, \tag{2.18}$$

$$\begin{Bmatrix} M_{xx}^{*} \\ M_{yy}^{*} \\ M_{xy}^{*} \end{Bmatrix} = -\int_{-½}^{½} \begin{bmatrix} Q_{11} & Q_{12} & Q_{16} \\ Q_{12} & Q_{22} & Q_{26} \\ Q_{16} & Q_{26} & Q_{66} \end{bmatrix} \begin{Bmatrix} \alpha_{xx} \\ \alpha_{yy} \\ 2\alpha_{xy} \end{Bmatrix} z dz. \tag{2.19}$$

The mass properties for the shells are also obtained by integrating the material property through the thickness of a shell. The mass per unit area, ρ_0, is given by:

$$\rho_0 = \int_{-½}^{½} \rho dz, \tag{2.20}$$

where ρ is the density of the material.

The rotary inertia per unit area, ρ_2, is given by:

$$\rho_2 = \int_{-½}^{½} \rho z^2 dz. \tag{2.21}$$

2.4 Equivalent Stiffness Matrices

In the present approach the ESM is described using Mindlin theory [59]:

$$\begin{aligned}[N]&=[A]\{\varepsilon\}+[B]\{k\},\\ [M]&=[B]\{\varepsilon\}+[D]\{k\},\\ [V]&=[H]\{\gamma\},\end{aligned} \tag{2.22}$$

where $[N]$, $[M]$ and $[V]$ are the in-plane stress resultant vector, the bending moment resultant vector and the out-of-plane shear resultant vector respectively. $\{\varepsilon\}$ and $\{k\}$ are the in-plane strain and curvature vectors respectively. $[A]$, $[B]$, $[D]$ and $[H]$ are the extension, coupling, flexural and transverse shear stiffness matrices of the structure respectively and are given as:

$$\begin{aligned}[A]&=[A]^{skin}+[A]^{rib},\\ [B]&=[B]^{skin}+[B]^{rib},\\ [D]&=[D]^{skin}+[D]^{rib},\\ [H]&=[H]^{skin}+[H]^{rib}.\end{aligned} \tag{2.23}$$

Notations with indices *skin* and *rib* are the stiffness matrices corresponding separately to the ribs and outer skins respectively.

2.4.1 Equivalent Stiffness of the Ribs

For the isogrid structure subjected to in-plane loading, axial forces will dominate in the ribs. In this case the bending and shear effect of the ribs tangential to midplane can be neglected. The total stiffness of the ribs can be obtained by summing the stiffness of each unidirectional set of parallel ribs using the principle of superposition, so that the stiffness matrices for the ribs can be expressed as:

$$[A]^{rib}=\begin{bmatrix} \frac{E_xA_0}{d_0}+2\frac{E_xA_\theta}{d_\theta}m^4 & 2\frac{E_xA_\theta}{d_\theta}m^2n^2 & 0 \\ 2\frac{E_xA_\theta}{d_\theta}m^2n^2 & \frac{E_xA_{90}}{d_{90}}+2\frac{E_xA_\theta}{d_\theta}n^4 & 0 \\ 0 & 0 & 2\frac{E_xA_\theta}{d_\theta}m^2n^2 \end{bmatrix},$$

$$[D]^{rib}=\begin{bmatrix} D_{11}^{rib} & D_{12}^{rib} & 0 \\ D_{21}^{rib} & D_{22}^{rib} & 0 \\ 0 & 0 & D_{66}^{rib} \end{bmatrix}, \tag{2.24}$$

$$[H]^{rib}=\begin{bmatrix} \frac{E_sA_0}{d_0}+2\chi\frac{E_sA_\theta}{d_\theta}m^2 & 0 \\ 0 & \frac{E_sA_{90}}{d_{90}}+2\chi\frac{E_sA_\theta}{d_\theta}n^2 \end{bmatrix},$$

$$\begin{aligned} D_{11}^{rib}&=\frac{E_xI_0}{d_0}+2\frac{E_xI_\theta}{d_\theta}m^4+2\frac{E_xJ_\theta}{d_\theta}m^2n^2, \\ D_{22}^{rib}&=\frac{E_xI_{90}}{d_{90}}+2\frac{E_xI_\theta}{d_\theta}m^4+2\frac{E_xJ_\theta}{d_\theta}m^2n^2, \\ D_{12}^{rib}&=D_{21}^{rib}=2\frac{E_xI_\theta}{d_\theta}m^2n^2-2\frac{E_xJ_\theta}{d_\theta}m^2n^2, \\ D_{66}^{rib}&=2\frac{E_xJ_\theta}{d_\theta}m^2n^2+\frac{E_sJ_0}{4d_0}+\frac{E_sJ_{90}}{4d_{90}}+\frac{E_sJ_\theta}{2d_\theta}\left(m^2-n^2\right)^2, \end{aligned} \tag{2.25}$$

$$m=\cos\theta, \qquad n=\sin\theta, \tag{2.26}$$

where subscripts *0*, *90* and θ indicate differently oriented sets of ribs; E_x and E_s are the longitudinal and shear module respectively; d is the spacing for each set of ribs; J's, A's and I are the torsion constant, area and second moment of inertia of the ribs respectively; χ is the shear correction factor. For the rectangular cross-section of the ribs these values are calculated from [95]:

$$I_1=\frac{bh^3}{12}, \qquad I_2=\frac{hb^3}{12}, \qquad J=\frac{hb^3}{16}\left(\frac{16}{3}-3.36\frac{b}{h}\left(1-\frac{b^4}{12h^4}\right)\right), \qquad \chi=\frac{5}{6}. \tag{2.27}$$

2.4.2 Stiffness of Composite Skins

Calculations for the skin's stiffness matrices are performed as for a regular laminate (Figure 2.4) [59] and are given by:

$$\begin{aligned}
[A]^{skin} &= \int [Q] dz, \\
[B]^{skin} &= \int [Q] z dz, \\
[D]^{skin} &= \int [Q] z^2 dz, \\
[H]^{skin} &= \chi \int \begin{bmatrix} C_{55} & C_{45} \\ C_{45} & C_{44} \end{bmatrix} dz.
\end{aligned} \tag{2.28}$$

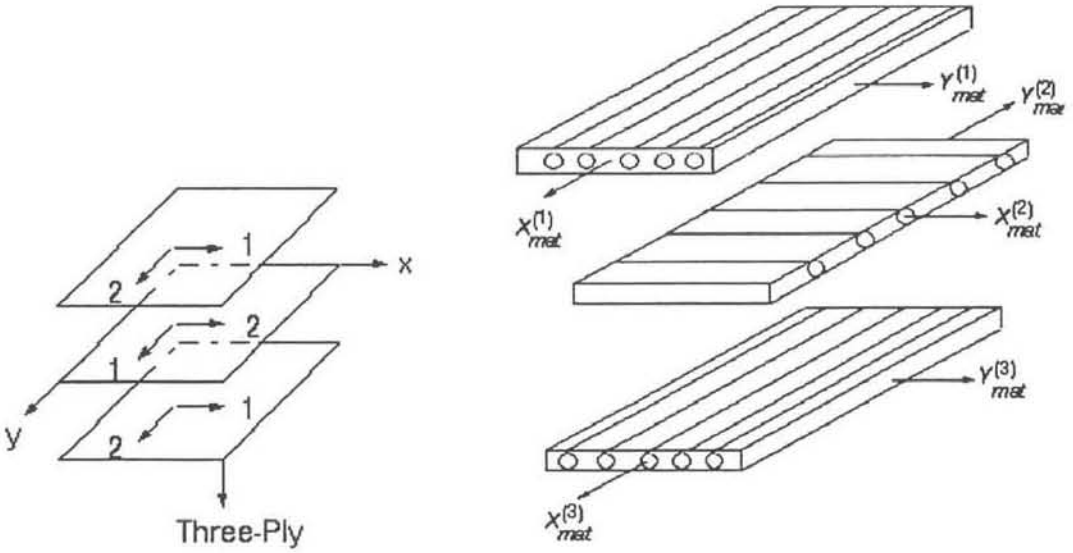

Figure 2.4 Laminae arranged to form a laminate

The stiffness matrices for each layer in the laminate are calculated using the formulae of the theory of laminates [41]:

$$Q = \begin{bmatrix} \dfrac{E_{11}}{1-\nu_{12}\nu_{21}} & \dfrac{\nu_{21}E_{11}}{1-\nu_{12}\nu_{21}} & 0 \\ \dfrac{\nu_{21}E_{11}}{1-\nu_{12}\nu_{21}} & \dfrac{E_{22}}{1-\nu_{12}\nu_{21}} & 0 \\ 0 & 0 & \dfrac{1}{G_{12}} \end{bmatrix}, \tag{2.29}$$

where E_{11}, E_{22} are Young's module of the orthotropic material in the first and second material directions; ν_{12}, ν_{21} are Poisson's ratios; G_{12} is shear modulus. For the layers

rotated with the respect to the global material axes of the composite laminate, the members of the stiffness matrix Q are:

$$\begin{aligned}
\overline{Q}_{11} &= Q_{11}m^4 + 2(Q_{12} + 2Q_{33})n^2m^2 + Q_{22}n^4, \\
\overline{Q}_{22} &= Q_{11}n^4 + 2(Q_{12} + 2Q_{33})n^2m^2 + Q_{22}m^4, \\
\overline{Q}_{12} &= (Q_{11} + Q_{22} - 4Q_{33})n^2m^2 + Q_{12}(m^4 + n^4), \\
\overline{Q}_{33} &= (Q_{11} + Q_{22} - 2Q_{12} - 2Q_{33})n^2m^2 + Q_{33}(m^4 + n^4), \\
\overline{Q}_{13} &= (Q_{11} - Q_{12} - 2Q_{33})nm^3 + (Q_{12} - Q_{22} + 2Q_{33})n^3m, \\
\overline{Q}_{23} &= (Q_{11} - Q_{12} - 2Q_{33})n^3m + (Q_{12} - Q_{22} + 2Q_{33})nm^3.
\end{aligned} \tag{2.30}$$

Stiffness matrices for the skins were calculated using PROMAL software for composites [55].

2.5 *Verification of the Model*

For the verification of the model presented, comparative analysis has been undertaken for ESM and the exact model using two different FEM packages. The structure under consideration is a circular cylinder (Figure 2.5) which is fixed on at one end and loaded at the other with a distributed load of 10^6 N/m. The core of the cylinder is a grid with equilateral triangular cell (Figure 2.5) representing a repetitive structural unit of the isogrid. The outer skin that covers the grid core of the structure (Figure 2.6) is a symmetrical laminate $(0/90)_s$. General dimensions of the structure are presented on the Figure 2.5 and numerical values are given in the Table 2.1:

H	*D*	φ	*h*	*b*
7.56 m	5.44 m	60°	0.02 m	0.00667 m

Table 2.1 Dimensions of the structure

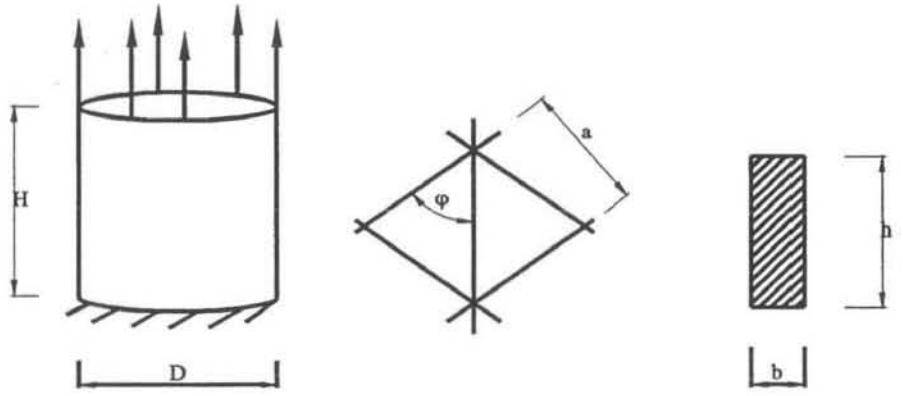

Figure 2.5 Considered structure and cell pattern

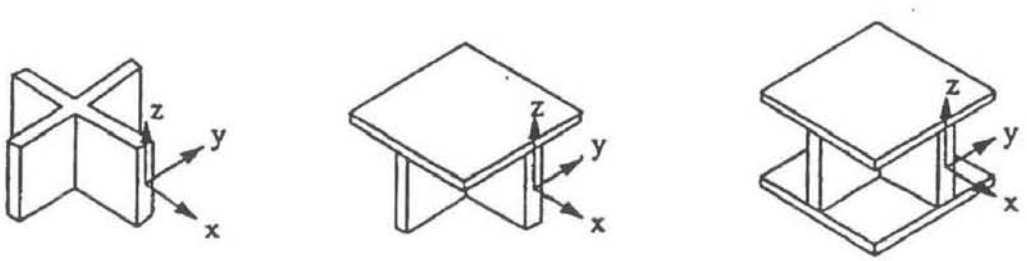

Figure 2.6 A unit cell

2.5.1 Equivalent Stiffness Model

The equivalent stiffness model (Figure 2.7) has been developed on the basis of homogenised stiffness matrices (2.23). A computer routine for the calculation of equivalent homogenised properties from given original grid properties (Appendix 1) has been written using the symbolic computation package *Mathematica* [117]. These properties were subsequently used as input parameters for the ESM FEM model. The FEM code used for the creation of ESM was *Pro/Mechanica* [21]. This particular FEM package was chosen because it allows input of the element's non-homogeneous material properties by means of inputting extension, coupling, flexural and transverse shear stiffness matrices. Rectangular shell p-elements were used.

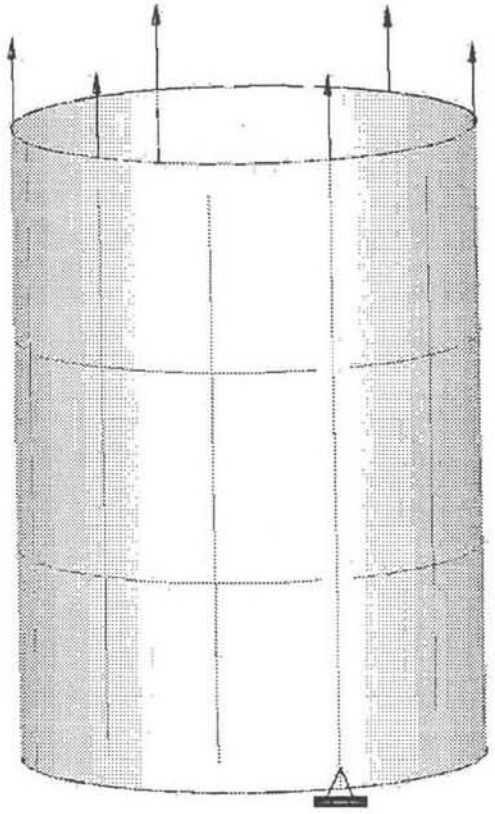

Figure 2.7 Equivalent stiffness model

2.5.2 Exact FEM Model

The exact FEM model (Figure 2.8) was created using the FEM package *MSC/NASTRAN.*

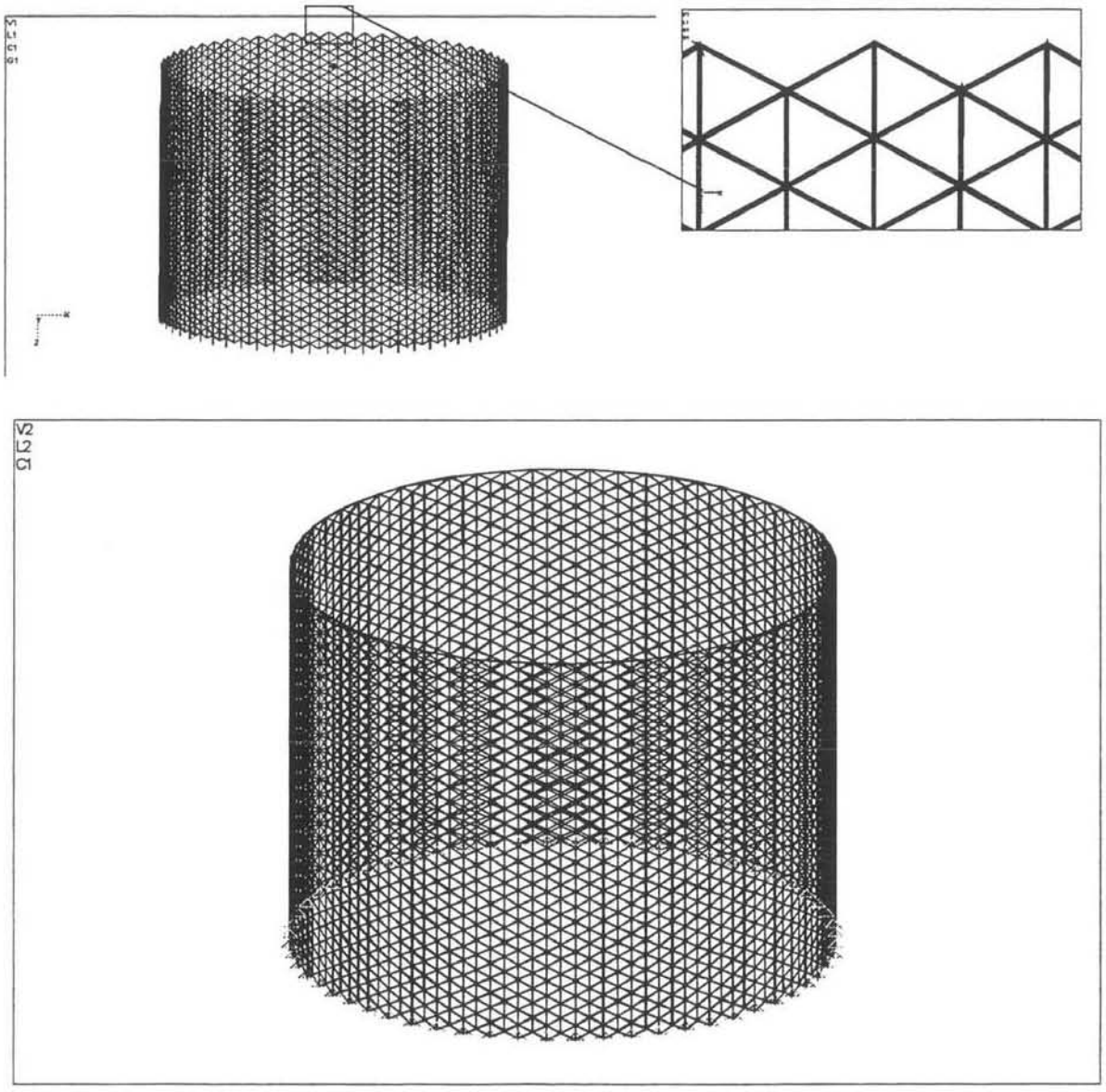

Figure 2.8 Exact FEM model

First, the unit cell of the structure (Figure 2.9) was developed. The unit cell of the considered structure can be modelled in a way that is usually used for modelling stiffened plates (Figure 2.10). A number of approaches were used previously [19], [62], [70]. One of them is to use plate elements to model the stiffener. The resulting

model turns out to be excessively stiff and does not transfer loads properly. The stiffener portion of the component resists a load by bending action, which requires a cubic displacement function to model, while the plate elements in membrane action are capable of representing only a linear displacement. Therefore, using a single plate as a stiffener almost always results in a model that is too stiff for most applications. Normally the most preferred approach for the modelling of similar structures is the one where offset beam elements (Figure 2.11) are used to model the stiffener. This is the recommended method for modelling a stiffened plate.

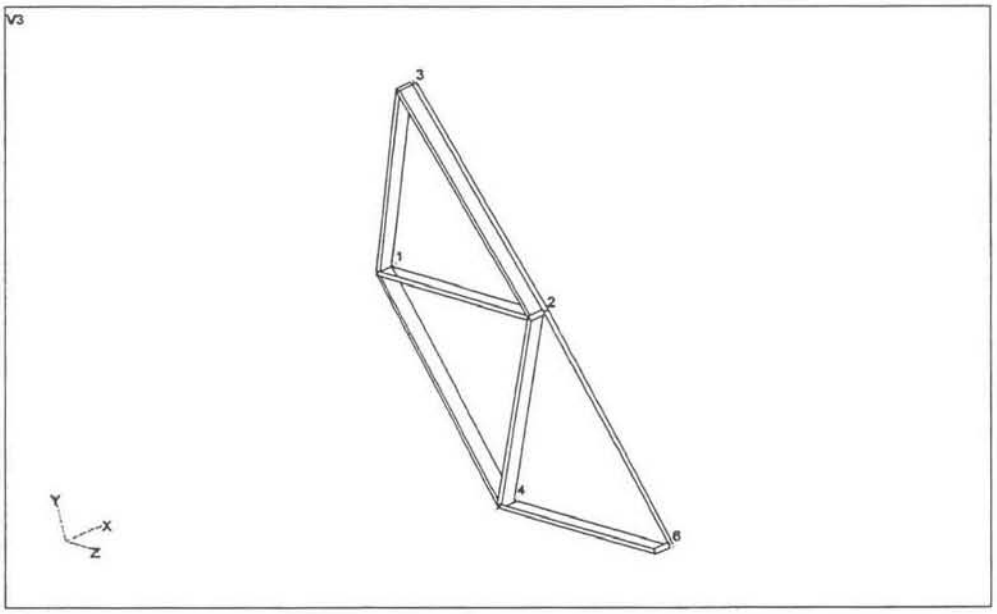

Figure 2.9 A unit cell

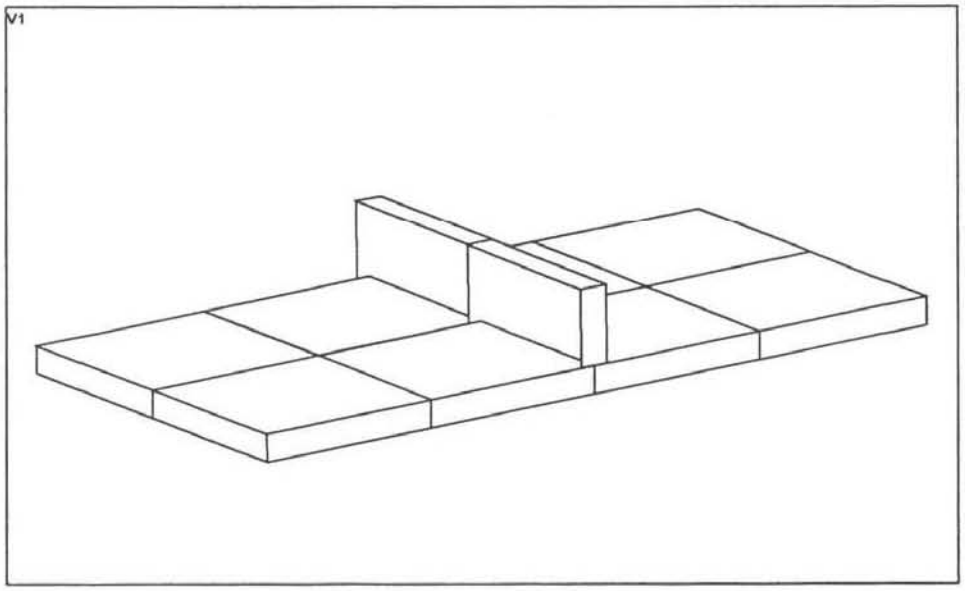

Figure 2.10 Stiffened plate

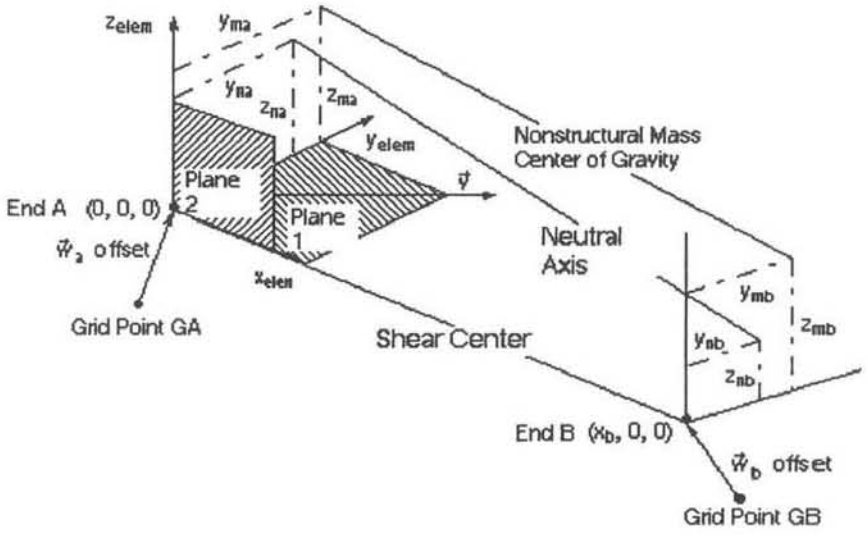

Figure 2.11 3D Offset BEAM element

In the exact FEM analysis, the rib to skin ratio was taken as 3.5 as is recommended in the "Isogrid Design Hand Book" [39]. This ratio was kept constant through the analysis whereas the aspect ratio of the rib's cross-section varied. The extra dimensions of the unit cell and its components that have not been listed above are:

Ribs: b=0.007 m; h=0.02 m; d_{90}=0.262 m; d_{θ}=0.302 m;

Skin thickness: h_{sk}=5.714e-3 m; Lay-up: $(0/90)_s$

Angle of isogrid rib's orientation: θ=60°.

H=7.56 m; D=5.44 m; φ=60°; a=0.302 m; h=0.02 m; b=0.00666667 m;

The skin section of the isogrid was taken as a $(0/90)_s$ laminate with four identical layers. Carbon/Epoxy composite was used as the material for the isogrid structure. The material properties used for the structure are taken from [12] and given in Table 2.2. Triangular laminate composite shell finite elements that take into account transverse shear stress were used in the model.

Material T300/5208				
Stiffness Pareameters				
E_1, *Pa*	E_2, *Pa*	ν_{12}		G_{12}, *Pa*
$1.81\ 10^{11}$	$1.03\ 10^{10}$	0.28		$7.17\ 10^{9}$
Strength Pareameters, MPa				
Tensile		*Compressive*		*Shear*
X_t	Y_t	X_c	Y_c	S
1500	57	1340	212	68

Table 2.2 Material properties of the ribs

At the second stage of the model development the unit cell was revolved around and translated along the global axis of the cylinder to represent the complete cylindrical structure. The final model had 23000 elements.

2.5.3 Comparison of the Results

In order to verify the results, normal and shear components of the strains obtained from linear static analysis of the ESM must be recalculated back to strain components acting in the ribs and skin using the following formulae:

$$\varepsilon_x^{skin} = \varepsilon_x^0 + k_x z, \qquad \varepsilon_y^{skin} = \varepsilon_y^0 + k_y z, \qquad \gamma_{xy}^{skin} = \gamma_{xy}^0 + k_{xy} z. \tag{2.31}$$

There superscript *skin* denotes strains acting in the skin; ε_x^0, ε_y^0, γ_{xy}^0 are normal and shear midsurface strains; and k_x , k_y , γ_{xy}^0 are curvature changes of the midsurface of the homogenised shell.

For the ribs, axial strains are calculated as:

$$\begin{aligned} &\varepsilon_x^{rib} = \varepsilon_x^0 m^2 + \varepsilon_x^0 n^2 + \gamma_{xy}^0 mn, \\ &m = \cos\theta, \qquad n = \sin\theta. \end{aligned} \tag{2.32}$$

Strains in the vertical and diagonal families of the ribs and also skin are plotted versus the vertical co-ordinate z (Figure 2.12 - Figure 2.29)

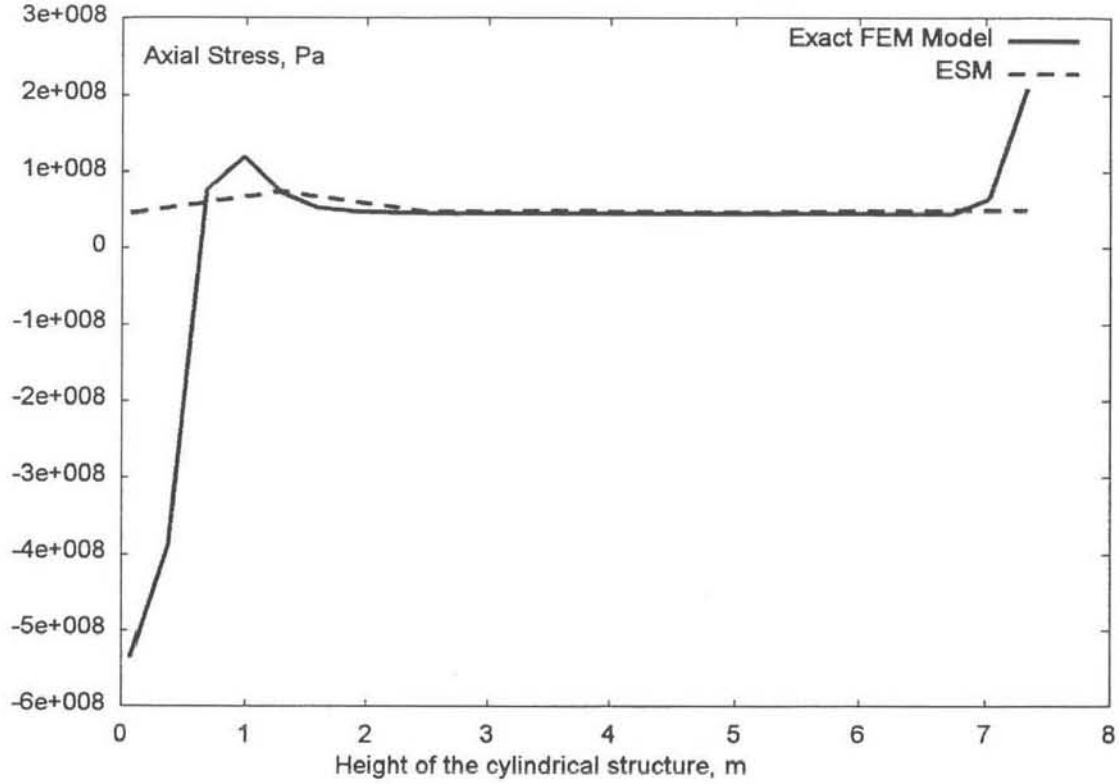

Figure 2.12 Beam axial stress for the diagonal families of ribs

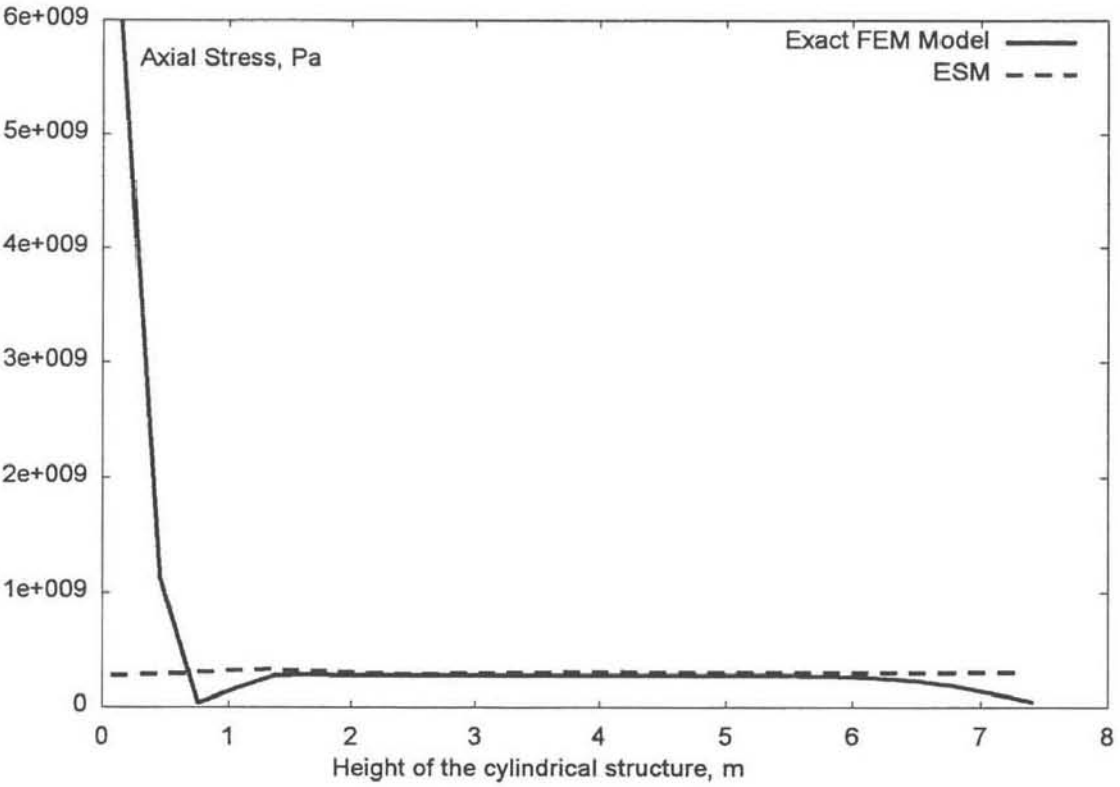

Figure 2.13 Beam axial stress for the vertical families of ribs

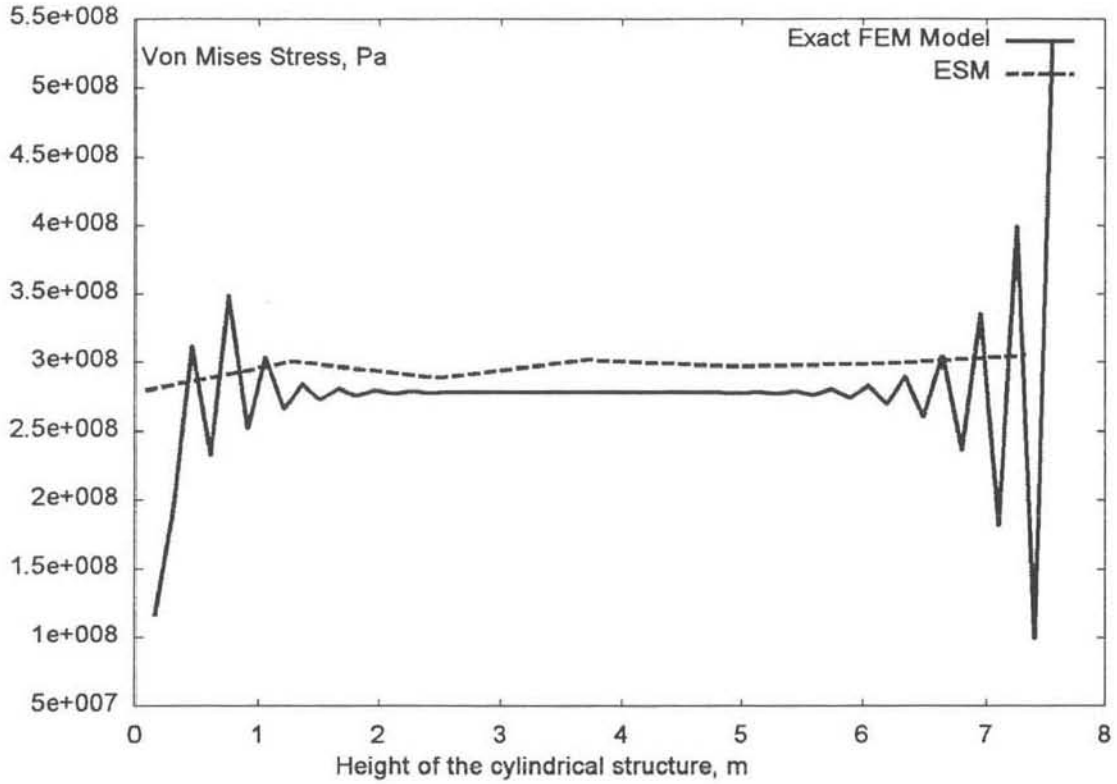

Figure 2.14 Von Mises stress for the ply 1

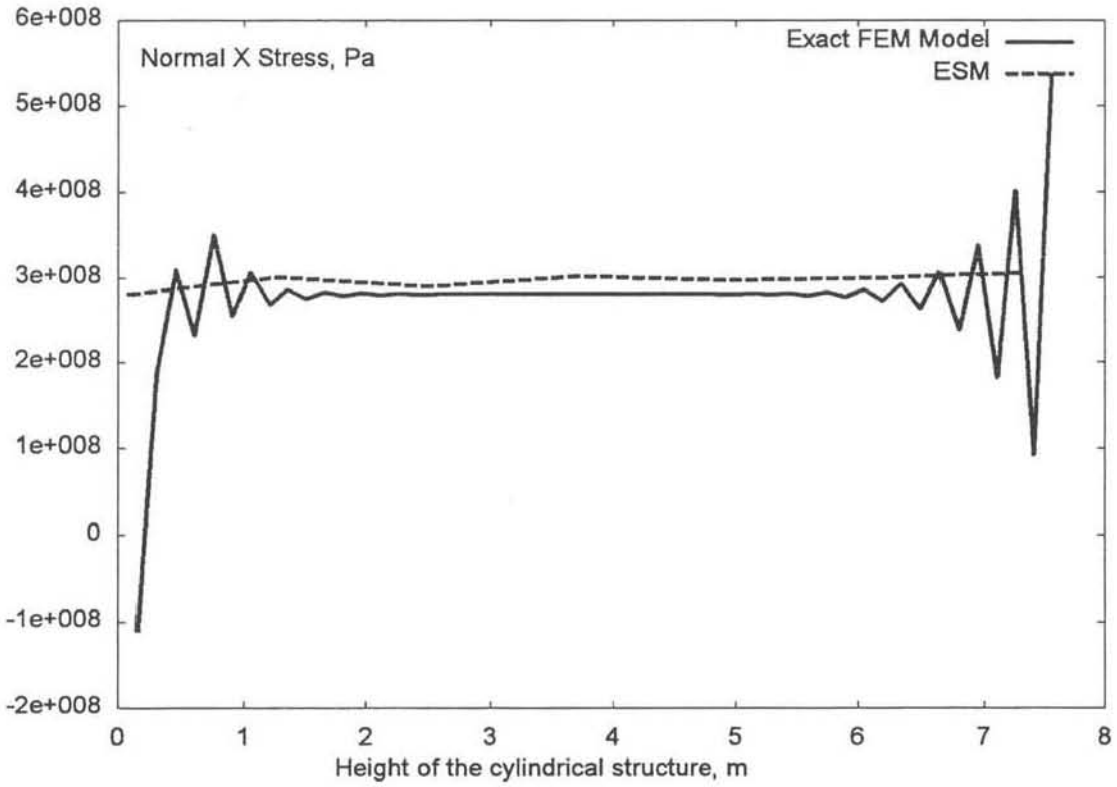

Figure 2.15 Normal X stress for the ply 1

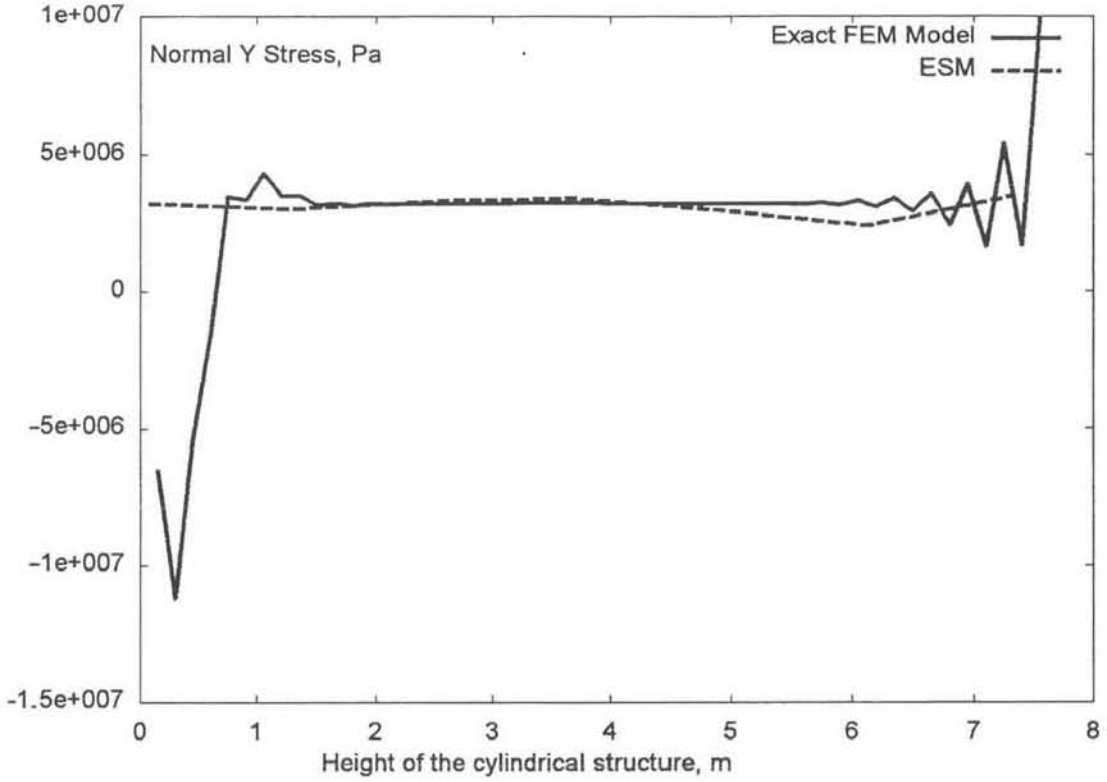

Figure 2.16 Normal Y stress for the ply 1

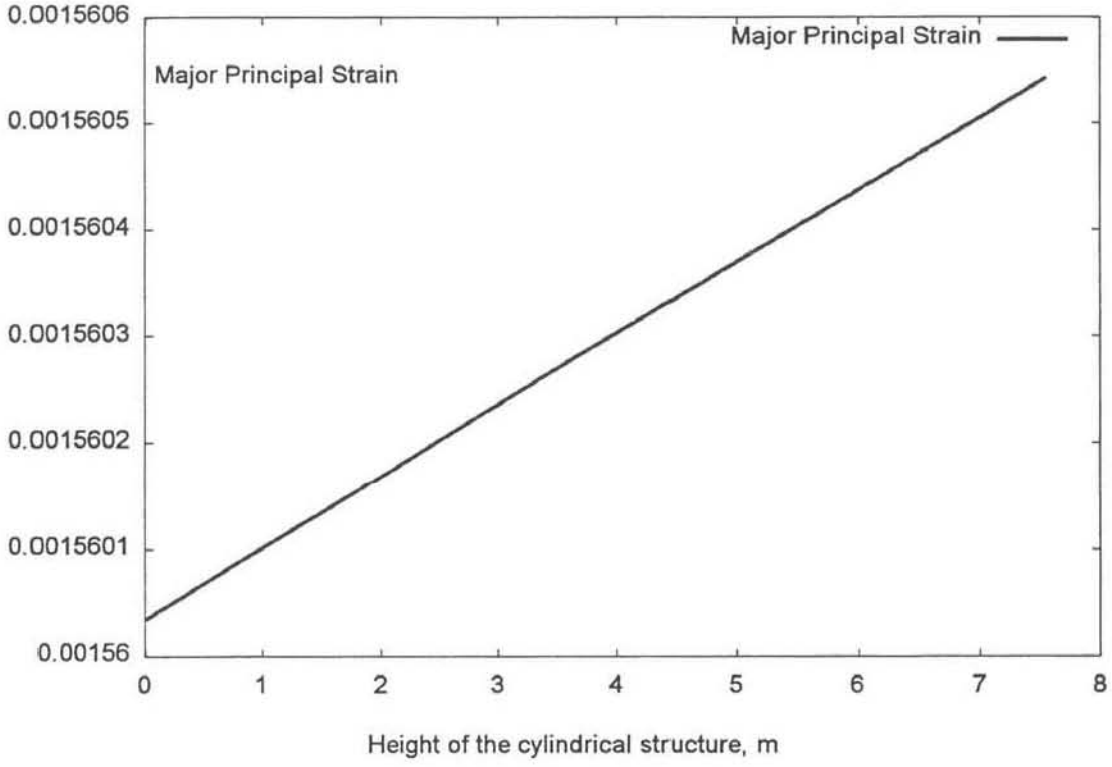

Figure 2.17 Major principal strain in ESM

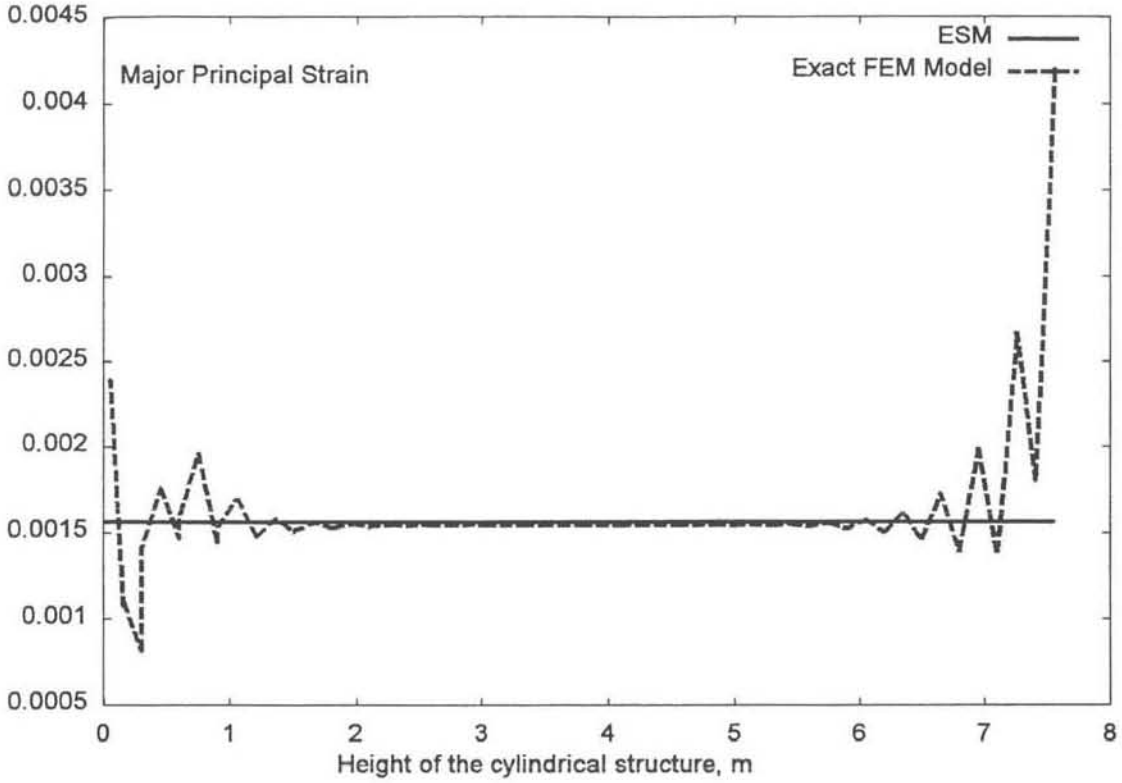

Figure 2.18 Major principal strain comparison

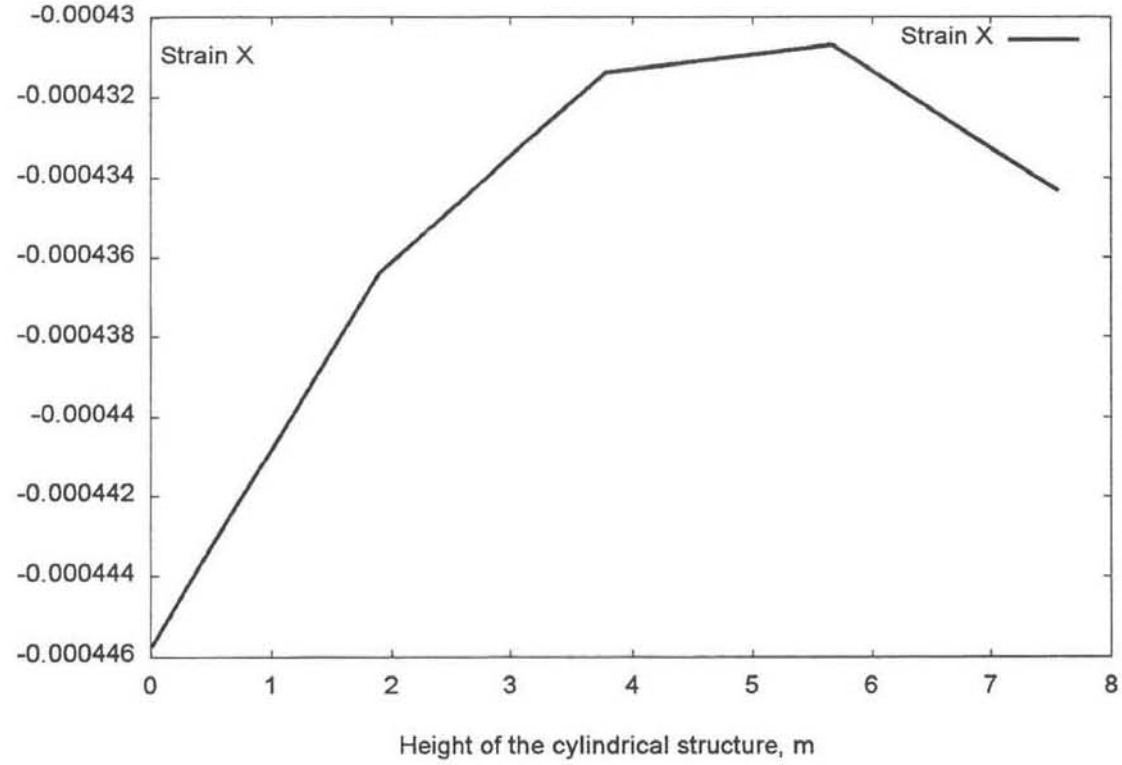

Figure 2.19 Strain X in ESM

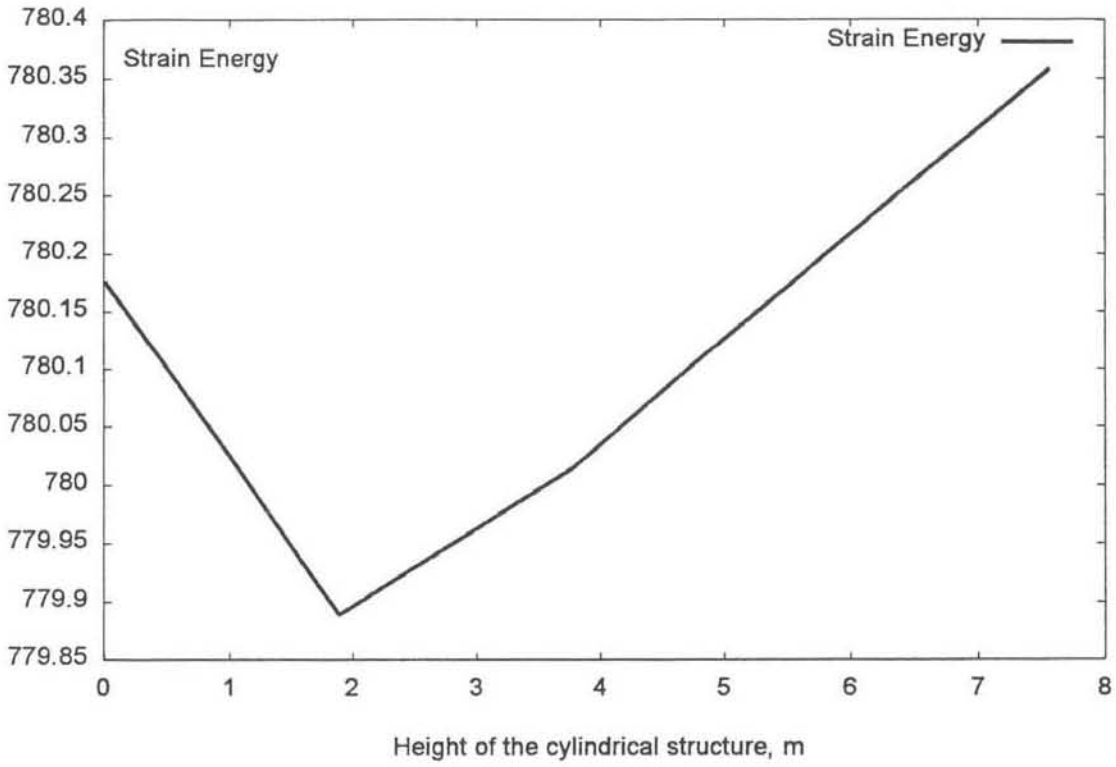

Figure 2.20 Strain energy in ESM

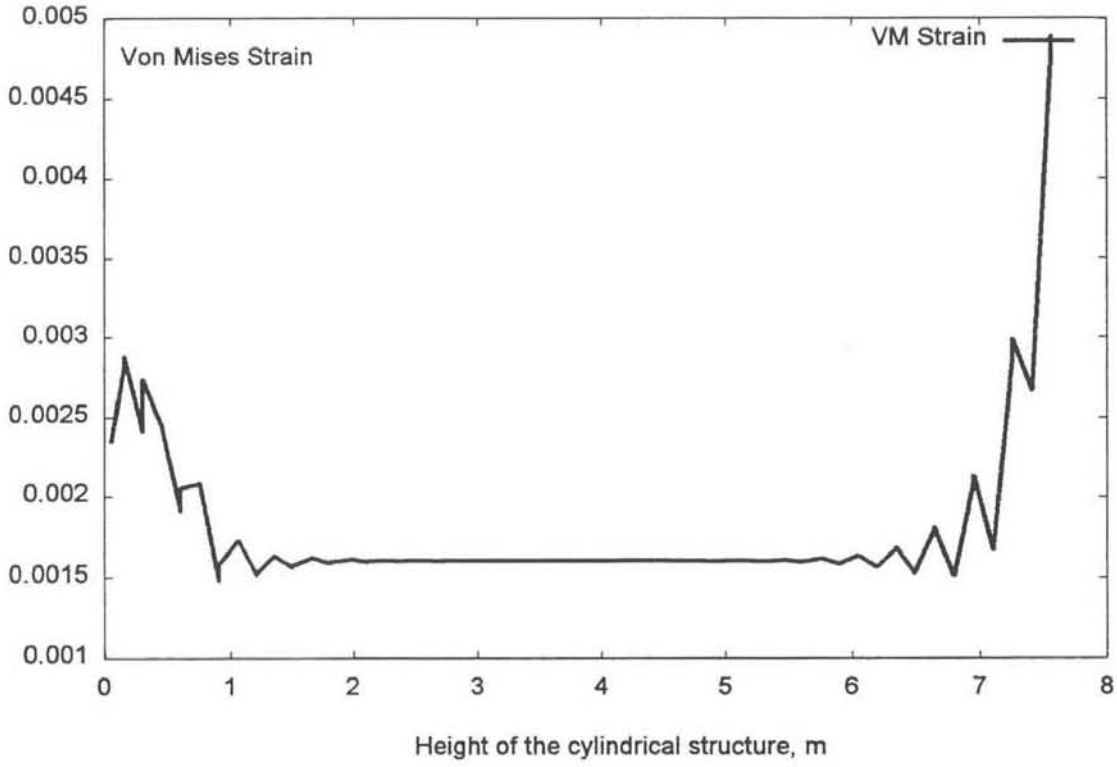

Figure 2.21 Von Mises strain (exact model)

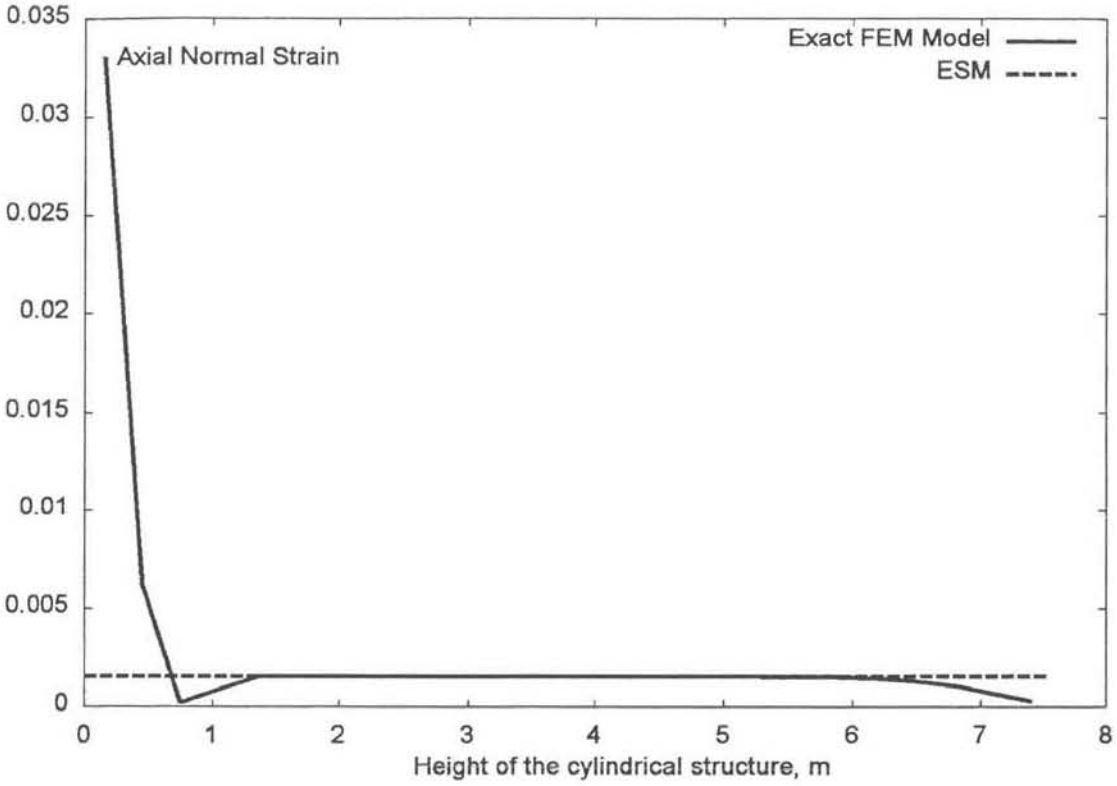

Figure 2.22 Axial normal strains in the vertical ribs

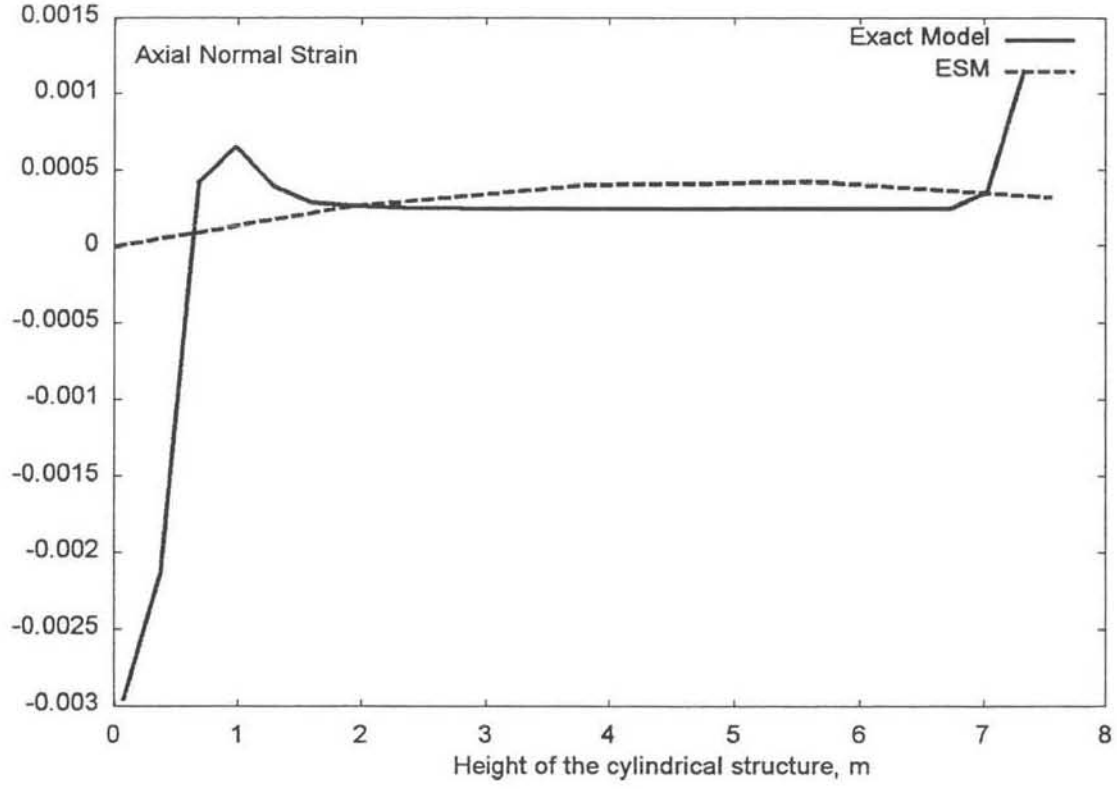

Figure 2.23 Axial normal strains in the diagonal ribs

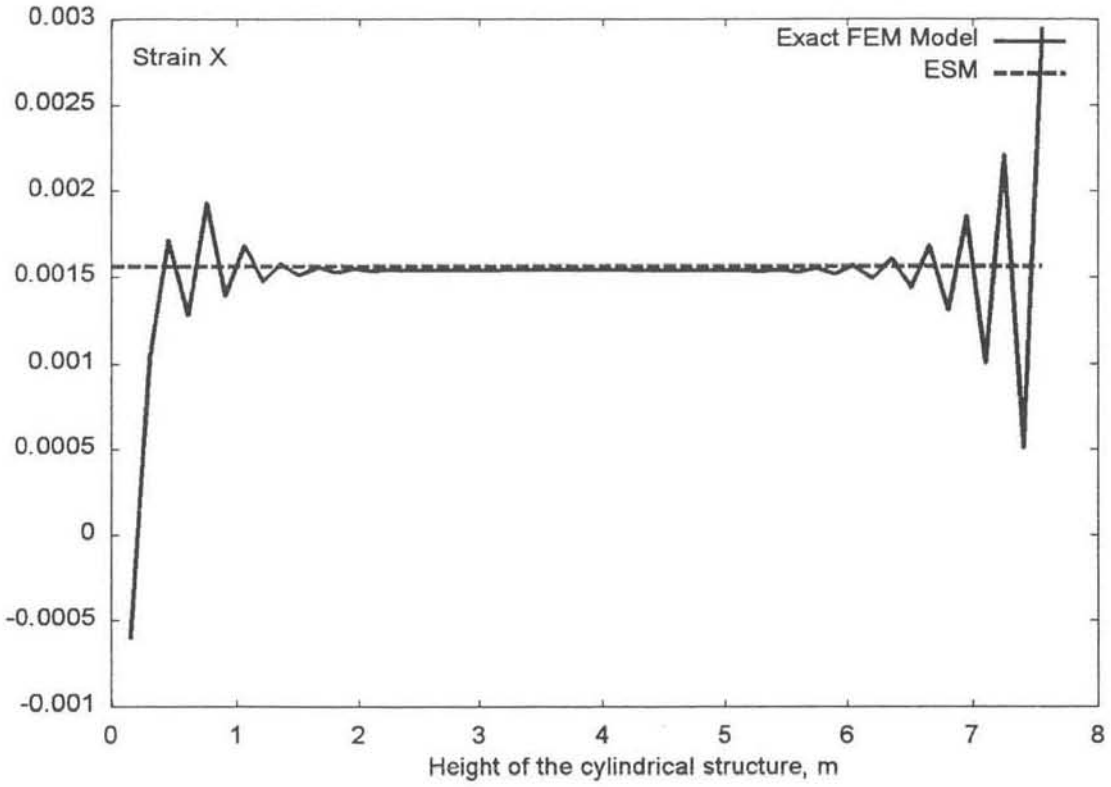

Figure 2.24 Strain X in the composite skin (top)

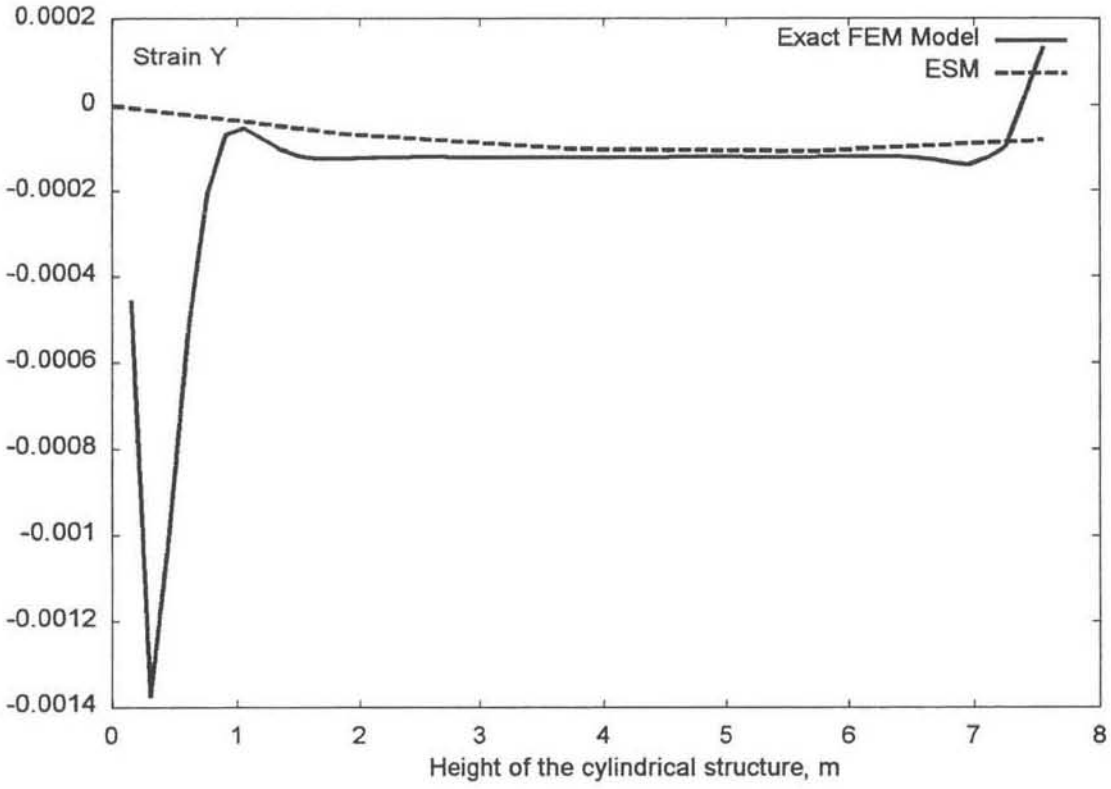

Figure 2.25 Strain Y in the composite skin (top)

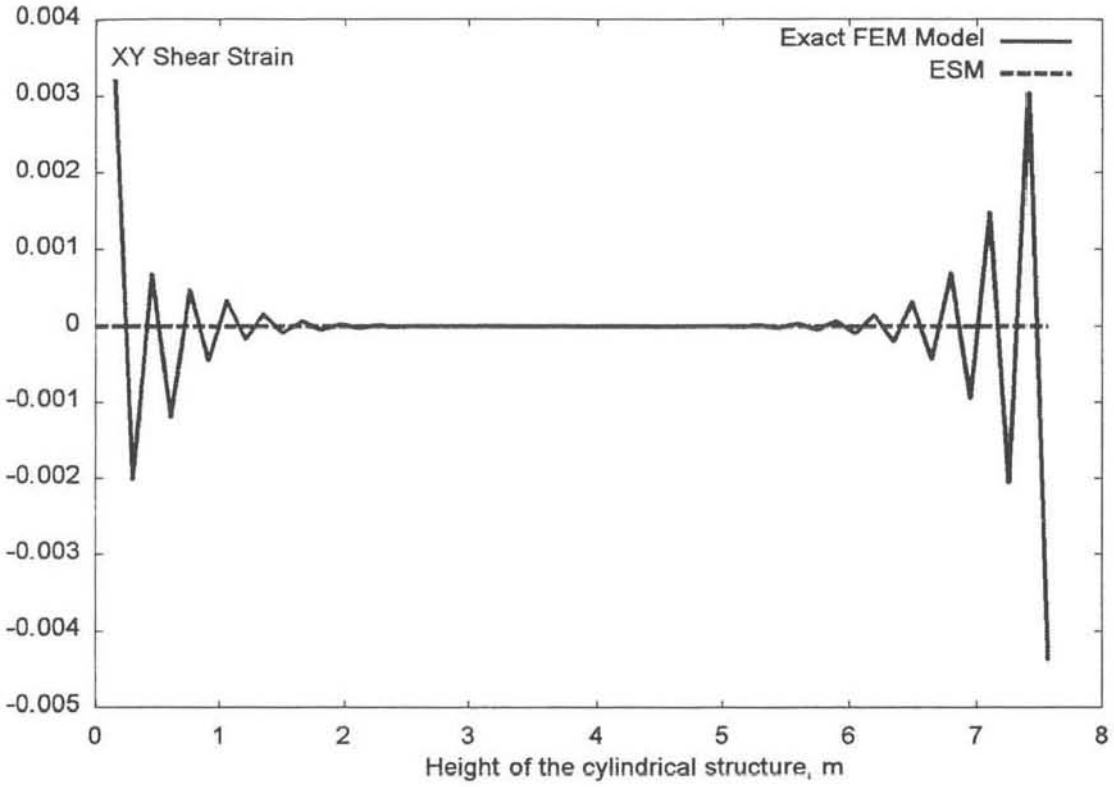

Figure 2.26 XY Shear strain in the composite skin (top)

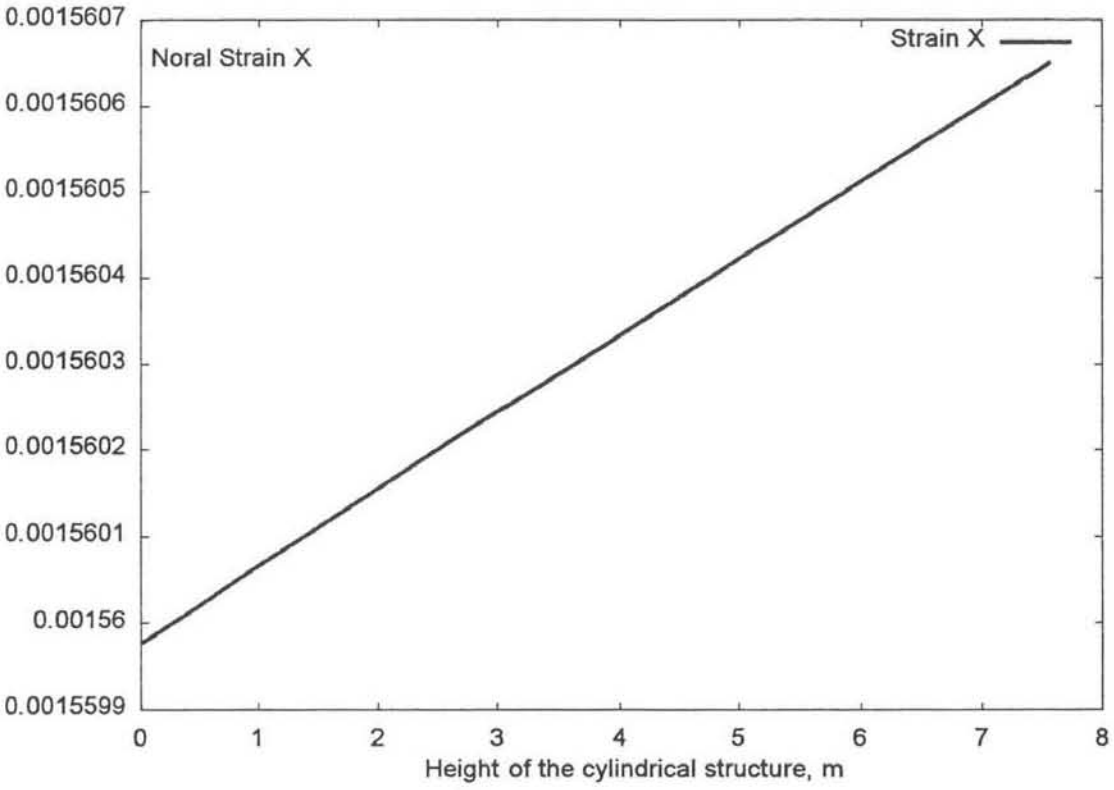

Figure 2.27 Normal strain X in the middle surface of the shells (ESM)

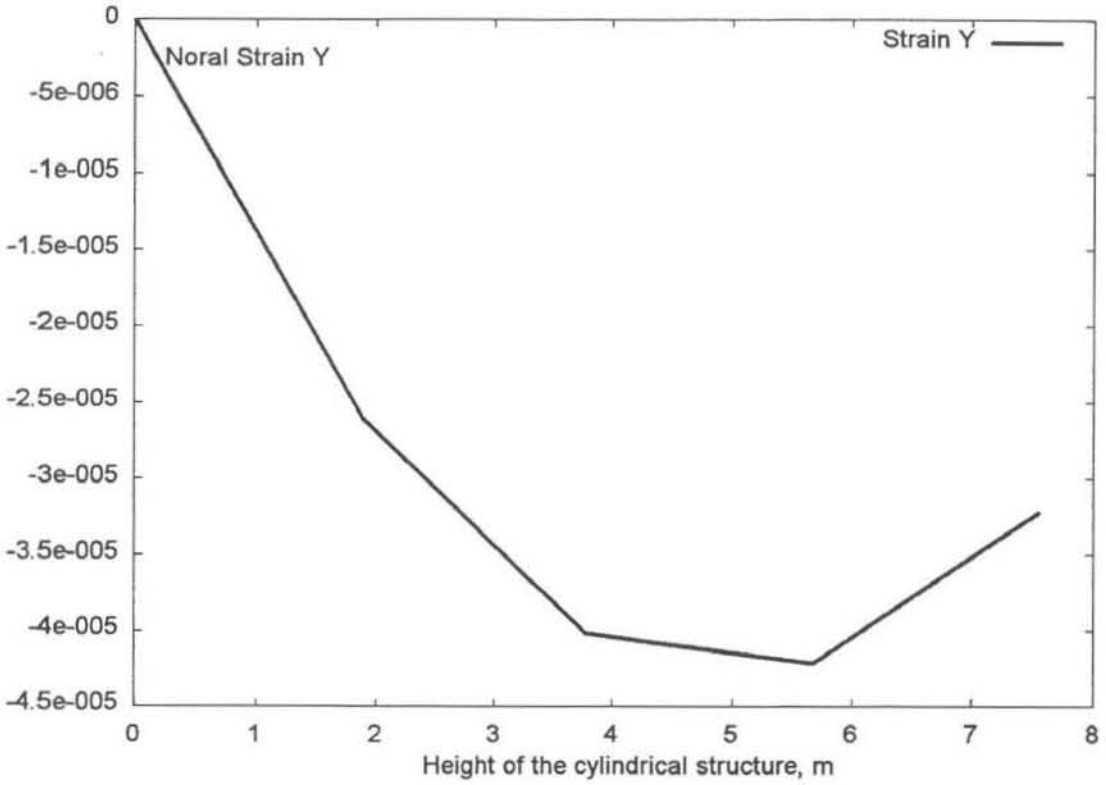

Figure 2.28 Normal strain Y in the middle surface of the shells (ESM)

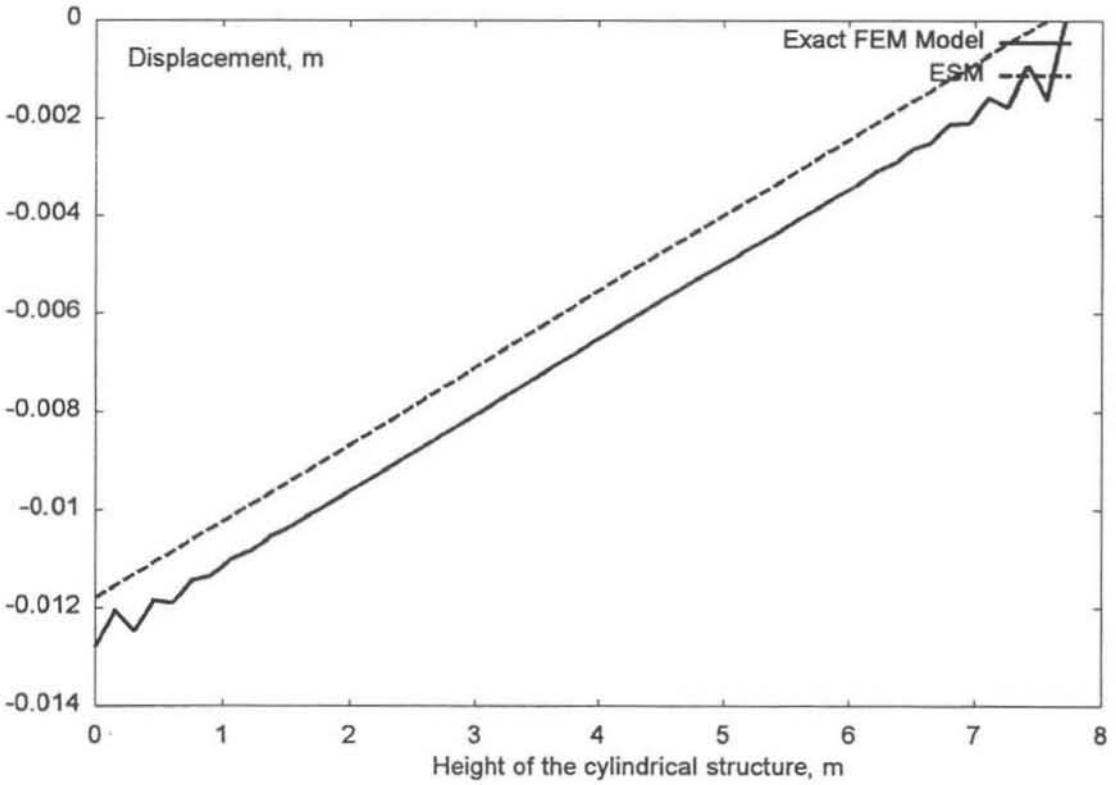

Figure 2.29 Displacement *z*

The results presented in Figure 2.22 - Figure 2.26 and Figure 2.29 show good correlation. The discrepancy does not exceed 10% for most of the elements of the model except for those elements subjected to the local effects. Considerable differences in the results can be seen in the vicinity of the constrained contour and the loaded edge of the cylinder. This inconsistency can be overcome by taking into account boundary effects: by combining exact beam and shell elements with equivalent stiffness shell elements in the regions where there are boundary effects. However, this is not considered in this thesis since it was not set as a goal of this research. In the following comparison of the obtained results, the primary focus is made on middle section of the structure which is not subjected to the edge effects.

Error estimation is given in Table 2.1 and Table 2.2 for the elements in the middle section of the structure in order to minimise the influence of the boundary effects on the results.

The results of this part of the research were summarised in [81].

	FEM		*ESM*			
	Axial strain	*Displacement, m*	*Axial strain*	*Displacement, m*	*Difference, %*	
	ε_x	z	ε_x	z	ε_x	z
Vertical family of ribs	1.551784E-3	7.5524E-3	1.5603143E-3	6.91125E-3	0.55	8.49
Diagonal family of ribs	3.512564E-4	7.5412E-3	0.3512564E-4	6.92331E-3	9.9	8.51

Table 2.1 Comparison of strains and displacements of the ribs

FEM			*ESM*					
Strain component			*Strain component*			*Difference, %*		
ε_x	ε_y	γ_{xy}	ε_x	ε_y	γ_{xy}	ε_x	ε_y	γ_{xy}
1.551784E-3	-1.332556E-4	0	1.5603143E-3	-0.101274E-4	0	0.57	7.6	0

Table 2.2 Comparison of strains components for the skin elements

2.5.4 Conclusions

The verification of the ESM has been undertaken by comparing it with the exact FEM model. The general verification of the homogenisation concept has been made and the estimation of the accuracy of the results has been performed. The comparison of the strains (both normal and shear) and displacements of the elements in two models shows that the difference in the results obtained from the analysis of the exact and equivalent stiffness models does not exceed 10%. The inconsistency in the stress resultants is localised in the boundary areas where the load and constraints are applied. At this stage the developed homogenised model fails to predict stress resultants with the reasonable accuracy in the vicinity of the areas where boundary effect is taking place. However, the homogenisation approach presented shows the possibility of replacing complex and extensive stress analysis on the basis of an exact FEM model by analysis based on an equivalent stiffness model of reasonable accuracy.

3 Proposed Homogenisation Approach

3.1 Introduction

Composite isogrid structures can offer a wide variety of properties for different sequences of geometric parameters (rib's cross-section, skin thickness, configuration of a unit cell) and skin lay-ups. All these advantages in the design can only be utilised by incorporating the optimisation methods.

During the optimisation process the design responses of a structure are usually calculated from the stress resultants in structural members. Calculation of the stress resultants themselves in the isogrid using the finite element method can be simplified by means of incorporating a homogenised model to replace the exact model [13], [36]. The finite element method (FEM) has proven to work reasonably well for calculating structural responses and characteristics [16]. Usually the geometry of the FEM models of lattice structures is highly dependent on rib stiffener spacing and angle, making these models very difficult to modify to accommodate small changes in rib pattern. This disadvantage limits the usefulness of the application of the FEM method for design/optimisation purposes.

Transition from the exact model to a ESM was shown in detail in the previous chapter. The optimisation requires a great number of finite element analyses to be performed for the constantly iteratively changing optimisation variables (usually the geometric characteristics of the unit cell). The complexity arises when equivalent stiffness matrices $[A]$, $[B]$, $[D]$ and $[H]$ have to be recalculated each time to update the stiffness characteristics of the finite element model. Calculation of equivalent stiffness matrices (2.23) for the isogrid is not a part of the FEM code so they should be calculated manually and subsequently the FEM model must be manually updated. Considering the amount of optimisation iterations required for obtaining the final optimum design with the reasonable convergence tolerance [10] this task will obviously be extremely intensive. The number and type of design variables that can be possibly assigned in commercially available FEM packages [21], [5], [17] is limited. That is why the optimisation of the isogrid structures must be performed using an optimisation routine that is not based on the FEM calculation of the design responses.

The above-mentioned inefficiency of the FEM method for the purpose of design/optimisation (though quite accurate for static structural analysis), makes it impossible to adopt for the solution of the design/optimisation problem stipulated for this research work. The further study will be focused on developing different homogenisation representations of equivalent stiffness of a lattice structure, which is not based on FEM, but rather on static equations and equations of motion, geometric equations and constitutive equations of a shells.

3.2 Basic Approach

The proposed approach deals with the elastic shell as a continuous system, i.e. external loads and the stress-strain states are described by the functions. This approach allows the effective implementation of the methods of solid mechanics [14] in the analysis of an isogrid shell.

Most of the grid shells represent complex spatial frames comprising elastic members. The axes of the structural members (the ribs) are assumed to form families of curves on the median surface of a shell. These families are further referred to as "families of ribs". There are three families for the isogrid structure and two for both the orthogrid and the anglegrid structures (Figure 1.4). The median surface of a continuous model is assumed to be coincident with the one of the exact model. Axes of the ribs that belong to any particular family do not intersect. The high accuracy of the calculations on the basis of the proposed homogenisation technique can be achieved for the parts of the model that are not situated in the immediate vicinity of the constraints or the applied load. For these regions the boundary effects must be taken into account or analysis should be performed on the basis of the exact model.

In the approach developed, three groups of equations are used:

1. Static equations and equations of motion written in terms of forces and moments [97]
2. Geometric equations that link the displacements to the deformations [6]
3. Constitutive equations of the shell [6].

3.3 Basic Equations of the Theory of Anisotropic Shells

Consider a median surface of a shell in the curvilinear co-ordinate system α, β. The projections of the displacement vector of the point on the median surface of a shell to the directions of the unit co-ordinate vectors α, β and the outer normal to the considered surface (Figure 3.1) are denoted as u, v, w.

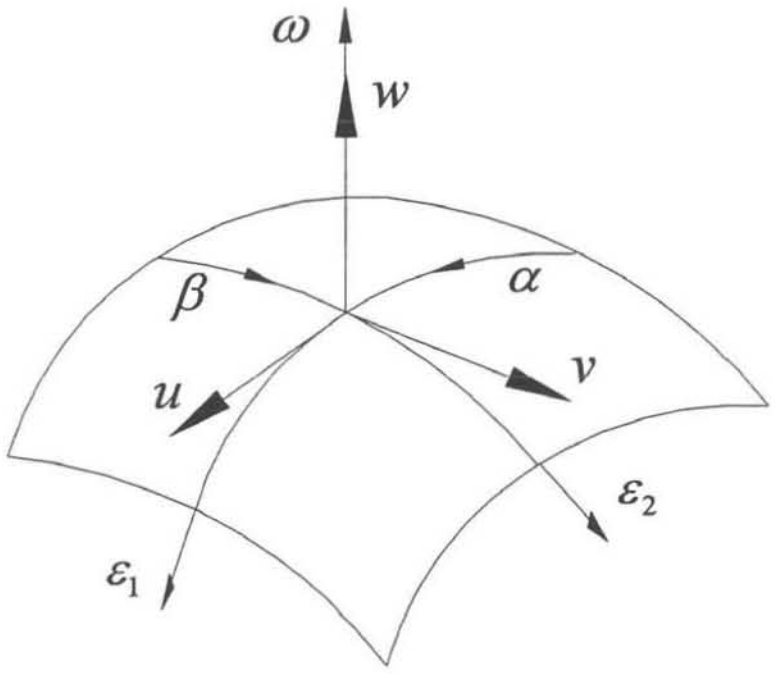

Figure 3.1 Median surface of a shell in curvilinear co-ordinates

ε_1, ε_2, ω, χ_1, χ_2 and τ are the components of the deformation of the median surface of the shell (Figure 3.1).

3.3.1 Static Equations

Positive directions of the distributed forces and moments are shown on the Figure 3.2. Positive directions correspond to the moments causing clockwise rotation when viewed from the positive side of the corresponding vector.

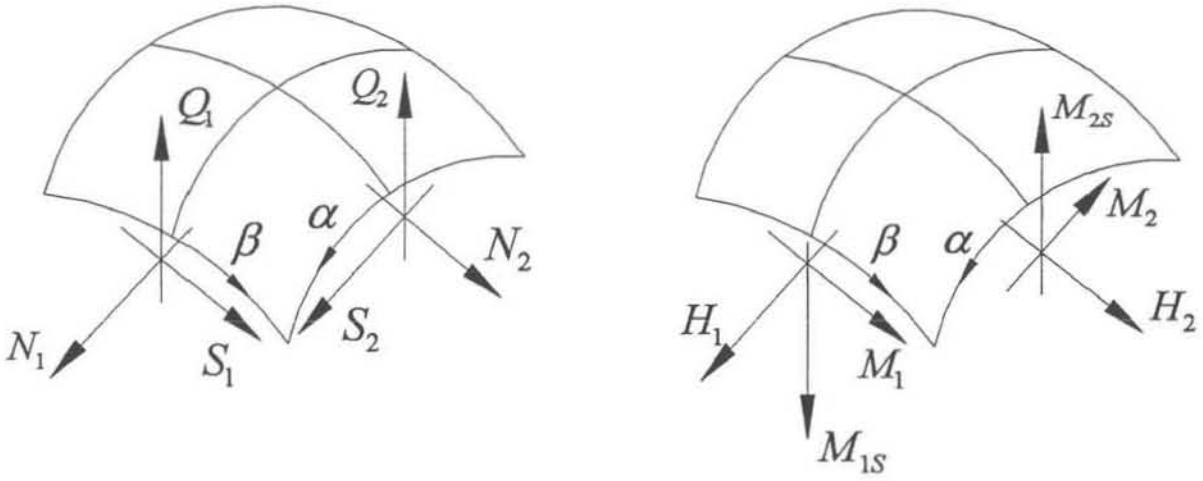

Figure 3.2 Direction of the forces and moments acting in the shell

Forces and moments S_j, Q_j, M_j, H_j $(j=1,2)$ must satisfy the following six equations [6]:

$$\begin{aligned}
&\frac{\partial B^* N_1}{\partial \alpha}+\frac{\partial A^* S_2}{\partial \beta}+S_1\frac{\partial A}{\partial \beta}-N_2\frac{\partial B^*}{\partial \alpha}+AB\left(Q_1 k_1^*+Q_2 k_{12}^*+X^*\right)=0,\\
&\frac{\partial A^* N_2}{\partial \beta}+\frac{\partial B^* S_1}{\partial \alpha}+S_2\frac{\partial B^*}{\partial \alpha}-N_1\frac{\partial A^*}{\partial \beta}+AB\left(Q_2 k_2^*+Q_1 k_{12}^*+Y^*\right)=0,\\
&\frac{\partial B Q_1}{\partial \alpha}+\frac{\partial A Q_2}{\partial \beta}-AB\left(N_1 k_1^*+N_2 k_2^*+S_1 k_{12}^*+S_2 k_{12}^*-Z^*\right)=0,\\
&\frac{\partial B M_1}{\partial \alpha}+\frac{\partial A H_2}{\partial \beta}+H_1\frac{\partial A}{\partial \beta}+M_2\frac{\partial B}{\partial \alpha}-AB\left(Q_1-m_\alpha^*\right)=0,\\
&\frac{\partial A M_2}{\partial \beta}+\frac{\partial B H_1}{\partial \alpha}+H_2\frac{\partial B}{\partial \alpha}+M_1\frac{\partial A}{\partial \beta}-AB\left(Q_2-m_\beta^*\right)=0,\\
&S_1-S_2+H_1 k_1^*+H_2 k_2^*+k_{12}^*\left(M_2-M_1\right)=0.
\end{aligned} \tag{3.1}$$

In (3.1) the superscript * shows that this term corresponds to the median surface in deformed state: X^*, Y^*, Z^* are projections of the vector of load intensity in the directions of the unit co-ordinate vectors and outer normal to the median surface; m_α^* and m_β^* are the intensities of distributed moments. A and B are coefficients of the first

quadratic form for the median surface; k_1, k_2 are curvatures of the normal sections of the median surface along co-ordinate lines; k_{12} is the torsion of the co-ordinate lines:

$$\begin{aligned} &k_1 = \frac{1}{R_1}, && k_2 = \frac{1}{R_2}, && k_{12} = \frac{1}{R_{12}}, \\ &k_1^* = k_1 + \chi_1, && k_2^* = k_2 + \chi_2, && k_{12}^* = k_{12} + \tau, \\ &A^* = (1+\varepsilon_1)A, && B^* = (1+\varepsilon_2)B. \end{aligned} \tag{3.2}$$

3.3.2 Geometric Equations

Tangential (ε_1, ε_2, ω) and bending (χ_1, χ_2, τ) components of strain tensor for median surface of a shell must satisfy the following three equations of continuity [6]:

$$\begin{aligned} &\frac{\partial}{\partial\alpha}\frac{1}{A}\left[\frac{\partial B\varepsilon_2}{\partial\alpha} - \varepsilon_1\frac{\partial B}{\partial\alpha} - \frac{1}{2}\left(\frac{\partial A\omega}{\partial\beta} + \omega\frac{\partial A}{\partial\beta}\right)\right] + \\ &+\frac{\partial}{\partial\beta}\frac{1}{A}\left[\frac{\partial A\varepsilon_1}{\partial\beta} - \varepsilon_2\frac{\partial A}{\partial\beta} - \frac{1}{2}\left(\frac{\partial B\omega}{\partial\alpha} + \omega\frac{\partial B}{\partial\alpha}\right)\right] = AB\left(\tau^2 - \chi_1\chi_2 - \chi_1 k_2 - \chi_2 k_1 + 2\tau k_{12}\right), \\ &\frac{\partial A\chi_1}{\partial\beta} - \frac{\partial B\tau}{\partial\alpha} - \chi_2\frac{\partial A}{\partial\beta} - \tau\frac{\partial B}{\partial\alpha} + (k_1+\chi_1)\left(\omega\frac{\partial B}{\partial\alpha} - A\frac{\partial\varepsilon_1}{\partial\beta}\right) + \\ &+(k_{12}+\tau)\left(2\omega\frac{\partial A}{\partial\beta} + B\frac{\partial(\varepsilon_1-\varepsilon_2)}{\partial\alpha}\right) + (k_2+\chi_2)\left(\frac{\partial B\omega}{\partial\alpha} - 2(\varepsilon_1-\varepsilon_2)\frac{\partial A}{\partial\beta} - A\frac{\partial\varepsilon_1}{\partial\beta}\right) = 0, \\ &\frac{\partial B\chi_2}{\partial\beta} - \frac{\partial B\tau}{\partial\beta} - \chi_2\frac{\partial B}{\partial\beta} - \tau\frac{\partial B}{\partial\beta} + (k_2+\chi_2)\left(\omega\frac{\partial B}{\partial\beta} - B\frac{\partial\varepsilon_1}{\partial\beta}\right) + \\ &+(k_{12}+\tau)\left(2\omega\frac{\partial B}{\partial\beta} + B\frac{\partial(\varepsilon_1-\varepsilon_2)}{\partial\beta}\right) + (k_2+\chi_2)\left(\frac{\partial B\omega}{\partial\beta} - 2(\varepsilon_1-\varepsilon_2)\frac{\partial B}{\partial\beta} - B\frac{\partial\varepsilon_1}{\partial\beta}\right) = 0. \end{aligned} \tag{3.3}$$

3.3.2.1 Small Deformations

In the case of small deformations it is assumed that angles of rotation are small compared to a unit. Components of the strain tensor (ε_1, ε_2, ω, χ_1, χ_2 and τ) can be found from the components of the displacement vector u, v and w using the following transformations [58].

$$\begin{aligned} &\varepsilon_1 = e_{11}, && \varepsilon_2 = e_{22}, && w = e_{12} + e_{21}, \\ &\chi_1 = k_1\varepsilon_1 - k_{12}\varepsilon_{21} - \frac{1}{A}\frac{\partial\gamma_1}{\partial\alpha} - \frac{\gamma_2}{AB}\frac{\partial A}{\partial\beta}, \\ &\chi_2 = k_2\varepsilon_1 - k_{12}\varepsilon_{12} - \frac{1}{B}\frac{\partial\gamma_2}{\partial\beta} - \frac{\gamma_1}{AB}\frac{\partial B}{\partial\alpha}, \\ &\tau = k_{12}\varepsilon_1 - k_1\varepsilon_{21} - \frac{1}{A}\frac{\partial\gamma_2}{\partial\alpha} + \frac{\gamma_1}{AB}\frac{\partial A}{\partial\beta}. \end{aligned} \tag{3.4}$$

In (3.4) the following notations are used:

$$
\begin{aligned}
e_{11} &= \frac{1}{A}\frac{\partial u}{\partial \alpha} + \frac{v}{AB}\frac{\partial A}{\partial \beta} + k_1 w, \quad e_{22} = \frac{1}{B}\frac{\partial v}{\partial \beta} + \frac{u}{AB}\frac{\partial B}{\partial \alpha} + k_2 w, \\
e_{12} &= \frac{1}{A}\frac{\partial v}{\partial \alpha} + \frac{u}{AB}\frac{\partial A}{\partial \beta} + k_{12} w, \quad e_{21} = \frac{1}{B}\frac{\partial u}{\partial \beta} + \frac{v}{AB}\frac{\partial B}{\partial \alpha} + k_{12} w, \\
\gamma_1 &= \frac{1}{A}\frac{\partial w}{\partial \alpha} - k_1 u - k_{12} v, \qquad \gamma_2 = \frac{1}{B}\frac{\partial w}{\partial \beta} - k_2 v - k_{12} u.
\end{aligned}
\tag{3.5}
$$

There are several methods which can be used to determine the bending components of the strain tensor [26], [115]. This is due to the fact that the right hand sides of the expressions for these components have additional terms containing product of the tangential component of a strain tensor and a curvature of the median surface of a shell.

If summand $k_{12}\omega/2$ is added to the right hand side of the formulae (3.4) in the expressions for χ_1 and χ_2, and also the term $2k_1 e_{21} + k_{12}(\varepsilon_2 - \varepsilon_1)$ in the expressions for τ we have:

$$
\begin{aligned}
\varepsilon_1 &= \frac{1}{A}\frac{\partial u}{\partial \alpha} + \frac{v}{AB}\frac{\partial A}{\partial \beta} + \frac{w}{R_1}, \qquad \varepsilon_2 = \frac{1}{B}\frac{\partial v}{\partial \beta} + \frac{u}{AB}\frac{\partial B}{\partial \alpha} + \frac{w}{R_2}, \\
\omega &= \frac{A}{B}\frac{\partial}{\partial \beta}\left(\frac{u}{A}\right) + \frac{B}{A}\frac{\partial}{\partial \alpha}\left(\frac{v}{B}\right) - \frac{2w}{R_{12}}, \\
\chi_1 &= \frac{1}{A}\frac{\partial}{\partial \alpha}\left(-\frac{1}{A}\frac{\partial w}{\partial \alpha} + \frac{u}{R_1} - \frac{v}{R_{12}}\right) + \frac{1}{AB}\frac{\partial A}{\partial \beta}\left(-\frac{1}{B}\frac{\partial w}{\partial \beta} + \frac{v}{R_2} - \frac{u}{R_{12}}\right) + \\
&+ \frac{1}{2ABR_{12}}\left(\frac{\partial}{\partial \beta}(Au) - \frac{\partial}{\partial \alpha}(Bv)\right), \\
\chi_2 &= \frac{1}{B}\frac{\partial}{\partial \beta}\left(-\frac{1}{B}\frac{\partial w}{\partial \beta} + \frac{v}{R_2} - \frac{u}{R_{12}}\right) + \frac{1}{AB}\frac{\partial B}{\partial \alpha}\left(-\frac{1}{A}\frac{\partial w}{\partial \alpha} + \frac{u}{R_1} - \frac{v}{R_{12}}\right) + \\
&+ \frac{1}{2ABR_{12}}\left(\frac{\partial}{\partial \alpha}(Bv) - \frac{\partial}{\partial \beta}(Au)\right), \\
\tau &= \frac{1}{A}\frac{\partial}{\partial \alpha}\left(-\frac{1}{B}\frac{\partial w}{\partial \beta} + \frac{v}{R_2} - \frac{u}{R_{12}}\right) + \frac{1}{AB}\frac{\partial A}{\partial \beta}\left(\frac{1}{A}\frac{\partial w}{\partial \alpha} + \frac{u}{R_2} - \frac{v}{R_{12}}\right) + \\
&+ \frac{1}{R_1}\left(\frac{1}{B}\frac{\partial u}{\partial \beta} - \frac{v}{AB}\frac{\partial B}{\partial \alpha} - \frac{w}{R_{12}}\right) - \frac{1}{R_{12}}\left(\frac{1}{B}\frac{\partial v}{\partial \beta} + \frac{u}{AB}\frac{\partial B}{\partial \alpha} + \frac{w}{R_2}\right).
\end{aligned}
\tag{3.6}
$$

In this case $k_{12} = -1/R_{12}$

The angle of in-plane rotation of a midplane surface about the normal to the median surface according to [60] is:

$$\mathrm{tg}\psi = \frac{-2\delta + (e_{12} + e_{21})\cos 2\varphi + (e_{22} + e_{11})\sin 2\varphi}{2\left(1 + e_{11}\cos^2\varphi + e_{22}\sin^2\varphi\right) + (e_{12} + e_{21})\sin 2\varphi}, \tag{3.7}$$

where

$$\delta = \frac{1}{2AB}\left[\frac{\partial}{\partial\beta}(Au) - \frac{\partial}{\partial\alpha}(Bv)\right]. \tag{3.8}$$

3.3.3 Constitutive Equations for Anisotropic Shells

If the material of a shell has a plane of elastic symmetry that is parallel to the tangent surface of the median surface, the constitutive equations take the following form [6]:

$$\begin{aligned}
N_1 &= C_{11}\varepsilon_1 + C_{12}\varepsilon_2 + C_{16}\omega, \\
N_2 &= C_{21}\varepsilon_1 + C_{22}\varepsilon_2 + C_{26}\omega, \\
S &= C_{16}\varepsilon_1 + C_{26}\varepsilon_2 + C_{66}\omega, \\
H &= D_{16}\varepsilon_1 + D_{26}\varepsilon_2 + D_{66}\tau, \\
M_1 &= -\left(D_{11}\chi_1 + D_{12}\chi_2 + D_{16}\tau\right), \\
M_2 &= -\left(D_{12}\chi_1 + D_{22}\chi_2 + D_{26}\tau\right).
\end{aligned} \tag{3.9}$$

In the case of an orthotropic material with main axes of elastic symmetry coincident with the direction of the co-ordinate lines, equation (3.9) simplifies, and the following terms vanish:

$$C_{16} = C_{12} = D_{16} = D_{26} = 0. \tag{3.10}$$

For the case of an isotropic material, equation (3.9) simplifies even further by satisfying conditions (3.11) as well as conditions (3.10).

$$\begin{aligned}
C_{11} = C_{22} = C_{12}/\nu = 2C_{66}/(1-\nu) = Eh/\left(1-\nu^2\right), \\
D_{11} = D_{22} = D_{12}/\nu = D_{66}/(1-\nu) = Eh^3/12\left(1-\nu^2\right),
\end{aligned} \tag{3.11}$$

where E and ν are Young's modulus and Poisson's ratio, respectively for the material of the shell.

3.4 Constitutive Equations of the Grid Shell Theory.

In this section constitutive equations are developed, which represent forces and moments acting in a homogenised model of a lattice shell as functions of the strain components of the median surface of the lattice shell. These constitutive equations will allow for the first stage of analysis: homogenisation of the actual grid structure and calculation of stress resultants in the homogenised model.

In the next section the second stage of lattice structure analysis will be shown: the reverse calculation of stress components in the ribs of the actual grid from the "homogenised" stress components. In a general form, the algorithm for the analysis of lattice structures is shown in Figure 3.3

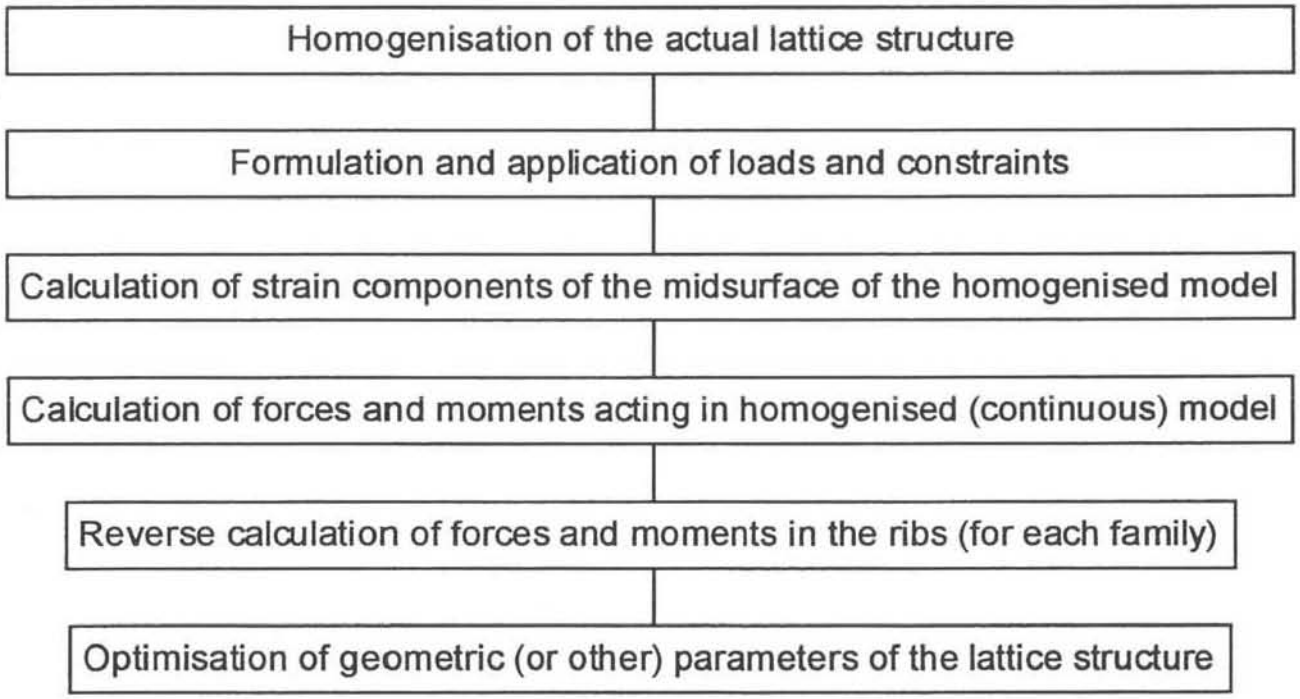

Figure 3.3 The algorithm for the analysis of lattice structures

3.4.1 Deformation of the Ribs in a Lattice Shell.

Assuming that the deformation of an axis of any particular rib is equal to the deformation of a line coincident with the axis of this rib and fix one (i-th, $1 \le i \le n$) of the presented n rib families in a shell. The orientation of a rib's axes on the median surface of a shell is characterised by the angle φ_i.

Using transformation formulae of the theory of elasticity for the components of a strain tensor [97] and also their linear distribution in the direction normal to the median surface, expressions for the deformations of an axis of a rib that belong to the i-th family of a grid shell can be derived as follows:

$$\begin{aligned} \varepsilon_i^* &= \varepsilon_1 c_i^2 + \varepsilon_2 s_i^2 + \omega s_i c_i, \\ \chi_i^* &= \chi_1 c_i^2 + \chi_2 s_i^2 + \tau \sin(2\varphi_i), \\ \tau_i^* &= (\chi_2 - \chi_1) s_i c_i + \tau \cos(2\varphi_i). \end{aligned} \tag{3.12}$$

Here the following notations have been used:

$$\begin{aligned} s_i &= \sin(\varphi_i), \\ c_i &= \cos(\varphi_i). \end{aligned} \tag{3.13}$$

The change in the curvature of a rib's axis in the plane tangential to the median surface of a shell can be calculated as:

$$\begin{aligned} \chi_i^0 &= -\nabla_i \psi_i, \\ \nabla_i &= \frac{c_i}{A}\frac{\partial}{\partial \alpha} + \frac{s_i}{B}\frac{\partial}{\partial \beta}. \end{aligned} \tag{3.14}$$

The value of ψ_i is calculated using (3.15) depending on the considered problem

$$\psi = 0.5(-2\delta + \omega \cos 2\varphi + (\varepsilon_2 - \varepsilon_1)\sin 2\varphi). \tag{3.15}$$

3.4.2 Forces and Moments Acting in the Ribs of a Grid Shell

Constitutive equations for the ribs in the lattice shell are developed in this subsection. Consider that one of the main central axes of rib's cross-section is coincident with the direction normal to the median surface of a shell.

Positive directions of forces and moments, acting in the cross-section of a rib that belong to i-th family are shown in Figure 3.4.

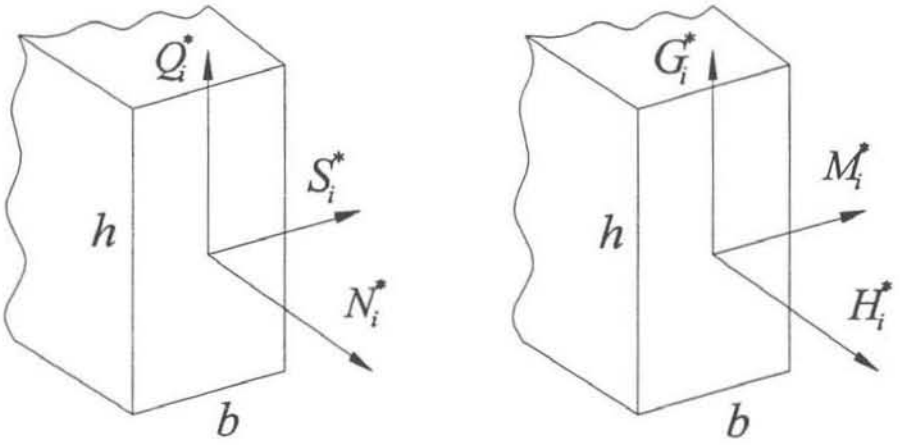

Figure 3.4 Positive directions of forces and moments in the cross-section of a rib

The relationship between the forces and moments and components of a strain tensor takes the following form:

$$\begin{aligned} N_i^* &= E_i F_i \varepsilon_i^*, & M_i^* &= -E_i J_{1i} \chi_i^*, & G_i^* &= -E_i J_{2i} \chi_i^0, \\ H_i^* &= G_i J_{3i} \tau_i^*, & Q_i^* &= -\nabla_i M_i^*, & S_i^* &= -\nabla_i G_i^*. \end{aligned} \tag{3.16}$$

Where F_i, J_{1i}, J_{2i}, J_{3i} are the area inertia of the cross-section, main central and torsional moment of inertia of the rib's cross-section respectively; E_i, G_i - the Young's and shear module of the ribs.

Formulae (3.16) allow the evaluation of the forces and moments acting in the ribs when the load is applied to the grid nodes. In the case of load application "out-of-

node" it is necessary to assess the deformation of a rib from the locally applied loads, distributed along the axes of the ribs.

3.4.3 Continuous Model.

A continuous model of a lattice shell is considered. A set of constitutive equations is developed for the equivalent homogenised model which allows the calculation of the stress resultants in the equivalent model from the strain components of its median surface.

3.4.3.1 Calculation of the Deformations from the Forces and Moments in the Ribs.

Let us assume that the forces N_i^*, Q_i^*, S_i^* and moments M_i^*, G_i^*, H_i^* (Figure 3.4) acting in the ribs are distributed continuously along the cross-section of the equivalent model.

Linear forces and moments (Figure 3.2) acting in the model of a shell that consists of n families of ribs are:

$$
\begin{aligned}
N_1 &= \sum_{i=1}^{n}\left(N_i^* c_i^2 - S_i^* c_i s_i\right)/a_i, & N_2 &= \sum_{i=1}^{n}\left(N_i^* s_i^2 + S_i^* c_i s_i\right)/a_i,\\
S_1 &= \sum_{i=1}^{n}\left(N_i^* c_i s_i + S_i^* c_i^2\right)/a_i, & S_2 &= \sum_{i=1}^{n}\left(N_i^* c_i s_i + S_i^* s_i^2\right)/a_i,\\
Q_1 &= \sum_{i=1}^{n} Q_i^* c_i / a_i, & Q_2 &= \sum_{i=1}^{n} Q_i^* s_i / a_i,\\
M_1 &= \sum_{i=1}^{n}\left(M_i^* c_i^2 + H_i^* c_i s_i\right)/a_i, & M_2 &= \sum_{i=1}^{n}\left(M_i^* s_i^2 - H_i^* c_i s_i\right)/a_i,\\
H_1 &= -\sum_{i=1}^{n}\left(M_i^* c_i s_i + H_i^* c_i^2\right)/a_i, & H_2 &= -\sum_{i=1}^{n}\left(M_i^* c_i s_i + H_i^* s_i\right)/a_i,\\
M_{1s} &= \sum_{i=1}^{n} G_i^* c_i / a_i, & M_{2s} &= -\sum_{i=1}^{n} G_i^* s_i / a_i,
\end{aligned}
\qquad (3.17)
$$

where a_i is spacing between the ribs that belong to the i-th family.

3.4.3.2 Constitutive Equations of Continuous Model

- *General case.*

Substituting (3.16) into (3.17), and taking into consideration (3.12), the following constitutive equations for a model of a grid shell can be obtained:

$$
\begin{aligned}
N_1 &= C_{11}\varepsilon_1 + C_{12}\varepsilon_2 + C_{16}\omega - \sum_{i=1}^{n} s_i\, c_i\, \chi_i', \\
N_2 &= C_{21}\varepsilon_1 + C_{22}\varepsilon_2 + C_{26}\omega + \sum_{i=1}^{n} s_i\, c_i\, \chi_i', \\
S_1 &= C_{61}\varepsilon_1 + C_{62}\varepsilon_2 + C_{66}\omega + \sum_{i=1}^{n} c_i^2\, \chi_i', \\
S_2 &= C_{61}\varepsilon_1 + C_{62}\varepsilon_2 + C_{66}\omega - \sum_{i=1}^{n} s_i^2\, \chi_i',
\end{aligned}
\tag{3.18}
$$

$$
\begin{aligned}
M_1 &= -\left[(D_{11}+K_{11})\chi_1 + (D_{12}+K_{12})\chi_2 + (2D_{16}+K_{16})\tau\right], \\
M_2 &= -\left[(D_{21}+K_{21})\chi_1 + (D_{22}+K_{22})\chi_2 + (2D_{26}+K_{26})\tau\right], \\
H_1 &= \left(D_{61}+K_{61}^{(1)}\right)\chi_1 + \left(D_{62}+K_{62}^{(1)}\right)\chi_2 + \left(2D_{66}+K_{66}^{(1)}\right)\tau, \\
H_2 &= \left(D_{61}+K_{61}^{(2)}\right)\chi_1 + \left(D_{62}+K_{62}^{(2)}\right)\chi_2 + \left(2D_{66}+K_{66}^{(2)}\right)\tau, \\
M_{1s} &= -\sum_{i=1}^{n} I_i^0 c_i\, \chi_i^0, \qquad M_{2s} = -\sum_{i=1}^{n} I_i^0 s_i\, \chi_i^0.
\end{aligned}
\tag{3.19}
$$

The following notations are used above:

$$
\begin{aligned}
&C_{11} = \sum_{i=1}^{n} K_i c_i^4, && C_{12} = C_{66} = \sum_{i=1}^{n} K_i s_i^2 c_i^2, && C_{16} = \sum_{i=1}^{n} K_i s_i\, c_i^3, \\
&C_{22} = \sum_{i=1}^{n} K_i s_i^4, && C_{26} = \sum_{i=1}^{n} K_i s_i^3 c_i, && C_{ij} = C_{ji}, \\
&D_{11} = \sum_{i=1}^{n} I_i c_i^4, && D_{12} = \frac{D_{66}}{2} = \sum_{i=1}^{n} I_i s_i^2 c_i^2, && D_{16} = \sum_{i=1}^{n} I_i s_i\, c_i^3, \\
&D_{22} = \sum_{i=1}^{n} I_i s_i^4, && D_{26} = \sum_{i=1}^{n} I_i s_i^3 c_i, && D_{ij} = D_{ji}.
\end{aligned}
\tag{3.20}
$$

$$
\begin{aligned}
&K_{11} = K_{22} = K_{12} = K_{21} = \sum_{i=1}^{n} C_i s_i^2 c_i^2, && K_{66}^{(1)} = \sum_{i=1}^{n} C_i c_i^2 \cos 2\varphi_i, \\
&K_{16} = K_{26} = \sum_{i=1}^{n} C_i s_i\, c_i \cos 2\varphi_i, && K_{61}^{(2)} = K_{62}^{(2)} = \sum_{i=1}^{n} C_i s_i^3 c_i, \\
&K_{61}^{(1)} = K_{62}^{(1)} = \sum_{i=1}^{n} C_i s_i\, c_i^3, && K_{66}^{(2)} = \sum_{i=1}^{n} C_i s_i^2 \cos 2\varphi_i, \\
&I_i^0 = \frac{E_i J_{2i}}{a_i}, && \chi_i' = \frac{\nabla_i \left(E_i J_{2i} \chi_i^0\right)}{a_i}, \\
&K_{16} = K_{61}^{(1)} - K_{61}^{(2)}.
\end{aligned}
\tag{3.21}
$$

Where

$$K_i = \frac{E_i F_i}{a_i}, \quad I_i = \frac{E_i J_{1i}}{a_i}, \quad C_i = \frac{G_i J_{3i}}{a_i}. \tag{3.22}$$

Parameters K_i, I_i, I_i^0, C_i show the relationship between the corresponding stiffness characteristics of the ribs and the distance between their axes.

In contrast to the conventional continuous shell in the case when $J_{2i} \neq 0$ additional bending moments M_{1s} and M_{2s} acting in the plane tangential to the median surface (Figure 3.2) must also be taken into account.

3.4.3.3 Some Particular Cases

In this subsection some particular cases are considered. Constitutive equations are derived for some of the most common patterns of a lattice.

In practical calculations we can assume $J_{2i} = 0$ provided it does not turn the model into an imperfect frame. There is a similarity with the analysis of a frame where the rigid joints of its members are assumed to be hinges. Bending stresses of the ribs acting in the plane tangential to the median surface are found using deformations of the median surface. In further calculations the value of J_{2i} is assumed to be equal to zero. This assumption essentially simplifies some of the constitutive equations (3.18). Tangential forces in this case are:

$$\begin{aligned} N_1 &= C_{11}\varepsilon_1 + C_{12}\varepsilon_2 + C_{16}\omega, \\ N_2 &= C_{21}\varepsilon_1 + C_{22}\varepsilon_2 + C_{26}\omega, \\ S &= C_{61}\varepsilon_1 + C_{62}\varepsilon_2 + C_{66}\omega. \end{aligned} \tag{3.23}$$

The last equation in (3.18) also shows that

$$M_{1s} = M_{2s} = 0. \tag{3.24}$$

Now constitutive equations for homogenised model will be written for several particular cases of the grid arrangement. The above mentioned assumption $J_{2i} = 0$ is used in each of the considered cases.

1. The torsion stiffness of the ribs equals zero ($J_{3i} = 0$). The constitutive equations take the following form:

$$
\begin{aligned}
N_1 &= C_{11}\varepsilon_1 + C_{12}\varepsilon_2 + C_{16}\omega, \\
N_2 &= C_{21}\varepsilon_1 + C_{22}\varepsilon_2 + C_{26}\omega, \\
S &= C_{16}\varepsilon_1 + C_{26}\varepsilon_2 + C_{66}\omega, \\
H &= D_{16}\varepsilon_1 + D_{26}\varepsilon_2 + D_{66}\tau, \\
M_1 &= -\left(D_{11}\chi_1 + D_{12}\chi_2 + D_{16}\tau\right), \\
M_2 &= -\left(D_{12}\chi_1 + D_{22}\chi_2 + D_{26}\tau\right).
\end{aligned}
\tag{3.25}
$$

For a particular grid pattern equations (3.25) will be the same as the constitutive equation for anisotropic shells, the material of which has a plane of elastic symmetry parallel to the plane that is tangential to the median surface. If these constitutive equations also satisfy the following equality:

$$
C_{16} = C_{12} = D_{16} = D_{26} = 0, \tag{3.26}
$$

then they transform into constitutive equations for an orthotropic shell, where the co-ordinate axes α, β, and the normal to the median surface are the principal elasticity axes:

$$
\begin{aligned}
&N_1 = C_{11}\varepsilon_1 + C_{12}\varepsilon_2, && N_2 = C_{21}\varepsilon_1 + C_{22}\varepsilon_2, && S = C_{66}\omega, \\
&M_1 = -\left(D_{11}\chi_1 + D_{12}\chi_2\right), && M_2 = -\left(D_{21}\chi_1 + K_{22}\chi_2\right), && H = D_{66}\tau.
\end{aligned}
\tag{3.27}
$$

Let us consider some possible grid arrangements where conditions (3.27) are satisfied. In this case it is enough to consider only the first two of these conditions because the last two may be obtained from the first, substituting K_i with I_i according to (3.20) and (3.21).

If the number of families of ribs, n, is two (orthogrid and anglegrid, see Figure 3.5) there are only two possible cases:

1. $\varphi_2 = -\varphi_1$, $K_2 = K_1$ (((3.22) because $a_2 = a_1$ for this geometry) (Figure 3.5(a))

2. $\varphi_1 = 0$, $\varphi_2 = \frac{\pi}{2}$, K_1, K_2 are arbitrary (Figure 3.5 (b))

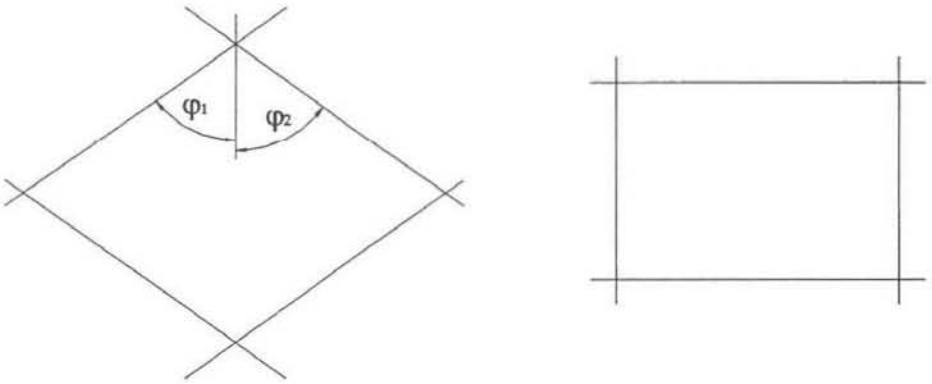

Figure 3.5 Isogrid and orthogrid unit cells

For $n=3$ (Isogrid), the constitutive equations (3.27) can be used for the following grid patterns: $\varphi_2=-\varphi_1$, $K_2=K_1$, $\varphi_3=0$ or $\varphi_3=\frac{\pi}{2}$ for any value of K_3;

$$K_1=\frac{\sin 2\varphi_3 \sin(\varphi_3-\varphi_2)\sin(\varphi_3+\varphi_2)}{\sin 2\varphi_1 \sin(\varphi_2-\varphi_1)\sin(\varphi_2+\varphi_1)}K_3,$$
$$K_2=\frac{\sin 2\varphi_3 \sin(\varphi_1-\varphi_3)\sin(\varphi_1+\varphi_3)}{\sin 2\varphi_2 \sin(\varphi_2-\varphi_1)\sin(\varphi_2+\varphi_1)}K_3. \tag{3.28}$$

The range of values for φ_i is determined by the condition $K_i>0$.

3. The grid pattern is rhombic $(n=2)$ (Figure 3.5). Ribs that belong to each family are assumed to be the same and we have $a_1=a_2=a$, $\varphi_1=\varphi_2=\varphi$, $K_1=K_2=K$.

For the considered rhombic grid pattern, the constitutive equations can be written as:

$$
\begin{aligned}
N_1 &= N_2 ctg^2\varphi = 2Kc^2\left(c^2\varepsilon_1 + s^2\varepsilon_2\right),\\
M_1 &= -2c^2\left(\left(Ic^2 + Cs^2\right)\chi_1 + (I-C)s^2\chi_2\right),\\
M_2 &= -2s^2\left((I+C)c^2\chi_1 + \left(Is^2 - Cc^2\right)\chi_2\right),\\
H_1 &= 2c^2\left(2Is^2 + C\cos 2\varphi\right)\tau,\\
H_2 &= 2s^2\left(2Ic^2 - C\cos 2\varphi\right)\tau,\\
S &= 2Ks^2c^2\omega.
\end{aligned}
\tag{3.29}
$$

It can be seen that forces N_1 and N_2 are linked. A similar link will occur between bending moments M_1 and M_2 when the torsion stiffness is equal to zero. This shows the significant difference of these equations in comparison with those used in the conventional solid shell theory [59].

4. A grid pattern consisting of four families of ribs $(n=4)$ (Figure 1.4). Ribs comprising families 1 and 2 are assumed to be the same:

$$
a_1 = a_2 = a, \qquad \varphi_1 = -\varphi_2 = \varphi, \qquad K_1 = K_2 = K. \tag{3.30}
$$

Using the relations for rib spacing $a = 2a_3 s = 2a_4 c$ the constitutive equations are given as:

$$
\begin{aligned}
&N_1 = C_{11}\varepsilon_1 + C_{12}\varepsilon_2, \quad N_2 = C_{21}\varepsilon_1 + C_{22}\varepsilon_2, && H_1 = \beta_{31}\tau, \quad S = C_{66}\omega,\\
&M_1 = \beta_{11}\chi_1 + \beta_{12}\chi_2, \quad M_2 = \beta_{12}\chi_1 + \beta_{22}\chi_2, && H_2 = \beta_{41}\tau.
\end{aligned}
\tag{3.31}
$$

where:

$$
\begin{aligned}
C_{11} &= 2Kc^4 + K_4,\\
C_{12} &= C_{66} = 2Ks^2c^2,\\
C_{22} &= 2Ks^4 + K_3,\\
\beta_{11} &= -\left(2Ic^4 + I_4 + 2Cs^2c^2\right),\\
\beta_{12} &= -2s^2c^2(I-C),\\
\beta_{22} &= -\left(2Is^4 + I_3 + 2Cs^2c^2\right),\\
\beta_{31} &= I\sin^2 2\varphi + 2Cc^2\cos 2\varphi + C_4,\\
\beta_{41} &= I\sin^2 2\varphi - 2Cs^2\cos 2\varphi + C_3.
\end{aligned}
\tag{3.32}
$$

3.5 Calculation of the Deformations and Forces in the Ribs from the Forces and Moments in Homogenised Model

The constitutive equations that were obtained above represent forces and moments acting in the homogenised model of a grid shell as functions of the strain components of its median surface. In this section the question of finding the reverse dependencies (strain components as functions of acting forces and moments) is considered.

In this section the deformations, forces and moments acting on the ribs are calculated for lattice structures with:

- two families of ribs
- more than two families of ribs.

The solutions are derived for the cases of statically determinate and statically indeterminate lattice shells.

3.5.1 Tangential Strain Components

Let us consider the tangential strain components ε_1, ε_2, ω in the equations of equilibrium (3.23) as unknowns. The determinant of this system of algebraic equations is:

$$D=\sum_{i,j,k=1}^{n} K_i K_j K_k \left(c_i^4 s_j^2 c_j^2 s_k^4 + 2 s_i^2 c_i^2 s_j c_j^3 s_k^3 c_k - c_i^4 s_j^3 c_j s_k^3 c_k - s_i^2 c_i^2 s_j^2 c_j^2 s_k^2 c_k^2 - s_i c_i^3 s_j c_j^3 s_k^4\right). \quad (3.33)$$

In order to simplify the expression, let us fix three arbitrary integer numbers μ, m, ν. Each of these numbers is greater than zero and smaller than $n+1$. According to further permutations of these numbers, the indices in equation (3.33) change their value in the following way:

$$\begin{aligned} &i=\mu,\ j=m,\ k=\nu;\ i=\mu,\ j=\nu,\ k=m;\\ &i=m,\ j=\mu,\ k=\nu;\ i=m,\ j=\nu,\ k=\mu;\\ &i=\nu,\ j=\mu,\ k=m;\ i=\nu,\ j=m,\ k=\mu. \end{aligned} \quad (3.34)$$

The final sum of all six members mentioned above, after certain trigonometric transformations, is:

$$\frac{1}{16}K_\mu K_m K_\nu\left[\sin 2(\varphi_\nu-\varphi_\mu)+\sin 2(\varphi_\mu-\varphi_m)+\sin 2(\varphi_m-\varphi_\nu)\right]^2. \qquad (3.35)$$

Consequently (3.33) will be:

$$D=\frac{1}{16}\sum_{\mu,m,\nu=1}^{n}{}' K_\mu K_m K_\nu\left[\sin 2(\varphi_\nu-\varphi_\mu)+\sin 2(\varphi_\mu-\varphi_m)+\sin 2(\varphi_m-\varphi_\nu)\right]^2. \qquad (3.36)$$

A prime next to the sum symbol means that there is only one member that corresponds to each sequence of indices μ, m, ν (the total number of these indices is six).

The value of the considered determinant does not depend on the choice of the co-ordinate axis of the median surface because (3.36) includes only the differences in angles.

3.5.1.1 The Number of Families of Ribs Is More Than Two

For all indices that satisfy the condition:

$$\mu\neq m, \qquad \mu\neq\nu, \qquad m\neq\nu, \qquad (3.37)$$

the expression (3.36) in the square brackets is non zero. Consequently, $D>0$ for $n>2$, because the number of combinations of indices μ, m, ν, which satisfy the conditions in (3.37), in this case $n(n-1)(n-2)/6$, and the system of algebraic equations (3.23) for unknowns ε_1, ε_2, ω always has a unique solution ($D>0$). This result is unique because for $n>2$ families a grid shell consists of the system of ribs, which is stiff in the plane tangential to the median surface: the system of homogeneous equations (3.21) should have only a trivial solution.

The solution of this system is:

$$\begin{aligned}\varepsilon_1&=a_{11}N_1+a_{12}N_2+a_{13}S,\\ \varepsilon_2&=a_{21}N_1+a_{22}N_2+a_{23}S,\\ \omega&=a_{31}N_1+a_{32}N_2+a_{33}S,\end{aligned} \qquad (3.38)$$

where:

$$
\begin{aligned}
a_{11} &= \frac{1}{2D}\sum_{i,j=1}^{n} K_i K_j s_i^2 s_j^2 \sin^2(\varphi_i - \varphi_j),\\
a_{12} &= \frac{1}{2D}\sum_{i,j=1}^{n} K_i K_j s_i c_i s_j c_j \sin^2(\varphi_i - \varphi_j),\\
a_{13} &= -\frac{1}{2D}\sum_{i,j=1}^{n} K_i K_j s_i s_j \sin(\varphi_i + \varphi_j)\sin^2(\varphi_i - \varphi_j),\\
a_{22} &= \frac{1}{2D}\sum_{i,j=1}^{n} K_i K_j c_i^2 c_j^2 \sin^2(\varphi_i - \varphi_j),\\
a_{23} &= -\frac{1}{2D}\sum_{i,j=1}^{n} K_i K_j c_i c_j \sin(\varphi_i + \varphi_j)\sin^2(\varphi_i - \varphi_j),\\
a_{33} &= \frac{1}{2D}\sum_{i,j=1}^{n} K_i K_j c_i c_j \sin^2(\varphi_i + \varphi_j)\sin^2(\varphi_i - \varphi_j),\\
a_{ij} &= a_{ji}.
\end{aligned}
\tag{3.39}
$$

3.5.1.2 The Number of Families of Ribs is Two

Formula (3.36) shows that if at least one of three conditions: $\mu = m$, $\mu = \nu$, $\mu = \nu$, is satisfied, then the corresponding sum equals zero. Therefore $D = 0$ for $n = 2$, since the combination of indices (3.37) in this case is excluded. Consequently, the system of equations (3.23) for $N_1 = N_2 = S = 0$ has also a nontrivial solution. That means that the model is not fully constrained and represents an imperfect frame.

In the considered case the tangential forces N_1, N_2, S are related in the following way:

$$
N_1 s_1 s_2 + N_2 c_1 c_2 - S\sin(\varphi_1 + \varphi_2) = 0, \tag{3.40}
$$

which represents the condition of compatibility for the inhomogeneous system of equations (3.23) for ε_1, ε_2, ω.

If $\varphi_1 + \varphi_2 \neq 0$, then the solution of this system of equations is

$$
\begin{aligned}
\varepsilon_1 &= -\frac{s_1 s_2}{\sin(\varphi_1 - \varphi_2)}\omega + \frac{C_{22}N_1 - C_{12}N_2}{K_1 K_2 \sin^2(\varphi_1 + \varphi_2)\sin^2(\varphi_1 - \varphi_2)},\\
\varepsilon_2 &= -\frac{c_1 c_2}{\sin(\varphi_1 + \varphi_2)}\omega + \frac{C_{11}N_2 - C_{12}N_1}{K_1 K_2 \sin^2(\varphi_1 + \varphi_2)\sin^2(\varphi_1 - \varphi_2)},
\end{aligned}
\tag{3.41}
$$

where ω has an arbitrary value.

The condition $\varphi_1 + \varphi_2 = 0$ results in $(\varphi_1 = -\varphi_2)$:

$$\varepsilon_1 = -\varepsilon_2 tg^2\varphi + \frac{C_{66}N_1 - C_{16}S}{K_1K_2c^4\sin^2 2\varphi}, \qquad \omega = \frac{C_{11}S - C_{16}N_1}{K_1K_2c^4\sin^2 2\varphi}. \tag{3.42}$$

Here ε_2 is arbitrary.

This leads to the conclusion that this model of a grid shell is unconstrained on its sides and therefore will represent an imperfect frame since its median surface can deform without any applied load.

3.5.2 Calculation of the Bending Components of a Strain Tensor

Let us derive bending components χ_1, χ_2, τ of a strain tensor from the following system of equations:

$$\begin{aligned}
M_1 &= -\left[(D_{11} + K_{11})\chi_1 + (D_{12} + K_{12})\chi_2 + (2D_{16} + K_{16})\tau\right],\\
M_2 &= -\left[(D_{21} + K_{21})\chi_1 + (D_{22} + K_{22})\chi_2 + (2D_{26} + K_{66})\tau\right],\\
H_1 &= \left(D_{61} + K_{61}^{(1)}\right)\chi_1 + \left(D_{62} + K_{62}^{(1)}\right)\chi_2 + \left(2D_{66} + K_{66}^{(1)}\right)\tau,\\
H_2 &= \left(D_{61} + K_{61}^{(2)}\right)\chi_1 + \left(D_{62} + K_{62}^{(2)}\right)\chi_2 + \left(2D_{66} + K_{66}^{(2)}\right)\tau,
\end{aligned} \tag{3.43}$$

which represents a part of the equations (3.19).

When $E_iJ_{1i} >> G_iJ_{3i}$ the torsional stiffness of ribs need not be taken into consideration if this assumption does not lead to the transformation of an analysis model into an imperfect frame (geometrically unstable model). Then the torque moments acting in the ribs of a grid shell are found from

$$H_i^* = G_iJ_{3i}\tau_i^*, \tag{3.44}$$

where the values of τ_i^* are calculated using equations (3.12).

Considering $J_{3i} = 0$ from (3.43) we obtain:

$$\begin{aligned}
M_1 &= -(D_{11}\chi_1 + D_{12}\chi_2 + 2D_{16}\tau),\\
M_2 &= -(D_{21}\chi_1 + D_{22}\chi_2 + 2D_{26}\tau),\\
H &= D_{61}\chi_1 + D_{62}\chi_2 + 2D_{66}\tau.\\
H &= H_1 = H_2.
\end{aligned} \tag{3.45}$$

Comparing systems of equations (3.23) (for ε_1, ε_2, ω) to (3.45) (for χ_1, χ_2, τ) we can conclude that one may be transformed into the other when substituting

$$\varepsilon_1, \varepsilon_2, \omega, N_1, N_2, S, F_i \tag{3.46}$$

for

$$\chi_1, \chi_2, 2\tau, -M_1, -M_2, H, J_{1i}. \tag{3.47}$$

It is also true for the system of equations (3.45), and in particular equations (3.36) (3.38) remain true (for arbitrary n), (3.40) (for $n>2$), (3.40) and (3.42) (for $n=2$) when substituting (3.46) with (3.47).

In the case when torsional stiffness of ribs can not be neglected $(J_{3i} \neq 0)$, parameters χ_1, χ_2, τ are calculated from the system of equations (3.43).

The system of equations (3.43) has only a trivial solution for $M_1 = M_2 = H_1 = H_2 = 0$. Bending and torque moments are related so that system (3.43) has a unique solution.

3.5.3 Forces and Moments Acting in the Ribs of a Cylindrical Shell

3.5.3.1 Statically Determinate Cases

If the reverse dependencies of (3.17) are single-valued, then they can be used for the calculation of forces and moments in the ribs of a grid shell from known strain-stress distributions (for statically determinate cases). Lets consider some of these cases.

For the grid pattern that has three families of ribs $(n=3)$, the solution of the first three equations from (3.17) is:

$$\begin{aligned} DN_1^* &= \left[N_1 s_2 s_3 \sin(\varphi_3 - \varphi_2) + N_2 c_2 c_3 \sin(\varphi_3 - \varphi_2) + S(c_3^2 - c_2^2)\right]\alpha_1, \\ DN_2^* &= \left[N_1 s_1 s_3 \sin(\varphi_1 - \varphi_3) + N_2 c_1 c_3 \sin(\varphi_1 - \varphi_3) + S(c_1^2 - c_3^2)\right]\alpha_2, \\ DN_3^* &= \left[N_1 s_1 s_2 \sin(\varphi_2 - \varphi_1) + N_2 c_1 c_2 \sin(\varphi_2 - \varphi_1) + S(c_2^2 - c_1^2)\right]\alpha_3, \end{aligned} \tag{3.48}$$

where $S_1 = S_2 = S$ because $S_i^* = 0$ and

$$D = c_1 c_2 \sin(\varphi_2 + \varphi_1) + c_1 c_3 \sin(\varphi_1 - \varphi_3) + c_2 c_3 \sin(\varphi_3 - \varphi_2). \tag{3.49}$$

In this case the value of D is not equal to zero if the axes of ribs which belong to the same family do not have a common tangent with the axes that belong to the different families. When subjected to the following conditions:

$$\varphi = \varphi_1 = -\varphi_2,\ a = a_1 = a_2, \tag{3.50}$$

these formulae simplify to:

$$\begin{aligned} D_0 N_1^* &= \left[-N_1 s s_3 \sin(\varphi+\varphi_3) + N_2 c c_3 \sin(\varphi-\varphi_3) + S\left(c_3^2 - c^2\right)\right]a, \\ D_0 N_2^* &= \left[N_1 s s_3 \sin(\varphi-\varphi_3) + N_2 c c_3 \sin(\varphi-\varphi_3) + S\left(c^2 - c_3^2\right)\right]a, \\ N_3^* &= a_3\left(N_1 s^2 - N_2 c^2\right)\left(c_3^2 - c^2\right)^{-1}, \end{aligned} \tag{3.51}$$

where

$$D_0 = \left(c_3^2 - c^2\right)\sin 2\varphi. \tag{3.52}$$

It follows from the equations (3.17), formulae for the bending moments can be obtained from (3.51) by substituting N_1^*, N_j, S with $M_1^*, M_j, -H$, respectively for $(i = 1, 2, 3;\ j = 1, 2)$. Torsional stiffness of the ribs in this case is neglected. After the substitution we have:

$$\begin{aligned} D_0 M_1^* &= \left[-M_1 s s_3 \sin(\varphi+\varphi_3) + M_2 c c_3 \sin(\varphi-\varphi_3) + H\left(c_3^2 - c^2\right)\right]a, \\ D_0 M_2^* &= \left[M_1 s s_3 \sin(\varphi-\varphi_3) + M_2 c c_3 \sin(\varphi-\varphi_3) + H\left(c^2 - c_3^2\right)\right]a, \\ M_3^* &= a_3\left(M_1 s^2 - M_2 c^2\right)\left(c_3^2 - c^2\right)^{-1}. \end{aligned} \tag{3.53}$$

Let us consider the case when $n = 2$, and all stiffness characteristics of the ribs (including J_{2i}) are non zero. Then the number of unknowns in the equations for unknown forces and moments acting in the ribs of a grid are equal to the number of equations for each of the separate systems appearing in (3.17).

Solutions for these systems can be written as:

$$
\begin{aligned}
N_1^* &= a_1(c_1 s_2 N_1 - s_1 c_2 N_2 - s_1 s_2 S_1 - c_1 c_2 S_2)\sin^{-1}(\varphi_2 - \varphi_1),\\
N_2^* &= a_2(s_1 c_2 N_1 - c_1 s_2 N_2 - s_1 s_2 S_1 - c_1 c_2 S_2)\sin^{-1}(\varphi_1 - \varphi_2),\\
S_1^* &= a_1(s_1 s_2 N_1 - c_1 c_2 N_2 - c_1 s_2 S_1 - s_1 c_2 S_2)\sin^{-1}(\varphi_1 - \varphi_2),\\
S_2^* &= a_2(s_1 s_2 N_1 - c_1 c_2 N_2 - s_1 c_2 S_1 - c_1 s_2 S_2)\sin^{-1}(\varphi_2 - \varphi_1),\\
G_1^* &= \frac{(s_2 M_{1s} + c_2 M_{2s})a_1}{\sin(\varphi_2 - \varphi_1)}, \qquad G_2^* = \frac{(s_1 M_{1s} + c_1 M_{2s})a_2}{\sin(\varphi_1 - \varphi_2)},\\
Q_1^* &= \frac{(s_2 Q_1 + c_2 Q_2)a_1}{\sin(\varphi_2 - \varphi_1)}, \qquad Q_2^* = \frac{(s_1 Q_1 + c_1 Q_2)a_2}{\sin(\varphi_1 - \varphi_2)}.
\end{aligned}
\tag{3.54}
$$

If consider $\varphi = \varphi_1 = -\varphi_2$, $a = a_1 = a_2$ these formulae transform into:

$$
\begin{aligned}
N_{1,2}^* &= 0.5a\left[N_1 + N_2 \pm (S_1 \operatorname{tg}\varphi + S_2 \operatorname{ctg}\varphi)\right],\\
S_{1,2}^* &= 0.5a\left[S_1 + S_2 \mp (N_1 \operatorname{tg}\varphi + N_2 \operatorname{ctg}\varphi)\right],\\
Q_{1,2}^* &= 0.5a\left(Q_1 c^{-1} \pm Q_2 s^{-1}\right),\\
G_{1,2}^* &= 0.5a\left(M_{1s} c^{-1} \pm M_{2s} s^{-1}\right).
\end{aligned}
\tag{3.55}
$$

On the basis of (3.17) the conclusion can be made that the formulae for bending and twist moments acting on the ribs of a considered grid can be obtained from (3.55), when the strain-stress distribution is known and N_i^*, S_i^*, N_i, S_i are replaced by $M_i^*, -H_i^*, M_i, -H_i$ $(i = 1, 2)$ respectively. Then we can write:

$$
\begin{aligned}
M_{1,2}^* &= 0.5a\left[M_1 + M_2 \mp (H_1 \operatorname{tg}\varphi + H_2 \operatorname{ctg}\varphi)\right],\\
H_{1,2}^* &= 0.5a\left[H_1 + H_2 \pm (M_1 \operatorname{tg}\varphi + M_2 \operatorname{ctg}\varphi)\right].
\end{aligned}
\tag{3.56}
$$

For the case of a grid pattern that consists of two families of ribs, and assuming that $J_{2i} = 0\ (S_i^* = 0)$, the linear loads of a model N_1, N_2, S are related through (3.40). This relationship represents the compatibility conditions for the first three equations of (3.17) that have two unknown forces in ribs N_1^* and N_2^*. Solution of these equations for $\varphi_1 + \varphi_2 \neq 0$ is:

$$
N_1^* = \frac{(N_1 s_2^2 - N_2 c_2^2)a_1}{c_1^2 - c_2^2}, \qquad N_2^* = \frac{(N_1 s_1^2 - N_2 c_1^2)a_2}{c_2^2 - c_1^2}. \tag{3.57}
$$

When $\varphi_1 + \varphi_2 = 0$ we have $(\varphi_1 = -\varphi_2)$ and

$$N_1^* = \left(\frac{N_1}{c} + \frac{S}{s}\right)\frac{a_1}{2c}, \qquad N_2^* = \left(\frac{N_1}{c} + \frac{S}{s}\right)\frac{a_2}{2c}. \tag{3.58}$$

If the torsional stiffness of the ribs are neglected $(J_{3i} = 0)$, then $H_i^* = 0$. The formulae for the bending moments in the ribs of a shell are obtained from (3.57), (3.58) after replacing N_i^*, N_i, S with $M_i^*, M_i, -H$ $(i = 1, 2)$. This leads to the following formulae for the bending moments:

$$M_1^* = \frac{\left(M_1 s_2^2 - M_2 c_2^2\right)a_1}{c_1^2 - c_2^2}, \qquad M_2^* = \frac{\left(M_1 s_1^2 - M_2 c_1^2\right)a_2}{c_2^2 - c_1^2} \tag{3.59}$$

for the case when $\varphi_1 + \varphi_2 \neq 0$ and

$$M_1^* = \left(\frac{M_1}{c} + \frac{H}{s}\right)\frac{a_1}{2c}, \qquad M_2^* = \left(\frac{M_1}{c} + \frac{H}{s}\right)\frac{a_2}{2c} \tag{3.60}$$

for the case $\varphi = \varphi_1 = -\varphi_2$.

3.5.3.2 Statically Indeterminate Cases

If a grid pattern of a shell is such that the number of equations (3.17) is less than the number of unknowns, we are faced with the statically indeterminate problem for calculation of unknown forces and moments in the ribs from the known stress-strain distribution in the shell.

Nevertheless, this problem can be solved relatively easily: first the strain components of a median surface can be obtained from a given stress distribution in the model (3.33), (3.35); and then formulae (3.12) and (3.16) can be incorporated.

We now calculate the forces and moments acting on the ribs of a grid (Figure 3.4) for a known stress distribution. Ribs of the first two families $(i = 1, 2)$ are considered to be the same. Index i $(i = 1)$ is skipped for all notations which correspond to the first family of ribs excluding those for the forces and moments.

Constitutive equations for the considered grid pattern are given by (3.17).

Equations for tangential strain components can be found after applying relations (3.38) as:

$$
\begin{aligned}
D\varepsilon_1 &= \left[2N_1\left(2Ks^4 + K_3\right) - KN_2 \sin^2 2\varphi\right]Ks^2c^2, \\
D\varepsilon_2 &= \left[-KN_1 \sin^2 2\varphi + 2N_2\left(2Kc^4 + K_4\right)\right]Ks^2c^2, \\
D\omega &= \left(2KK_3c^4 + 2KK_4s^4 + K_3K_4\right)S,
\end{aligned} \tag{3.61}
$$

where according to (3.35)

$$
D = \left[\left(K_3c^4 + K_4s^4\right)K + K_3K_4/2\right]K \sin^2 2\varphi. \tag{3.62}
$$

Now formulae (3.12) and (3.16) allow the unknown axial forces in the ribs to be found for any of the four families:

$$
\begin{aligned}
N_{1,2}^{*} &= \left[\left(K_3N_1c^2 + K_4N_2s^2\right)K^0 \pm SK(\sin 2\varphi)^{-1}\right] EF, \\
N_3^{*} &= \left[\left(2Kc^4 + K_4\right)N_2 - 2KN_1s^2c^2\right]K^0E_3F_3, \\
N_4^{*} &= \left[\left(2Ks^4 + K_3\right)N_1 - 2KN_2s^2c^2\right]K^0E_4F_4,
\end{aligned} \tag{3.63}
$$

where

$$
K^0 = \left[2K\left(K_3c^4 + K_4s^4\right) + K_3K_4\right]^{-1}. \tag{3.64}
$$

The sign before the second summand in the expression for $N_{1,2}^{*}$ is negative for the second family and positive for the first family.

The expressions for the bending and twisting moments of the median surface of a shell are found by expressing the components of bending deformation χ_1, χ_2, τ in terms of distributed moments M_1, M_2, H_1, using constitutive equations (3.18). Then after applying (3.12) and (3.16), the final expressions for bending and twisting moments of the median surface are found as:

$$
\begin{aligned}
M_{1,2}^{*} &= \{\left[\left(I_3c^3 + 2Cs^2c^2\right)M_1 + \left(I_4s^2 + 2Cs^2c^2\right)M_2\right]I_0 \mp \\
&\mp H_1\left(I \sin 2\varphi + 2Cc^2 \operatorname{ctg} 2\varphi + C_4 \sin^{-1} 2\varphi\right)^{-1}\}EJ_1, \\
M_3^{*} &= \left[\left(2Ic^4 + I_4 + 2Cs^2c^2\right)M_2 - 2M_1s^2c^2(I - C)\right]I_0E_3J_{13}, \\
M_4^{*} &= \left[\left(2Is^4 + I_3 + 2Cs^2c^2\right)M_1 - 2M_2s^2c^2(I - C)\right]I_0E_4J_{14}, \\
H_{1,2}^{*} &= \left\{\pm\left[\left(Is^2 + I_3\right)M_1 - \left(2Ic^2 + I_4\right)M_2\right]I_0 + 2H_1\beta_{31}^{-1} \cos 2\varphi\right\}GJ_3, \\
H_3^{*} &= -2G_3J_{33}H_1\beta_{31}^{-1}, \qquad H_4^{*} = -2G_4J_{34}H_1\beta_{31}^{-1},
\end{aligned} \tag{3.65}
$$

where

$$I_0 = \left[2I\left(I_3 c^4 + I_4 s^4\right) + I_3 I_4 + 2Cs^2 c^2\left(2I + I_3 + I_4\right)\right]^{-1}. \qquad (3.66)$$

The term β_{31} is calculated using (3.32).

3.6 Boundary Conditions

In this section the boundary conditions imposed on the considered structure are discussed.

If the stiffness of the members of a grid structure in the plane tangent to the median surface of a shell is neglected (3.67)

$$J_{2i} = 0, \qquad \left(i = \overline{1, n}\right), \tag{3.67}$$

then the order of the system of differential equations of the stress-strain state for both grid and solid shells are the same. In this case the boundary conditions are the same for the both shells.

When the stiffness of the ribs J_{2i} is not neglected, the order of the system of differential equations increases from the eighth to the twelfth order. In this case six boundary conditions are required to be specified instead of four. Consider the form of these two extra boundary conditions required for a grid shell in the case of non-zero bending stiffness of the ribs $\left(J_{2i} \neq 0\right)$. Practically there is only one case when the bending stiffness of the ribs in the plane tangential to a median surface should be taken into account. This is the case of a grid comprised of two families of ribs (n=2).

The additional boundary conditions are formulated along the contour of a shell, which is coincident with the co-ordinate line $\beta = \beta_0$.

The most typical boundary conditions are:

1. The members of a grid structure are joined along the contour of a shell by means of a hinged connection, which allows free rotation of the members of each family about the normal to the median surface of a shell (Figure 3.6a).

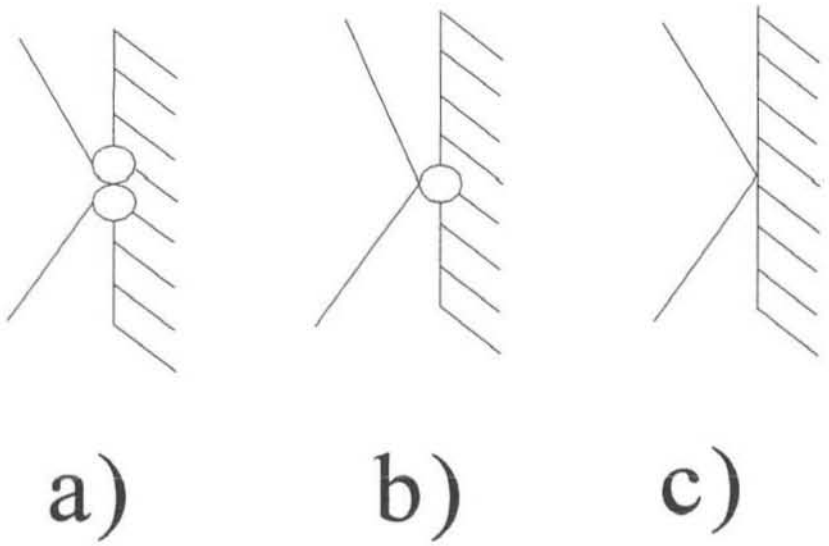

Figure 3.6 Types of a constraint contour

In this case, according to (3.20) and (3.21), the two additional boundary conditions along the contour $G_1^* = G_2^* = 0$ are:

$$M_{1s} = M_{2s} = 0 \qquad \text{for} \quad \beta = \beta_0. \tag{3.68}$$

2. The members of a grid structure are rigidly connected to each other (Figure 3.6b) along the contour of a shell: the rotational angles about the normal to the median surface of a shell of two adjacent members that belong to different families are equal. Additionally, the value of a linear bending moment in the plane tangential to the median surface of a shell is given.

In this case one of the two additional boundary conditions is:

$$M_{2s} = M_{2s}^0(\alpha) = 0 \qquad \text{for} \quad \beta = \beta_0, \tag{3.69}$$

where $M_{2s}^0(\alpha)$ is a given function.

The second additional boundary condition is obtained by equating the angles of rotation of two adjacent members about the normal to the median surface of a shell (3.15):

$$\omega(\cos 2\varphi_1 - \cos 2\varphi_2) + (\varepsilon_2 - \varepsilon_1)(\sin 2\varphi_1 - \sin 2\varphi_2) = 0. \tag{3.70}$$

3. The members of a grid structure are rigidly connected to each other along the contour of a shell. No rotation about the normal to the median surface of a shell is allowed (Figure 3.6c).

Two additional boundary conditions, according to (3.15), are:

$$-2\delta+\omega\cos 2\varphi_i+(\varepsilon_2-\varepsilon_1)\sin 2\varphi_i=0 \qquad \text{for} \qquad \beta=\beta_0. \tag{3.71}$$

For the case of $\varphi=\varphi_1=\varphi_2$, boundary conditions (3.70) and (3.71) become:

$$\varepsilon_2-\varepsilon_1=0 \qquad \text{for} \qquad \beta=\beta_0, \tag{3.72}$$

$$\varepsilon_2-\varepsilon_1=\omega\cos 2\varphi-2\delta=0 \qquad \text{for} \qquad \beta=\beta_0. \tag{3.73}$$

4. The members of a grid structure are rigidly connected to each other, but the connection with the contour of a shell is linear elastic with the respect to the angle about the normal to the median surface of a shell.

In this case one of the two additional boundary conditions must be taken in the form of (3.70) and the other as (3.74):

$$M_{2s}=k(\alpha)\psi_1=k(\alpha)\psi_2 \qquad \text{for} \qquad \beta=\beta_0, \tag{3.74}$$

where $k(\alpha)$ is a function of the rigidity of the elastic constraint, ψ_1 and ψ_2 are angles of rotation about the normal to a median surface of the axes of two adjacent members of two different families. These angles are found from the formulae (3.15) depending on the type of the considered boundary problem. In later formulae the members ψ and φ must be substituted with ψ_i and φ_i.

3.7 Analysis of the Lattice Plates

In this section the problem of a rectangular plate with rhombic and rectangular types of grid patterns is considered. The forces and moment resultants are calculated.

3.7.1 A Plate with the Number of Families of Ribs More than Two

Lets consider the median surface of a plate in the Cartesian co-ordinate system x, y. The differential equations of equilibrium in this case are given as:

$$\frac{\partial N_1}{\partial x}+\frac{\partial S}{\partial y}+X=0, \qquad \frac{\partial N_2}{\partial y}+\frac{\partial N_1}{\partial x}+Y=0. \tag{3.75}$$

The components of strain tensor in this case are given as:

$$\varepsilon_1=\frac{\partial u}{\partial x}, \qquad \varepsilon_2=\frac{\partial v}{\partial y}, \qquad \omega=\frac{\partial u}{\partial y}+\frac{\partial v}{\partial x}. \tag{3.76}$$

The constitutive equations (3.23) can be written in the following form:

$$N_1=\sum_{i=1}^{n}K_i c_i^2\nabla_i\left(c_i u+s_i v\right), \qquad N_2=\sum_{i=1}^{n}K_i s_i^2\nabla_i\left(c_i u+s_i v\right),$$
$$S=\sum_{i=1}^{n}K_i s_i c_i\nabla_i\left(c_i u+s_i v\right), \tag{3.77}$$

where the operator ∇_i denotes differentiation towards the tangent to the axis of a rib, which belongs to i-th family. This operator is given as:

$$\nabla_i=c_i\frac{\partial}{\partial x}+s_i\frac{\partial}{\partial y}. \tag{3.78}$$

The member $c_i u+s_i v$ represents the displacement of the point of the median surface in the direction of a tangent to the axis of a rib, which belongs to i-th family.

Incorporating the obtained constitutive equations and (3.75), the following system of differential equations is found in the displacement form:

$$L_{11}(u)+L_{12}(v)+X=0, \qquad L_{12}(u)+L_{22}(v)+Y=0, \tag{3.79}$$

where L_{ij} are linear differential operators:

$$L_{11} = C_{11}\frac{\partial^2}{\partial x^2} + 2C_{16}\frac{\partial^2}{\partial x \partial y} + C_{12}\frac{\partial^2}{\partial y^2} + C_1^0\frac{\partial}{\partial x} + C_3^0\frac{\partial}{\partial y},$$
$$L_{12} = C_{16}\frac{\partial^2}{\partial x^2} + 2C_{12}\frac{\partial^2}{\partial x \partial y} + C_{26}\frac{\partial^2}{\partial y^2} + C_3^0\frac{\partial}{\partial x} + C_2^0\frac{\partial}{\partial y}, \qquad (3.80)$$
$$L_{22} = C_{12}\frac{\partial^2}{\partial x^2} + 2C_{26}\frac{\partial^2}{\partial x \partial y} + C_{22}\frac{\partial^2}{\partial y^2} + C_2^0\frac{\partial}{\partial x} + C_4^0\frac{\partial}{\partial y}.$$

The notations used in (3.80) are given in (3.20) and (3.21), and the following additional notations are used:

$$C_1^0 = \frac{\partial C_{11}}{\partial x} + \frac{\partial C_{16}}{\partial y}, \qquad C_2^0 = \frac{\partial C_{12}}{\partial x} + \frac{\partial C_{26}}{\partial y},$$
$$C_3^0 = \frac{\partial C_{16}}{\partial x} + \frac{\partial C_{12}}{\partial y}, \qquad C_4^0 = \frac{\partial C_{26}}{\partial x} + \frac{\partial C_{22}}{\partial y}. \qquad (3.81)$$

If the geometric and material parameters are the same for all the families of ribs, the differential operators of the system of equations (3.79) can be simplified and are given as:

$$L_{11} = \sum_{i=1}^{n} K_i c_i^2 \nabla_i^2, \qquad L_{22} = \sum_{i=1}^{n} K_i s_i^2 \nabla_i^2, \qquad L_{22} = \sum_{i=1}^{n} K_i c_i s_i \nabla_i^2. \qquad (3.82)$$

Let us consider a grid plate which consists of three families of ribs. The grid parameters as well as the properties of the ribs are considered to be constant:

$$\varphi = \varphi_1 = -\varphi_2, \qquad \varphi_3 = 0, \qquad a = a_1 = a_2 = 2ca_3,$$
$$F = F_1 = F_2, \qquad E = E_1 = E_2 = E_3. \qquad (3.83)$$

This grid can be obtained from the one shown in Figure 1.4 (c) if the third family of ribs is absent. The subscript i for the first family of ribs in the further derivations is omitted.

In this case the equations of equilibrium of a grid plate are transformed into the formulae for N_1, N_2, S from the formulae (3.27) with the following notations:

$$C_{11} = 2Kc^4 + K_3, \qquad C_{12} = C_{66} = 2Ks^2c^2, \quad C_{11} = 2Ks^4. \qquad (3.84)$$

For the considered type of grid, the differential operators (3.82) of the system of equations (3.79) become

$$L_{11} = \left(2c^4K + K_3\right)\frac{\partial^2}{\partial x^2} + 2c^2s^2K\frac{\partial^2}{\partial y^2},$$
$$L_{22} = 2c^2s^2K\left(\frac{\partial^2}{\partial x^2} + \mathrm{tg}^2 2\varphi\frac{\partial^2}{\partial y^2}\right), \tag{3.85}$$
$$L_{12} = K\sin^2 2\varphi\frac{\partial^2}{\partial x\partial y},$$

where

$$u = -(a_3/EF)L_{22}(\Phi), \qquad v = (a_3/EF)L_{12}(\Phi). \tag{3.86}$$

The system of equations (3.79) can be reduced to a single equation

$$\left(K_1^0\frac{\partial^4}{\partial x^4} + K_3^0\frac{\partial^4}{\partial x^2\partial y^2} + K_2^0\frac{\partial^4}{\partial y^4}\right)\Phi = X, \tag{3.87}$$

where

$$\begin{aligned} &K_1^0 = a_{11}a_{12}, \quad K_2^0 = a_{22}a_{12}, \quad K_3^0 = a_{11}a_{12} - 3a_{12}^2, \\ &a_{11} = \delta_3 + c^3, \quad a_{12} = s^2c, \quad a_{22} = s^3\mathrm{tg}\varphi, \quad \delta_3 = F_3/F. \end{aligned} \tag{3.88}$$

Lets consider particular case where the boundary conditions are given as:

$$u = S = 0 \qquad \text{for} \quad x = 0, l, \tag{3.89}$$

where l is the dimension of a plate in the x direction. In this case the solution of the differential equation (3.87) is found by expansion into a series

$$\Phi(x, y) = \sum_{m=1}^{\infty}\varphi_m(y)\sin\lambda_m x, \qquad \left(\lambda_m = \frac{m\pi}{l}\right). \tag{3.90}$$

The solution for the function $\varphi_m(y)$ corresponds to the solution of the homogeneous equation (3.87) for $X \equiv 0$ and can be reduced to the solution of the characteristic equation

$$s_m^4 - 2\lambda_m^2 s_m^2\frac{\alpha_2}{\alpha_1} + \frac{\lambda_m^4}{\alpha_1^2} = 0, \tag{3.91}$$

where

$$\alpha_1 = \sqrt{\frac{K_2^0}{K_1^0}}, \qquad 2\alpha_2 = \frac{K_3^0}{\sqrt{\frac{K_2^0}{K_1^0}}}. \tag{3.92}$$

The forces in the members of each of the families are obtained from the known stress-strain state using the following equations:

$$N_{1,2}^{*}=\left(\frac{N_2}{s}\pm\frac{S}{c}\right)\frac{a}{2s},\quad N_3^{*}=\left(\frac{N_1}{c}-\frac{N_2 c}{s^2}\right)\frac{a}{2}, \tag{3.93}$$

which were obtained from (3.51), for the case of $\varphi_3=0$, $a=2ca_3$.

3.7.2 A Plate with Two Families of Ribs

Consider a problem that takes into account the in-plane stiffness of the ribs. On the basis of equations (3.7), (3.8), (3.15) and (3.76), the angle of twist of the axis of a rib that belongs to the i-th family about the normal to the median surface of a shell is

$$\psi_i=\left(c_i\frac{\partial}{\partial x}-s_i\frac{\partial}{\partial y}\right)(c_i v-s_i u). \tag{3.94}$$

The changes in the in-plane curvature of the axis of a rib, that belongs to the same family, according to (3.14) is

$$\chi_i^0=-\left(c_i^2\frac{\partial^2}{\partial x^2}+\sin 2\varphi_i\frac{\partial^2}{\partial x\partial y}+s_i^2\frac{\partial^2}{\partial y^2}\right)(c_i v-s_i u). \tag{3.95}$$

The constitutive equations of the grid plate can be written using formulae (3.18), considering the number of the families of ribs: $n=2$.

The stress-strain state of a model allows the calculation of the forces and moments in the members of a grid using the formulae in Section 3.5.3.

3.7.2.1 A Plate With a Rectangular Grid

Consider the case when the co-ordinate axes are coincident with the grid families, so that $\varphi_1=0$, $\varphi_2=\pi/2$. Then the formulae for the forces and moments can be obtained from the relationships (3.18), (3.76) and (3.95).

$$\begin{aligned} &N_1=K_1\frac{\partial u}{\partial x},\quad N_2=K_2\frac{\partial v}{\partial y},\quad S_1=-I_1^0\frac{\partial^3 v}{\partial x^3},\\ &S_2=-I_2^0\frac{\partial^3 u}{\partial y^3},\quad M_{1s}=I_1^0\frac{\partial^2 v}{\partial x^2},\quad M_{2s}=I_2^0\frac{\partial^2 u}{\partial y^2}, \end{aligned} \tag{3.96}$$

where

$$I_1^0=\frac{EJ_{2i}}{a_i}\qquad (i=1,2). \tag{3.97}$$

The equations of equilibrium

$$\frac{\partial N_1}{\partial x}+\frac{\partial S_2}{\partial y}+X=0,\quad \frac{\partial N_2}{\partial y}+\frac{\partial S_1}{\partial x}+Y=0 \tag{3.98}$$

can be reduced to the following form

$$K_1\frac{\partial^2 u}{\partial x^2}-I_2^0\frac{\partial^4 u}{\partial y^4}=-X,\qquad K_2\frac{\partial^2 v}{\partial y^2}-I_1^0\frac{\partial^4 v}{\partial x^4}=-Y. \tag{3.99}$$

The above system of equations for a plate with considered grid pattern is written in terms of displacements.

3.7.2.2 A Plate With a Rhombic Grid

Let us consider the diagonals of a grid to be coincident with the co-ordinate lines of the median surface of a plate $(\varphi=\varphi_1=-\varphi_2)$. The ribs are considered to have equal length and to have the same cross-section.

The constitutive equations (3.100) for a plate with a rhombic grid are obtained using formulae (3.18), (3.76) and (3.95):

$$\begin{aligned}
&N_1=N^{(1)}-N^{(2)}, \qquad N_2=N^{(1)}\mathrm{tg}^2\varphi+N^{(2)},\\
&S_1=S^{(1)}+S^{(2)}, \qquad S_2=S^{(1)}-S^{(2)}\mathrm{tg}^2\varphi,\\
&M_{1s}=\frac{I^0}{2}\left(4c^4\frac{\partial^2 v}{\partial x^2}+\frac{\partial^2 v}{\partial y^2}\sin^2 2\varphi-2\frac{\partial^2 u}{\partial x\partial y}\sin^2 2\varphi\right),\\
&M_{2s}=\frac{I^0}{2}\left(4s^4\frac{\partial^2 u}{\partial y^2}+\frac{\partial^2 u}{\partial x^2}\sin^2 2\varphi-2\frac{\partial^2 v}{\partial x\partial y}\sin^2 2\varphi\right),
\end{aligned} \tag{3.100}$$

where

$$\begin{aligned}
&N^{(1)}=\frac{K\sin^2 2\varphi}{2}\left(\frac{\partial u}{\partial x}\mathrm{ctg}^2\varphi+\frac{\partial v}{\partial y}\right), \qquad S^{(1)}=\frac{K\sin^2 2\varphi}{2}\left(\frac{\partial v}{\partial x}+\frac{\partial u}{\partial y}\right),\\
&N^{(2)}=\left(c^2\frac{\partial^3 u}{\partial x^3}+3s^2\frac{\partial^3 u}{\partial x\partial y^2}-3c^2\frac{\partial^3 v}{\partial x^2\partial y}-s^2\frac{\partial^3 v}{\partial y^3}\right)I^0\sin^2 2\varphi,\\
&S^{(2)}=\left(s^2\frac{\partial^3 u}{\partial y^3}+3c^2\frac{\partial^3 u}{\partial x^2\partial y}-3c^2\frac{\partial^3 v}{\partial x\partial y^2}-\frac{c^4}{s^2}\frac{\partial^3 v}{\partial x^3}\right)I^0\sin^2 2\varphi.
\end{aligned} \tag{3.101}$$

The forces and moments in the members of a grid are calculated using (3.55) for the known stress-strain state of the model of a grid shell.

The following system of equations in terms of displacements (3.102) is obtained by substituting (3.100) into the equations of equilibrium (3.98):

$$\begin{aligned}
&L_{11}(u)+L_{12}(v)+\frac{2X}{K\sin^2 2\varphi}=0,\\
&L_{12}(u)+L_{22}(v)+\frac{2Y}{K\sin^2 2\varphi}=0,
\end{aligned} \tag{3.102}$$

where

$$
\begin{aligned}
L_{11} &= L - \rho_2^2 T, \\
L_{22} &= L\mathrm{tg}^2\varphi - \rho_2^2 T\mathrm{ctg}^2\varphi, \\
L_{12} &= 2\frac{\partial^2}{\partial x\partial y} + 4\rho_2^2\left(c^2\frac{\partial^4}{\partial x^3\partial y} + s^2\frac{\partial^4}{\partial x\partial y^3}\right), \\
T &= c^2\frac{\partial^4}{\partial x^4} + 6s^2\frac{\partial^4}{\partial x^2\partial y^2} + \frac{s^4}{c^2}\frac{\partial^4}{\partial y^4}, \\
L &= \mathrm{ctg}^2\varphi\frac{\partial^2}{\partial x^2} + \frac{\partial^2}{\partial y^2}.
\end{aligned}
\tag{3.103}
$$

Here $\rho_2^2 = J_2/F$; ρ is a radius of inertia of the rib's cross-section for the case of in-plane bending of a grid plate.

Taking $Y \equiv 0$ and also considering

$$
u = L_{22}(\Phi), \qquad v = L_{12}(\Phi), \tag{3.104}
$$

the system of equations (3.102) is reduced to the following differential equation expressed in terms of the function Φ:

$$
\begin{aligned}
&\left\{\mathrm{ctg}^2\varphi\frac{\partial^4}{\partial x^4} - 2\frac{\partial^4}{\partial x^2\partial y^2} + \mathrm{tg}^2\varphi\frac{\partial^4}{\partial y^4} - \rho_2^2\left[c^2\left(1+\mathrm{tg}^4\varphi\right)\frac{\partial^6}{\partial x^6} + \right.\right. \\
&c^2\left(16+7\mathrm{tg}^2\varphi+7\mathrm{ctg}^2\varphi\right)\frac{\partial^6}{\partial x^4\partial y^2} + s^2\left(16+7\mathrm{tg}^2\varphi+7\mathrm{ctg}^2\varphi\right)\frac{\partial^6}{\partial x^2\partial y^4} + \\
&\left.+s^2\left(1+\mathrm{tg}^4\varphi\right)\frac{\partial^6}{\partial y^6}\right] + \rho_2^4\left(c^4\mathrm{ctg}^2\varphi\frac{\partial^8}{\partial x^8} - 4c^2\frac{\partial^8}{\partial x^6\partial y^2} + 6c^2s^2\frac{\partial^8}{\partial x^4\partial y^4} - 4s^2\frac{\partial^8}{\partial x^2\partial y^6} + \right. \\
&\left.\left.+s^4\mathrm{tg}^2\varphi\frac{\partial^8}{\partial x^8}\right)\right\}\Phi = \frac{2X}{K\sin^2 2\varphi}.
\end{aligned}
\tag{3.105}
$$

As can be seen from the above equation, consideration of the in-plane bending stiffness of the ribs $(\rho_2 \neq 0)$ increases the order of the equation from four to eight. This fact points towards the necessity of the formulation of additional boundary conditions.

Additional boundary conditions (3.71) that restrict the rotation of the axes of the ribs of both families about the normal to the median surface of a plate can be used. Substituting equations (3.8) and (3.76) into (3.71), these additional boundary conditions are written in the following form:

$$c^2\frac{\partial v}{\partial x}-s^2\frac{\partial u}{\partial y}=\frac{\partial u}{\partial x}-\frac{\partial v}{\partial y}=0 \quad \text{for} \quad y=y_0. \tag{3.106}$$

In the analysis of the plates with two families of ribs, the decision of whether to take into account in-plane bending deformation of the ribs depends on the particular formulation of the problem.

As can be observed, for $X=Y=J_{2i}=0$ and $\varphi_i=const$ $(i=1,2)$ the axial force in any of the members of a grid plate must remain constant. This can be shown by the following solution of the equations of equilibrium.

Co-ordinate axes are chosen in such a way that they satisfy the following conditions $\varphi=\varphi_1=-\varphi_2$. Then from the equations (3.40) we obtain

$$N_2=N_1\mathrm{tg}^2\varphi, \tag{3.107}$$

and the equations (3.75) are written as

$$\frac{\partial N_1}{\partial x}+\frac{\partial S}{\partial y}=0, \qquad \frac{\partial N_1}{\partial y}\mathrm{tg}^2\varphi\frac{\partial S}{\partial x}=0. \tag{3.108}$$

The solution of this system of equations is given as:

$$\begin{aligned} N_1&=\psi_2(y+x\mathrm{tg}\varphi)+\psi_1(y-x\mathrm{tg}\varphi),\\ S&=\left[-\psi_2(y+x\mathrm{tg}\varphi)+\psi_1(y-x\mathrm{tg}\varphi)\right]\mathrm{tg}\varphi, \end{aligned} \tag{3.109}$$

where ψ_1 and ψ_2 are arbitrary functions.

In this case the forces in the ribs (3.111) are obtained incorporating formulae (3.110) for the case of $\varphi=\varphi_1=-\varphi_2$ as

$$2N^*_{1,2}=\left(N_1c^{-2}\pm 2S\sin^{-1}2\varphi\right)a, \tag{3.110}$$

$$N^*_1=ac^{-2}\psi_1(y-x\mathrm{tg}\varphi), \qquad N^*_2=ac^{-2}\psi_2(y+x\mathrm{tg}\varphi). \tag{3.111}$$

The axial forces N^*_1 and N^*_2 do not change if the following conditions are satisfied

$$y-x\mathrm{tg}\varphi=\text{const}, \qquad y+x\mathrm{tg}\varphi=\text{const}. \tag{3.112}$$

The conditions (3.112) are the equations of the axes of the first and the second families of ribs.

3.8 Bending of the Grid Plates

This section presents analysis of bending and shear deformation of the lattice plates with two, three and four families of ribs.

3.8.1 Differential Equations of Bending of the Plates

The equations of equilibrium for an element of a plate in the Cartesian co-ordinate system are:

$$\begin{aligned} &\frac{\partial Q_1}{\partial x}+\frac{\partial Q_2}{\partial y}+\mathrm{Z}=0, \\ &\frac{\partial H_1}{\partial x}+\frac{\partial M_2}{\partial y}-Q_2=0, \\ &\frac{\partial H_2}{\partial y}-\frac{\partial M_1}{\partial x}-Q_1=0. \end{aligned} \tag{3.113}$$

The expressions for the linear shear forces (3.115) are obtained from the last two equations (3.113) taking into account the constitutive equations (3.17) and the conditions (3.114):

$$\chi_1=-\frac{\partial^2 w}{\partial x^2}, \quad \chi_2=-\frac{\partial^2 w}{\partial y^2}, \quad \tau=-\frac{\partial^2 w}{\partial x \partial y}. \tag{3.114}$$

$$
\begin{aligned}
Q_1 = -\Big\{&\left(D_{11}+K_{11}\right)\frac{\partial^3 w}{\partial x^3}+\left(3D_{61}-K_{16}+K_{61}^{(2)}\right)\frac{\partial^3 w}{\partial x^2\partial y}+\\
&+\left(D_{66}+D_{12}-K_{11}+K_{66}^{(2)}\right)\frac{\partial^3 w}{\partial x\partial y^2}+\left(D_{62}-K_{61}^{(2)}\right)\frac{\partial^3 w}{\partial y^3}+\\
&+\left[\frac{\partial}{\partial x}\left(D_{11}+K_{11}\right)+\frac{\partial}{\partial y}\left(D_{61}+K_{61}^{(2)}\right)\right]\frac{\partial^2 w}{\partial x^2}+\\
&+\left[\frac{\partial}{\partial x}\left(2D_{61}-K_{16}\right)+\frac{\partial}{\partial y}\left(D_{66}+K_{66}^{(2)}\right)\right]\frac{\partial^2 w}{\partial x\partial y}+\\
&+\left[\frac{\partial}{\partial x}\left(2D_{12}-K_{11}\right)+\frac{\partial}{\partial y}\left(D_{62}+K_{61}^{(2)}\right)\right]\frac{\partial^2 w}{\partial y^2}\Big\},\\
Q_2 = -\Big\{&\left(D_{61}+K_{61}^{(1)}\right)\frac{\partial^3 w}{\partial x^3}+\left(D_{66}+D_{12}-K_{11}+K_{66}^{(1)}\right)\frac{\partial^3 w}{\partial x^2\partial y}+\\
&+\left(3D_{62}+K_{16}+K_{61}^{(1)}\right)\frac{\partial^3 w}{\partial x\partial y^2}+\left(D_{22}+K_{11}\right)\frac{\partial^3 w}{\partial y^3}+\\
&+\left[\frac{\partial}{\partial x}\left(D_{61}-K_{61}^{(1)}\right)+\frac{\partial}{\partial y}\left(D_{12}-K_{11}\right)\right]\frac{\partial^2 w}{\partial x^2}+\\
&+\left[\frac{\partial}{\partial x}\left(D_{66}+K_{66}^{(1)}\right)+\frac{\partial}{\partial y}\left(2D_{62}+K_{16}\right)\right]\frac{\partial^2 w}{\partial x\partial y}+\\
&+\left[\frac{\partial}{\partial x}\left(D_{62}+K_{61}^{(1)}\right)+\frac{\partial}{\partial y}\left(D_{22}+K_{11}\right)\right]\frac{\partial^2 w}{\partial y^2}\Big\}.
\end{aligned}
\tag{3.115}
$$

Coefficients D_{ij} and K_{ij} are defined in (3.20) and (3.21).

The differential equation of the bending of a grid plate, taking into account the values from the first equation of equilibrium (3.113), can then be written in a form of

$$L(w)-Z=0, \tag{3.116}$$

where linear differential operator $L(w)$, is defined as

$$
\begin{aligned}
L(w) &= (D_{11}+K_{11})\frac{\partial^4 w}{\partial x^4} + 2(2D_{61}+K_{16})\frac{\partial^4 w}{\partial x^3 \partial y} + \\
&+(3D_{66}+K_1^0)\frac{\partial^4 w}{\partial x^2 \partial y^2} + 2(2D_{62}-K_{61})\frac{\partial^4 w}{\partial x \partial y^3} + (D_{22}+K_{11})\frac{\partial^4 w}{\partial y^4} + \\
&+\left[2\frac{\partial}{\partial x}(D_{11}-K_{11}) + \frac{\partial}{\partial y}(3D_{61}+K_{16})\right]\frac{\partial^3 w}{\partial x^3} + \\
&+\left[3\frac{\partial}{\partial x}(2D_{61}-K_{16}) + \frac{\partial}{\partial y}(3D_{66}+K_1^0)\right]\frac{\partial^3 w}{\partial x^2 \partial y} + \\
&+\left[\frac{\partial}{\partial x}(3D_{66}+K_1^0) + 3\frac{\partial}{\partial y}(D_{62}+K_{16})\right]\frac{\partial^3 w}{\partial x \partial y^2} + \\
&+\left[\frac{\partial}{\partial x}(2D_{62}-K_{16}) + 2\frac{\partial}{\partial y}(D_{22}+K_{11})\right]\frac{\partial^3 w}{\partial y^3} + \\
&+\frac{\partial^2}{\partial x^2}(D_{11}+K_{11}) + \frac{\partial}{\partial x \partial y}(2D_{61}+K_{16}) + \frac{\partial^2}{\partial y^2}(D_{12}-K_{11})\frac{\partial^2 w}{\partial x^2} + \\
&+\left[\frac{\partial^2}{\partial x^2}(2D_{61}+K_{16}) + \frac{\partial}{\partial x \partial y}(2D_{66}+K_2^0) + \right. \\
&\left.+\frac{\partial^2}{\partial y^2}(2D_{62}-K_{16})\right]\frac{\partial^2 w}{\partial x \partial y} + \frac{\partial^2}{\partial x^2}(D_{12}-K_{11}) + \frac{\partial^2 w}{\partial x \partial y}(2D_{62}+K_{16}) + \\
&+\frac{\partial^2}{\partial y^2}(D_{22}+K_{11})\Bigg]\frac{\partial^2 w}{\partial y^2}.
\end{aligned}
\tag{3.117}
$$

The following additional notations were used in the above equation (3.117):

$$
K_1^0 = \sum_{i=1}^{n}(1-6s_i^2c_i^2)C_i, \qquad K_2^0 = \sum_{i=1}^{n} C_i \cos^2 2\varphi_i. \tag{3.118}
$$

The equations for the moments are given as:

$$
\begin{aligned}
M_1 &= \sum_{i=1}^{n} c_i \nabla_i (I_i c_i \nabla_i + C_i s_i \Delta_i) w, \\
M_2 &= \sum_{i=1}^{n} s_i \nabla_i (I_i s_i \nabla_i - C_i c_i \Delta_i) w, \\
H_1 &= -\sum_{i=1}^{n} c_i \nabla_i (I_i s_i \nabla_i - C_i c_i \Delta_i) w, \\
H_2 &= -\sum_{i=1}^{n} s_i \nabla_i (I_i c_i \nabla_i + C_i s_i \Delta_i) w,
\end{aligned}
\tag{3.119}
$$

where the differentiation is introduced in the direction orthogonal to the tangent to the axis of the i-th family in addition to (3.14):

$$
\Delta_i = s_i \partial/\partial x - c_i \partial/\partial y. \tag{3.120}
$$

Equations (3.115) for the shear forces of a grid plate are written in the form:

$$Q_1 = -\sum_{i=1}^{n} \nabla_i^2 \left(I_i c_i \nabla_i + C_i s_i \Delta_i \right) w,$$
$$Q_2 = -\sum_{i=1}^{n} \nabla_i^2 \left(I_i s_i \nabla_i - C_i c_i \Delta_i \right) w. \tag{3.121}$$

The differential operator (3.117) in the (3.116) is transformed into

$$L(w) = \sum_{i=1}^{n} \nabla_i^2 \left(I_i \nabla_i^2 + C_i \Delta_i^2 \right) w. \tag{3.122}$$

3.8.2 A Plate With a Rhombic Grid

The type of grid considered is the same as the one analysed in the section 3.7.2.2: the diagonals of rhombic grid are coincident with the co-ordinate lines of the median surface of a plate: $\varphi = \varphi_1 = -\varphi_2$, $a = a_1 = a_2$. The cross-sections of the ribs which belong to both families are considered to be the same. From the above considerations and using equations (3.119) we obtain the expressions for the bending moments as:

$$\begin{aligned}
M_1 &= 2c^2 \left[\left(Ic^2 + Cs^2 \right) \partial^2 w / \partial x^2 + (I - C) s^2 \, \partial^2 w / \partial y^2 \right], \\
M_2 &= 2s^2 \left[(I - C) c^2 \, \partial^2 w / \partial x^2 + \left(Is^2 + Cc^2 \right) \partial^2 w / \partial y^2 \right], \\
H_1 &= -2c^2 \left(2Is^2 + C \cos 2\varphi \right) \partial^2 w / \partial x \partial y, \\
H_2 &= 2s^2 \left(C \cos 2\varphi - 2Ic^2 \right) \partial^2 w / \partial x \partial y.
\end{aligned} \tag{3.123}$$

The formulae (3.121) for the shear forces are simplified considerably:

$$\begin{aligned}
Q_1 &= -2c^2 I \left(c^2 \frac{\partial^3 w}{\partial x^3} + 3s^2 \frac{\partial^3 w}{\partial x \partial y^2} \right) - 2s^2 C \left(c^2 \frac{\partial^3 w}{\partial x^3} + \left(1 - 3c^2 \right) \frac{\partial^3 w}{\partial x \partial y^2} \right), \\
Q_2 &= -2s^2 I \left(3c^2 \frac{\partial^3 w}{\partial x^2 \partial y} + s^2 \frac{\partial^3 w}{\partial y^3} \right) - 2c^2 C \left(s^2 \frac{\partial^3 w}{\partial y^3} + \left(1 - 3s^2 \right) \frac{\partial^3 w}{\partial x^2 \partial y} \right).
\end{aligned} \tag{3.124}$$

After the update of the differential operator (3.122) for the rhombic grid pattern, the differential equation of bending of a grid plate (3.116) transforms into the following equation:

$$D_1 \frac{\partial^4 w}{\partial x^4} + D_3 \frac{\partial^4 w}{\partial x^2 \partial y^2} + D_2 \frac{\partial^4 w}{\partial y^4} = \frac{Z}{I}. \tag{3.125}$$

The coefficients in (3.125) are given as:

$$\begin{aligned}
D_1 &= 2 \left(c^4 + \gamma a_0 \right), \\
D_2 &= 2 \left(s^4 + \gamma a_0 \right), \\
D_3 &= 12 a_0 + 2\gamma \left(1 - 6 a_0 \right),
\end{aligned} \tag{3.126}$$

where

$$\gamma = \frac{GJ_3}{EJ_1}, \qquad a_0 = s^2 c^2. \tag{3.127}$$

The bending and twisting moments and also shear forces acting directly on the members of a grid plate are calculated using (3.55), (3.56).

3.8.3 A Plate With More Than Two Families of Ribs

In this section the transverse bending of the grid plates with three and four families of ribs is discussed.

3.8.3.1 Three Families of Ribs

Let us consider a rectangular plate with three families of ribs. The solution for this case can be obtained from the generalised case (Figure 1.4, with four families), where the family number 3 is absent. In order to utilise already derived equations for the plate with four families of ribs, the family number four will be referred as number three. The members which belong to the first and the second families are considered to have the same cross-sections. For the considered grid pattern the length of the ribs which belong to the first two families is

$$a = 2ca_3. \tag{3.128}$$

Constitutive equations for this model of plate are obtained from (3.27), if the coefficients β_{ij} in the formulae for linear bending and torque moments are substituted with

$$\begin{aligned}
\beta_{11} &= -\left(2Ic^4 + I_3 + 2Cs^2c^2\right), \\
\beta_{22} &= -2s^2\left(Is^2 + Cc^2\right), \\
\beta_{12} &= -2s^2c^2(I - C), \\
\beta_{31} &= I\sin^2 2\varphi + 2Cc^2\cos 2\varphi + C_3, \\
\beta_{41} &= I\sin^2 2\varphi - 2Cs^2\cos 2\varphi.
\end{aligned} \tag{3.129}$$

The shear forces acting in the grid plate are obtained from the equations (3.121) with an adjustment to the current grid pattern:

$$\begin{aligned}
Q_1 &= -\frac{EJ_1}{a_3}\left\{D_1\frac{\partial^3 w}{\partial x^3} + s\left[3sc + \gamma\left(\mathrm{tg}\varphi - 3sc\right)\right]\frac{\partial^3 w}{\partial x\partial y^2}\right\}, \\
Q_2 &= -\frac{EJ_1}{a_3}\left\{D_2\frac{\partial^3 w}{\partial y^3} + c\left[3s^2 + \gamma\left(1 - 3s^2 + e_3\right)\right]\frac{\partial^3 w}{\partial x^2\partial y}\right\},
\end{aligned} \tag{3.130}$$

where

$$D_1 = c^3 + d_3 + \gamma s^2 c, \qquad D_2 = (s\mathrm{tg}\varphi + \gamma c)s^2,$$
$$\gamma = \frac{GJ_3}{EJ_1}, \qquad e_3 = \frac{G_3 J_{33}}{GJ_3}, \qquad d_3 = \frac{E_3 J_{13}}{EJ_1}. \tag{3.131}$$

The equations of bending of a plate (3.132) are obtained from the formulae (3.116) and (3.122)

$$D_1 \frac{\partial^4 w}{\partial x^4} + D_3 \frac{\partial^4 w}{\partial x^2 \partial y^2} + D_2 \frac{\partial^4 w}{\partial y^4} = \frac{a_3}{EJ_1} Z, \tag{3.132}$$

where

$$D_3 = 6s^2 c + \left(c^{-1} - 6s^2 c + e_3\right)\gamma. \tag{3.133}$$

If the torsion stiffness of the ribs can be neglected, the bending moments acting on the ribs are obtained using formulae (3.53), where $\varphi_3 = 0$, $a = 2ca_3$:

$$M_{1,2}^{*} = \left(\frac{M_2}{s} \mp \frac{H}{c}\right)\frac{a}{2s}, \qquad M_s^{*} = \left(\frac{M_1}{c} - \frac{M_2 c}{s^2}\right)\frac{a}{2}. \tag{3.134}$$

Otherwise, formulae for bending and twist moments are obtained from (3.65). In order to do that, all the quantities which correspond to the third family must be taken as equal to zero and the quantities which correspond to the fourth family must be considered as third family. After these changes we obtain

$$\begin{aligned}
M_{1,2}^{*} &= \left\{\left[2Cs^2c^2 M_1 + \left(I_3 s^2 + 2Cs^2c^2\right)M_2\right]I_0 \mp \right. \\
&\left. \mp H_1\left(I\sin 2\varphi + 2Cc^2 \mathrm{ctg}2\varphi + C_3 \sin^{-1} 2\varphi\right)^{-1}\right\}EJ_1, \\
M_3^{*} &= \left[\left(2Is^4 + 2Cs^2c^2\right)M_1 - 2M_2 s^2 c^2 (I - C)I_0 E_3 J_{13}\right], \\
H_{1,2}^{*} &= \left\{\pm\left[2Is^2 M_1 - \left(2Ic^2 + I_3\right)M_2\right]I_0 + \right. \\
&\left. + 2H_1 \beta_{31}^{-1} \cos 2\varphi\right\}GJ_3, \\
H_3^{*} &= 2G_3 J_{33} H_1 \beta_{31}^{-1},
\end{aligned} \tag{3.135}$$

where

$$\begin{aligned}
I_0 &= \left[2II_3 s^4 + 2Cs^2c^2(2I + I_3)\right]^{-1}, \\
\beta_{31} &= I\sin^2 2\varphi + 2Cc^2 \cos 2\varphi + C_3.
\end{aligned} \tag{3.136}$$

For the rectangular grid plate, which is pinned at its opposite ends $(x = \mathrm{const})$, the solution of the equation (3.132) is found using an ordinary trigonometric series:

$$w(x,y) = \sum_{m=1}^{\infty} w_m(y)\sin\lambda_m x \qquad \left(\lambda_m = \frac{m\pi}{l}\right). \tag{3.137}$$

The characteristic equation, which corresponds to (3.132) is

$$s_m^4 - 2\frac{\alpha_2}{\alpha_1}\lambda_m^2 s_m^2 + \frac{\lambda_m^4}{\alpha_1^2} = 0,$$
$$\alpha_1 = \sqrt{\frac{D_2}{D_1}}, \qquad 2\alpha_2 = \frac{D_3}{\sqrt{\frac{D_2}{D_1}}}. \tag{3.138}$$

3.8.3.2 Four Families of Ribs

Lets consider a plate with four families of ribs $(n=4)$. The cross-sections of the ribs of the first two families are considered to be the same and $\varphi = \varphi_1 = -\varphi_2$, $a = a_1 = a_2 = 2sa_3 = 2ca_4$ (See Figure 1.4 (c)).

The constitutive equations for this model are written in the form of expressions for linear bending and twist moments (3.27).

For the considered case of a plate with four families of ribs, the expressions for shear forces (3.139) are obtained from the formulae (3.121) and are written as a function of deflections

$$Q_1 = -\frac{EJ}{a_4}\left\{D_1\frac{\partial^3 w}{\partial x^3} + \left[3s^2c + \gamma\left(s\mathrm{tg}\varphi - 3s^2c + e_3\mathrm{tg}\varphi\right)\right]\frac{\partial^3 w}{\partial x\partial y^2}\right\},$$
$$Q_2 = -\frac{EJ}{a_4}\left\{D_2\frac{\partial^3 w}{\partial y^3} + \left[3s^2c + \gamma\left(c - 3s^2c + e_4\right)\right]\frac{\partial^3 w}{\partial x^2\partial y}\right\}, \tag{3.139}$$

where

$$D_1 = c^3 + d_4 + \gamma s^2 c, \qquad D_2 = s^3\mathrm{tg}\varphi + d_3\mathrm{tg}\varphi + \gamma s^2 c,$$
$$e_i = G_i J_{3i}/GJ_3, \qquad d_i = E_i J_{1i}/EJ_1 \qquad (i=3,4). \tag{3.140}$$

The subscript i is omitted when its value is equal to zero.

The differential equation for the deflection of a grid shell comprised of four families of ribs is found by means of substituting (3.122) into (3.116):

$$D_1\frac{\partial^4 w}{\partial x^4} + D_3\frac{\partial^4 w}{\partial x^2\partial y^2} + D_2\frac{\partial^4 w}{\partial y^4} = \frac{a_4}{EJ_1}Z, \tag{3.141}$$

where

$$D_3 = 6s^2c + \gamma\left(c^{-1} - 6s^2c + e_3\mathrm{tg}\varphi + e_4\right). \tag{3.142}$$

For the case of isogrid plate this differential equation changes into (3.27). In this case the third family of ribs considered to be absent, and the fourth family is notated as a third.

In order to obtain an equation for deflection of a plate with rhombic grid (3.125), the coefficients which correspond to the third and the fourth family in the equation (3.141) must be taken as equal to zero. For the known stress-strain state of a plate, the values of bending moments acting in each of the four members of a grid are calculated using the formulae (3.65).

3.8.4 Shear Deformation

The classical theory of shells, based on the Kirchhoff-Love hypothesis [86] allows the analysis of a wide variety of problems with an accuracy that is often sufficient for practical applications.

However, in many engineering applications some refined theories should be used. Higher-order theories of laminated plates and shells, which take into account transverse shear and normal deformation were developed by V. E. Verijenko *et. al.* [64], [107] for the solution of the dynamic problems. These theories are capable of treating plates and shells with arbitrary numbers and sequences of layers which may differ significantly in their physical and mechanical properties. The use of the refined higher-order theories can be very beneficial especially for shells made of composite materials where the matrix has a relatively low stiffness. In the present chapter the transverse shear of the ribs comprising a lattice shell is taken into consideration by applying the well known principle of Timoshenko [97].

3.8.4.1 The System of Differential Equations for the Deflection of a Plate

Let us denote the angles of rotation of the normal to a median surface of a plate in the planes x=const, y=const as θ_1 and θ_2. The corresponding angles of transverse shear for the considered model of a grid shell are

$$\beta_1 = \frac{\partial w}{\partial x} + \theta_1, \quad \beta_2 = \frac{\partial w}{\partial y} + \theta_2. \tag{3.143}$$

Shear forces and bending moments for the members of i-th family of the ribs are

$$Q_i^* = k_i^2 G_i F_i \beta_i^*, \quad M_i^* = -E_i J_{1i} \nabla_i \theta^*{}_i, \tag{3.144}$$

where

$$\theta_i^* = \theta_1 c_i + \theta_2 s_i, \quad \beta_i^* = \beta_1 c_i + \beta_2 s_i. \tag{3.145}$$

The torsional stiffness of the ribs is neglected. The value of k_i^2 depends on the shape of the cross-section of the ribs.

Substituting (3.143)-(3.145) into the corresponding equations (3.17) and after some simplifications we obtain the expressions for the shear forces, bending and twist moments of the plate as:

$$\begin{aligned}
Q_1 &= \sum_{i=1}^{n} c_i K_i^* (\nabla_i w + c_i\theta_1 + s_i\theta_2), \\
Q_2 &= \sum_{i=1}^{n} s_i K_i^* (\nabla_i w + c_i\theta_1 + s_i\theta_2), \\
M_1 &= -\sum_{i=1}^{n} c_i^2 I_i \nabla_i (\theta_1 c_i + \theta_2 s_i), \\
M_2 &= -\sum_{i=1}^{n} s_i^2 I_i \nabla_i (\theta_1 c_i + \theta_2 s_i), \\
H &= \sum_{i=1}^{n} s_i c_i I_i \nabla_i (\theta_1 c_i + \theta_2 s_i),
\end{aligned} \tag{3.146}$$

where

$$K_i^* = k_i^2 G_i F_i / a_i. \tag{3.147}$$

Differential equations for the deflection of a plate (3.116) can be reduced to the system of differential equations in terms of the functions w, θ_1 and θ_2 using formulae (3.146):

$$\begin{aligned}
L_{11}(w) + L_{12}(\theta_1) + L_{13}(\theta_2) &= Z, \\
L_{12}(w) + L_{22}(\theta_1) + L_{23}(\theta_2) &= 0, \\
L_{13}(w) + L_{23}(\theta_1) + L_{33}(\theta_2) &= 0,
\end{aligned} \tag{3.148}$$

where

$$\begin{aligned}
L_{11} &= \sum_{i=1}^{n} K_i^* \nabla_i^2, & L_{12} &= \sum_{i=1}^{n} c_i K_i^* \nabla_i, \\
L_{13} &= \sum_{i=1}^{n} s_i K_i^* \nabla_i, & L_{22} &= \sum_{i=1}^{n} c_i^2 (K_i^* - I_i \nabla_i^2), \\
L_{23} &= \sum_{i=1}^{n} s_i c_i (K_i^* - I_i \nabla_i^2), & L_{33} &= \sum_{i=1}^{n} s_i^2 (K_i^* - I_i \nabla_i^2)
\end{aligned} \tag{3.149}$$

3.8.4.2 A Plate With a Rhombic Grid

Let us consider the case when the directions of the families of ribs coincide with the co-ordinate axes, and when all members to be the same. In this case the system of differential equations (3.149) can be written as:

$$
\begin{aligned}
&c^2\frac{\partial^2 w}{\partial x^2}+s^2\frac{\partial^2 w}{\partial y^2}+c^2\frac{\partial \theta_1}{\partial x}+s^2\frac{\partial \theta_2}{\partial y}=\frac{Z}{2K^*},\\
&\frac{\partial w}{\partial x}-\frac{I}{K^*}\left(c^2\frac{\partial^2\theta_1}{\partial x^2}+s^2\frac{\partial^2\theta_1}{\partial y^2}+2s^2\frac{\partial^2\theta_2}{\partial x\partial y}\right)+\theta_1=0,\\
&\frac{\partial w}{\partial y}-\frac{I}{K^*}\left(2c^2\frac{\partial^2\theta_1}{\partial x\partial y}+c^2\frac{\partial^2\theta_2}{\partial x^2}+s^2\frac{\partial^2\theta_2}{\partial y^2}\right)+\theta_2=0.
\end{aligned}
\tag{3.150}
$$

Formulae (3.146) for the calculation of forces and moments are simplified to

$$
\begin{aligned}
&Q_1=2K^*c^2\left(\frac{\partial w}{\partial x}+\theta_1\right),\quad Q_2=2K^*s^2\left(\frac{\partial w}{\partial y}+\theta_2\right),\\
&M_1=M_2\operatorname{ctg}\varphi=-2Ic^2\left(c^2\frac{\partial\theta_1}{\partial x}+s^2\frac{\partial\theta_2}{\partial y}\right),\\
&H=2Is^2c^2\left(\frac{\partial\theta_1}{\partial y}+\frac{\partial\theta_2}{\partial x}\right).
\end{aligned}
\tag{3.151}
$$

For the particular case of a square grid $(\varphi=\pi/4)$, the equations (3.150) take the following form:

$$
\begin{aligned}
&\frac{\partial^2 w}{\partial x^2}+\frac{\partial^2 w}{\partial y^2}+\frac{\partial\theta_1}{\partial x}+\frac{\partial\theta_2}{\partial y}=\frac{Z}{K^*},\\
&\frac{\partial w}{\partial x}-\frac{I}{2K^*}\left(\frac{\partial^2\theta_1}{\partial x^2}+\frac{\partial^2\theta_1}{\partial y^2}+2\frac{\partial^2\theta_2}{\partial x\partial y}\right)+\theta_1=0,\\
&\frac{\partial w}{\partial y}-\frac{I}{2K^*}\left(2\frac{\partial^2\theta_1}{\partial x\partial y}+\frac{\partial^2\theta_2}{\partial x^2}+\frac{\partial^2\theta_2}{\partial y^2}\right)+\theta_2=0.
\end{aligned}
\tag{3.152}
$$

The forces and moments acting in the square grid can be obtained from equation (3.151), considering $\varphi=\pi/4$:

$$
\begin{aligned}
&Q_1=K^*\left(\frac{\partial w}{\partial x}+\theta_1\right), && Q_2=K^*\left(\frac{\partial w}{\partial y}+\theta_2\right),\\
&M_1=M_2=M=-\frac{I}{2}\left(\frac{\partial\theta_1}{\partial x}+\frac{\partial\theta_2}{\partial y}\right), && H=\frac{I}{2}\left(\frac{\partial\theta_1}{\partial y}+\frac{\partial\theta_2}{\partial x}\right).
\end{aligned}
\tag{3.153}
$$

The solutions of the boundary value problem for the grid plates with the rhombic and square grid pattern can be linked. In order to do this the following substitution of the variables is introduced:

$$
x=\xi\operatorname{ctg}\varphi,\qquad \theta_1=\theta_1{}^0\operatorname{tg}\varphi. \tag{3.154}
$$

The formulae (3.151) then can be written as:

$$Q_1 = K^* \sin 2\varphi \left(\frac{\partial w}{\partial \xi} + \theta_1^{\,0} \right), \qquad Q_2 = 2K^* s^2 \left(\frac{\partial w}{\partial y} + \theta_2 \right),$$

$$M_1 = M_2 \operatorname{ctg}\varphi = -2Is^2 c^2 \left(\frac{\partial \theta_1^{\,0}}{\partial \xi} + \frac{\partial \theta_2}{\partial y} \right), \tag{3.155}$$

$$H = 2Is^3 c \left(\frac{\partial \theta_1^{\,0}}{\partial y} + \frac{\partial \theta_2}{\partial \xi} \right),$$

and the system of differential equations (3.150) becomes

$$\begin{aligned}
&\frac{\partial^2 w}{\partial \xi^2} + \frac{\partial^2 w}{\partial y^2} + \frac{\partial \theta_1^{\,0}}{\partial \xi} + \frac{\partial \theta_2}{\partial y} = \frac{Z}{2K^* s^2}, \\
&\frac{\partial w}{\partial \xi} - \frac{Is^2}{K^*} \left(\frac{\partial^2 \theta_1^{\,0}}{\partial \xi^2} + \frac{\partial^2 \theta_1^{\,0}}{\partial y^2} + 2\frac{\partial^2 \theta_2}{\partial \xi \partial y} \right) + \theta_1^{\,0} = 0, \\
&\frac{\partial w}{\partial y} - \frac{Is^2}{K^*} \left(2\frac{\partial^2 \theta_1^{\,0}}{\partial \xi \partial y} + \frac{\partial^2 \theta_2}{\partial \xi^2} + \frac{\partial^2 \theta_2}{\partial y^2} \right) + \theta_2 = 0.
\end{aligned} \tag{3.156}$$

It can be observed that the system of equations (3.152) for the plate with a square grid is the same as (3.156). The following substitution of variables is made:

$$x, \theta_1, K^*, Z \qquad \text{with} \qquad \xi, \theta_1^{\,0}, K_*, Z_*, \tag{3.157}$$

where

$$K_* = K^*/2s^2, \qquad Z_* = Z/4s^4. \tag{3.158}$$

Comparing the linear forces and moments for the models of a plate with the rhombic and square grids calculated using formulae (3.155) and (3.153), it is found that for the case of rhombic grid we have:

$$\begin{aligned}
&Q_1 = Q_{1*} \sin 2\varphi, \quad Q_2 = 2s^2 Q_{2*}, \\
&H = 4s^3 c H_*, \qquad M_1 = M_2 \operatorname{ctg}\varphi = 4s^2 c^2 M_*,
\end{aligned} \tag{3.159}$$

where the quantities denoted with the index * are calculated using the formulae (3.153) for the case of the square grid after the substitution of x and θ_1 with ξ and θ_1^0 correspondingly.

The last formulae are obtained satisfying the condition that K^* for the rhombic and square grids are equal. For the case of substitution of variables in (3.145), where K^* is substituted with $K^*/2s^2$, formulae (3.159) must be modified to the following form:

$$\begin{aligned}
&Q_1 = 4s^3 c Q_{1*}, \quad Q_2 = 4s^4 Q_{2*}, \\
&H = 4s^3 c H_*, \qquad M_1 = M_2 \operatorname{ctg}\varphi = 4s^2 c^2 M_*.
\end{aligned} \tag{3.160}$$

These transformations allow substitution of the problem of analysis of a plate with a rhombic grid with the solution of a certain boundary value problem for a square grid. This can be done by following the proposed scheme:

1. The side dimension l of a plate with a rhombic grid pattern in the direction x is substituted with $l\,\mathrm{tg}\varphi$ in accordance with (3.154).
2. The given value of K^* is substituted with $K = K^*/2s^2$.
3. Transverse load Z is considered to be equal $Z = Z^*/4s^4$.
4. The values on the outer boundary of the functions with * superscript and also θ_1^0 are found using second formula of (3.154) and (3.160).

This substitution will result in a boundary value problem for the system of equations (3.156), where $0 \le \xi \le l\,\mathrm{tg}\varphi$. The solution of this problem is actually the solution for the plate with a square grid with the set of altered (substituted) parameters, shown above.

After completing the analysis of such a lattice plate, the reverse transition from the obtained functions with * superscript and θ_1^0 is performed using (3.154) and (3.160) considering also that $\xi = x\,\mathrm{tg}\varphi$.

3.9 Circular Cylindrical Shells

In the previous sections (3.1-3.8) a technique was developed for the analysis of various types of lattice plates. The solutions obtained for lattice plates will be used for the development of a similar analysis technique for lattice structures of revolution. This technique is based on the same homogenisation principles. In the present section the analysis of a circular cylindrical shell with several grid patterns is considered.

3.9.1 System of Differential Equations

Let us take the expressions for the components of deformation of the median surface of a shell in the following form:

$$\begin{aligned} &\varepsilon_1 = \frac{1}{R}\frac{\partial u}{\partial \alpha}, \qquad \varepsilon_2 = \frac{1}{R}\left(\frac{\partial v}{\partial \beta} + w\right), \qquad \omega = \frac{1}{R}\left(\frac{\partial u}{\partial \beta} + \frac{\partial v}{\partial \alpha}\right), \\ &\chi_1 = -\frac{1}{R^2}\frac{\partial^2 w}{\partial \alpha^2}, \qquad \chi_2 = -\frac{1}{R^2}\frac{\partial^2 w}{\partial \beta^2}, \qquad \chi_1 = -\frac{1}{R^2}\frac{\partial^2 w}{\partial \alpha \partial \beta}. \end{aligned} \tag{3.161}$$

Then the constitutive equations (3.18) can be transformed and written as:

$$\begin{aligned} &N_1 = \frac{1}{R}\sum_{i=1}^{n} d_i c_i^2, \qquad N_2 = \frac{1}{R}\sum_{i=1}^{n} d_i s_i^2, \qquad S = \frac{1}{R}\sum_{i=1}^{n} d_i c_i s_i, \\ &M_1 = \frac{1}{R^2}\sum_{i=1}^{n}\left(p_i c_i^2 + q_i c_i s_i\right), \qquad M_2 = \frac{1}{R^2}\sum_{i=1}^{n}\left(p_i s_i^2 + q_i c_i s_i\right), \\ &H_1 = \frac{1}{R^2}\sum_{i=1}^{n}\left(q_i c_i^2 + p_i c_i s_i\right), \qquad H_2 = -\frac{1}{R^2}\sum_{i=1}^{n}\left(q_i s_i^2 + p_i c_i s_i\right), \end{aligned} \tag{3.162}$$

where $J_{2i} = 0$ and the following notations were used:

$$\begin{aligned} &d_i = K_i\left[c_i^2\frac{\partial u}{\partial \alpha} + s_i^2\left(\frac{\partial v}{\partial \beta} + w\right) + s_i c_i\left(\frac{\partial u}{\partial \beta} + \frac{\partial v}{\partial \alpha}\right)\right], \\ &p_i = I_i\left(c_i^2\frac{\partial^2 w}{\partial \alpha^2} + s_i^2\frac{\partial^2 w}{\partial \beta^2} + \sin 2\varphi_i\frac{\partial^2 w}{\partial \alpha \partial \beta}\right), \\ &p_i = C_i\left[\left(\frac{\partial^2 w}{\partial \alpha^2} - \frac{\partial^2 w}{\partial \beta^2}\right)s_i c_i - \cos 2\varphi_i\frac{\partial^2 w}{\partial \alpha \partial \beta}\right]. \end{aligned} \tag{3.163}$$

Let us write the differential equations of equilibrium for the element of cylindrical shell [59]:

$$\frac{\partial N_1}{\partial \alpha}+\frac{\partial S}{\partial \beta}=-RX, \qquad \frac{\partial N_2}{\partial \beta}+\frac{\partial S}{\partial \alpha}=-RY, \qquad -N_2+\frac{\partial Q_1}{\partial \alpha}+\frac{\partial Q_2}{\partial \beta}=-RZ,$$
$$\frac{\partial H_1}{\partial \alpha}+\frac{\partial M_2}{\partial \beta}=-RQ_2, \quad \frac{\partial H_2}{\partial \beta}+\frac{\partial M_1}{\partial \alpha}=-RQ_1. \tag{3.164}$$

The terms K_i, I_i, C_i, φ_i, in the further derivations are considered to be constant but may have different values for different indices i. From the last two equations of the (3.164), taking into account formulae (3.162), obtain:

$$Q_1=-\frac{1}{R^3}\sum_{i=1}^{n}\left\{c_i^4 I_i\left[c_i^2\frac{\partial^3 w}{\partial \alpha^3}+3\mathrm{tg}\varphi_i\frac{\partial^3 w}{\partial \alpha^2\partial \beta}+3\mathrm{tg}^2\varphi_i\frac{\partial^3 w}{\partial \alpha\partial \beta^2}+\mathrm{tg}^3\varphi_i\frac{\partial^3 w}{\partial \beta^3}\right]+\right.$$
$$\left.+C_i\left(c_i^2 s_i^2\frac{\partial^3 w}{\partial \alpha^3}+c_i s_i\left(3s_i^2-1\right)\frac{\partial^3 w}{\partial \alpha^2\partial \beta}+s_i^2\left(1-3c_i^2\right)\frac{\partial^3 w}{\partial \alpha\partial \beta^2}-s_i^3 c_i\frac{\partial^3 w}{\partial \beta^3}\right)\right\},$$
$$Q_2=-\frac{1}{R^3}\sum_{i=1}^{n}\left\{s_i c_i^3 I_i\left[c_i^2\frac{\partial^3 w}{\partial \alpha^3}+3\mathrm{tg}\varphi_i\frac{\partial^3 w}{\partial \alpha^2\partial \beta}+3\mathrm{tg}^2\varphi_i\frac{\partial^3 w}{\partial \alpha\partial \beta^2}+\mathrm{tg}^3\varphi_i\frac{\partial^3 w}{\partial \beta^3}\right]-\right. \tag{3.165}$$
$$\left.-C_i\mathrm{ctg}\varphi_i\left(c_i^2 s_i^2\frac{\partial^3 w}{\partial \alpha^3}+c_i s_i\left(3s_i^2-1\right)\frac{\partial^3 w}{\partial \alpha^2\partial \beta}+s_i^2\left(1-3c_i^2\right)\frac{\partial^3 w}{\partial \alpha\partial \beta^2}-s_i^3 c_i\frac{\partial^3 w}{\partial \beta^3}\right)\right\}.$$

Substituting the values of terms (3.162) and (3.165) into the first three equations of system (3.164), obtain the following system of differential equations of equilibrium in terms of displacements:

$$\begin{aligned} L_{11}(u)+L_{12}(v)+L_{13}(w)&=-R^2X,\\ L_{21}(u)+L_{22}(v)+L_{23}(w)&=-R^2Y,\\ L_{31}(u)+L_{32}(v)+L_{33}(w)&=-R^2Z, \end{aligned} \tag{3.166}$$

where differential operators L_{ij} are given:

$$L_{11}=\sum_{i=1}^{n}c_i{}^4K_iL_i, \qquad L_{12}=\sum_{i=1}^{n}s_ic_i{}^3K_iL_i,$$
$$L_{13}=\sum_{i=1}^{n}s_i{}^2c_i{}^2K_i\left(\frac{\partial}{\partial \alpha}+\mathrm{tg}\varphi_i\frac{\partial}{\partial \beta}\right),$$
$$L_{22}=\sum_{i=1}^{n}s_i{}^2c_i{}^2K_iL_i, \qquad L_{23}=\sum_{i=1}^{n}s_i{}^3c_iK_i\left(\frac{\partial}{\partial \alpha}+\mathrm{tg}\varphi_i\frac{\partial}{\partial \beta}\right),$$
$$L_3=\sum_{i=1}^{n}K_i\left\{r_{1i}{}^2c_i{}^4\left(\frac{\partial^4}{\partial \alpha^4}+4\mathrm{tg}\varphi_i\frac{\partial^4}{\partial \alpha^3\partial \beta}+6\mathrm{tg}^2\varphi_i\frac{\partial^4}{\partial \alpha^2\partial \beta^2}+4\mathrm{tg}^3\varphi_i\frac{\partial^4}{\partial \alpha\partial \beta^3}+\right.\right. \tag{3.167}$$
$$\left.+\mathrm{tg}^4\varphi_i\frac{\partial^4}{\partial \beta^4}\right)+r_{3i}{}^2\left[s_i{}^2c_i{}^2\left(\frac{\partial^4}{\partial \alpha^4}+\frac{\partial^4}{\partial \beta^4}\right)+\sin 2\varphi_i\left(2s_i{}^2-1\right)\frac{\partial^2}{\partial \alpha\partial \beta}\left(\frac{\partial^2}{\partial \alpha^2}-\frac{\partial^2}{\partial \beta^2}\right)+\right.$$
$$\left.\left.+\left(1-6s_i{}^2c_i{}^2\right)\frac{\partial^4}{\partial \alpha^2\partial \beta^2}\right]+s_i{}^4\right\} \qquad (L_{ik}=L_{ki}),$$

where

$$L_i = \frac{\partial^2}{\partial\alpha^2} + 2\mathrm{tg}\varphi_i \frac{\partial^2}{\partial\alpha\partial\beta} + \mathrm{tg}^2\varphi_i \frac{\partial^2}{\partial\beta^2},$$
$$r_{1i}^{\ 2} = J_{1i}/R^2 F_i, \qquad r_{3i}^{\ 2} = G_i J_{3i}/R^2 E_i F_i. \tag{3.168}$$

The term r_{1i} is a non-dimensional section radius of inertia of a rib, that belong to the i-th family. The final system of differential equations (3.166) is symmetric. For a grid plate this system splits into two independent systems which correspond to the plane and bending problems (in this case the following values must be taken: $x = R\alpha$, $y = R\beta$, $R \to \infty$).

3.9.2 Cylindrical Shell with Rhombic Grid

Let us consider a cylindrical shell with a rhombic grid (n=2) comprised of the same rib members. Let us take one of the diagonals of a rhombic unit cell to be coincident with the generating line of the median surface of a shell ($\varphi_1 = \varphi$, $\varphi_2 = -\varphi$). The torsional stiffness of the ribs comprising the grid is neglected: $J_{3i} = 0$ (i=1, 2). In this case from the formulae (3.162), (3.165) we obtain

$$\begin{aligned}
N_1 &= N_2\mathrm{ctg}^2\varphi = \frac{2Kc^2}{R}\left[c^2\frac{\partial u}{\partial\alpha} + s^2\left(\frac{\partial v}{\partial\beta} + w\right)\right],\\
S &= \frac{2Ks^2c^2}{R}\left(\frac{\partial u}{\partial\beta} + \frac{\partial v}{\partial\alpha}\right),\\
H &= -\frac{4Is^2c^2}{R^2}\frac{\partial^2 w}{\partial\alpha\partial\beta},\\
M_1 &= M_2\mathrm{ctg}^2\varphi = \frac{2Ic^2}{R^2}\left(c^2\frac{\partial^2 w}{\partial\alpha^2} + s^2\frac{\partial^2 w}{\partial\beta^2}\right),\\
Q_1 &= -\frac{2Ic^2}{R^3}\left(c^2\frac{\partial^3 w}{\partial\alpha^3} + 3s^2\frac{\partial^3 w}{\partial\alpha\partial\beta^2}\right),\\
Q_2 &= -\frac{2Ic^2}{R^3}\left(3c^2\frac{\partial^3 w}{\partial\alpha^2\partial\beta} + s^2\frac{\partial^3 w}{\partial\beta^3}\right).
\end{aligned} \tag{3.169}$$

The system of differential equations (3.166) now transforms into

$$
\begin{aligned}
&\frac{\partial^2 u}{\partial \alpha^2}\operatorname{ctg}^2\varphi+\frac{\partial^2 u}{\partial \beta^2}+2\frac{\partial^2 v}{\partial \alpha\partial \beta}+\frac{\partial w}{\partial \alpha}=-\frac{2R^2X}{K\sin^2 2\varphi},\\
&2\frac{\partial^2 u}{\partial \alpha\partial \beta}+\frac{\partial^2 v}{\partial \alpha^2}+\frac{\partial^2 v}{\partial \beta^2}\operatorname{tg}^2\varphi+\frac{\partial w}{\partial \beta}\operatorname{tg}^2\varphi=-\frac{2R^2Y}{K\sin^2 2\varphi},\\
&\frac{\partial u}{\partial \alpha}+\frac{\partial v}{\partial \beta}\operatorname{tg}^2\varphi+\left(\frac{\partial^4 w}{\partial \alpha^4}\operatorname{ctg}^2\varphi+6\frac{\partial^4 w}{\partial \alpha^2\partial \beta^2}+\frac{\partial^4 w}{\partial \beta^4}\operatorname{tg}^2\varphi\right)r_1^{\,2}+\\
&+w\operatorname{tg}^2\varphi=\frac{2R^2Z}{K\sin^2 2\varphi}.
\end{aligned}
\tag{3.170}
$$

The solution of the problem in the case of a rhombic grid shell (arbitrary angle φ of a unit cell) can also be applied to the case of a shell with a square unit cell ($\varphi=\pi/4$), for a certain reduced length of the shell and dummy surface loading. Some transformations must be carried out to allow this.

The following notations are used in the further derivations:

$$
\begin{aligned}
&\xi=\alpha\operatorname{tg}\varphi, \qquad u_*=u\operatorname{ctg}\varphi,\\
&X=4s^3cX_*, \quad Y=4s^4Y_*, \qquad Z=4s^4Z_*.
\end{aligned}
\tag{3.171}
$$

Substituting the notations (3.171) into the system (3.170) obtain:

$$
\begin{aligned}
&\frac{\partial^2 u_*}{\partial \xi^2}+\frac{\partial^2 u_*}{\partial \beta^2}+2\frac{\partial^2 v}{\partial \xi\partial \beta}+\frac{\partial w}{\partial \xi}=-\frac{2R^2X_*}{K},\\
&2\frac{\partial^2 u_*}{\partial \xi\partial \beta}+\frac{\partial^2 v}{\partial \xi^2}+\frac{\partial^2 v}{\partial \beta^2}+\frac{\partial w}{\partial \beta}=-\frac{2R^2Y_*}{K},\\
&\frac{\partial u_*}{\partial \xi}+\frac{\partial v}{\partial \beta}+\left(\frac{\partial^4 w}{\partial \xi^4}+6\frac{\partial^4 w}{\partial \xi^2\partial \beta^2}+\frac{\partial^4 w}{\partial \beta^4}\right)r_1^{\,2}+w=\frac{2R^2Z_*}{K}.
\end{aligned}
\tag{3.172}
$$

It is important to mention that functions u_*, v, w are linked to co-ordinates ξ, β (subjected to the load components X_*, Y_*, Z_*) by the same differential relations as u, v, w to the co-ordinates α, β (subjected to the load components X, Y, Z) for the case of a square unit cell. This can be clearly seen if the system of differential equations (3.172) for the shell with a rhombic cell are compared to the system of differential equations for the shell with a square cell. The latter is obtained from equation (3.170) for $\varphi=\pi/4$,

$$\frac{\partial^2 u}{\partial \alpha^2}+\frac{\partial^2 u}{\partial \beta^2}+2\frac{\partial^2 v}{\partial \alpha \partial \beta}+\frac{\partial w}{\partial \alpha}=-\frac{2R^2 X}{K},$$
$$2\frac{\partial^2 u}{\partial \alpha \partial \beta}+\frac{\partial^2 v}{\partial \alpha^2}+\frac{\partial^2 v}{\partial \beta^2}+\frac{\partial w}{\partial \beta}=-\frac{2R^2 Y}{K}, \tag{3.173}$$
$$\frac{\partial u}{\partial \alpha}+\frac{\partial v}{\partial \beta}+\left(\frac{\partial^4 w}{\partial \alpha^4}+6\frac{\partial^4 w}{\partial \alpha^2 \partial \beta^2}+\frac{\partial^4 w}{\partial \beta^4}\right)r_1^2+w=\frac{2R^2 Z}{K}.$$

The formulae (3.169) for the cylindrical shell with a square grid ($\varphi=\pi/4$) are transformed into:

$$N=N_1=N_2=\frac{K}{2R}\left(\frac{\partial u}{\partial \alpha}+\frac{\partial v}{\partial \beta}+w\right),$$
$$S=\frac{K}{2R}\left(\frac{\partial u}{\partial \beta}+\frac{\partial v}{\partial \alpha}\right),$$
$$H=-\frac{I}{R^2}\frac{\partial^2 w}{\partial \alpha \partial \beta}, \tag{3.174}$$
$$M=M_1=M_2=\frac{I}{2R^2}\left(\frac{\partial^2 w}{\partial \alpha^2}+\frac{\partial^2 w}{\partial \beta^2}\right),$$
$$Q_1=\frac{I}{2R^3}\left(\frac{\partial^3 w}{\partial \alpha^3}+3\frac{\partial^3 w}{\partial \alpha \partial \beta^2}\right),\quad Q_2=-\frac{I}{2R^3}\left(3\frac{\partial^3 w}{\partial \alpha^2 \partial \beta}+\frac{\partial^3 w}{\partial \beta^3}\right).$$

The formulae (3.171) for the shell with a rhombic unit cell can be written in the following form:

$$\begin{aligned} N_1&=N_2\mathrm{ctg}^2\varphi=N_*\sin^2 2\varphi, & S&=4S_* s^3 c,\\ M_1&=M_2\mathrm{ctg}^2\varphi=M_*\sin^2 2\varphi, & H&=4H_* s^3 c,\\ Q_1&=4Q_{1*}s^3 c, & Q_2&=4Q_{2*}s^4. \end{aligned} \tag{3.175}$$

The expressions for N_*, S_*, M_*, H_*, Q_{1*}, Q_{2*} are obtained from (3.174) by substituting α and u with ξ and u_* respectively.

The relationships (3.171) and (3.175) allow a transition from the boundary conditions prescribed for a shell with a rhombic unit cell to the boundary conditions for equivalent shell with a square unit cell to be made. In other words, to analyse a shell with a rhombic unit cell and a length l, subjected to the load X, Y, Z and continuous boundary conditions, it is sufficient to analyse a shell with a square grid with a reduced length $l_*=l\,\mathrm{tg}\varphi$ and a surface loading X_*, Y_*, Z_* for the same boundary

conditions. Then the values of the forces and moments are recalculated using (3.175) and applying

$$u = u_* \mathrm{tg}\varphi, \qquad \alpha = \xi \mathrm{ctg}\varphi. \tag{3.176}$$

The described method allows the simplification of the further analyses of grid shells with two families by considering only a cylindrical shell with a square unit cell.

3.9.3 Cylindrical Shell with a Square Unit Cell

3.9.3.1 Introduction of Resolving Function

In the case of homogeneous problem $(X = Y = Z \equiv 0)$ the system of equations (3.173) can be reduced to a homogeneous differential equation of the eighth order relative to the function $\Phi = \Phi(\alpha, \beta)$:

$$L(\Phi) = 0, \tag{3.177}$$

where L is a differential operator:

$$L = \frac{\partial^8}{\partial\alpha^8} = 4\frac{\partial^8}{\partial\alpha^6\partial\beta^2} - 10\frac{\partial^8}{\partial\alpha^4\partial\beta^4} + 4\frac{\partial^8}{\partial\alpha^2\partial\beta^6} + \frac{\partial^8}{\partial\beta^8}. \tag{3.178}$$

The components of the displacement vector are found using function Φ in the following way:

$$\begin{aligned} u &= \left[\left(\frac{\partial^6}{\partial\alpha^6} + 7\frac{\partial^6}{\partial\alpha^4\partial\beta^2} + 7\frac{\partial^6}{\partial\alpha^2\partial\beta^4} + \frac{\partial^6}{\partial\beta^6}\right) r_1^{\,2} + \frac{\partial^2}{\partial\alpha^2}\right]\Phi, \\ v &= -\left[2r_1^{\,2}\left(\frac{\partial^6}{\partial\alpha^5\partial\beta} + 6\frac{\partial^6}{\partial\alpha^3\partial\beta^3} + \frac{\partial^6}{\partial\alpha\partial\beta^5}\right) + \frac{\partial^2}{\partial\alpha\partial\beta}\right]\Phi, \\ w &= \left(\frac{\partial^3}{\partial\alpha\partial\beta^2} - \frac{\partial^3}{\partial\alpha^3}\right)\Phi. \end{aligned} \tag{3.179}$$

Substituting (3.179) into (3.174) we have:

$$
\begin{aligned}
N &= \frac{Kr_1^2}{2R}\left(\frac{\partial^7}{\partial\alpha^7}+5\frac{\partial^7}{\partial\alpha^5\partial\beta^2}-5\frac{\partial^7}{\partial\alpha^3\partial\beta^4}+\frac{\partial^7}{\partial\alpha\partial\beta^6}\right)\Phi,\\
S &= \frac{Kr_1^2}{2R}\left(-\frac{\partial^7}{\partial\alpha^6\partial\beta}-5\frac{\partial^7}{\partial\alpha^4\partial\beta^3}+5\frac{\partial^7}{\partial\alpha^2\partial\beta^5}+\frac{\partial^7}{\partial\beta^7}\right)\Phi,\\
M &= \frac{I}{2R^2}\left(-\frac{\partial^5}{\partial\alpha^5}+\frac{\partial^5}{\partial\alpha\partial\beta^4}\right)\Phi,\\
H &= -\frac{I}{R^2}\left(\frac{\partial^5}{\partial\alpha^2\partial\beta^3}-\frac{\partial^5}{\partial\alpha^4\partial\beta}\right)\Phi,\\
Q_1 &= -\frac{I}{2R^3}\left(-\frac{\partial^6}{\partial\alpha^6}-2\frac{\partial^6}{\partial\alpha^4\partial\beta^2}+3\frac{\partial^6}{\partial\alpha^2\partial\beta^4}\right)\Phi,\\
Q_2 &= -\frac{I}{2R^3}\left(-3\frac{\partial^6}{\partial\alpha^5\partial\beta}+2\frac{\partial^6}{\partial\alpha^3\partial\beta^3}+\frac{\partial^6}{\partial\alpha\ \partial\beta^5}\right)\Phi.
\end{aligned}
\tag{3.180}
$$

Partial solution of the system of differential equations (3.173) is found in the form of three summands, each of them corresponding to only one component of the surface load X, Y, Z.

1 If $Y = Z \equiv 0$, then the system of equations (3.173) is reduced to one differential equation:

$$L\Phi_x = -(2R^4 / I)X. \tag{3.181}$$

The displacements, linear forces and moments are calculated using formulae (3.179), (3.180), where the function Φ is substituted with Φ_x.

2 If $X = Z \equiv 0$, then resolving equation is

$$L\Phi_y = -(2R^4 / I)Y. \tag{3.182}$$

The components of the displacement vector of any point on the median surface of a shell are

$$
\begin{aligned}
u_y &= -\left[2r_1^2\left(\frac{\partial^6}{\partial\alpha^5\partial\beta}+6\frac{\partial^6}{\partial\alpha^3\partial\beta^3}+\frac{\partial^6}{\partial\alpha\partial\beta^5}\right)+\frac{\partial^2}{\partial\alpha\partial\beta}\right]\Phi_y,\\
v_y &= \left[\left(\frac{\partial^6}{\partial\alpha^6}+7\frac{\partial^6}{\partial\alpha^4\partial\beta^2}+7\frac{\partial^6}{\partial\alpha^2\partial\beta^4}+\frac{\partial^6}{\partial\beta^6}\right)d^2+\frac{\partial^2}{\partial\beta^2}\right]\Phi_y,\\
w_y &= \left(\frac{\partial^3}{\partial\alpha^2\partial\beta}-\frac{\partial^3}{\partial\beta^3}\right)\Phi_y.
\end{aligned}
\tag{3.183}
$$

Then formulae (3.174) for linear forces and moments become

$$
\begin{aligned}
N_y &= \frac{Kr_1^{\,2}}{2R}\left(-\frac{\partial^7}{\partial\alpha^6\partial\beta}-5\frac{\partial^7}{\partial\alpha^4\partial\beta^3}+5\frac{\partial^7}{\partial\alpha^2\partial\beta^5}+\frac{\partial^7}{\partial\beta^7}\right)\Phi_y,\\
S_y &= \frac{Kr_3^{\,2}}{2R}\left(\frac{\partial^7}{\partial\alpha^7}+5\frac{\partial^7}{\partial\alpha^5\partial\beta^2}-5\frac{\partial^7}{\partial\alpha^3\partial\beta^4}-\frac{\partial^7}{\partial\alpha\partial\beta^6}\right)\Phi_y,\\
M_y &= \frac{I}{2R^2}\left(\frac{\partial^5}{\partial\alpha^4\partial\beta}-\frac{\partial^5}{\partial\beta^5}\right)\Phi_y,\\
H_y &= -\frac{I}{R^2}\left(\frac{\partial^5}{\partial\alpha^3\partial\beta^2}-\frac{\partial^5}{\partial\alpha\partial\beta^4}\right)\Phi_y,\\
Q_{1y} &= -\frac{I}{2R^3}\left(\frac{\partial^6}{\partial\alpha^5\partial\beta}+2\frac{\partial^6}{\partial\alpha^3\partial\beta^3}-3\frac{\partial^6}{\partial\alpha\partial\beta^5}\right)\Phi_y,\\
Q_{2y} &= -\frac{I}{2R^3}\left(3\frac{\partial^6}{\partial\alpha^4\partial\beta^2}-2\frac{\partial^6}{\partial\alpha^2\partial\beta^4}-\frac{\partial^6}{\partial\beta^6}\right)\Phi_y.
\end{aligned}
\tag{3.184}
$$

3 If $X = Y \equiv 0$, then this problem reduces to the solution of the following differential equation:

$$
L\Phi_z = \left(2R^4 / I\right)Z. \tag{3.185}
$$

The state of deformation of the considered model is defined by the formulae

$$
\begin{aligned}
u_z &= \left(\frac{\partial^3}{\partial\alpha\partial\beta^2}-\frac{\partial^3}{\partial\alpha^3}\right)\Phi_z,\\
v_z &= \left(\frac{\partial^3}{\partial\alpha^2\partial\beta}-\frac{\partial^3}{\partial\beta^3}\right)\Phi_z,\\
w_z &= \left(\frac{\partial^4}{\partial\alpha^4}-2\frac{\partial^4}{\partial\alpha^2\partial\beta^2}+\frac{\partial^4}{\partial\beta^4}\right)\Phi_z.
\end{aligned}
\tag{3.186}
$$

These formulae as well as relationships (3.174) allow the analysis of the stress state using the following equations:

$$
\begin{aligned}
N_z &= S_z = 0,\ M_z = \frac{I}{2R^2}\left(\frac{\partial^6}{\partial\alpha^6}-\frac{\partial^6}{\partial\alpha^4\partial\beta^2}-\frac{\partial^6}{\partial\alpha^2\partial\beta^4}+\frac{\partial^6}{\partial\beta^6}\right)\Phi_z,\\
H_z &= \frac{I}{R^2}\left(\frac{\partial^6}{\partial\alpha^5\partial\beta}-2\frac{\partial^6}{\partial\alpha^3\partial\beta^3}+\frac{\partial^6}{\partial\alpha\partial\beta^5}\right)\Phi_z,\\
Q_{1z} &= -\frac{I}{2R^3}\left(\frac{\partial^7}{\partial\alpha^7}+\frac{\partial^7}{\partial\alpha^5\partial\beta^2}-5\frac{\partial^7}{\partial\alpha^3\partial\beta^4}+3\frac{\partial^7}{\partial\alpha\partial\beta^6}\right)\Phi_z,\\
Q_{2z} &= -\frac{I}{2R^3}\left(3\frac{\partial^7}{\partial\alpha^6\partial\beta}-5\frac{\partial^7}{\partial\alpha^4\partial\beta^3}+\frac{\partial^7}{\partial\alpha^2\partial\beta^5}+\frac{\partial^7}{\partial\beta^7}\right)\Phi_z.
\end{aligned}
\tag{3.187}
$$

3.10 Equations for the Shell of Revolution

The main relationships and equations for a shell of revolution are discussed in this section. A cylindrical co-ordinate system is used to describe the location of the points on the surface. The expressions for the main radii of curvature of the surface $(R_1,\ R_2)$ and coefficients of the first quadratic form (A,B) are:

$$\begin{aligned} A &= \left(1+r'^2\right)^{1/2}, & B &= r, \\ r''R_1 &= -\left(1+r'^2\right)^{3/2}, & R_2 &= r\left(1+r'^2\right)^{1/2}, \end{aligned} \tag{3.188}$$

where r is the equation of the median surface of a shell.

The angle between the normal to the median surface of a shell and the axis of revolution is:

$$\psi = \arcsin\left(\left(1+r'^2\right)^{-1/2}\right). \tag{3.189}$$

The static equations of the shell theory [94] are:

$$\begin{aligned} &\frac{\partial AN_2}{\partial\beta}+\frac{\partial BS_1}{\partial\alpha}+S_2\frac{\partial B}{\partial\alpha}-N_1\frac{\partial A}{\partial\beta}+AB\left(Q_2k_2+Q_1k_{12}+Y\right)=0,\\ &\frac{\partial BQ_1}{\partial\alpha}+\frac{\partial BQ_2}{\partial\beta}+AB\left(N_1k_1+N_2k_2+S_1k_{12}+S_2k_{12}-Z\right)=0,\\ &\frac{\partial BM_1}{\partial\alpha}+\frac{\partial AH_2}{\partial\beta}+H_1\frac{\partial A}{\partial\beta}+M_2\frac{\partial B}{\partial\beta}-AB\left(Q_1-m_\alpha\right)=0,\\ &\frac{\partial AM_2}{\partial\beta}+\frac{\partial BH_1}{\partial\alpha}+H_2\frac{\partial B}{\partial\alpha}+M_1\frac{\partial A}{\partial\beta}-AB\left(Q_2-m_\beta\right)=0,\\ &S_1-S_2+H_1k_1+H_2k_2+k_{12}\left(M_2-M_1\right)=0. \end{aligned} \tag{3.190}$$

In the case of the linear problems for a shell of revolution, the functions A, B, R_1 and R_2 are independent of the θ co-ordinate. Thus, the static equations transform to:

$$\frac{\partial BN_1}{\partial z}+A\frac{\partial S}{\partial \theta}-N_2\frac{\partial B}{\partial z}+\frac{AB}{R_1}Q_1+ABX=0,$$
$$A\frac{\partial N_2}{\partial \theta}+\frac{\partial B^2 S}{\partial z}+\frac{AB}{R_2}Q_2+ABY=0,$$
$$\frac{\partial BQ_1}{\partial z}+A\frac{\partial Q_2}{\partial \theta}-AB\left(\frac{N_1}{R_1}+\frac{N_2}{R_2}\right)+ABZ=0, \qquad (3.191)$$
$$\frac{\partial BM_1}{\partial z}+A\frac{\partial H_2}{\partial \theta}+\frac{\partial B}{\partial z}M_2-ABQ_1=0,$$
$$-A\frac{\partial M_2}{\partial \theta}+\frac{\partial BH_1}{\partial z}+\frac{\partial B}{\partial z}H_2-ABQ_2=0.$$

Here, the bending stiffness of the ribs in the plane tangential to median surface of a shell are assumed to be equal to zero.

Using geometric equations, the deformation components of the median surface are written as:

$$\varepsilon_1=\frac{1}{A}\frac{\partial u}{\partial z}+k_1 w, \qquad \varepsilon_2=\frac{\partial B}{\partial z}\frac{u}{AB}+\frac{1}{B}\frac{\partial v}{\partial \theta}+k_2 w,$$
$$\omega=\frac{1}{B}\frac{\partial u}{\partial \theta}+\frac{B}{A}\frac{\partial}{\partial z}\left(\frac{v}{B}\right),$$
$$\chi_1=\frac{\partial k_1}{\partial z}\frac{u}{A}-k_1^2 w-\frac{1}{A}\frac{\partial}{\partial z}\left(\frac{1}{A}\frac{\partial w}{\partial z}\right), \qquad (3.192)$$
$$\chi_2=\frac{\partial k_2}{\partial z}\frac{u}{A}-k_2^2 w-\frac{1}{B}\frac{\partial}{\partial \theta}\left(\frac{1}{B}\frac{\partial w}{\partial \theta}\right)-\frac{1}{A^2 B}\frac{\partial B}{\partial z}\frac{\partial w}{\partial z},$$
$$\tau=\left[\frac{1}{B}\frac{\partial u}{\partial \theta}-\frac{B}{A}\frac{\partial}{\partial z}\left(\frac{v}{B}\right)\frac{k_1-k_2}{2}-\frac{1}{AB}\left(\frac{\partial^2 w}{\partial z\partial \theta}-\frac{1}{B}\frac{\partial B}{\partial z}\frac{\partial w}{\partial \theta}\right)\right].$$

The angles of rotation and generalised distributed forces are:

$$\gamma_1=\frac{1}{A}\frac{\partial w}{\partial z}-k_1 u, \qquad \gamma_2=\frac{1}{B}\frac{\partial w}{\partial \theta}-k_2 v,$$
$$Q_{1H}=Q_1+\frac{1}{B}\frac{\partial H_1}{\partial \theta}, \qquad Q_{2H}=Q_2+\frac{1}{B}\frac{\partial H_2}{\partial z}. \qquad (3.193)$$

For the general case of a shell that consists of four families of ribs, we assume that the ribs, which belong to families one and two have the same properties and are made of the same material.

Constitutive equations for a shell with this grid pattern have been derived earlier and are given by (3.31). The reverse calculation of axial forces, bending and twisting moments acting in the ribs of each family can be made from known stress resultants in the homogenised model using (3.63), (3.65).

For convenience further calculations are carried out in the non-dimensional form. The non-dimensional equivalents of the quantities used before are denoted with the superscript *0* are:

$$
\begin{aligned}
&u = R_0 u^0 \left[v,w,B,r,z,a_i \left(i=\overline{1,4}\right)\right], \\
&G = EG^0\left[X,Y,Z,g\right], \quad k_1^0 = R_0 k_1\left[k_2,\chi_{1.},\chi_2,\tau\right], \\
&S = ER_0 S^0\left[N_i,Q_i\right], \qquad M_i = ER_0^2 M_i{}^0\left[H_i\right] \quad \left(i=1,2\right), \\
&F_i = R_0^2 F_i^0, \qquad J_{ji} = R_0^4 J_{ji}^0 \quad \left(j=1,3\right), \\
&N_i^* = ER_0^2 N_{i0} \qquad M_i^* = ER_0^3 M_{i0}\left[H_i^*\right] \quad \left(i=\overline{1,4}\right),
\end{aligned}
\tag{3.194}
$$

where: R_0 is a linear dimension of a shell; g is the distributed surface load. Functions are listed in the square brackets are reduced to non-dimensional form in a similar way as the expression, which preceded it.

The constitutive equations (3.31) for a shell with considered grid pattern in non-dimensional form are:

$$
\begin{aligned}
&N_1^0 = \alpha_{11}\varepsilon_1 + \alpha_{12}\varepsilon_2, \quad N_2^0 = \alpha_{12}\varepsilon_1 + \alpha_{22}\varepsilon_2, \quad S^0 = \alpha_{12}\omega, \\
&M_1^0 = \gamma_{11}\chi_1^0 + \gamma_{12}\chi_2^0, \quad M_2^0 = \gamma_{12}\chi_1^0 + \gamma_{22}\chi_1^0, \\
&H_1^0 = \gamma_{31}\tau^0, \qquad H_2^0 = \gamma_{41}\tau^0.
\end{aligned}
\tag{3.195}
$$

The non-dimensional coefficients entering these formulae are:

$$\alpha_{11}=\frac{2F^0c^4}{a^0}+\frac{F_4^0}{a_4^0},\quad \alpha_{12}=\frac{F^0\sin^2(2\varphi)}{2a^0},\quad \alpha_{22}=\frac{2F^0s^4}{a^0}+\frac{F_3^0}{a_3^0},$$

$$\gamma_{11}=-\left(\frac{2J_1^0c^4}{a^0}+\frac{J_{14}^0}{a_4^0}+\frac{G^0J_3^0\sin^2(2\varphi)}{2a^0}\right),$$

$$\gamma_{12}=-\left(J_1^0-G^0J_3^0\right)\frac{\sin^2(2\varphi)}{2a^0},$$

$$\gamma_{22}=-\left(\frac{2J_1^0s^4}{a^0}+\frac{J_{13}^0}{a_3^0}+\frac{G^0J_3^0\sin^2(2\varphi)}{2a^0}\right), \qquad (3.196)$$

$$\gamma_{31}=\frac{J_1^0\sin^2(2\varphi)}{a^0}+\frac{G^0J_{34}^0}{a_4^0}+\frac{2G^0J_3^0c^2\cos(2\varphi)}{a^0},$$

$$\gamma_{41}=\frac{J_1^0\sin^2(2\varphi)}{a^0}+\frac{G^0J_{33}^0}{a_3^0}+\frac{2G^0J_3^0s^2\cos(2\varphi)}{a^0}.$$

3.11 Axisymmetric Deformations of the Grid Shells

For an axisymmetric state of stress all the unknown stress resultants are the functions the of co-ordinate z only:

$$v = \omega = \tau = \gamma_2 = S = Q_2 = H_1 = H_2 = Y = 0. \tag{3.197}$$

In this case, after certain transformations (3.191) - (3.195), the final system of differential equations in the matrix form can be obtained as:

$$y'(z^0) = P(z^0)y(z^0) + f(z^0), \tag{3.198}$$

where y is the vector of unknown functions:

$$y_1 = u^0, y_2 = w^0, y_3 = \gamma_1, y_4 = N_1^0, y_5 = M_1^0, y_6 = Q_1^0; \tag{3.199}$$

f is a known vector which describes the loading conditions of the shell:

$$f_1 = f_2 = f_3 = f_5 = 0, \qquad f_4 = -AX, \qquad f_6 = -AZ; \tag{3.200}$$

P is a square matrix with known coefficients that are calculated from the stiffness properties and geometric characteristics of the considered shell. Non zero members of the matrix are given:

$$p_{11}=-\frac{\alpha_{12}B^{0'}}{\alpha_{11}B^0},\qquad p_{12}=-\frac{\alpha_{12}mA}{\alpha_{11}B^0},\qquad p_{13}=-A\left(k_1^0+\frac{\alpha_{12}}{\alpha_{11}}k_2^0\right),\qquad p_{21}=-\frac{mA}{B^0},$$

$$p_{22}=\frac{B^{0'}}{B^0},\qquad p_{31}=Ak_1^0,\qquad p_{41}=\frac{\gamma_{11}\psi_0}{\gamma_{12}}+\frac{\alpha_{12}k_1^0B^{0'}}{\alpha_{11}B^0},\qquad p_{34}=A,$$

$$p_{42}=\frac{\alpha_{12}mk_1^0A}{\alpha_{11}B^0},\qquad p_{44}=-\frac{\gamma_{12}B^{0'}}{\gamma_{11}B^0},\qquad p_{43}=A\left(\frac{\gamma_{12}\psi_1}{\gamma_{11}}+\frac{\alpha_{12}}{\alpha_{11}}k_1^0k_2^0\right),\quad p_{45}=-\frac{k_1^0A}{\alpha_{11}},$$

$$p_{51}=\frac{1}{B^{0^2}}\left(\alpha_0\frac{\left(B^{0'}\right)^2}{A}+m^2k_1^0k_2^0\gamma_{31}A\right),\qquad p_{52}=m\alpha_0\frac{B^{0'}}{B^{0^2}},\qquad p_{62}=(\alpha_0-\psi_3)\frac{m^2\psi_2A}{B^{0^2}},$$

$$p_{56}=-\frac{mA}{B^0}\left(1+\frac{k_1^0\gamma_{31}\left(k_1^0-k_2^0\right)}{2\alpha_{12}}\right),\qquad p_{53}=\frac{B^{0'}}{B^0}\left(\alpha_0k_2^0-\frac{\gamma_{31}}{B^{0^2}}m^2k_1^0\right),$$

$$p_{61}=\frac{m\psi_2}{B^{0^2}}\left[\left(\alpha_0-\psi_3-\beta_1k_2^{0^2}\right)B^{0'}-\left(\beta_0+\beta_2\gamma_{31}\right)\psi_0k_2^0B^0-\beta_3k_2^{0^2}\right],$$

$$p_{63}=\frac{m\psi_2k_2^0A}{B^0}\left[\begin{array}{l}\alpha_0+\dfrac{\beta_1\left(B^{0'}\right)^2}{A^2B^{0^2}}+\dfrac{\gamma_{31}\left(B^0\right)''}{A^2B^0}-\psi_1\left(\beta_0+\dfrac{\gamma_{12}\gamma_{31}}{\gamma_{11}}\right)+\\ k_2^0\gamma_{31}\left[k_1^0+\left(k_2^0-k_1^0\right)\dfrac{\alpha_{12}}{\alpha_{11}}\right]+\dfrac{B^{0'}}{A^3B^{0^3}}\left[\gamma_{31}{}'AB^{0^2}-\gamma_{31}B^0\left(A'B^0+2AB^{0'},\right)\right]\end{array}\right],\qquad (3.201)$$

$$p_{64}=\frac{m\psi_2k_2^0}{B^{0^2}}\left[\left(\beta_0-\beta_1+\beta_2\gamma_{31}\right)B^{0'}-\beta_3\right],\qquad p_{65}=\frac{m\psi_2A}{\alpha_{11}B^0}\left[\alpha_{12}\left(k_1^0-k_2^0\right)k_2^0\gamma_{31}\right],$$

$$p_{66}=-\psi_2\left[\frac{2B^{0'}}{B^0}+\left(k_2^{0'}-k_1^{0'}\right)\frac{k_2^0\gamma_{31}}{2\alpha_{12}}+\frac{k_2^0\left(k_2^0-k_1^0\right)}{2\alpha_{12}}\left[\frac{\beta_1B^{0'}}{B^0}+\left(\gamma_{31}{}'-\frac{\gamma_{31}\alpha_{12}{}'}{\alpha_{12}}\right)\right]\right].$$

The solution of this system must satisfy the following boundary conditions:

$$B_0y\left(z^0\right)=b_0\,\text{for}\,z^0=z_0^0,\qquad B_1y\left(z^0\right)=b_1\,\text{for}\,z^0=z_1^0,\qquad (3.202)$$

where B_0 and B_1 are known rectangular matrices; b_0 and b_1 are given column vectors.

The given system of differential equations represents a boundary value problem that can be solved numerically reducing it to the solution of Cauchy problem using the Runge-Kutta method [105].

The rest of the unknowns, which do not enter the system (3.198) must be calculated using the following formulae:

$$N_2^0 = \left(\alpha_{22} - \frac{\alpha_{12}^2}{\alpha_{11}}\right)\left(\frac{B^{0\prime}}{AB^0}u^0 + k_2^0 w^0\right) + \frac{\alpha_{12}}{\alpha_{11}}N_1^0,$$

$$M_2^0 = \left(\gamma_{22} - \frac{\gamma_{12}^2}{\gamma_{11}}\right)\left(\left(k_2^{0\prime} - \frac{B^{0\prime}}{B^0}k_1^0\right)\frac{u^0}{A} - k_2^{0\,2} w^0 - \frac{B^{0\prime}}{AB^0}\gamma_1\right) + \frac{\gamma_{12}}{\gamma_{11}}M_1^0. \qquad (3.203)$$

The calculation of forces in the members with known state of stress is done using formulae (3.63) that were obtained for the case of a plate with the same grid pattern. For calculation of bending and twisting moments in the members of a shell, the expressions (3.65) are used.

3.12 Boundary Effects

The mathematical model described earlier allows calculations to be made for the lattice cylindrical structure subjected to different sets of loading conditions and their combination. Providing a reasonable range of accuracy with the exception of the areas that are in the immediate vicinity of the loaded/constrained regions. For the sake of the improving the accuracy of results in these areas, an approach that takes into account boundary effects is proposed.

3.12.1 Equation of a Simple Boundary

Boundary effects in the grid shells are similar to those in continuous shells. The local state of stress in a shell in the vicinity of the line $(\alpha = \text{const})$ close to the boundary is now analysed. A grid shell with more than two families of ribs is considered. The solution of the stress-strain state of a shell is based on the following conditions:

1. The boundary effect is caused by the distortion of the stress state along the line $(\alpha = \text{const})$. The solution of the system of homogeneous equations in this case is $(X=Y=Z=0)$.
2. Differentiation of any unknown function over the co-ordinate α causes significant growth of this function (3.204) compared to differentiation over the co-ordinate β $(A \approx B \approx R_2)$. This is caused by a quick tapering off of the solution with the increase of the distance from the line $(\alpha = \text{const})$.

$$\left|\frac{\partial^{k+1} f}{\partial \alpha^{k+1}}\right| >> \left|\frac{\partial^{k} f}{\partial \alpha^{k}}\right|. \tag{3.204}$$

3. The direction of the displacement vector for the point on the median surface of a shell is very close to the direction of its normal at this point. In this case the following relationship

$$\left|\frac{\partial u}{\partial \alpha}\right| \approx \left|\frac{\partial v}{\partial \alpha}\right| \approx |w| \tag{3.205}$$

is taking place.

4. The main contribution to the stress state comes from the load N_2:

$$\left|\frac{\partial N_1}{\partial \alpha}\right| \approx \left|\frac{\partial S}{\partial \alpha}\right| \approx |N_2|. \tag{3.206}$$

Considering (3.205) and (3.206), formulae for deformation components of the median surface of a shell are:

$$\begin{aligned} &\varepsilon_1 = \frac{1}{A}\frac{\partial u}{\partial \alpha} + \frac{w}{R_1}, \qquad \varepsilon_2 = \frac{w}{R_2}, \qquad \omega = \frac{1}{A}\frac{\partial v}{\partial \alpha} - \frac{2w}{R_{12}}, \\ &\chi_1 = -\frac{1}{A^2}\frac{\partial^2 w}{\partial \alpha^2}, \qquad |\chi_2| << |\chi_1|, \quad |\tau| << |\chi_1|. \end{aligned} \tag{3.207}$$

The main component of the bending deformation of the median surface of a shell in the case of boundary effect is χ_1. The constitutive equations (3.18) in terms of bending and twisting moments are written as

$$\begin{aligned} &M_1 = -(D_{11} + K_{11})\chi_1, \qquad M_2 = -(D_{12} + K_{11})\chi_1, \\ &H_1 = \left(D_{16} + K_{61}^{(1)}\right)\chi_1, \qquad H_2 = \left(D_{16} + K_{61}^{(2)}\right)\chi_1. \end{aligned} \tag{3.208}$$

Shear forces in this case are

$$Q_1 = -\frac{1}{A}\frac{\partial M_1}{\partial \alpha}, \qquad Q_2 = \frac{1}{A}\frac{\partial H_1}{\partial \alpha}, \tag{3.209}$$

considering equations (3.207), (3.208)

$$Q_1 = -\frac{D_{11} + K_{11}}{A^3}\frac{\partial^3 w}{\partial \alpha^3}, \qquad Q_2 = \frac{D_{16} + K_{61}^{(1)}}{A^3}\frac{\partial^3 w}{\partial \alpha^3}. \tag{3.210}$$

Using the expression for the function ε_2 that enters equations (3.38), using (3.206) and taking into account $a_{22} \neq 0$ we have

$$\varepsilon_{22} = a_{22} N_{22}. \tag{3.211}$$

Considering (3.207),

$$N_2 = \frac{w}{a_{22} R_{22}}. \tag{3.212}$$

Equations (3.206) and (3.210) in conjunction with static equations allow another expression for N_2 to be obtained:

$$N_2 = -\frac{(D_{11} + K_{11})R_2}{A^4}\frac{\partial^4 w}{\partial \alpha^4}. \tag{3.213}$$

After equating the right sides of (3.212) and (3.213), the following equation of a simple boundary effect can be obtained:

$$\frac{\partial^4 w}{\partial \alpha^4} + \frac{A^4}{a_{22}R_{22}^2(D_{11} + K_{11})}w = 0. \tag{3.214}$$

Now formulae (3.208) for bending and twisting moments incorporating (3.207) are:

$$\begin{aligned} M_1 &= \frac{D_{11} + K_{11}}{A^2}\frac{\partial^2 w}{\partial \alpha^2}, & M_2 &= \frac{D_{12} - K_{11}}{A^3}\frac{\partial^2 w}{\partial \alpha^2}, \\ H_1 &= -\frac{D_{16} - K_{61}^{(1)}}{A^2}\frac{\partial^2 w}{\partial \alpha^2}, & H_2 &= -\frac{D_{16} + K_{61}^{(2)}}{A^2}\frac{\partial^2 w}{\partial \alpha^2}. \end{aligned} \tag{3.215}$$

The obtained formulae (3.210), (3.213) and (3.215) allow all the unknown functions of the stress state for a grid shell to be calculated.

3.12.2 Integration of the Boundary Effect

Let us consider that the distortion line of the stress state coincides with the co-ordinate line $\alpha = \alpha_*$.

The stress-strain state of a shell for the case of the boundary effect is localised in the vicinity of this line. All the coefficients in the obtained formulae are functions of co-ordinate β only and are equal to their values for $\alpha = \alpha_*$. In this case the coefficients of the equation of the boundary effect (3.214) do not depend on α. The solution of the equation (3.214) for the case of $\alpha \le \alpha_*$ is:

$$\begin{aligned} w &= (\psi_1 c_0 + \psi_2 s_0)E^+, \\ \gamma_1 &\approx \frac{\partial w}{\partial \alpha}\left[(\psi_1 + \psi_2)c_0 + (\psi_2 - \psi_1)s_0\right]gE^+, \\ N_2 &= N_2^0(\psi_1 c_0 + \psi_2 s_0)E^+, \\ Q_i &= Q_i^0\left[(\psi_1 - \psi_2)c_0 + (\psi_1 + \psi_2)s_0\right]E^+, \\ M_i &= M_i^0(\psi_2 c_0 - \psi_1 s_0)E^+, \\ H_i &= H_i^0(\psi_1 s_0 - \psi_2 c_0)E^+ \qquad (i = 1, 2). \end{aligned} \tag{3.216}$$

The notations in the formulae (3.216) are:

$$
\begin{aligned}
&s_0 = \sin g(\alpha - \alpha_*), \qquad c_0 = \cos g(\alpha - \alpha_*),\\
&E^+ = e^{g(\alpha-\alpha_*)}, \qquad E^- = e^{-g(\alpha-\alpha_*)},\\
&g = \frac{A}{\sqrt{R_2}\sqrt[4]{4(D_{11}+K_{11})a_{22}}},\\
&N_2^0 = \frac{1}{a_{22}R_2}, \qquad Q_1^0 = \frac{A}{2ga_{22}R_2^2}, \qquad Q_2^0 = \frac{D_{16}-K_{61}^{(1)}}{D_{11}+K_{11}}Q_1^0,\\
&M_1^0 = 2g^2A^{-2}(D_{11}+K_{11}), \qquad M_2^0 = 2g^2A^{-2}(D_{12}+K_{11}),\\
&H_1^0 = 2g^2A^{-2}\left(D_{16}+K_{61}^{(1)}\right), \qquad H_2^0 = 2g^2A^{-2}\left(D_{16}+K_{61}^{(2)}\right).
\end{aligned}
\tag{3.217}
$$

In these formulae $\psi_i\ \left(\overline{1,4}\right)$ are arbitrary functions of the co-ordinate β. They can be determined from the boundary conditions at $\alpha = \alpha_*$.

3.12.3 Simple Boundary Effect for a Shell of Revolution Subjected to Axisymmetric Loading

The solution for the boundary effect in the vicinity of the distortion line of the stress state is determined by the main state of the stress and nontangential boundary conditions. Addition of the solution part for the boundary effect to the conventional solution violates the tangential boundary conditions. The proposed approach allows nontangential boundary conditions to be considered without violating tangential boundary conditions.

Let us introduce a rigid body displacement of a shell along its axis of revolution.

For an orthotropic grid shell we have:

$$
\frac{C_{11}}{A}\frac{\partial u}{\partial \alpha} + (C_{11}k_1 + C_{12}k_2)w = 0. \tag{3.218}
$$

After the integration of this equation and considering formulae (3.216) for w it can be found that:

$$
u = -\frac{A}{2g}\left(\frac{1}{R_1} + \frac{C_{12}}{R_2C_{11}}\right)\left[(\psi_1 - \psi_2)c_0 + (\psi_1 + \psi_2)s_0\right]E^+. \tag{3.219}
$$

Writing the components of the displacement vector of the median surface as a sum of three terms:

$$
u = u_1 + u_2 - C\sin\psi, \qquad w = w_1 + w_2 - C\cos\psi, \tag{3.220}
$$

where u_1, w_1 are conventional solutions of the problem, u_2, w_2 are solutions of the simple boundary effect, C is a rigid body displacement of a shell in the direction of the outer normal to the median surface, ψ is the angle between the normal to the median surface of a shell and the axis of revolution.

Functions u_1, w_1 are considered known from the solution of the boundary value problem subjected to a set of tangential boundary conditions.

Lets consider the case when one of the edges of a shell is fixed at $\alpha = \alpha_*$. The boundary conditions in this case are:

$$u = w = \gamma_1 = 0 \qquad \text{at} \qquad \alpha = \alpha_*. \tag{3.221}$$

Taking into account (3.219), (3.220), the boundary conditions (3.221) can be rewritten as

$$u_2 - C\sin\psi = w = \gamma_1 = 0 \qquad \text{at} \qquad \alpha = \alpha_*. \tag{3.222}$$

Substituting (3.219), (3.220) and (3.216) into the boundary conditions (3.222), the following system of three equations for unknowns ψ_1, ψ_2, C can be obtained:

$$\begin{aligned} &\frac{A}{2g}\left(\frac{1}{R_1}+\frac{C_{12}}{R_2C_{11}}\right)(\psi_1-\psi_2)+C\sin\psi_* = 0, \\ &w(\alpha_*)+\psi_1+C\cos\psi_* = 0, \qquad \psi_1+\psi_2 = 0. \end{aligned} \tag{3.223}$$

In the system (3.223) all the functions are calculated for $\alpha = \alpha_*$ and $\psi_* = \psi(\alpha_*)$.

The solution of this system is

$$\psi_1 = -\frac{2w_1(\alpha_*)}{2-\varepsilon\,\mathrm{ctg}\,\psi_*}, \quad \psi_2 = 0 \qquad C = \frac{\varepsilon w_1(\alpha_*)}{2\sin\psi_* - \varepsilon\cos\psi_*}, \tag{3.224}$$

where

$$\varepsilon = \frac{A}{g}\left(\frac{1}{R_1}+\frac{C_{12}}{R_2C_{11}}\right). \tag{3.225}$$

3.13 Conclusions

In this chapter a new approach has been developed. This approach is shown to be more efficient when applied to the design/optimisation of lattice structures than the Equivalent Stiffness Method (which is quite effective in simple static analysis).

Constitutive equations are developed and the expressions for the components of stress and strain tensors are derived for the following cases:

1. **Plane problem:**

   Lattice plates with two, three and four families of ribs loaded in-plane and transverse to the plane.

2. **Shell of revolution:**

   Cylindrical shells with different lattice patterns. The cases of axisymmetric deformation and boundary effect are considered.

The models for the cylindrical lattice shells were realised in computer code using symbolic computation. Numeric verification of the mathematical models is given in the next chapter.

An advantage of the new homogenisation approach is the ability to calculate structural stress resultants without performing FEM analysis. This allows higher computational efficiency to be achieved. Also this approach allows more design variables to be assigned in the further optimisation analyses.

4 Numerical Verification of the Mathematical Model.

Numerical implementation of the proposed homogenisation approach was performed using the general-purpose symbolic computation package *Mathematica* [117]. A list of the *Mathematica* code used for the solution of the problem described above, is presented in the Appendix 2

This code solves the problem in the following steps:

1. Calculation of the equivalent stiffness parameters.
2. Analytical solution of the boundary value problem (system of six governing differential equations (3.198)).
3. Calculation of the homogenised stress resultants.
4. Conversion of the homogenised stress resultants to the stress resultants in the members of two diagonal and one vertical families of ribs.
5. Subsequent calculation of the failure coefficients.
6. Analytical derivation of the objective function.
7. Maximisation of the objective function.

Using the method outlined in the Chapter 3, numerical results are obtained for the isogrid cylindrical structure with the geometric parameters given for the ribs (Table 2.2) and the cell configuration shown on the structure (Figure 2.5), subjected to combined tension and torsional loading. Surfaces of optimisation are shown in Figure 5.5-Figure 5.12, and the optimal values for the critical load and optimal design parameters are given in Table 5.2-Table 5.4. Results presented here are given for the model that neglects the influence of the boundary effects on the general state of the stress. The contribution of the boundary effect will be discussed and implemented in the further chapters. The obtained results are compared to the solution of the same problem using the Finite Element Method, using the commercial FEM code *MSC/NASTRAN*. The stress (axial force, moments, etc.) distribution in the structural members of the different families is shown in Figure 4.1- Figure 4.16.

In order to verify its validity, the developed mathematical model was analysed and the results obtained were compared to the exact FEM solution. The following load cases were considered:

4.1 Uniaxial Tension.

The load has been applied to the top edge of the isogrid cylinder as a uniformly distributed load 10^6 N/m.

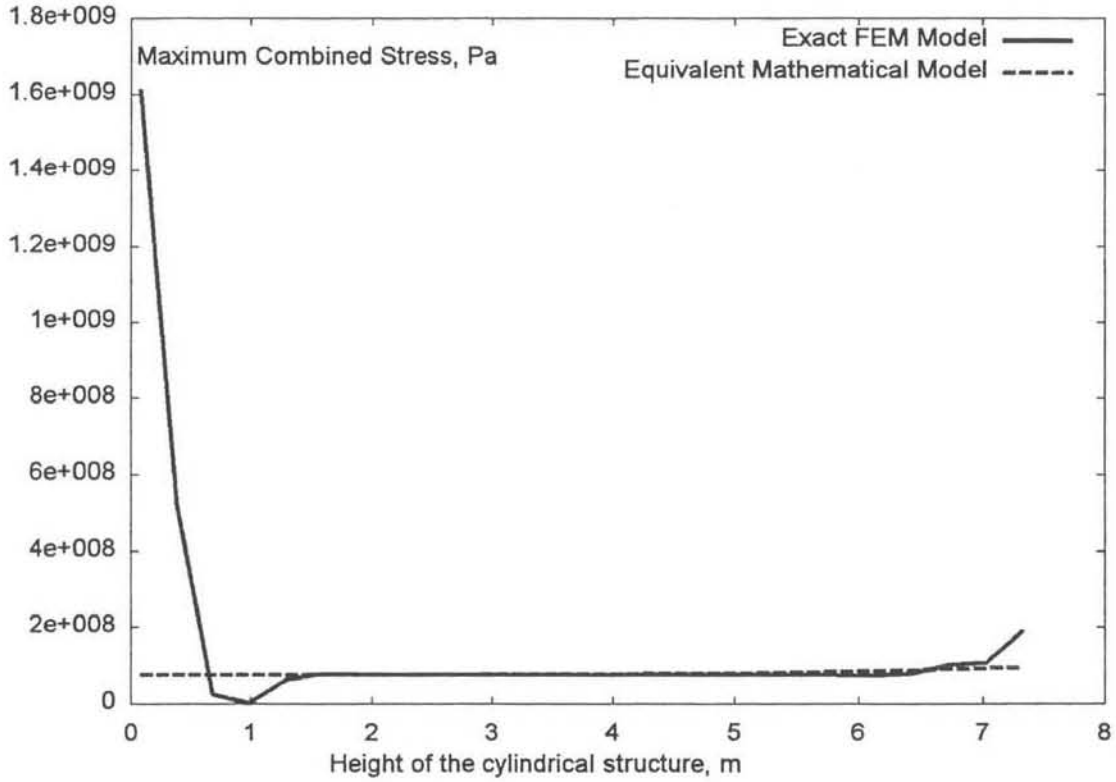

Figure 4.1 Maximum combined stress for the diagonal family of ribs

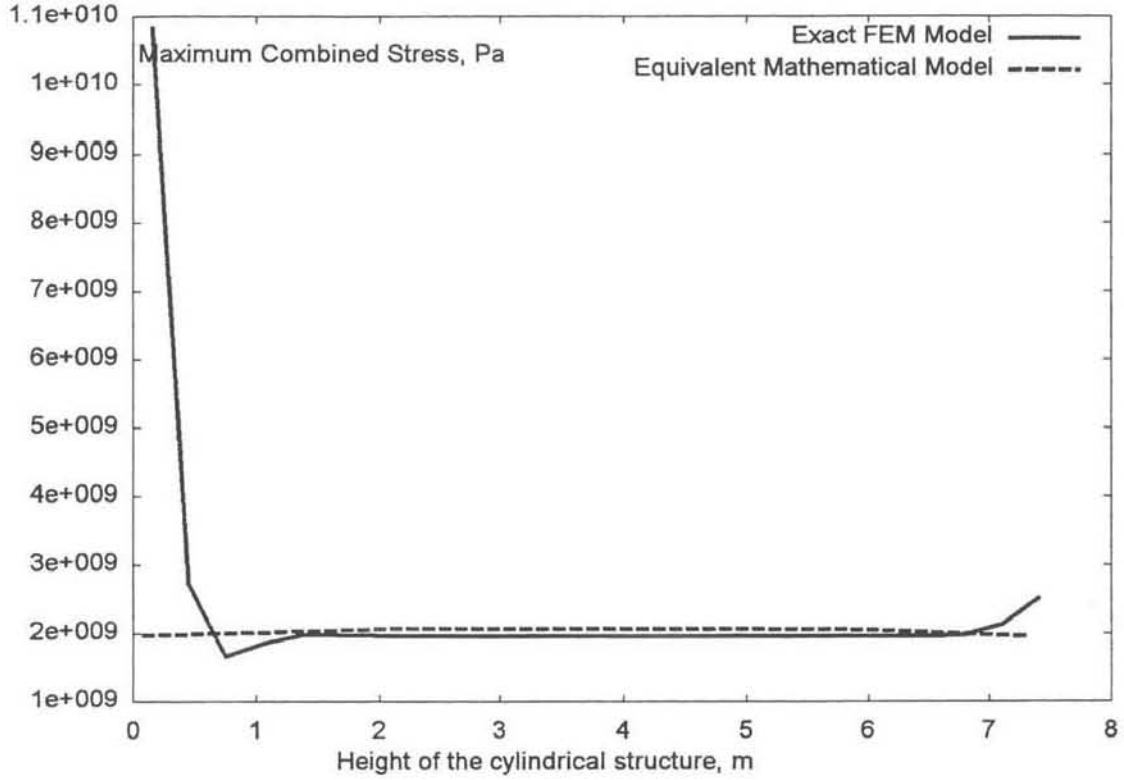

Figure 4.2 Maximum combined stress for the vertical family of ribs

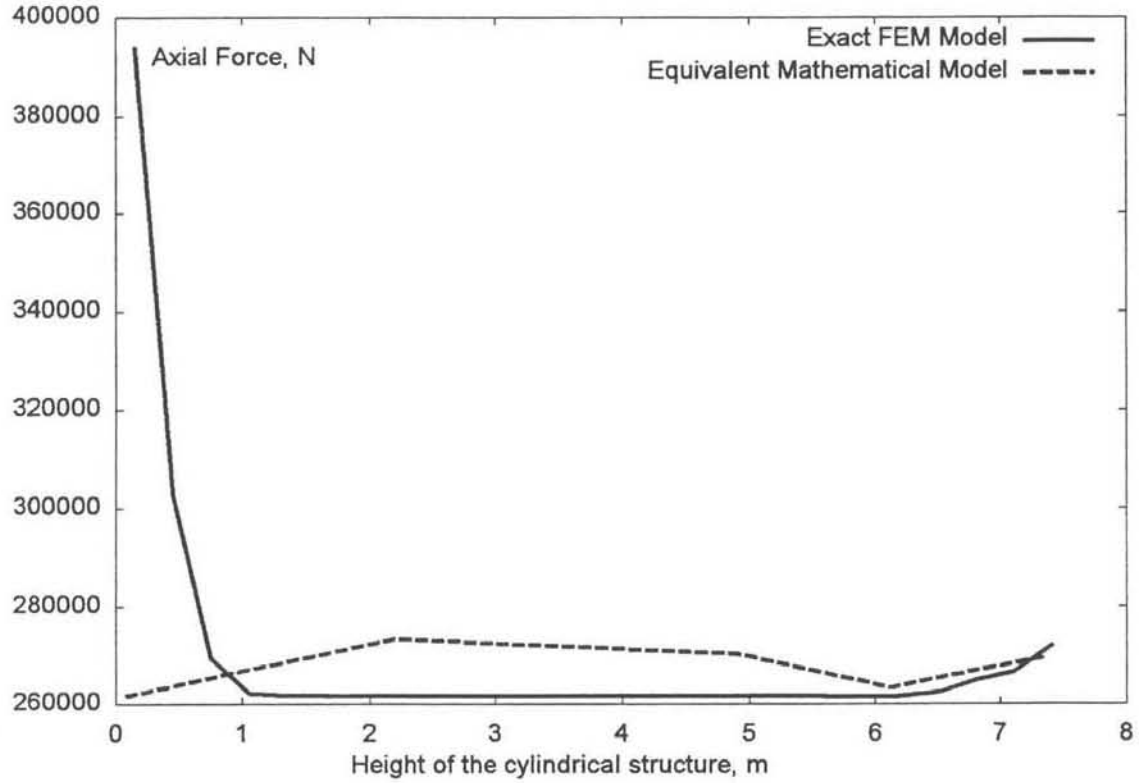

Figure 4.3 Axial force for the vertical family of ribs

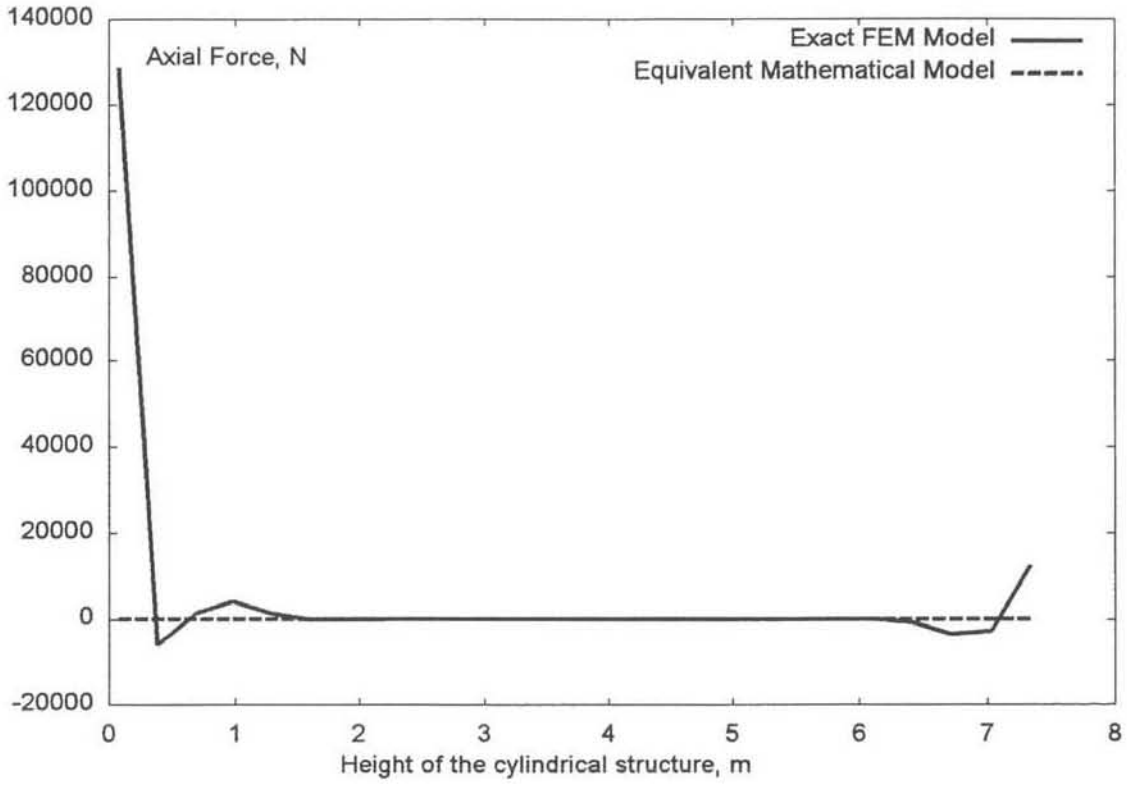

Figure 4.4 Axial force for the vertical family of ribs

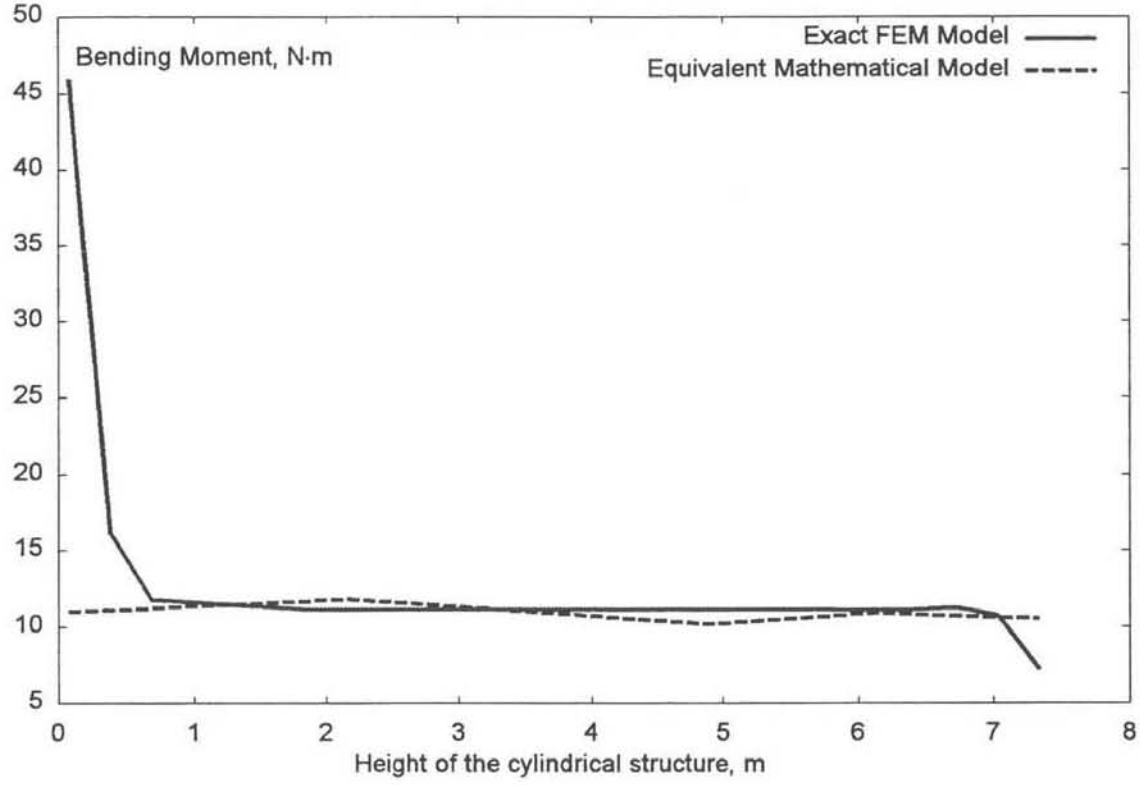

Figure 4.5 Bending moment M1 for the diagonal family of ribs

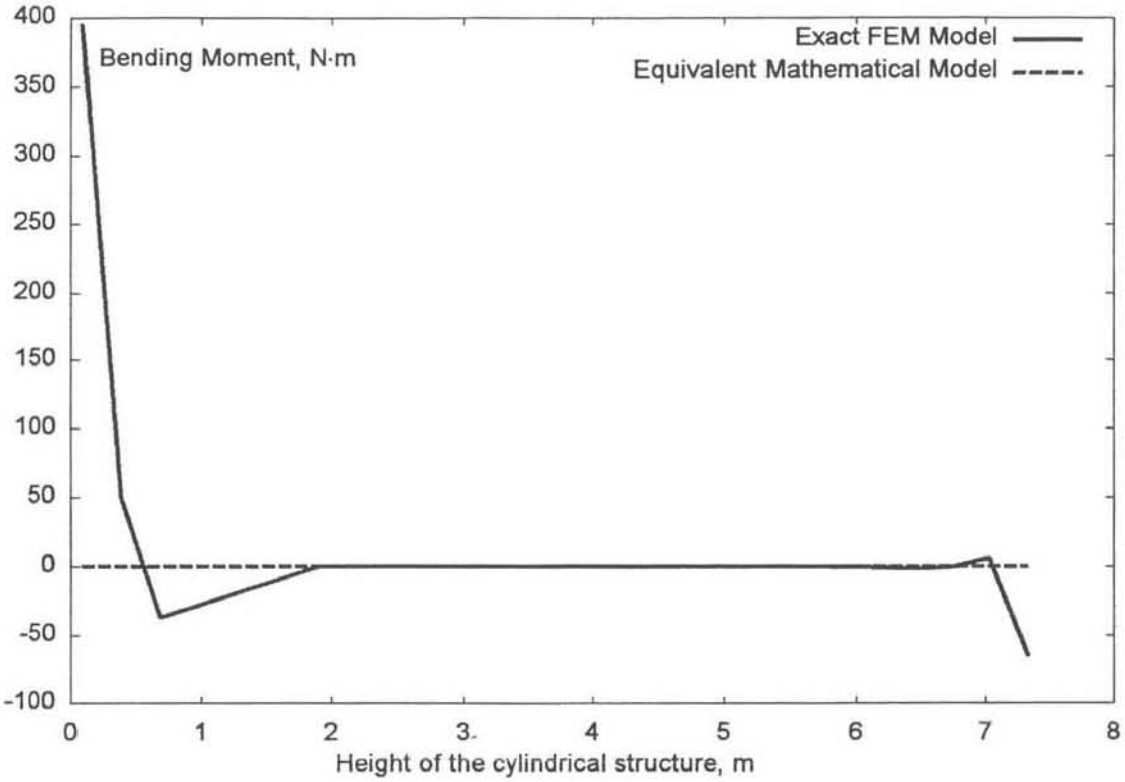

Figure 4.6 Bending moment M2 for the diagonal family of ribs

4.1.1 Torsion.

The torque load has been applied as an uniformly distributed equivalent force 10^5 N/m in the hoop direction.

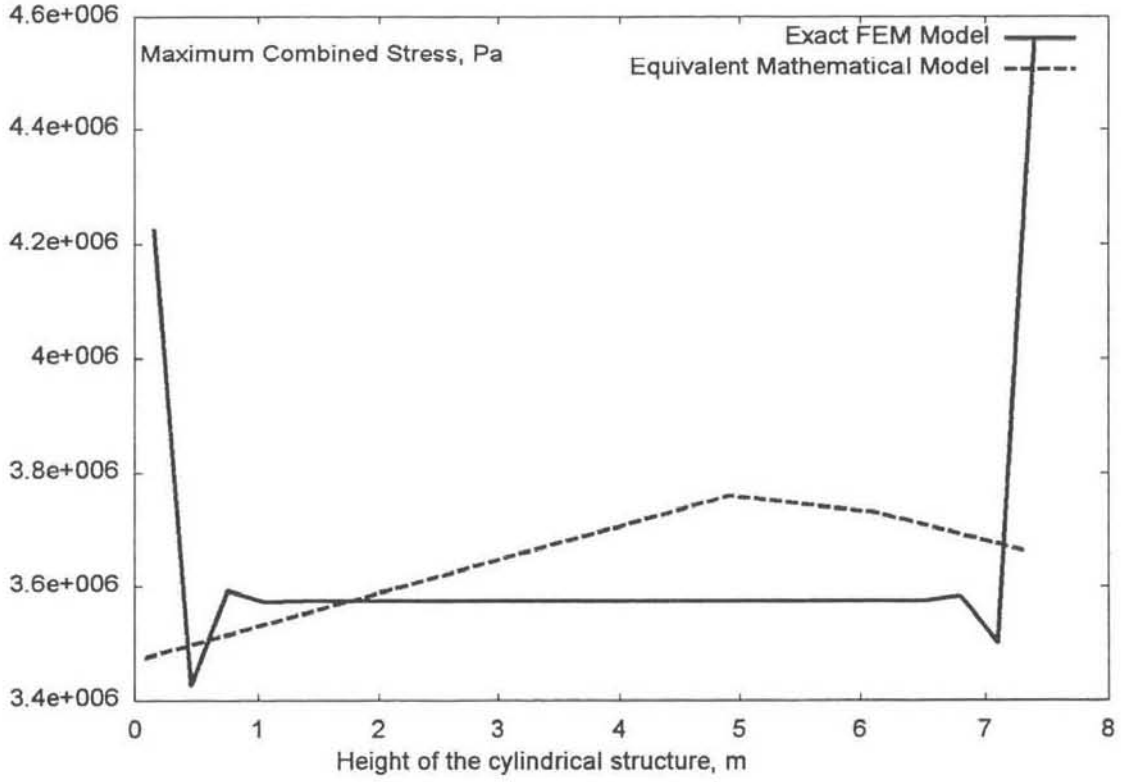

Figure 4.7 Maximum combined stress for the vertical family of ribs

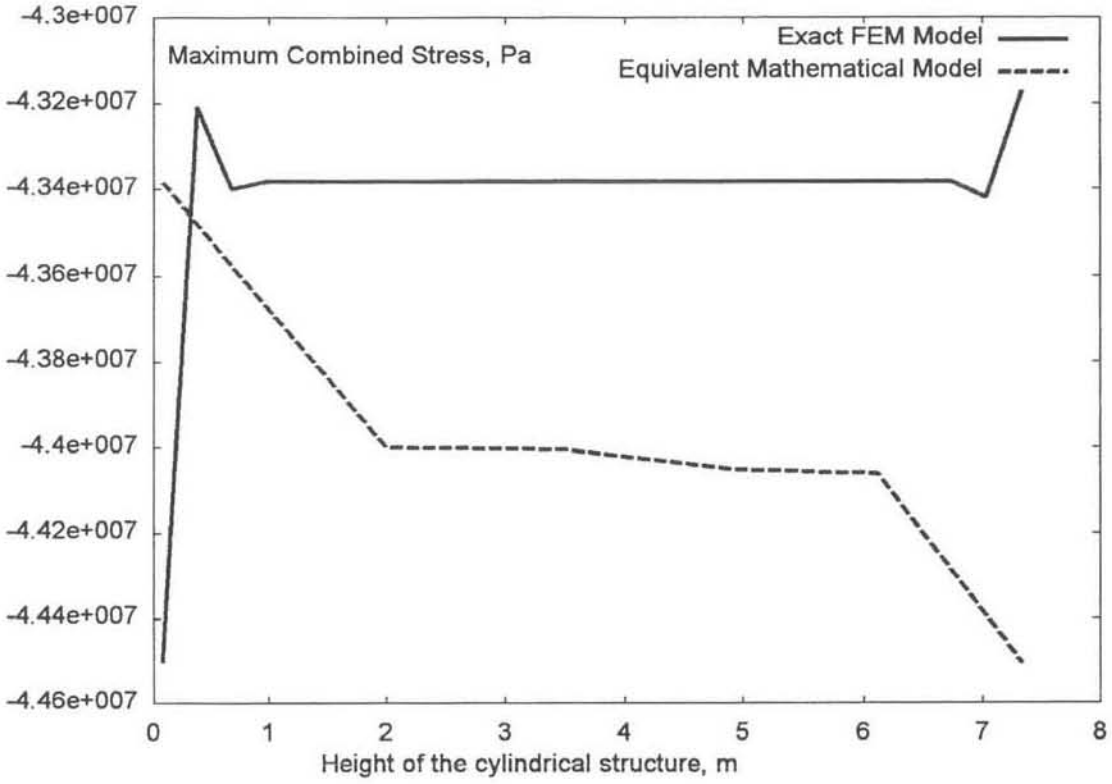

Figure 4.8 Maximum combined stress for the diagonal family of ribs

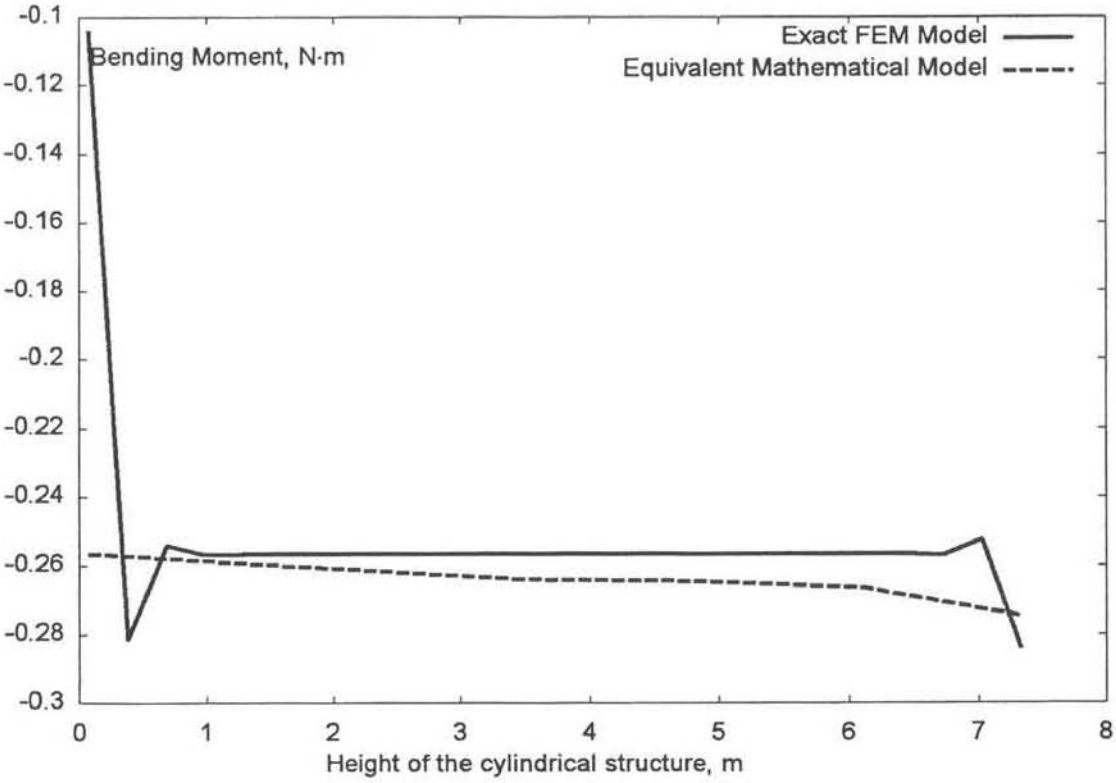

Figure 4.9 Bending moment M1 for the diagonal family of ribs

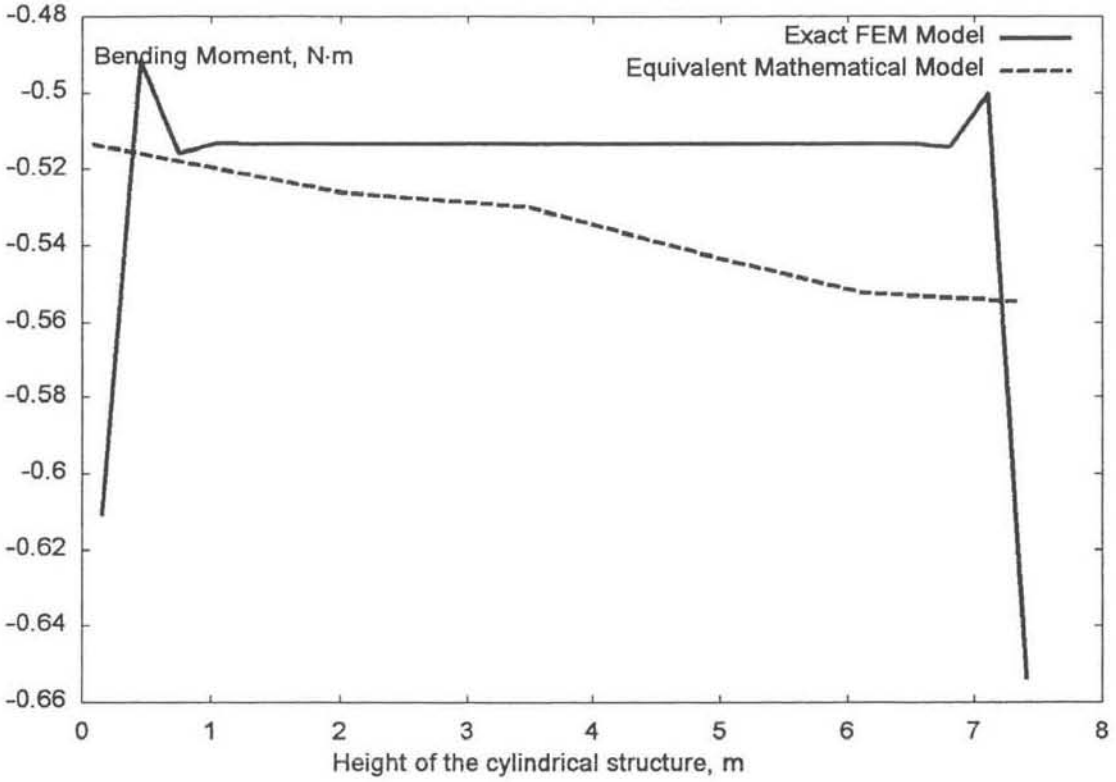

Figure 4.10 Bending moment M1 for the vertical family of ribs

The bending moment M2 is almost an order smaller compared to the moment M1 so the further graphs will only be plotted for the moment M1.

In this case the dominating stress appears in the vertical family of ribs will be due to the deformation of bending and for diagonal families the additional contribution of the stress state comes from the appearance of the axial force.

4.1.2 Combined Tension and Torsion

Loading was considered as a combination of the two previous loading conditions.

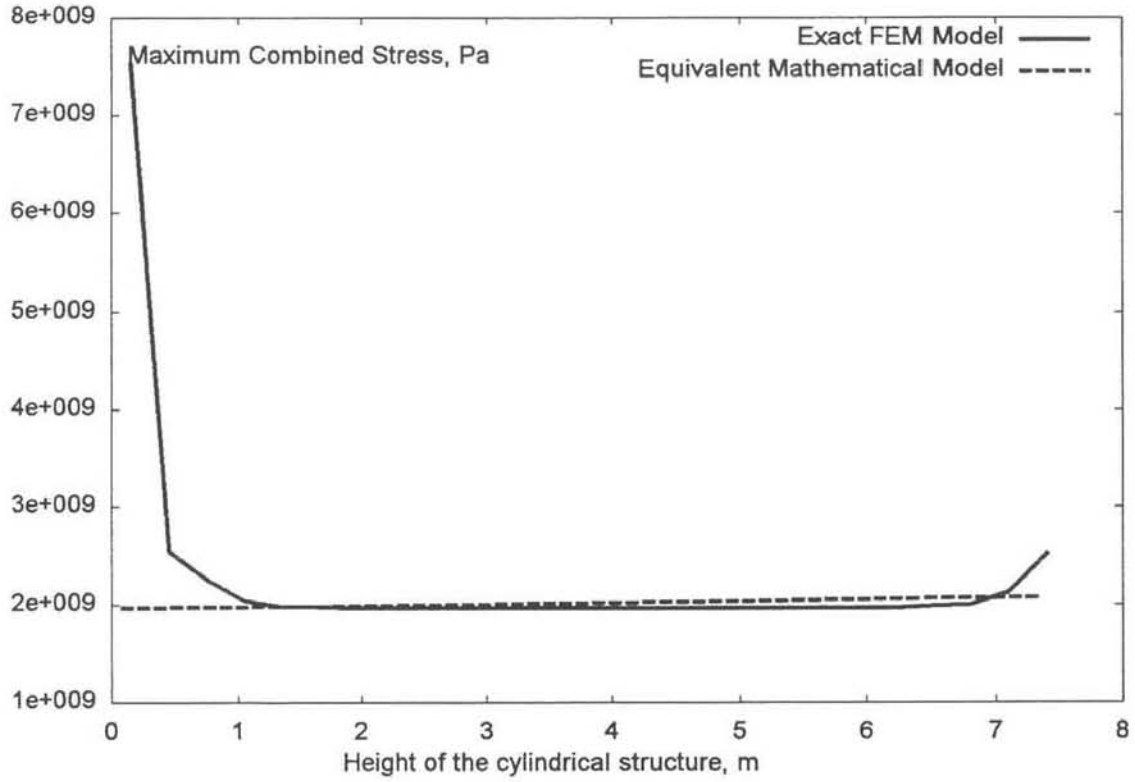

Figure 4.11 Maximum combined stress for the vertical family of ribs

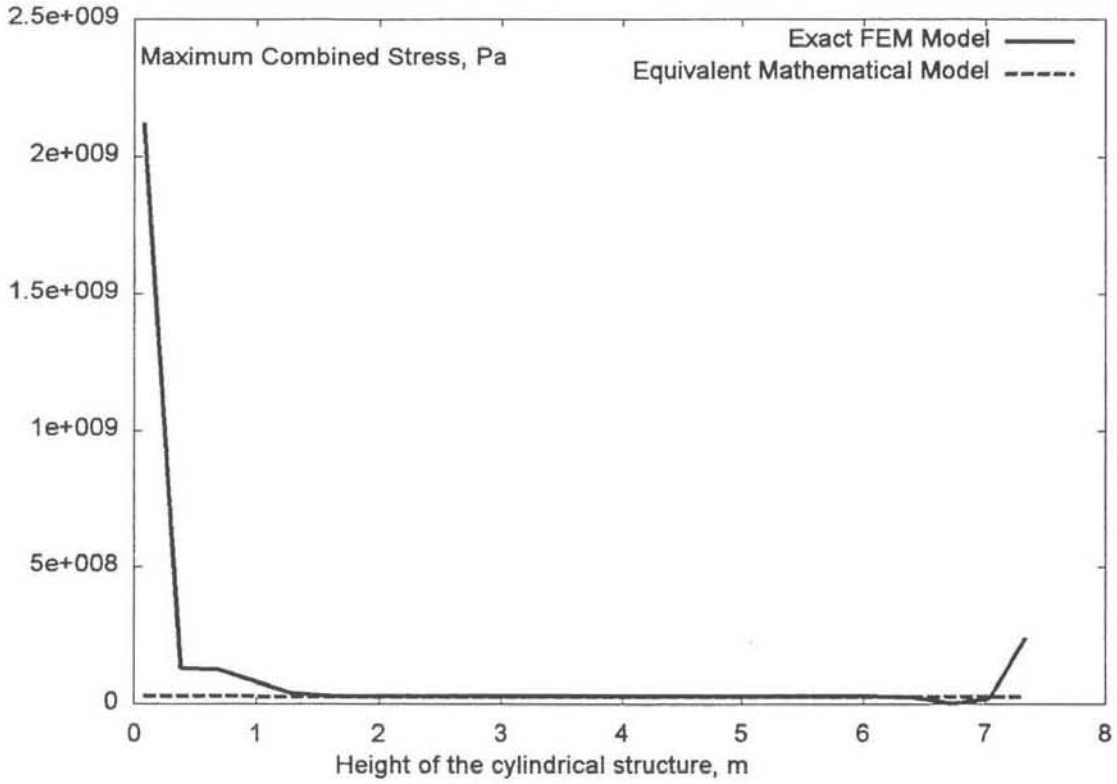

Figure 4.12 Maximum combined stress for the diagonal family of ribs

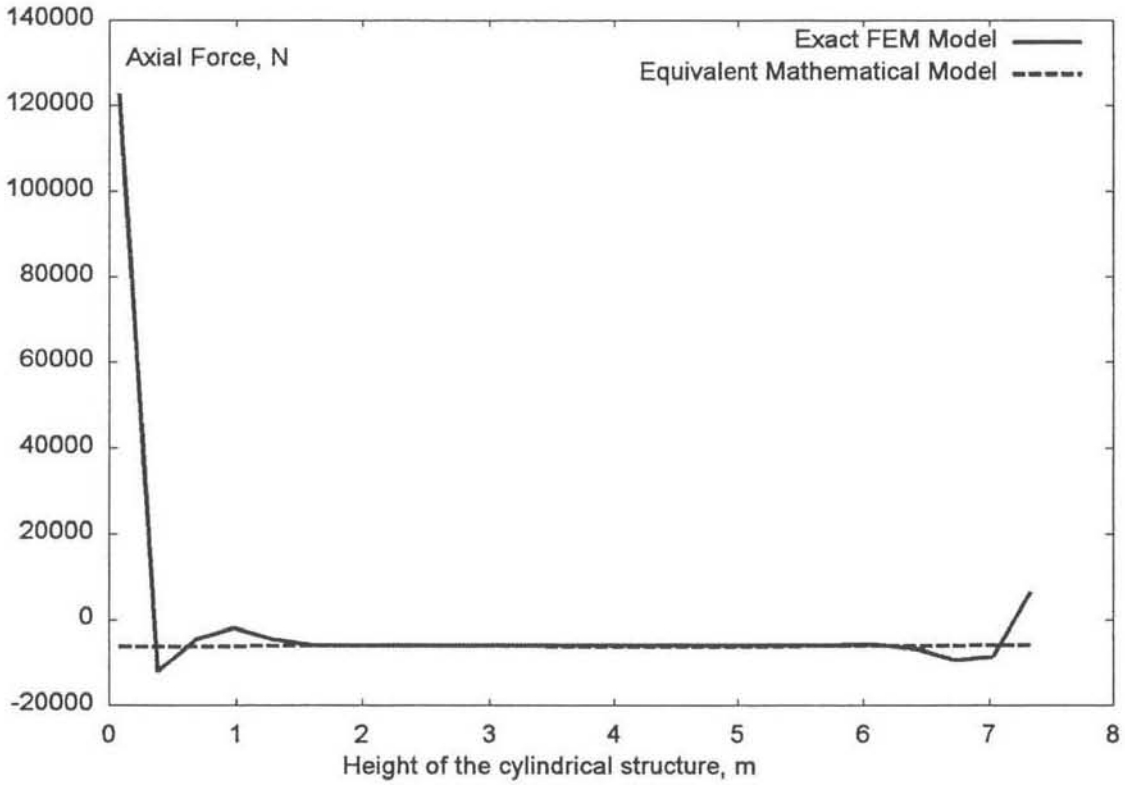

Figure 4.13 Axial force for the diagonal family of ribs

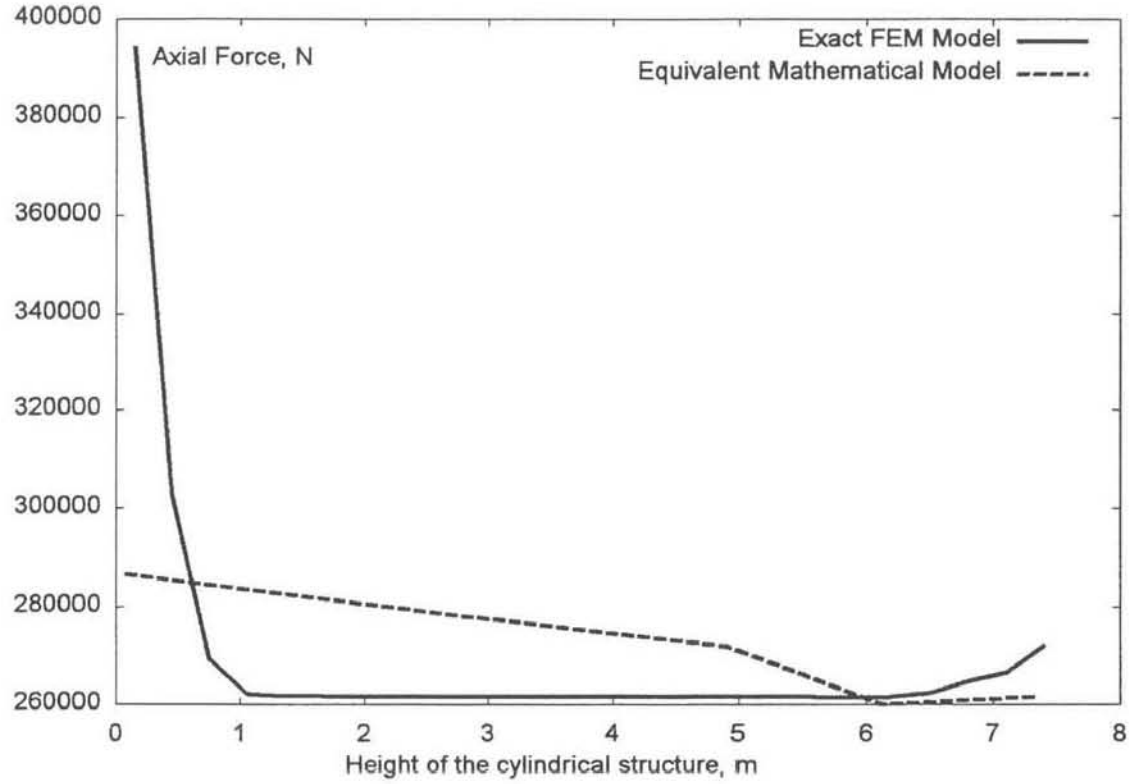

Figure 4.14 Axial force for the vertical family of ribs

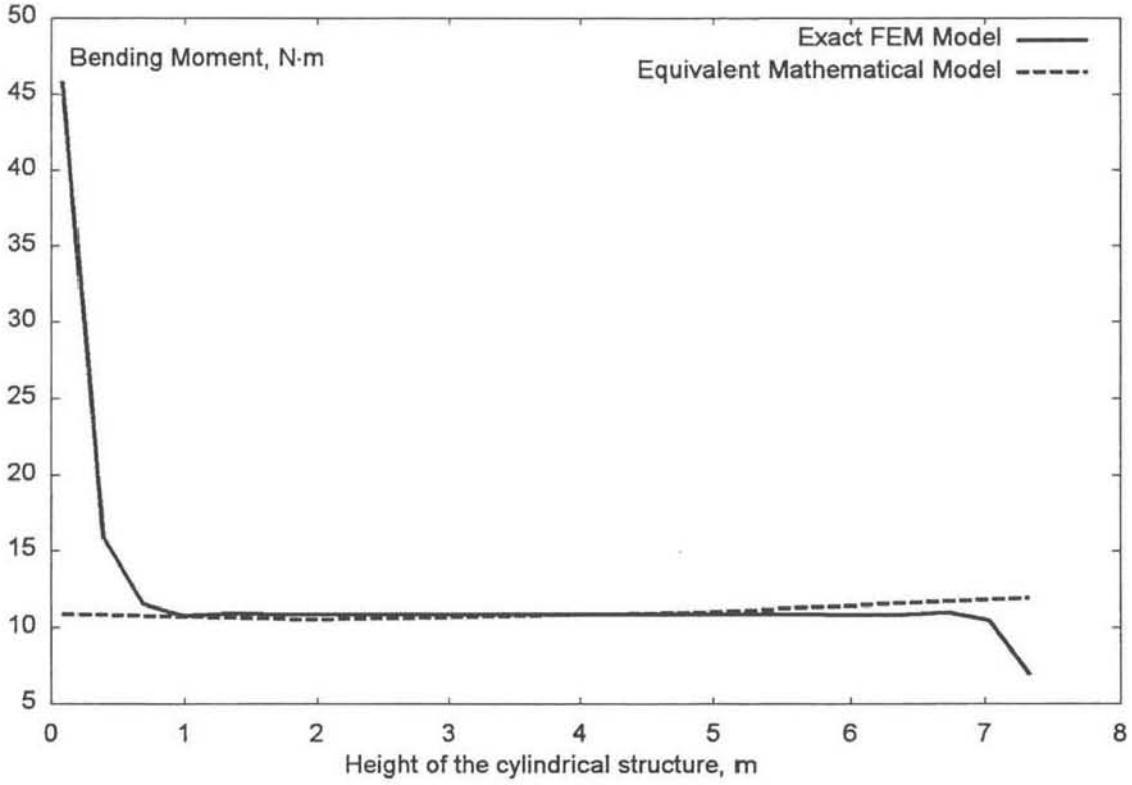

Figure 4.15 Bending moment M1 for the diagonal family of ribs

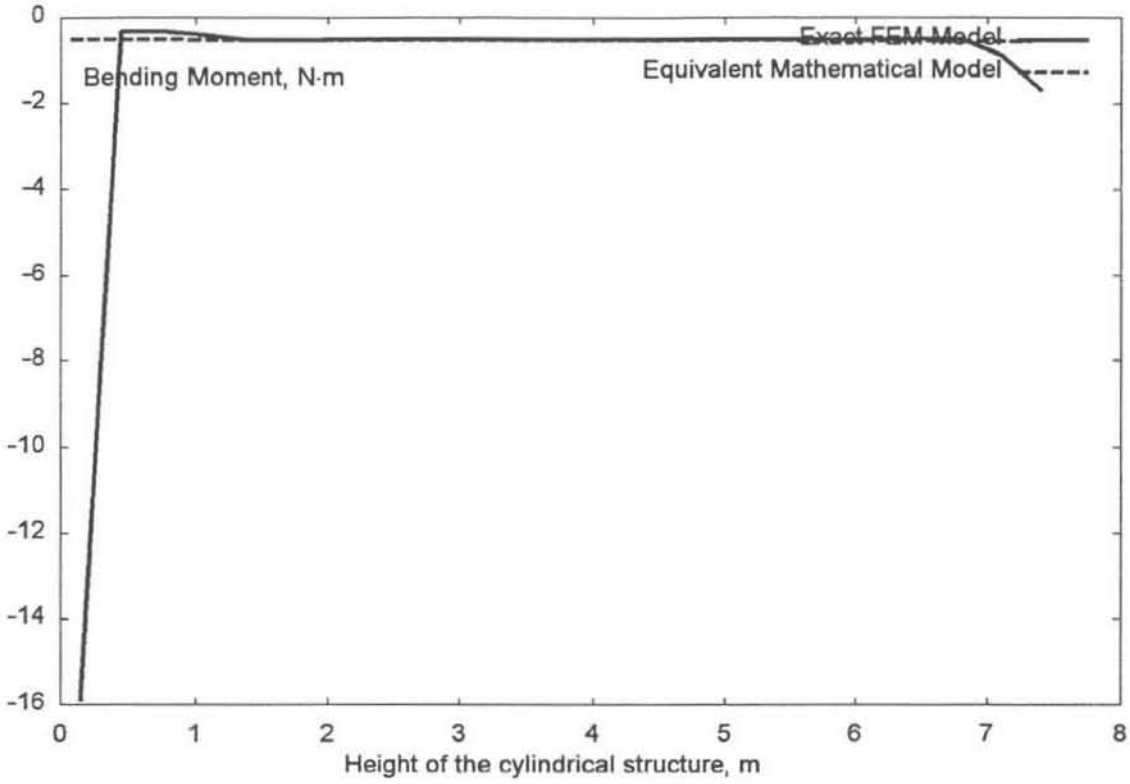

Figure 4.16 Bending moment M1 for the vertical family of ribs

	Exact Model		Equivalent Stiffness Model		Difference, %	
	Diagonal family	Vertical family	Diagonal family	Vertical family	Diagonal family	Vertical family
N_{ax}, N	6081	0.00928	6587.7	0.0100224	6.7	8.7
M_1, Nm	0.064	0.12	0.07104	0.108	8.8	6.4
σ, Pa	$1.77\ 10^8$	$7.1\ 10^6$	$1.75\ 10^8$	$7.662\ 10^6$	1.1	7.3

Table 4.1 Comparison of stress resultants for the case of torsional load q=2 10^4 N/m

	Exact Model		Equivalent Stiffness Model		Difference, %	
	Diagonal family	Vertical family	Diagonal family	Vertical family	Diagonal family	Vertical family
N_{ax}, N	1924	0.0029	2058.6	0.003132	6.5	9.1
M_1, Nm	0.02	0.04	0.023	0.0426	9.1	6.3
σ, Pa	56486740	2276822	60440812	2463521	7.2	8.2

Table 4.2 Comparison of stress resultants for the case of torsional load q=6366 N/m

	Exact Model		Equivalent Stiffness Model		Difference, %	
	Diagonal family	Vertical family	Diagonal family	Vertical family	Diagonal family	Vertical family
N_{ax}, N	44.9	261659	47	273433	4.5	4.85
M_1, Nm	11	0	10.5	0	4.9	0
σ, Pa	73694487	1959789326	78565552	2061634048	6.2	4.94

Table 4.3 Comparison of stress resultants for the case of tension load q= 10^6 N/m

*The cross-section parameters of all ribs for the given analysis are: h=0.01m; b=0.0033m

	Exact Model		Equivalent Stiffness Model		Difference, %	
	Diagonal family	Vertical family	Diagonal family	Vertical family	Diagonal family	Vertical family
N_{ax}, N	6408	286708	6843.7	314231	6.8	9.6
M_1, Nm	10.8	0.51341	11.5	0.55191	6.9	7.5
σ, Pa	28370730	1966027008	30470164	2074158493	7.4	5.5

Table 4.4 Comparison of stress resultants for the case of combined tension 10^6 N/m and torsional load 2 10^4 N/m

*The cross-section parameters of all ribs for the given analysis are: h=0.01m; b=0.0033m

The values in the tables are given for the middle section of the grid structure. It is observed from Figure 4.1 - Figure 4.16 that the developed homogenised model is in a good agreement with the FEM solution. The main discrepancy of the results occurs in the immediate vicinity to the boundary edges of the model where the loading and boundary conditions are applied. The comparison of the results is shown in the Table 4.1-Table 4.4.

The analysis of the lattice structure presented in this chapter is aimed merely at verification of the accuracy of developed homogenised model and comparison of the values for stress resultants for the ESM and the FEM. The complete structural failure analysis is undertaken in the following chapter.

The numerical results of the proposed homogenisation technique are summarised in [83].

4.2 Conclusions

The proposed homogenisation approach is implemented using the *Mathematica* symbolic computation system and this application is used to derive analytical expressions for the objective functions with further calculation of the numerical results. Consideration of boundary effects (discussed in the chapter 3.12) is not realised in the software at current stage of the development due to the high computational complexity and subsequent high requirements on the computing hardware.

The model of the lattice cylindrical structure developed in the previous chapter is realised in the computer code. The static analysis is performed for the structure loaded in tension and torsion.

The numerical results obtained for the equivalent homogeneous model of the isogrid cylindrical structure are compared to those obtained on the basis of commercial FEM code in order to validate the homogenisation approach used. It is found that the developed homogenised mathematical model predicts stress resultants in the members of the structure with sufficient accuracy (the discrepancy of the results does not exceed 10% for most of the elements). However, it is observed that a high discrepancy of the results occurs in the regions subjected to the boundary effects.

5 Optimisation

The objective of this chapter is to present the optimisation study of the isogrid cylindrical structure on the basis of the homogenisation approach presented in Chapter 3.

On the basis of the derived system of differential equations, a variety of optimisation tasks can be stated:

1. Minimisation of the total weight of the structure subjected to the variable design parameters (cell configuration, cross-section of the ribs, etc.) without failure of the structure occuring. The failure of the structure is calculated on the basis of design responses (stresses, strains, etc.) using one of the composite failure criteria.

2. Maximisation of the applied load before the failure of the structure, subject to the same set of design variables.

The first case is obviously more complicated because the objective function (weight) is non-linear and optimisation requires constant verification of another non-linear function i. e. strength ratio of the structural members. The practical realisation of such an optimisation task requires the incorporation of a complex non-linear programming algorithms.

For the second case, the optimisation task is much simplified since we are dealing with only one function. This function is an objective function, which is derived in an analytical form from the solution of the boundary value problem (3.198). The failure coefficients enter the expression of the considered objective function and their calculation is performed inside the objective function during optimisation.

In the case of the isogrid cylinder subjected to a combination of different loading and different geometrical parameters of the structure need to be optimised to allow the structure sustain the maximum load before failure. The optimum combination of the design parameters subsequently contributes to the optimum mass of the system.

5.1 Problem Statement

The basic optimisation problem statement can be introduced by providing the definition of the design variables, objective, and constraints as

$$\begin{array}{lllll} \text{minimise} & F(\vec{X}) & & & \text{Objective function} \\ \text{subject to} & g_j(\vec{X}) \le 0 & j = 1, \ldots n_g & & \text{Inequality Constraints} \\ & h_k(\vec{X}) = 0 & k = 1, \ldots n_h & & \text{Equality Constraints} \\ & X_i^l \le X_i \le X_i^u & i = 1 & & \text{Side Costratints} \end{array} \tag{5.1}$$

where X is a vector of design variables.

It is within the design space defined by the above problem statement that the optimiser searches for a best design. At this time we have introduced the idea of a one-dimensional search and the steepest descent algorithm as a particular method of establishing this search direction. However, we have also noted that this method, in addition to not being particularly efficient, cannot address situations in which one or more constraints are active. The resolution of these issues is discussed in the section 5.4.

The design variable vector update can be written as

$$\vec{X}^1 = \vec{X}^0 + \alpha^* \vec{S}^1, \tag{5.2}$$

where $\vec{X}^0$ is the initial vector of design variables, $\vec{S}^1$ is the search vector, and α is the search parameter. Equation (5.2) represents a one-dimensional search since the update on $\vec{X}^1$ depends only on the single scalar parameter α. α^* is the value of α that yields the optimal design in the direction defined by $\vec{S}$.

In practice, there is a better choice of direction called a conjugate direction. However, regardless of the search direction used the concept is the same. The optimiser finds a search direction towards the highest gradient of the objective function and moves in that direction as far as possible.

If the optimiser has encountered some of the design constraints, in order to make any further improvement in the design, a new search direction S^2 must be found that continues to reduce the objective function within the design space. Here the optimiser is seeking for a "usable-feasible" direction, in which a usable direction is one that moves in the direction of the high gradient of the objective function and a feasible

direction is one that keeps the search inside the constraint boundaries. This situation is shown in Figure 5.1. The mathematical definition of a usable search direction is

$$\nabla F(\vec{X}) \cdot \vec{S} \leq 0. \tag{5.3}$$

Equation (5.3) is the scalar product (dot product) of the gradient of the objective function with the search direction. The dot product is the magnitude of $\nabla F(\vec{X})$ times the magnitude of $\vec{S}$ times the cosine of the angle between the two vectors. Thus, the cosine of the angle determines the sign of the product since the magnitudes are positive numbers. The optimiser has to find a search direction that makes the left-hand side of equation (5.3) as negative as possible. However, this direction must remain within a critical constraint. This is the feasibility requirement, which is similar to the usability requirement but now is stated with respect to the constraint

$$\nabla g_j(\vec{X}) \cdot \vec{S} \leq 0. \tag{5.4}$$

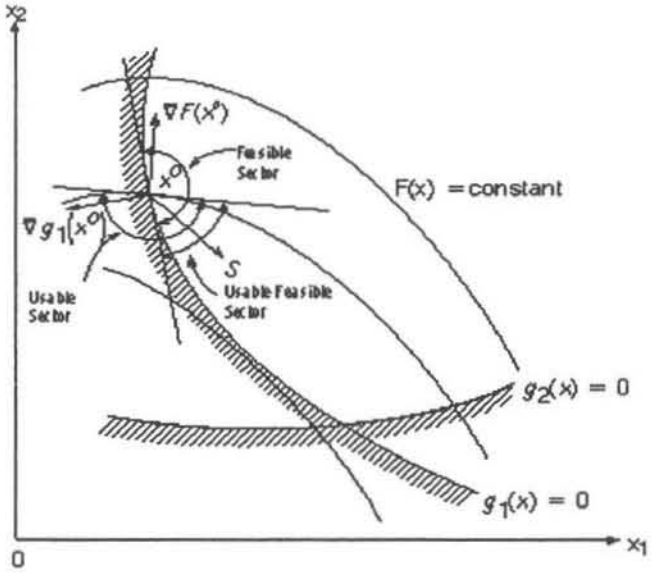

Figure 5.1 Usable-feasible search direction

Just as for the objective function, the angle between the search direction $\vec{S}$ and the gradient of the constraint must be between 90° and 270°. If the angle is exactly 90° or 270°, the search direction is tangent to the constraint boundary. To find the search direction that makes the greatest possible improvement in the objective function but still follows or moves inside the constraint boundary, the usability and feasibility requirements must be combined. This combination creates the following sub-

optimisation task: to find the components of the search direction $\vec{S}$ in order to minimise

$$\nabla F(\vec{X})\cdot(\vec{S}) \tag{5.5}$$

subject to:

$$\nabla g_j(\vec{X})\cdot(\vec{S}) \le 0 \qquad j \in J, \tag{5.6}$$

$$\vec{S}\cdot\vec{S} \le 1, \tag{5.7}$$

where J is the set of constraints whose values are zero within some numerical tolerance. This is the set of active constraints. The purpose of the equation (5.7) is simply to prevent an unbounded solution to the problem defined by (5.5) and (5.6). In the general case where there are numerous design variables as well as several active constraints, this becomes a sub-problem that is solved as part of the optimisation. This problem is linear in $\vec{S}$ except for the quadratic constraint of (5.7) [105].

Assuming that a usable-feasible search direction is found, the optimiser can now search in this direction until it can make no further improvement. The sub-problem of finding a new usable-feasible search direction is repeated and continues until no search direction can be found that improves the design without violating one or more constraints. That means that the optimum is reached.

The verification of the obtained values of the design variables that correspond to the real optimum can be done using the Kuhn-Tucker conditions [104]. In the case of an unconstrained problem (omitting second and third equations in (5.1)), this is simply the condition where the gradient objective function vanishes. In the case of the constrained optimisation problem considered here, the conditions of optimality are more complex. In this case, the governing equation is the stationary condition of the Lagrangian function:

$$L(\vec{X},\vec{\lambda}) = F(\vec{X}) + \sum_{j=1}^{M} \lambda_j g_j(\vec{X}), \tag{5.8}$$

$$\lambda_j \ge 0. \tag{5.9}$$

The Kuhn-Tucker conditions dictate that the Lagrangian function $L(X,\lambda)$ must have a vanishing gradient at the optimum design, X^*. When all of these conditions are considered, they lead to the statement of the Kuhn-Tucker necessary conditions for optimality:

Condition 1: $\vec{X}^*$ is feasible. Therefore, for all j, $g_j\left(\vec{X}^*\right) \leq 0$

Condition 2: $\lambda_j g_j\left(\vec{X}^*\right) = 0$ (the other product of λ_j and $g_j\left(\vec{X}^*\right)$ equals to zero)

Condition 3: $$F\left(\vec{X}^*\right) + \sum_{j=1}^{M} \lambda_j \nabla g_j\left(\vec{X}^*\right) = 0,$$
$$\lambda_j \geq 0 \qquad j = 1, 2, \ldots, M.$$

The physical interpretation of these conditions is that the sum of the gradients of the objective and scalars λ_j times the associated gradients of all active constraints must vectorally add to zero. This is much like the statement for static equilibrium where the sum of all internal and external forces at any given point must vectorally add to zero.

5.2 The Feasible Direction Search Method

The method described here is referred to as the Modified Method of Feasible Directions [104]. At this point it is assumed that both an objective function $F(\vec{X})$ and constraints $g_j(X) \leq 0$ for $j = 1,2,...,n_g$ as well as lower and upper bounds on the design variables are provided. Also, the gradients of the objective and constraints are available. Thus, we are solving the general problem defined by (5.1).

The optimiser is simply minimising a function subject to inequality constraints.

Given an initial x-vector x^0, the design will be updated according to

$$\vec{X}^q = \vec{X}^{q-1} + \alpha^* \vec{S}^q, \tag{5.10}$$

where q - iteration number, α^* - scalar move parameter.

The overall optimisation process proceeds in the following steps of the algorithm (Figure 5.2)

5.3 Finding the Search Direction

Often in design optimisation, the one-dimensional search is limited by the α at which a side constraint X_i^l or X_i^u becomes critical. Assume α^* corresponds to encountering the lower or upper bound on some variable X_k. Because this constraint is a function of X_k only, it may be possible to fix this at its bound and repeat the one-dimensional search from this point with respect to the remaining variables. To achieve this, the k-th component of S is set to zero. If other constraints are violated and a feasible design is being sought, the one-dimensional search is restarted from this point. If no constraints are currently violated, the scalar product $\nabla F\left(\vec{X}\right)\cdot\left(\vec{S}\right)$ is calculated. If this product is negative, the objective is assumed to be decreasing for a move in this modified direction. This is an assumption, since $\nabla F\left(\vec{X}\right)$ has not been re-evaluated for the current X. If the objective is, in fact, increasing in this new direction, the resulting α^* will be zero.

The advantage of this modification is that, in a design where many side constraints are active, the one-dimensional search can continue without the necessity of calculating new gradient information, usually a time-consuming process. For cases where this modification applies, it often considerably improves the efficiency of the optimisation process and is recommended when using this and other direct search algorithms.

An alternative here would be to simply set any X_i to its bound if, during the one-dimensional search, that bound is violated. This usually works well in practice, even though the objective and constraints now have discontinuous first derivatives with respect to α.

Figure 5.2 Algorithm for the method of feasible directions

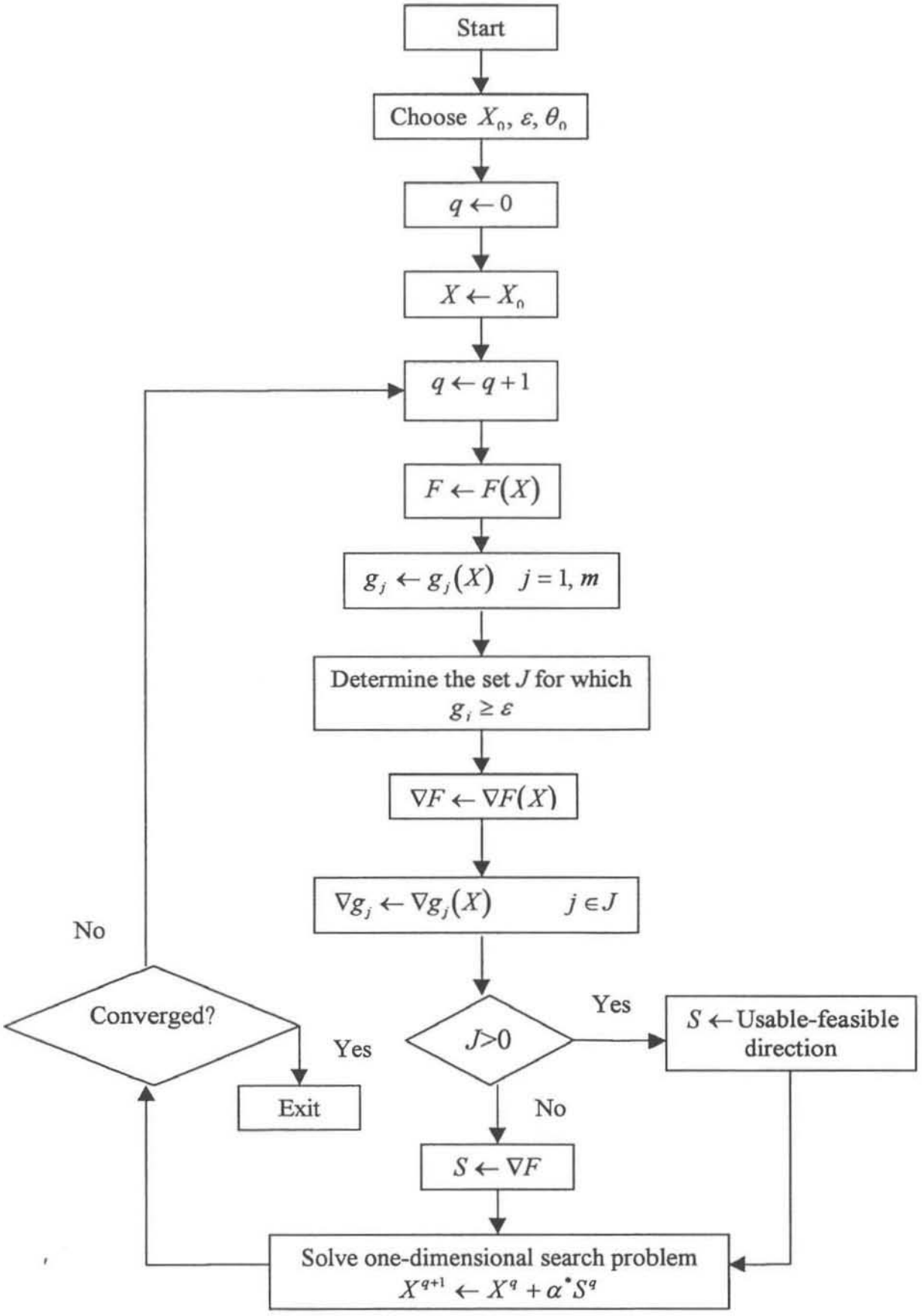

5.4 Sequential Quadratic Method

This method is considered to be an excellent method by many theoreticians [67], [105]. The basic concept is very similar to Sequential Linear Programming (SLP) [67], [104] [63], when first the objective and constraint functions are approximated using Taylor Series Approximations [67] and the search direction $\vec{S}$ is created. Then a one-dimensional search is performed in order to improve the design as much as possible in this direction. In this case the search direction is found using first order (gradient) information only. The first step in the one-dimensional search direction is somewhat arbitrary although, using gradient information, it is possible to provide a first order estimate for the solution to the one-dimensional search.

In contrast to the SLP, Sequential Quadratic Programming uses the technique where the search direction is found by solving a sub-problem with a quadratic objective and linear constraints. The objective function is an augmented using Lagrange multipliers $\left(\lambda_j,\ j=1,m\right)$ and an exterior penalty. The direction of the search is determined by incorporating a quadratic, rather than a linear approximation of the objective function. Linearised constraints are used with this to create a direction-finding problem of the form:

minimise

$$Q(S) = F^0 + \nabla F\, S + 0.5 S^T B S \tag{5.11}$$

subject to

$$\nabla g_j S + g_j^0 \le 0 \qquad j=1,\ m, \tag{5.12}$$

where $F(X)$ is an objective function and vector X contains design (or decision) variables; S is a vector of search direction; superscript 0 denotes the value at the beginning point; g_j defines the constraint boundaries; B is dependant variable matrix which contains gradient information.

Here the design variables are the components of S. The matrix B is a positive definite matrix which is initially the identity matrix. On subsequent iterations, B is updated to approach the Hessian of the Lagrangian functions. This sub-problem is solved using the Modified Method of Feasible Directions [104]. For this sub-optimisation problem, the functions and derivatives are easily and efficiently evaluated.

Now assuming the approximate problem of minimising Q subject to the linearised constraints has been solved. At the optimum for this problem, the Lagrange multipliers $\lambda_j,\ j=1,m$ associated with the solution of this direction-finding problem can be calculated.

With the Lagrange multipliers available, an approximate Lagrangian function can be constructed and used to search in the direction defined by $\vec{S}$. Having determined the search direction $\vec{S}$, the design is updated as a one-dimensional search problem in the usual manner, except here an exterior penalty function is used:

$$\Phi = F(\vec{X}) + \sum_{j=1}^{m} u_j \max\left[0, g_j(\vec{X})\right] \tag{5.13}$$

where

$$\vec{X} = \vec{X}^{q-1} + \alpha\vec{S}, \tag{5.14}$$

$$u_j = |\lambda_j|,\ j=1,m \qquad \text{for the first iteration,} \tag{5.15}$$

$$u_j = \max\left[|\lambda_j|, \frac{1}{2}\left(u'_j + |\lambda_j|\right)\right],\ j=1,m \qquad \text{for the subsequent iterations} \tag{5.16}$$

and $u'_j = u_j$ from the previous iteration.

Here: Φ is a pseudo-objective function; q is an iteration number; α^* defines the distance in the direction S where the optimiser should move to achieve the better design.

The task is to find α in order to minimise (5.13). This one-dimensional search problem is well conditioned and α=1 is a very good estimate for α^*. Usually, quadratic polynomial interpolation is adequate to refine the solution for α^*.

During the one-dimensional search, approximations are made to the components of Φ because this function has discontinuous derivatives at the constraint boundaries, but the components are smooth.

At this point the search direction $\vec{S}$ is determined and the one-dimensional search is performed to update the design. Then the matrix B needs to be updated to provide an improved quadratic approximation of the augmented design objective. Powell [67] recommends the Broydon-Fletcher-Shanno-Goldfarb (BFSG) [105] update formula:

$$[B^*] = [B] - \frac{[B]\{p\}\{p\}^T[B]}{\{p\}^T[B]\{p\}} + \frac{\{\eta\}\{\eta\}^T}{\{p\}^T\{\eta\}}, \tag{5.17}$$

where

$$
\begin{aligned}
&\{p\} = \vec{X}^{q} - \vec{X}^{q-1}, \\
&\{\eta\} = \theta\{y\} + (1-\theta)[B]\{p\}, \\
&\{y\} = \nabla_X \Phi^{q} - \nabla_X \Phi^{q-1}, \\
&\Phi = F(\vec{X}) + \sum_{j=1}^{m} \lambda_j g_j(\vec{X}),
\end{aligned}
\tag{5.18}
$$

$$
\theta = \begin{cases} 1 & \text{if } \{p\}^T\{y\} \geq 0.2\{p\}^T[B]\{p\} \\ \dfrac{0.12\{p\}^T[B]\{p\}}{\{p\}^T[B][B]\{p\} - \{p\}^T\{y\}} & \text{if } \{p\}^T\{y\} < 0.2\{p\}^T[B]\{p\} \end{cases}
$$

Here the constants 0.12 and 0.2 are chosen arbitrary from the numerical experience; θ is a push-off factor The new matrix $[B^*]$ now replaces $[B]$ in (5.11) and the optimisation process is repeated until convergence.

Figure 5.3 Algorithm for the sequential quadratic method

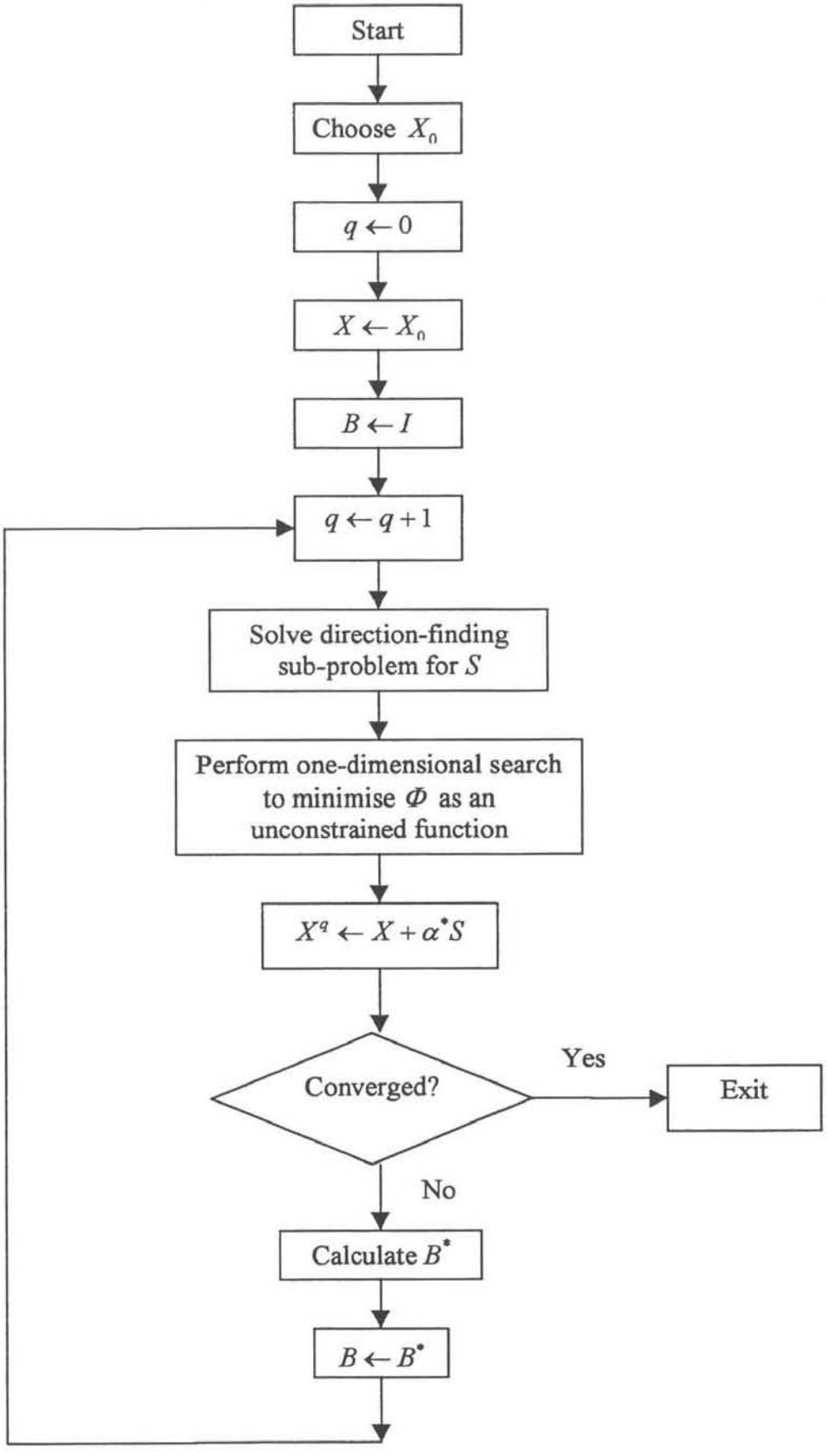

The algorithm of this method is given in Figure 5.3. From the outline of the algorithm, it is apparent that this method incorporates the best features of several concepts. First, the Lagrangian is approximated and then the approximating function is minimised. However, since the function is approximated with respect to the primal variables X alone, the minimisation sub-problem uses linear approximations to the constraints. The result is then used as a search direction to minimise the augmented Lagrangian. The form of the update of the B matrix is such that positive definiteness is maintained and thus is a variable metric method. The method deals well with equality constraints, as long as the sub-problem of the solving for $\vec{S}$ can treat linear equality constraints. Finally, the method deals with infeasible designs with no additional strategy required. The abovementioned confirms this technique to represent a very powerful optimisation tool.

5.5 Literature Survey

A number of optimisation studies have been undertaken for orthogrid, anglegrid and isogrid structures [13], [36], [32]. However they were mostly based on the different homogenisation approaches that required calculations of the stress resultants with the use of supplementary finite element package and subsequent input of the obtained results in the optimisation routine. These approaches make the optimisation process not completely automatic, which becomes an important issue considering the number of iterations required for achieving optimum.

5.6 Maximum Applied Load Design

The objective function in the present design study is applied load. The design problem can be stated as

$$\max_{\varphi,\, h,\, b} q(\varphi, h, b) \tag{5.19}$$

subjected to the following constraints

$$\varphi_{\min} \le \varphi \le \varphi_{\max}, \quad h_{\min} \le h \le h_{\max} \tag{5.20}$$

for the case of the constant aspect ratio, and also

$$b_{\min} \le b \le b_{\max} \tag{5.21}$$

for the generalised case.

The maximum load represents the maximum load the structure can sustain before failure. The failure of the isogrid cylinder is characterised by the failure coefficient (strength ratio) r, described later in Section 5.8.2 equation (5.33). The value of $r=1$ corresponds to the failure of the structure. The strength ratio is calculated for the vertical and diagonal families of ribs and the structure is considered to have failed when either of them is equal to one. The analytical expression for the objective function is derived for $r=1$.

The load scaling factor was introduced to link tension and torsional loads in order to reduce the number of system variables and subsequently reduce the required computational time. The load scaling factor is a ratio:

$$w_s = \frac{q_{ten}}{q_{tor}}, \tag{5.22}$$

where q_{ten} is a tension load and q_{tor} is an equivalent torsional load. The equivalent torsional load is an applied distributed load equivalent to the torque (T)

$$q_{tor} = \frac{T}{2\pi R^2}. \tag{5.23}$$

The maximum applied load design involves the computation of the width (b), height (h) of the ribs and angle of cell configuration (φ) so as to solve the optimisation problem (5.19). For a given h and φ the maximum P_{cr} is determined such that the inequality (5.20) is satisfied. The optimal h and φ are obtained by maximising the objective function P_{cr} over these variables. This yields the maximum (critical) load that can be applied to the structure just before its failure, having the optimal geometric parameters h, b and φ. A Sequential Quadratic Method (SQM) was used for calculating the optimum [105]. In this method, a quadratic programming subproblem is solved at each iteration. The values of the optimum sequences of the cross-sectional parameters are presented in Table 5.2-Table 5.4.

5.7 Stresses Acting in the Ribs

Components of the stress acting in the ribs of the isogrid structure comprise normal (direct) and shear components. According to the regular beam theory direct stress components σ_i are calculated on the faces that are normal to the direction denoted by a subscript (Figure 5.4). The notations of the shear stresses τ_{12} the first index denotes the direction of the normal to the surface where the stress component is acting and the second shows the direction of this stress (Figure 5.4); i shows that stresses are calculated for each family of ribs. The directions of the forces and moments acting in the rib are shown on the Figure 3.4

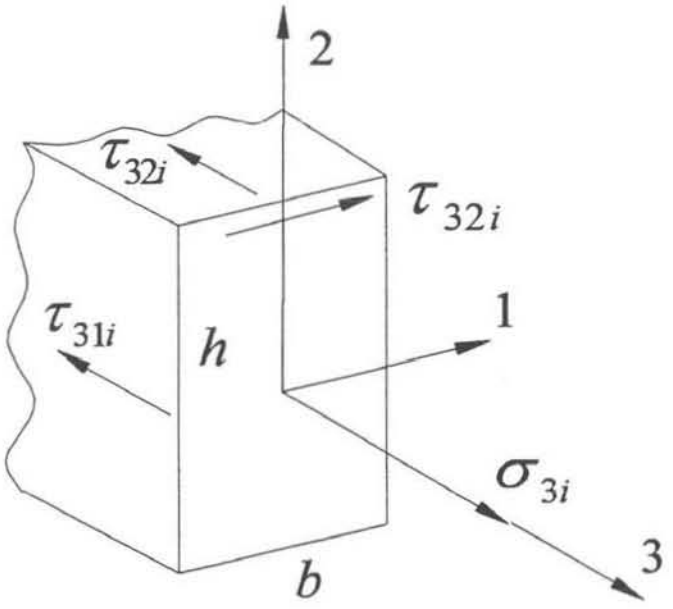

Figure 5.4 Direction of the normal and shear stress components

5.7.1 Normal Stresses

Normal stresses have two components:

1. From the contribution of the axial force in direction 3 [95]:

$$\sigma_{3i}(N_i)=\frac{N_{3i}}{A_i}. \tag{5.24}$$

Where N_3 is an axial force in the rib in direction 3; A is a cross-sectional area.

2. From the contribution of the bending moment about the axes 1 and 2 [95]:

$$\sigma_{3i}(M_i)=\frac{M_{1i}}{I_{1i}}x_{2i}-\frac{G_{2i}}{I_{2i}}x_{1i}. \tag{5.25}$$

Where Q_i are the shear forces.

The total normal stress is:

$$\sigma_{3i}=\sigma_{3i}(M_i)+\sigma_{3i}(N_i). \tag{5.26}$$

5.7.2 Shear Stresses

Shear stress has also two components:

1. From the contribution of the shear forces Q_i:

$$\begin{aligned}\tau_{31i}&=\frac{Q_{1i}}{I_{2i}}\left(\frac{b_i}{2}-|x_1|\right)\left(\frac{b_i}{4}-\frac{|x_{1i}|}{2}\right),\\ \tau_{32i}&=\frac{S_i}{I_{1i}}\left(\frac{h_i}{2}-|x_{2i}|\right)\left(\frac{h_i}{4}-\frac{|x_{2i}|}{2}\right).\end{aligned} \tag{5.27}$$

5.7.3 Torsion of the Ribs

Torsional stress in the ribs may be expressed as:

$$\tau_{12i}=\frac{H_i}{\alpha h_i b_i^{\,2}}, \tag{5.28}$$

where h_i is longer side of the cross-section and b_i is the shorter side, α is the coefficient that depends on the geometry, for the rectangular cross-section the values of this coefficient are given in Table 5.1.

h/b	1	1.5	2	2.5	3	4	6	10	∞
α	0.208	0.231	0.246	0.256	0.267	0.282	0.299	0.312	0.333

Table 5.1 The values of coefficient α

5.8 Material Failure in a Rib

In this section a quadratic failure criterion is derived to determine material failure in the ribs due to the stresses calculated in subsection 5.7.

5.8.1 Material Properties

The following material properties are considered for the material which is orthotropic in respect of the third direction:

X_3^t = Tensile strength in the 3-d direction;

X_3^c = Compressive strength in the 3-d direction;

S = Shear strength in the 31 and 32 directions.

5.8.2 Quadratic Failure Criterion for a Beam

Let us start derivation with the generic quadratic criterion [15]

$$F_{ij} \cdot \sigma_i \cdot \sigma_j + F_{ij} \cdot \sigma_i = 1 \qquad (i,\ j = 1,\ 2,\ 3,\ 4,\ 5,\ 6), \tag{5.29}$$

where the material is presumed to fail when equation (5.29) is satisfied at any point. Eliminating stress in the 1, 2, 12 directions from beam theory assumptions and removing the first order shear terms leaves us with

$$F_{33} \cdot \sigma_3^2 \cdot F_{44} \cdot \sigma_4^2 \cdot F_{55} \cdot \sigma_5^2 \cdot F_3 \cdot \sigma_3 = 1, \tag{5.30}$$

where only F_{ij} and F_i have to be determined from the material properties. When any two of the stresses are zero, the remaining stress is either X_3^t, X_3^c or S at failure, so we can determine that

$$\begin{aligned} F_{33} &= \frac{1}{X_3^t X_3^c}, \\ F_{44} &= \frac{1}{S^2}, \\ F_{55} &= \frac{1}{S^2}, \\ F_3 &= \frac{1}{X_3^t} - \frac{1}{X_3^c}, \end{aligned} \tag{5.31}$$

and our final failure criteria for a simple orthotropic beam is then

$$\frac{\sigma_3^2}{X_3^t X_3^c}+\frac{\sigma_4^2}{S^2}+\frac{\sigma_5^2}{S^2}+\left(\frac{1}{X_3^t}-\frac{1}{X_3^c}\right)\sigma_3=1. \tag{5.32}$$

If we now substitute $r\sigma_i$ for σ_i, the ratio of the failure loading to the applied loading can be determined as follows

$$r=\frac{S^2\sigma_3\left(X_3^t-X_3^c\right)+S\sqrt{S^2\sigma_3^2\left(X_3^t-X_3^c\right)+4X_3^tX_3^c\left(S^2\sigma_3^2+X_3^tX_3^c\left(\sigma_4^2+\sigma_5^2\right)\right)}}{2\left(S^2\sigma_3^2+X_3^tX_3^c\left(\sigma_4^2+\sigma_5^2\right)\right)}, \tag{5.33}$$

where r is a strength ratio for this case.

5.9 Optimisation Runs

Three optimum design problems for the isogrid structure are considered.

The first problem involves the maximum load design for the structure in the form of a cylinder subjected to combined tension and torsional loading. The design variables are chosen as the width (b) and the height (h) of the ribs' cross-section, and they considered to be the same for all the families of the structure. The design-optimisation is performed for the isogrid cylinder with the geometrical parameters given in Table 2.1 and material properties in Table 2.2. The relationship between these cross-sectional parameters is established. The effect of the design parameters on the extensional and torsional stiffness is investigated. The optimisation task has been performed for the different combinations of tension and torsional loads and the results are presented in Figure 5.5-Figure 5.6

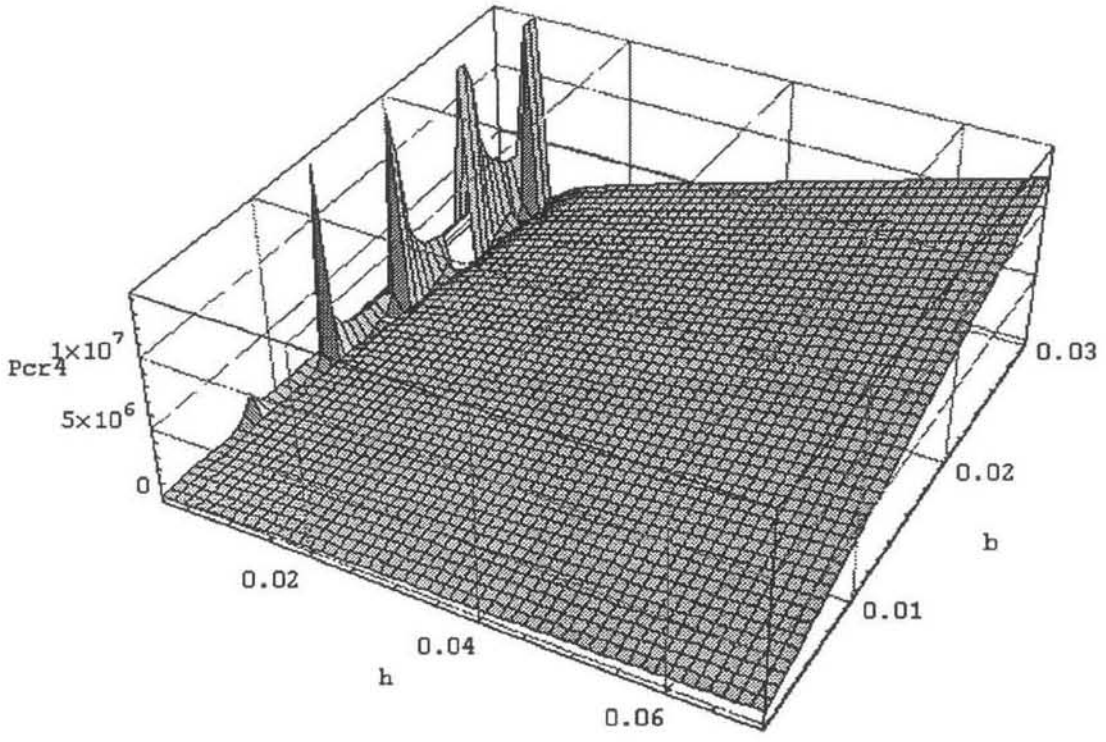

Figure 5.5 Critical load for the vertical family of ribs (w_s=1)

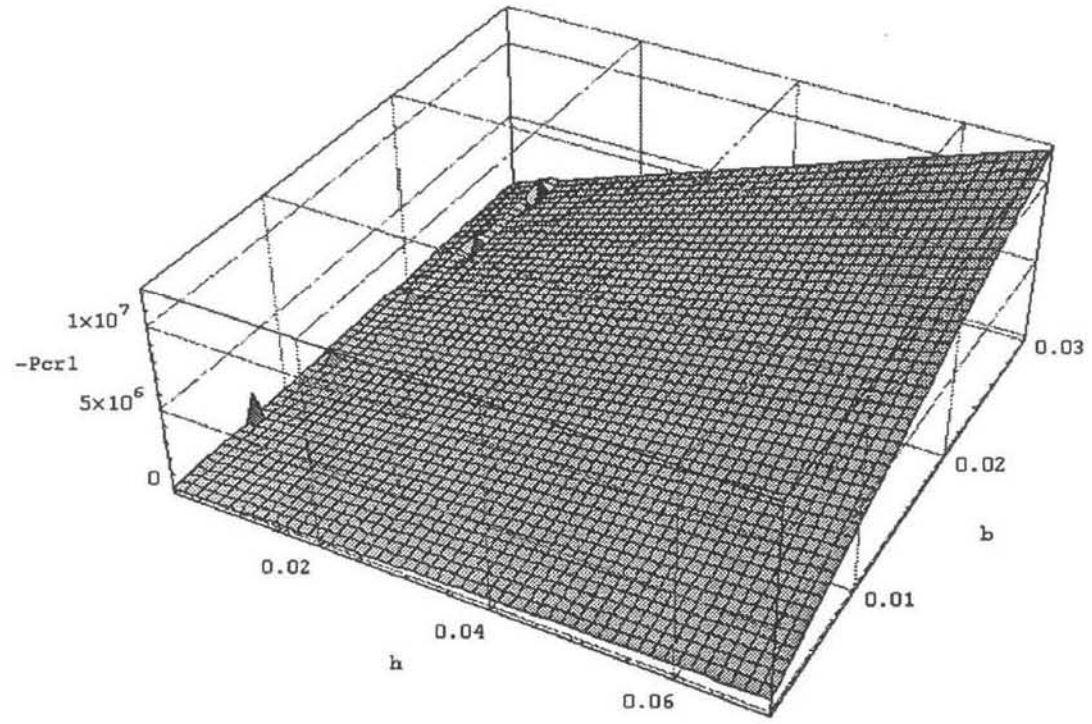

Figure 5.6 Critical load for the diagonal family of ribs (w_s=1)

The values of the optimum sequences of the cross-sectional parameters are presented in the Table 5.2. The optima are found in each case using the symbolic computation package *Mathematica* by means of multiple application of the Sequential Quadratic Method (SQM) with constant changing of the initial guess.

In the case of w_s=1 the failure occurs in both families of ribs almost simultaneously at the critical load combination: q_{ten}=q_{tor}=10^7 N/m. Surfaces of optimisation are shown in Figure 5.5 - Figure 5.6, where the critical applied (P_{cr}) load is plotted verses the design variables (b and h). Optimum sequences of geometric parameters for the rib's cross-section for this case are given in the Table 5.2.

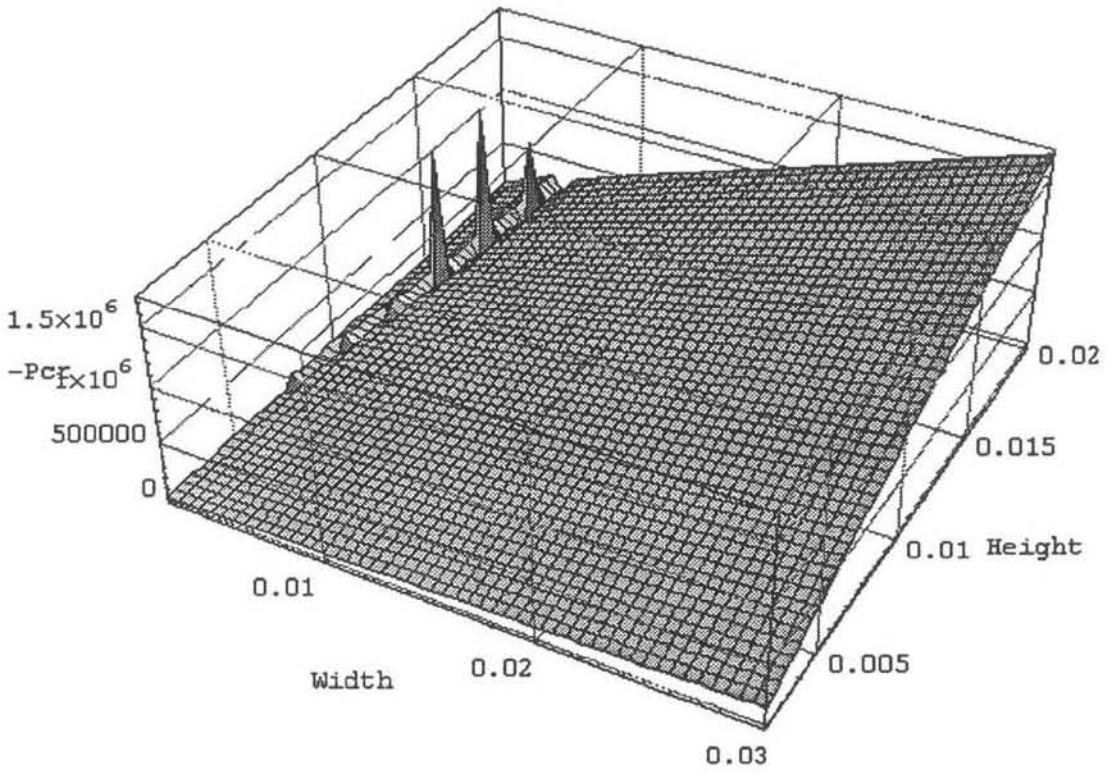

Figure 5.7 Critical load for the diagonal family of ribs (w_s=2)

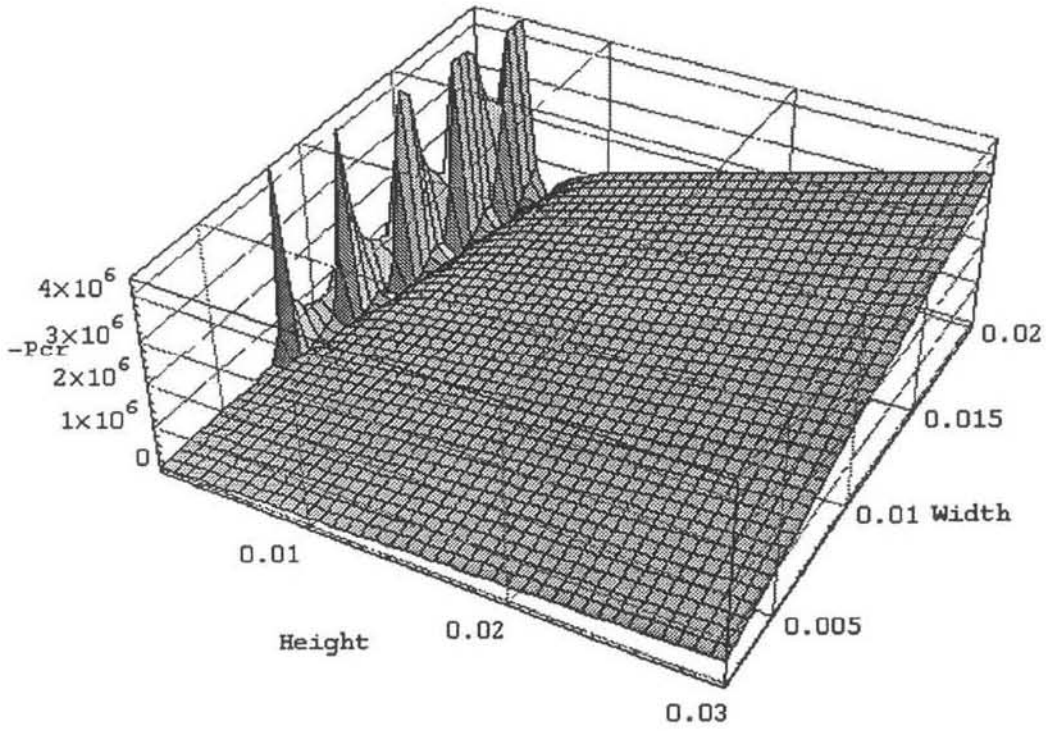

Figure 5.8 Critical load for the vertical family of ribs (w_s=2)

In the case of dominating tensile loading (w_s=2) as can be seen from Figure 5.7-Figure 5.8, the failure load for the diagonal families is much smaller than for the vertical families. The aspect ratios of the ribs that belong to the diagonal families tend to a unit. This occurs because of the increased tensile component of the axial force in the diagonal families of ribs. Considering the cross-section of the vertical and diagonal ribs to be the same during the optimisation process leads to the vertical family become much stiffer than the diagonal. This points towards the possibility of considering cross-sectional parameters b and h to be different for vertical and diagonal families of ribs, varying independently during the optimisation process. That can subsequently increase the stiffness of the structure in the critically loaded direction and reduce the total mass of the structure as a whole.

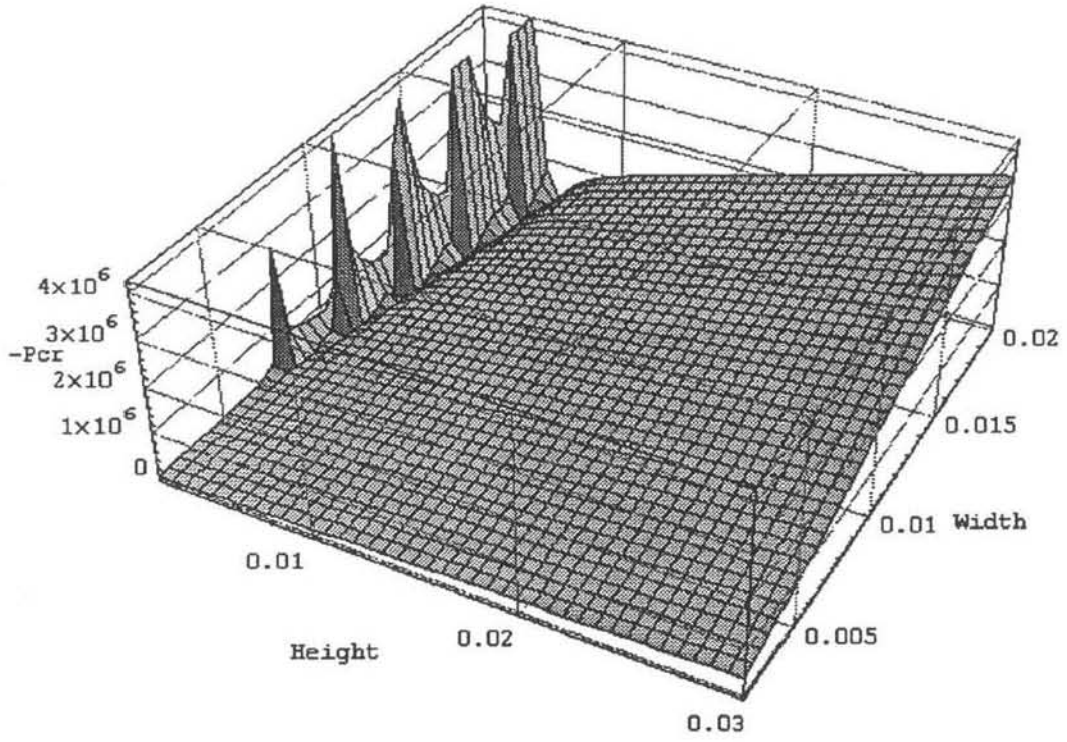

Figure 5.9 Critical load for the vertical family of ribs (w_s=0.5)

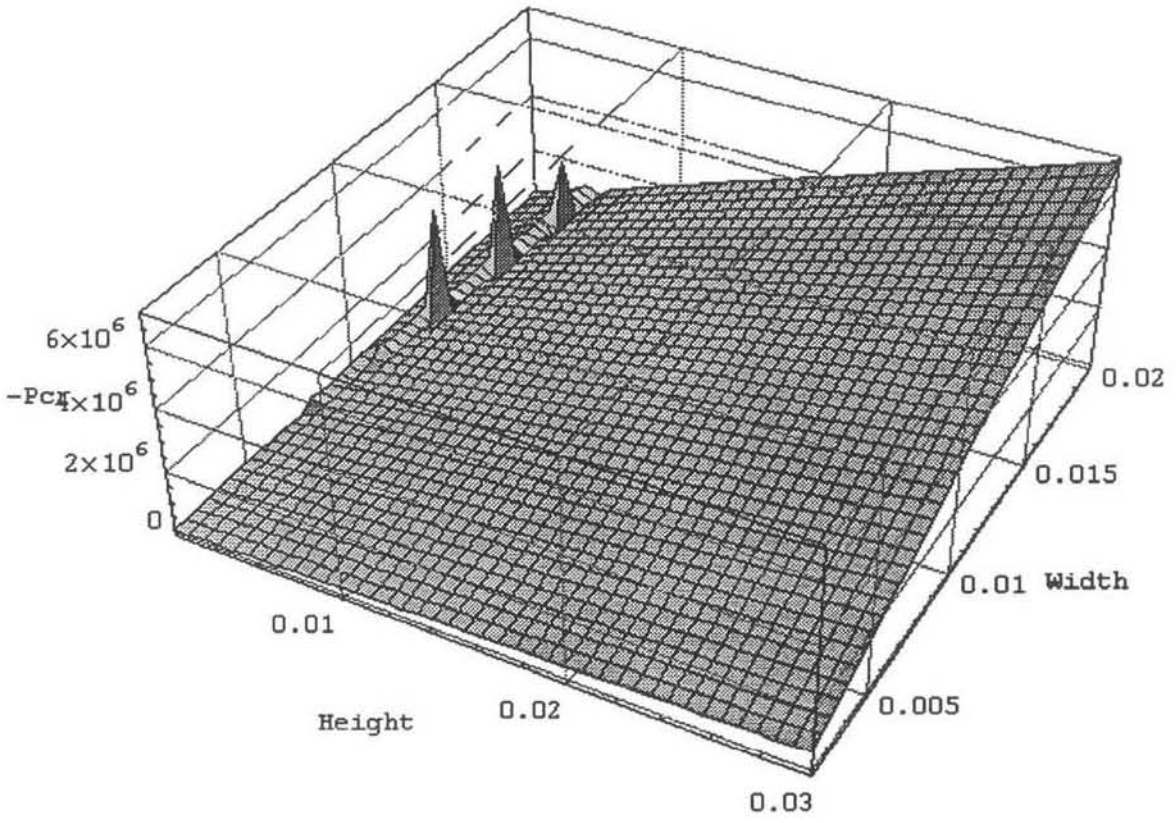

Figure 5.10 Critical load for the diagonal family of ribs (w_s=0.5)

For the case of w_s=0.5 the increase of the load scaling factor (which leads to the increase of the torsional component of the loading) as can be seen from the Figure 5.9 - Figure 5.10 does not influence much the stress-strain state of the ribs that belong to the vertical family. Increased strength of the diagonal ribs is observed. This is caused by the decreased contribution of the axial loading of the diagonal ribs subjected to the smaller torsional component of the applied load. There are several local maximums on the surface plots Figure 5.9 - Figure 5.10. The global optimum corresponds to the b=0.017m and h=0.035m for the critical loading combination: q_{ten}=3.8 10^6 N/m, q_{tor}=1.9 10^6 N/m. The cross-section of the vertical ribs tends to the high aspect ratio in the hoop (tangential) direction to increase the bending stiffness of the vertical ribs to sustain the bending component of the torsional load.

The second problem involves the maximum applied load design for the isogrid cylindrical structure subjected to the same combined loading, but the design variables are chosen as the height (h) of the cross-section of the rib in each of the families and the cell configuration described by the angle (φ) between the first family and the

generator of the cylindrical surface. The aspect ratio of the cross-section in this case is considered constant (equal to three as suggested in [39]). The relationship between the height of the rib, cell configuration and the maximum applied load is established. The effect of the design parameters on the extension and torsional stiffness is investigated.

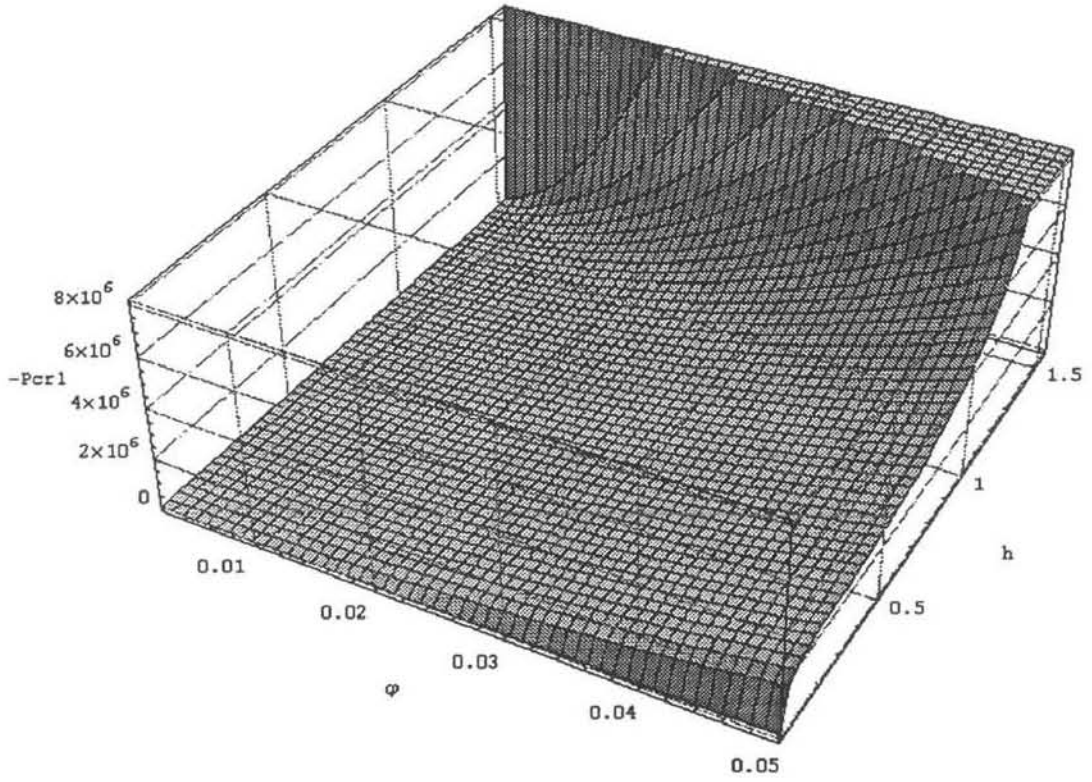

Figure 5.11 Critical load for vertical family of ribs (w_s=1)

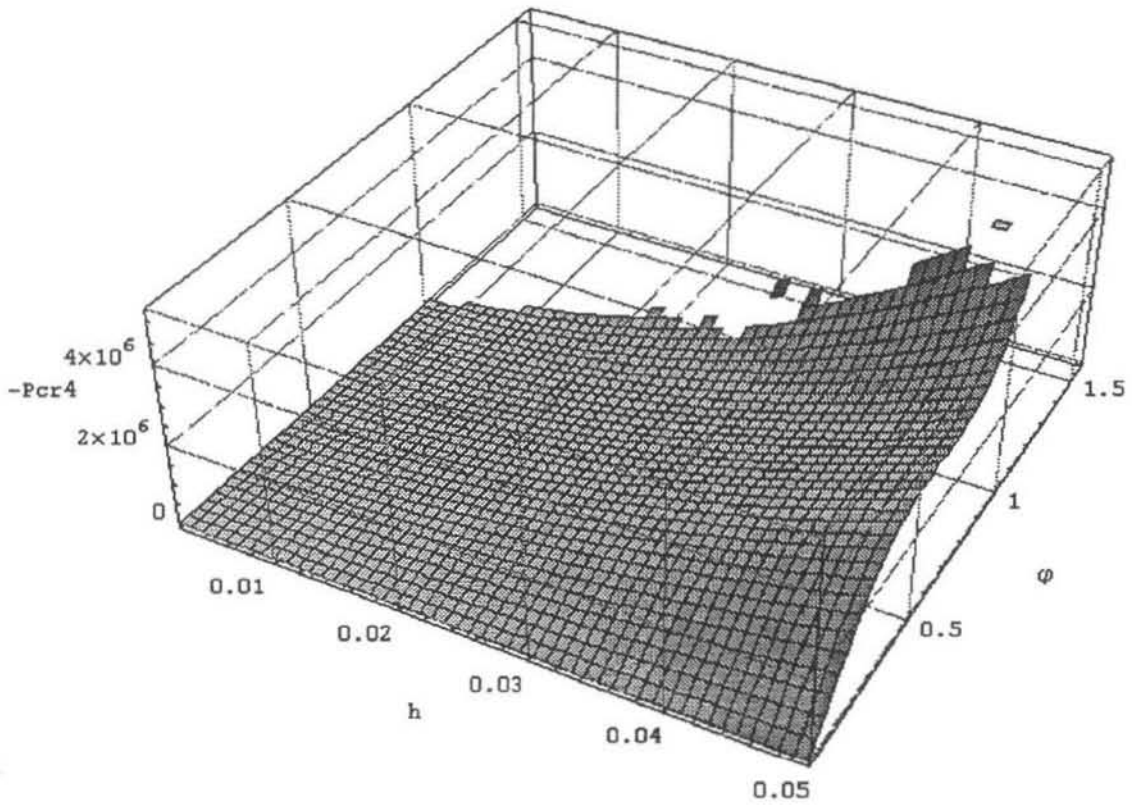

Figure 5.12 Critical load for diagonal family of ribs (w_s=1)

A number of cases were considered for different values of the aspect ratio of the cross-section. The optima are given in the Table 5.3.

With introducing a cell configuration angle φ as a design variable, the distribution of the optimum sequences becomes more complex. Extensional and torque stiffness of a cylindrical structure in this case is governed by the change in orientation of the two diagonal families. Torque stiffness increases for higher values of φ (60...70°). In contrast, the extensional stiffness is reverse dependant on φ: increasing for the lower φ values (40...50°). The change in cell configuration causes a change in cell density and subsequently a slight change in the diameter of an isogrid cylinder (the magnitude of this change also depends on the change in cell density). That is why, in practical design/optimisation of the isogrid structures it is recommended that the change in the design variable φ with a certain step be consider, to be able to manufacture an enclosed isogrid cylinder.

The range of the design variables were taken as $35°>\varphi>75°$, $0.002>h>0.07$ from the considerations of manufacturability of the isogrid structure. The optimisation results

show that with decreasing angle φ, the torsional stiffness of the structure decreases. The optimum cell configuration for the w_s=2 corresponds to the φ=62.1° and h=0.02394m at the critical load combination: q_{ten}=q_{tor}=1.2 10^7 N/m. Analysing the plots for different load scaling factors the following conclusions can be made:

1. For w_s=2 (dominant torsional load) and w_s=0.5 (dominant tension load): in the case of the smaller torsion load the diagonal ribs can sustain a higher load than in the case of w_s=2, but still the failure will be at the minimum load for both families. In this case it will be vertical family.
2. For the vertical family the value of the critical load does not change with the load factor (w_s).

The values of the optimum sequences of the cross-sectional parameters are presented in the Table 5.3. The optima are found in each case using symbolic computation package *Mathematica* by means of multiple application of the Sequential Quadratic Method (SQM). In this method, a quadratic programming subproblem is solved at each iteration with constant changing of the initial guess.

The objective of the design study for the third case is to maximise the applied loading subjected to the material failure constraint. Maximisation of the applied load (q_{ten}, q_{tor}) is achieved by optimally determining the width and height of the ribs cross-section (b and h respectively) and the angle (φ) between the first family and the generator of the cylindrical surface in order to prevent material failure occuring during the loading event. The design-optimisation problem is stated as (5.19) subjected to (5.20) and (5.21). The computational solution consists of successive stages of the calculation of the stiffness parameters with successive optimisation until a convergence is obtained and the optimal values of the design variables (5.20), (5.21) are determined within a specified range of accuracy. In this optimisation study the Sequential Quadratic Method (SQM) [105] is employed to determine the global optimum. The effect of the design parameters on the extension and torque stiffness is investigated. The optimisation task has been performed the different combinations of tension and torque loads. The numerical results are given in the Table 5.4 for the isogrid structure (Figure 2.5) with the dimensions shown in Table 2.1 and the material properties of the ribs shown in Table 2.2.

The numerical results obtained on the basis of optimisation study show that the vertical family of the ribs is more sensitive to the loading and will fail first at the lower values of the combined tension and torsion loading. This is true for all the three cases considered. The optimum configuration of the unit cell of the grid structure in the case of equal tensile and torsion loading corresponds to an almost equilateral triangle (φ_{opt}=61.3°). When the tensile loading starts to dominate (the case w_s=0.5), the unit cell will tend to stretch in the vertical (z) direction, and the optimum cell configuration corresponds to the isosceles triangle with the base angle φ_{opt}=40.5°; accordingly for the case of dominating torsion loading the base angle φ_{opt}=73.3° - the unit cell tends to stretch in the hoop (θ) direction. The rectangular cross-section parameters are also changing dependent on the dominant loading component. As expected, as the torsional component of the combined load increases (w_s=0.5, 1, 2) the aspect ratio of the rib's cross-section tends to increase in the hoop (θ) direction. Predominate torsion of the structure causes bending of the ribs in the θ direction, which subsequently governs the increasing aspect ratio of the ribs. The increased aspect ratio of the ribs accordingly increases the second moments of inertia of the cross-section in the direction of the induced bending.

The values of the optimum sequences of the cross-sectional parameters are presented in the Table 5.4. The optimums are found in each case using the symbolic computation package *Mathematica* by means of multiple application of the Sequential Quadratic Method (SQM).

Vertical Family						*Diagonal Family*				
w_s	b	h	φ	q_{ten}	q_{tor}	b	h	φ	q_{ten}	q_{tor}
1	0.025 m	0.004 m	0°	10^7 N/m	10^7 N/m	0.0218 m	0.0302 m	60°	10^7 N/m	10^7 N/m
2	0.029 m	0.002 m	0°	$4\ 10^6$ N/m	$8\ 10^6$ N/m	0.0301 m	0.069 m	60°	$1.5\ 10^6$ N/m	$3\ 10^6$ N/m
0.5	0.017 m	0.0035 m	0°	$3.8\ 10^6$ N/m	$1.9\ 10^6$ N/m	0.0219 m	0.0302 m	60°	$6\ 10^6$ N/m	$3\ 10^6$ N/m

Table 5.2 Optimum values for b, h

Vertical Family						*Diagonal Family*				
w_s	b	h	φ	q_{ten}	q_{tor}	b	h	φ	q_{ten}	q_{tor}
1	0.0091 m	0.0026 m	0°	$1.2\ 10^7$ N/m	$1.2\ 10^7$ N/m	0.02394 m	0.00684 m	62.1°	$1.3\ 10^7$ N/m	$1.3\ 10^7$ N/m
2	0.01295 m	0.0037 m	0°	$4.7\ 10^6$ N/m	$9.4\ 10^6$ N/m	0.0588 m	0.0168 m	71.4°	$1.8\ 10^6$ N/m	$3.6\ 10^6$ N/m
0.5	0.01155 m	0.0033 m	0°	$4.3\ 10^6$ N/m	$2.2\ 10^6$ N/m	0.06825 m	0.0195 m	38.2°	$7.2\ 10^6$ N/m	$3.6\ 10^6$ N/m

Table 5.3 Optimum values for h, φ, when aspect ratio is constant (3.5)

Vertical Family						*Diagonal Family*				
w_s	b	h	φ	q_{ten}	q_{tor}	b	h	φ	q_{ten}	q_{tor}
1	0.014 m	0.004 m	0°	$1.38\ 10^7$ N/m	$1.38\ 10^7$ N/m	0.021 m	0.014 m	61.3°	$1.4\ 10^7$ N/m	$1.4\ 10^7$ N/m
2	0.033 m	0.0063 m	0°	$5.43\ 10^6$ N/m	$1.1\ 10^7$ N/m	0.027 m	0.0057 m	73.3°	$6\ 10^6$ N/m	$1.2\ 10^7$ N/m
0.5	0.024 m	0.0135 m	0°	$4.9\ 10^6$ N/m	$2.45\ 10^6$ N/m	0.052 m	0.02625 m	40.5°	$8.64\ 10^6$ N/m	$4.32\ 10^6$ N/m

Table 5.4 Optimum values for b, h, φ

* Bold case indicates design variable

The range of design variables: $35^0 \le \varphi \le 75^0$ $\quad 0.002 \le b \le 0.07$ $\quad 0.002 \le h \le 0.07$

5.10 Analysis of the Results

The effects of tensile and torsion applied load on the optimum design have been investigated.

In the case of equal tensile and torsion loads (Figure 5.5, Figure 5.6, Table 5.2 - Table 5.4), the failure occurs in both families of ribs almost simultaneously at the critical load combination: $q_{ten}=q_{tor}=10^7$ /m.

In the case of dominating torque loading ($w_s=2$) as can be seen from Figure 5.7, Figure 5.8; Table 5.2, that the aspect ratio increases to increase the torsion stiffness of the structure. Ribs tend to get taller in the hoop direction. The failure load for the diagonal families is much smaller than for the vertical families. The aspect ratios of the ribs that belong to the diagonal families tend to a unit. This occurs because of the increased tensile component of the axial force in the diagonal families of ribs. Considering the cross-section of the vertical and diagonal ribs being the same during the optimisation process leads to the vertical family becoming much stiffer than the diagonal. This points towards the possibility of considering cross-sectional parameters b and h to be different for vertical and diagonal families of ribs, varying independently during the optimisation process. This can subsequently increase the stiffness of the structure in the critically loaded direction and reduce the total mass of the structure as a whole.

When introducing a cell configuration angle φ as a design variable, the distribution of the optimum sequences becomes more complex. Extensional and torsion stiffness of a cylindrical structure in this case is governed by the change in orientation of the two diagonal families. Torsion stiffness increases for higher values of φ (60...70°). In contrast, the extensional stiffness is reverse dependant on φ: increases for the lower φ values (40...50°). The change in cell configuration causes a change in cell density and subsequently a slight change in the diameter of an isogrid cylinder (the magnitude of this change also depends on the change in cell density). That is why, in the practical design/optimisation of the isogrid structures it is recommended that the change in the design variable φ with a certain step be considered, to allow manufacture of an enclosed isogrid cylinder. Results obtained for a number of design/optimisation studies are also summarised in [82], [84].

5.11 Conclusions

The procedure for optimally designing grid structures for a maximum applied loading using a failure criterion as a constraint is described. The objective is a maximum applied combined tensile and torsion load and the design variables are cell configuration and the cross-section parameters of the ribs comprising the grid. The equivalent stiffness homogenisation approach in conjunction with an optimum search routines is used to determine the design variables optimally. The numerical approach employed in the present study is necessitated by the computational inefficiency and conventional difficulties of linking the optimiser and the FEM analysis package for calculating the stress resultants used in the optimisation process. These were successfully overcome by the developing special purpose symbolic computation routines to compute stress resultants directly in the program using the new homogenisation approach for the model with equivalent stiffness. The proposed homogenisation approach shows high efficiency and good accuracy for the obtained results. It must be emphasised that different failure criteria may be used.

The effect of the optimisation was investigated by plotting surfaces of optimisation, where the critical applied load is plotted against the design variables. The results show that the difference in the value of the maximum load applied to the optimal and non-optimal isogrid structure can be quite substantial, emphasising the importance of optimisation for composite isogrid structures.

In order to demonstrate the complete procedure of implementation of the new homogenisation approach to the design-optimisation study, several isogrid cylinders were completely optimised, such that both width and height of the ribs comprising vertical and diagonal families and the angle of the cell configuration were determined optimally. These structures have been analysed for different loading conditions such as tension and torsion and their combination, and optimal designs of each were compared to the others. The extent of influence of the rib's geometry and unit cell configuration on extensional and torsion stiffness was established.

6 Areas of Further Research

This research is aimed at formulating new mathematical models for composite grid plates and shells which are subjected to a variety of loading combinations. The main objective of this research is to improve the accuracy and efficiency of the tools for design/optimisation of these structures. As a step towards obtaining practical results and further research in this area it is recommended that that the developed experimental computer code [Appendix 1, 2] written using symbolic computation package *Mathematica* should be made available in more accessible versions to the researchers working in the field of the design/optimisation of grid structures. Further work on this code should concentrate on considering the influence of boundary effects in the vicinities of loaded and constrained edges of a shell. The mechanism of application of internal pressure to the mathematical model should also be further investigated. In addition, experimental studies on a real isogrid structures should be carried out to investigate an accuracy of the homogenised mathematical model. In the case of a grid structure with outer layers of composite skins the homogenised representation of the skins must be developed so that the behaviour of the composite grid structure as a whole can be represented adequately.

Some of the areas of grid structure analysis which are still not well developed analytically, are typically resolved by the use of FEM. These areas include: local rib buckling, local skin 'pocket buckling', rib termination effects and the effects of grid pattern irregularities. The influence of manufacturing defects on the modelling of grid structures should also be addressed. Detailed geometry of a grid structure is heavily dependent on the manufacturing method used. The effects of different manufacturing processes on the behaviour of grid structures is currently not very well understood and was not implemented in the currently developed model. Further development of the current model must also address the following common manufacturing defects: material build-up at the nodes, skin print-through (markoff) near ribs where rubber tooling deforms the skin, wavy fibres in ribs due to lateral compaction, resin rich/dry areas at or near nodes, and non-uniform fibre volume fraction from rib top to rib bottom.

The analysis tool developed in this study is aimed at making the design of grid structures easier for the engineer. The tool of course has to be further developed not only to be able to incorporate the effects mentioned above, but also to address some of the guideline issues of the grid structures design which have not been fully understood and developed at present time. This issues include:

- Investigation of the effect of nodal offset.
- The best methods to terminate different types of grid patterns.
- The choice of the grid pattern for the lattice structures of revolution. What families of ribs should be included for the optimal structural performance?
- Adequate representation of discontinuities in grid structure patterns (cut-outs, doors, windows) and the boundary effect at the edges.
- Fabrication of a grid structure with a zero bending-coupling (B-matrix) which would not warp under a temperature change.

Development of reliable and accurate optimisation methods is also essential due to the expanded use of composite grid shells in high-tech industries. Therefore, there is a need to improve the current optimisation methods and approaches. Development of practical numerical techniques for predicting the failure initiation in composite grid shells subjected to different loading conditions is a logical sequel of the design optimisation and of a great importance in modern engineering. The results of this research can be used to assemble a computer code for the simulation of the deformation and stresses of the grid structure subjected to a variety of loads and their combination. The extended optimisation routines can also be further developed to handle more variables. This research would greatly enhance the scope and effectiveness of conventional tools for the design/optimisation of grid structures. Several problems which are cumbersome or exceedingly difficult to solve using conventional techniques could be treated using the proposed new homogenisation method.

7 General Conclusions

A model for the analysis of grid structures based on the equivalent stiffness approach has been developed. The model was verified by comparing the results obtained on its basis to those obtained using exact FEM model. The equivalent stiffness model was shown to be accurate in predicting resultant stresses and strains. However, the equivalent stiffness approach was found later to be inefficient for application in the design/optimisation of lattice structures, so a new homogenisation approach was proposed. The new homogenisation approach was developed and verified. This approach was implemented using the symbolic computational system of *Mathematica*. The developed software was used to derive analytical expressions for the objective functions with further calculation of the numerical results.

The numerical results were calculated for the problem of isogrid cylindrical structure subjected to tensile and torsion loads. The optimisation study shows the maximum values of the combination of the loads correspond to the values of optimum design parameters. Results are presented for a model, which neglects the influence of the boundary effects. The computational efficiency of the optimisation algorithm in the design optimisation of cylindrical isogrids was improved and good accuracy of the results has been achieved. The investigation based on failure analysis shows that the difference in the value of maximum load applied to the optimal and non-optimal isogrid structure can be quite substantial, emphasising the importance of optimisation for the composite isogrid structures. Several isogrid cylinders were completely optimised on the basis of the proposed homogenisation approach, such that both the width and height of the ribs comprising vertical and diagonal families and the angle of the cell configuration were determined optimally. These structures were analysed for different loading conditions such as tension and torsion, and their combination. The numerical results obtained during several optimisation runs can be used in the practical engineering design of isogrid structures to allow time consuming and inefficient trial and error methods to be avoided when the recommended values for cross-sectional parameters, cell configuration and cell density have to be determined for an arbitrary loading combination.

As a step towards improving the developed experimental computer code, further work should concentrate on considering the influence of boundary effects in the vicinities of loaded and constrained edges of a shell. The mechanism of applying of internal

pressure to the mathematical model should also be further investigated. The extended optimisation routines can also be further developed to handle more variables.

References

[1] Adali S. , Summers E. B. and Verijenko V. E., "Minimum Weight and Deflection Design of Thick Sandwich Laminates via Symbolic Computation", *Composite Structures,* Vol. 29, 1994, pp. 145-160.

[2] Adali S. , Richter A. and Verijenko V. E., "Multiobjective Design of Laminated Cylindrical Shells for Maximum Pressure and Buckling Load", *Microcomputers in Civil Engineering*, Vol. 10(4), 1995, pp. 269-280.

[3] Adali S. , Richter A. and Verijenko V. E., "Optimisation of Shear Deformable Laminated Plates under Buckling and Strength Criteria", *Composite Structures*, Vol. 39, 1997, pp. 167-178.

[4] Agarwal B. D. and Broutman L. J., *Analysis and Performance of Fiber Composites,* John Wiley & Sons, New York, NY, 1980.

[5] Ali H., Chang S., *COSMOS/M Advanced Modules User Guide*, SRAC, Santa Monica, USA, 1993.

[6] Ambartsumyan S. A., *General Theory of Anisotropic Shells.* Nauka, Moscow. 446p, Russian, 1974.

[7] Ashton J. E. and Whitney J. M., *Theory of Laminated Plates,* Technomic Publishing Co., Inc., Westport, CT, 1970.

[8] Belegundu A. D., and Rajan S. D., "Shape Optimal Design Using Isoparametric Elements", *Proceedings of 29th AIAA/ASME/ASCE/AHS/ASC Structures, Dynamics, and Materials Conference,* pp. 696-701, Williamsburg, VA, April 18-20, 1988.

[9] Beveridge Gordon S. G., *Optimization: Theory and Practice,* McGraw-Hill, New York, 1970.

[10] Broyden C. G., "The Convergence of a Class of Double Rank Minimization Algorithms, Parts I and II", *J. Inst. Math. Appl.,* Vol. 6, pp. 76-90, 222-231, 1970.

[11] Chang F. K., *AA250 Course Notes,* Stanford University., Stanford, CA, Autumn, 1992.

[12] Chen C. H. and Cheng S., "Mechanical Properties of Fiber Reinforced Composites", *Journal of Composite Materials,* Vol. 1, 1967, p. 30.

[13] Chen H.-J., Tsai S. "Analysis and Optimum Design of Composite Grid Structures", *Journal of Composite Materials,* vol. 30, NO 4/1996:503-532.

[14] Christensen R.M., *Mechanics of Composite Materials,* Wiley-Interscience, 1979.

[15] Cook R. D., Malkus D. S. and Plesha M. E., *Concepts and Applications of Finite Element Analysis,* John Wiley & Sons, New York, 1989.

[16] Cronin D., O'Mahoney P., Krishnaswami P., "Forced Response Optimization with MSC/NASTRAN", *1992 MSC World Users' Conf. Proc.,* Vol. II, Paper No. 31, May, 1992.

[17] Currie Andrew, "Structural Design Optimization in MSC/NASTRAN Version 66", *The Second Australasian MSC Users Conf. Proc.,* Paper No. 8, November, 1988.

[18] Dantzig G. B., *Linear Programming and Extensions,* Princeton University Press, Princeton, NJ, 1963.

[19] Deb A. and Booton M., "Finite Element Models for Stiffened Plates under Transverse Loading", *Computers and Structures,* 28(3):361-372, 1988.

[20] Dow N. F. and Grundfest I. J., "Determination of Most Needed Potentially Possible Improvements in Materials for Ballistic and Space Vehicles", *GE-TIS 60SD389,* June 1960.

[21] Enright C., *Pro/Mechanica User Guide,* Parametric Technology Corporation, USA, 1997.

[22] Fagan M. J., *Finite Element Analisis, Theory and Practice,* Longman Scientific & Technical, Singapore, 1992.

[23] Fletcher R. and Reeves C. M., "Function Minimization by Conjugate Gradients", *Br. Computer Journal,* Vol. 7, No. 2, pp. 149-154, 1964.

[24] Fletcher R., "A New Approach to Variable Metric Algorithms", *Computer Journal,* Vol.. 13 pp. 317-322, 1970.

[25] Flugge W., *Stresses in Shels.* 2nd Edition, Springer-Verlag, New York, 1973.

[26] Goldenveyzer A. L., *Theory of Thin Elastic Shells,* Moscow, Fizmatgis, 1976.

[27] Goldfarb D., "A Family of Variable Metric Methods Derived by Variational Means", *Math. Comput.,* Vol. 24 pp. 23-26, 1970.

[28] Hashin Z. and Rosen B. W., "The Elastic Moduli of Fiber-Reinforced Materials", *Journal of Appl. Mech.,* Vol. 31, 1964, p.223.

[29] Hashin Z., "Failure Criteria for Unidirectional Fiber Composites", *J. Appl. Mech.,* Vol. 47, 1980, p. 329.

[30] Hashin Z., "Theory of Fiber Reinforced Materials", *NASA CR*-1974, 1972.

[31] Hashin Z., "Analysis of Properties of Fiber Composites with Anisotropic Constituents", *Journal of Appl. Mech.,* Vol. 46, 1979, p.543.

[32] Hong-Ji Chen, *Analysis and Optimum Design of Composite Grid Structures*, Stanford University, Stanford, CA, 1994.

[33] Hughes T. J. R., *The Finite Element Method*, Prentice-Holl, Inc., Englewood Cliffs, New Jersey, 1987.

[34] Hughes T. J. R., *The Finite Element Method: Linear Static and Dynamic Finite Element Analysis*, Prentice-Hall, Englewood Cliffs, New Jersey, 1987.

[35] Hussein R. M, *Composite Panels/Plates: Analysis and Design*, Technomic Publishing Co., Inc., Westport, CT, 1986.

[36] Huybrechts S. M., Tsai S. "Analysis and Behaviour of Grid Structures", *Composite Science and Technology* 56/1996:1001-1015.

[37] Huybrechts S., Hahn S. E., Meink T. E. "Grid Stiffened Structures: A Survey of Fabrication, Analysis and Design Methods", *Proceedings of the Twelfth International Conference on Composite Materials ICCM/12*, July 1999, Paris, France.

[38] Huybrechts S., and Meink T. E., "Advanced Grid Stiffened Structures for the Next Generation of Launch Vehicles", *1997 IEEE Aerospace Conference Proceedings*, 1997.

[39] *Isogrid Design Handbook*, McDonnell Douglas Company, Report MDC G4295A, 1973.

[40] Jackson J. J. and Wirtz H. G., *Statics and Strength of Materials*, Schaum`s Outline Series, McGraw-Hill, Inc., New York, 1983.

[41] Jones R. M. *Mechanics of Composite Materials*, Scripta Book Company, Washington, D.C., 1975.

[42] Kalamkarov A. L., "Modelling and Design of Composites of a Regular Structure", *Proceeding of the Third International Conference on Composite Science and Technology ICCST/3*, pp. 21-22, January 2000, Durban, South Africa.

[43] Kalamkarov A. L. and Kolpakov A. G., *Analysis, Design and Optimisation of Composite Structures*, 1997, John Wiley & Sons: Chichester, New-York.

[44] Kalamkarov A. L., *Composite and Reinforced Elements of Construction*, 1992, John Wiley & Sons: Chichester, New-York.

[45] Kelly J. E., "The Cutting Plane Method for Solving Convex Programs", *J. SIAM*, Vol. 8, pp. 702-712, 1960.

[46] Kollar L. and Hegedus I., *Analysis and Design of Space Frames By the Continuum Method*, Elsevier Science Publishing Company, Amsterdam, 1985.

[47] Koury J. L., and Kim T. D., "Continuous Fiber Composite Isogrid Structures for Space Applications," *1993 ASM Conference*, Long Beach, CA, 1993.

[48] Lekhnitskii S. G., *Anisotropic Plates*, Gordon and Breach, Science Publishers, New York, 1968.

[49] Logan D. L., *A First Course in the Finite Element Method*, PWS-KENT Publishing Company, Boston, 1986.

[50] Megson T. H. G., *Aircraft Structures for Engineering Students*, Halsted Press, New York, 1975.

[51] Meink T. E., *Structural Analysis and Design of Composite Isogrid Panels for Increased Buckling Efficiency*. The Ohio State University, Columbus, OH, 1995.

[52] Meink T. E. and Gregoreck G., "Composite Grid vs. Composite Sandwich: A Comparison Based on Payload Shroud Requirements", *1998 IEEE Aerospace Conference Proceedings*, April, 1998.

[53] Meink T., Huybrechts S., Ganley J., and Shen H., "The Effect of Varying Thickness on the Buckling of Orthotropic Plates", *Journal of Composite Materials*, 1999.

[54] Meink T. E. and Huybrechts S., "Hybrid Tooling for Advanced Grid Stiffened (AGS) Structures", *1996 SAMPE Technical Conference Proceedings*, November 4-7, 1996.

[55] Monaco P., *PROMOL Software for Composites*, New York, USA, 1996.

[56] *MSC/NASTRAN V68 Design Sensitivity and Optimization User's Guide*

[57] Mukherjee A. and Mukhopadhyay. 1988 "Finite Element Free Vibration of Eccentrically Stiffened Plates", *Computers and Structures*, 30(6):1303-1317.

[58] Mushtari H. M, Galimov K. Z, *Nelineinaya teoria uprugih obolochek*, Kazan, Tatknigoizdat, USSR, 1957.

[59] Niordson F., *Shell theory / Frithiof I. Niordson*, Amsterdam : North-Holland, 1985.

[60] Novozhilov V. V., *Basics of Nonlinear Theory of Elasticity*, Leningrad, Moscow, Gostehizdat, 1948.

[61] Ochoa O. O. and Reddy J. N., *Finite Element Analysis of Composite Laminates*, Kluwer Academic Publishers, Dordrecht, 1992.

[62] Palani G. S., Lyer N. R. and Appa Rao T. V. S. R. 1992. "An Efficient Finite Element Model for Static and Vibration Analysis of Eccentrically Stiffened Plates/Shells", *Computers and Structures*, 43(4):651-661, pp. 53-66, 1992.

[63] Panne C. *Methods for Linear and Quadratic Programming*, Amsterdam, North-Holland, 1975.

[64] Piskunov V. G., Verijenko V. E., Adali S. and Tabakov P. Y., "Transverse Shear and Normal Deformation Higher-Order Theory for the Solution of Dynamic Problems of Laminated Plates and Shells", *International Journal of Solids and Structures*, vol. 31, No. 24, pp. 3345-3374, 1994.

[65] Powell M. J. D. *Nonlinear Optimization*, 1981 London, Academic Press, 1982.

[66] Powell M. J. D., *Approximation Theory and Methods*, Cambridge University Press, Cambridge, 1981.

[67] Powell M. J. D., *Nonlinear Optimization*, Proceedings of the NATO Advanced Research Institute, Academic Press, London, 1982.

[68] Powell M. J. D., "Algorithms for Nonlinear Constraints that use Lagrangian Functions", *Math. Prog.*, Vol. 14, No. 2 pp. 224-248, 1978.

[69] Przemieniecki J. S., *Theory of Matrix Structural Analysis*, Dover Publications, Inc., New York, 1968.

[70] Rao D. V., Sheikh A. H. and Mukopadhyay M. 1993. "A Finite Element Large Displacement Analysis of Stiffened Plates", *Computers and Structures*, 47(6):987-993.

[71] Reddy A. D., Rehfield L. W., Haag R. S. and Wildman C. G. "Compressive Buckling Behaviour of Graphite/Epoxy Isogrid Wide Column with Progressive Damage", *ASTM Symposium on Compression Testing of Homogeneous Materials and Composites*, ASTM-STP 808, pp. 187-199, 1983.

[72] Reddy A. D., Vasiletty R. R. and Rehfield L. W. "Continuous Filament Wound Composite Concepts for Aircraft Fuselage Structures", *Journal of Aircraft*, Vol. 22, 3, pp. 249-255, 1985.

[73] Reddy A. D., Valisetty R. R., and Rehfield L. W., "Continuous Filament Wound Composite Concepts for Aircraft Fuselage Structures", 1984 *AIAA/ASME/ASCE/AHS 25th Structures*, Structural Dynamics and Materials Conference, May 14-16, 1984.

[74] Reddy J. N., *Energy and Variational Method in Applied Mechanics*, John Wiley & Sons, New York, 1984.

[75] Rehfield L. W. and Reddy A. D. "Damage Tolerance of Continuous Filament Composite Isogrid Structures: A Preliminary Assessment", *Composite Materials:* Mechanics, Mechanical Properties and Fabrication, Japan - U.S. Conference, Tokyo, pp. 545-553, 1982.

[76] Roark R. J. and Young W. C., *Formulas for Stress and Strain,* 5th ed., McGraw-Hill, 1975.

[77] Rosen B. W., "Mechanics of Composite Strengthening", *Fiber Composite Materials,* Am. Soc. for Metals, Metals Park, Ohio, 1965.

[78] Saadat H., *Computational Aids in Control Systems Using MATLAB,* McGrow-Hill, Inc., New York, 1993.

[79] Sendeckyj G. P., "Elastic Behaviour of Composites", *Mechanics of Composite Materials,* Vol. II, ed. Sendeckyj, G.P., Academic Press, 1974.

[80] Shanno D. F., "Conditioning of Quasi-Newton Methods for Function Minimization", *Math. Comput.,* Vol. 24, pp. 647-656, 1970.

[81] Slinchenko D., Verijenko V. E., Adali S. and Sevostianov I. B. "Design/Optimisation of Isogrid Cylindrical Structures", *Proceeding of the Second International Conference on Composite Science and Technology ICCMS/2,* June 1998, Durban, South Africa, pp 265-270.

[82] Slinchenko D., Verijenko V. E., "Optimum Design of Grid Cylindrical Structures Using Homogenized Method", *Proceedings of the Twelfth International Conference on Composite Materials ICCM/12,* July 1999, Paris, France, p. 568.

[83] Slinchenko D., Verijenko V. E., "Optimum Design of Grid Structures of Revolution Using Homogenized Model", *Proceedings of the Sixth International Conference on Composite Engineering ICCE/6,* June 1999, Orlando, USA, pp. 783-784.

[84] Slinchenko D., Verijenko V. E. and Adali S., "Optimization of Lattice Structures Using Equivalent Homogenized Model", *Proceedings of the Third International Conference on Composite Science and Technology ICCST/3,* January 2000, Durban, South Africa, pp. 165-170.

[85] Slysh P., Dyer J. E., Furman J. H., and Key J. E., "Isogrid Structural Tests and Stability Analyses", *Journal of Aircraft,* Vol. 13, 3, pp. 778-785, 1976.

[86] Sokolnikoff I. S., *Mathematical Theory of Elasticity,* McGraw-Hill, New York, 1956.

[87] Subramanian G. and Jayachandrabose C., "Convenient Generating of Stiffness Matrices for the Family of Plane Triangular Elements", *Computers & Structures,* Vol. 15, No. 1, 1982, pp. 85-89.

[88] Sumec J., *Regular Lattice and Shells*, Elsevier Science Publishing Company, Amsterdam, 1990.

[89] Summers E., *PhD Thesis: Analysis and Design Optimization of Laminated Composite Structutes Using Symbolic Computation*, University of Natal, Durban, South Africa, October 1994.

[90] Tabakov P., *PhD Thesis: Computational and Analistical Modelling of Composite Structures Based on Exact and Higher Order Theories*, University of Natal, Durban, South Africa, November 1995.

[91] Tarnopol'skii Yu. M., Zhigun I.G., Polyakov V.A., *Spatially reinforced composites*, 1992.

[92] Tarnopol'skii Yu. M., Kincis T., *Static test methods for composites*, 1985.

[93] Thompson P. A., Bettess P. and Caldwell J. B. 1988. "An Isoparametric Eccentrically Stiffened Plate Bending Element", *Engineering Computation*, 5:110-116.

[94] Timoshenko S. P. and S. Woinowsky-Krieger, *Theory of Plates and Shells*, 2nd Ed., McGraw-Hill, New York, 1959.

[95] Timoshenko S. P., *Elements of Strength of Materials*, 4th ed, Princeton, N.J. : Van Nostrand, 1962.

[96] Timoshenko S. P., *Theory of Elastic Stability*, McGraw-Hill, New York, 1961.

[97] Timoshenko S. P., *Theory of Elasticity*, 3rd ed., Auckland : McGraw-Hill, 1970.

[98] Troitsky M. S., *Stiffened Plates: Bending, Stability and Vibrations*, Elsevier Science Publishing Company, Amsterdam, 1976.

[99] Tsai S. W., "Strength Characteristics of Composite Materials", *NASA CR-224*, 1965.

[100] Tsai S. W. and Wu E. M., "A General Theory of Strength for Anisotropic Materials", *Journal of Composite Materials*, Vol. 5, 1971, p. 58.

[101] Tsai S. W. and Hahn H. T., *Introduction to Composite Materials*, Technomic Publishing Co., Inc., Westport, CT, 1988.

[102] Tsai S. W., *Theory of Composites Design*, Think Composites, Dayton, Ohio, 1992.

[103] Ugural A. C., *Stresses in Plates and Shells*, McGraw-Hill Book Company, New York, 1981.

[104] Vanderplaats G. N., "An Efficient Feasible Direction Algorithm for Design Synthesis", *AIAA Journal*, Vol. 22, No. 11, Nov. 1984.

[105] Vanderplaats G. N., *Numerical Optimization Techniques for Engineering Design with Applications*, McGraw Hill, New York, 1984

[106] Vasiliev V. V., Baraynin V. A., Rasin A. F., "Composite Lattice Structures - Theory and Application", *Proceeding of the Third International Conference on Composite Science and Technology ICCST/3*, pp. 177- 187, January 2000, Durban, South Africa.

[107] Verijenko V. E., "Geometrically Nonlinear Higher Order Theory of Laminated Plates and Shells with Shear and Normal Deformation", *Composite Structures*, vol. 29 (1994), pp. 161-179.

[108] Verijenko V. E., "Nonlinear Deformation of Laminated Orthotropic Shells" *Strengths of Materials and Theory of Structures,* Vol. 59, 1989, pp. 48-53.

[109] Verijenko V. E., "Nonlinear Analysis of Laminated Composite Plates and Shells Including the Effects of Shear and Normal Deformation" *Composite Structures*, Vol. 25, 1993, pp. 173-185.

[110] Verijenko V. E., Adali S. and Summers E. B. , "Accurate Finite Elements Based on Shear Deformation Theory for the Analysis of Laminated Composite Plates", *SAIMechE R & D Journal*, Vol. 9, 1993, pp. 24-32.

[111] Verijenko V. E., Adali S. and Summers E. B. , "Applications of Refined Theory in the Nonlinear Analysis of Laminated Composite Structures", *Computational Mechanics*, Vol. 14(1), 1994, pp. 52-67.

[112] Verijenko V. E., "Geometrically Nonlinear Higher Order Theory of Laminated Plates and Shells with Shear and Normal Deformation", *Composite Structures,* Vol. 29, 1994, pp. 161-179.

[113] Verijenko V. E., , Galileev S. M. and Matrosov A. V., "Method of Initial Functions for Layered and Continuously Nonuniform Plates and Shells", *International Journal. Mechanics of Composite Materials*, Vol. 30 (4), 1994, pp. 531-539 (in Russian).

[114] Verijenko V. E., , Adali S. and Piskunov V. G., "Finite Elements Based on Shear and Normal Deformation Theory for the Analysis of Laminated Composite Plates", *Computers and Structures,* Vol. 54(5), 1995, pp. 789-807.

[115] Vlasov V. Z., *Izbrannie Trudi*, AN SSR, USSR, 1962.

[116] William H., *Numerical Recipes: the Art of Scientific Computing (FORTRAN version)*, Cambridge University Press, Cambridge, 1989.

[117] Wolfram S., *Mathematica, A System for Doing Mathimetics by Computer,* Addison-Wesley Publishing Company, New York, 1988.

[118] Wu E. M., "Phenomenological Anisotropic Failure Criterion", *Mechanics of Composite Materials,* ed. Sendeckyj, G.P., Academic Press, 1974.

[119] Zangwill W. I., *Nonlinear Programming: A Unified Approach*, Prentice-Hall, Englewood Cliffs, NJ, 1969.

[120] Zweben C., "Tensile Failure Analysis of Composites", *AIAA Journal,* Vol. 2, 1968, p. 2325.

Appendix 1

Symbolic computational routine used for the calculation of the equivalent stiffness matrices for the isogrid cylindrical structure.

Calculation of the Equivalent Stiffness Matrices for the Isogrid Structure

Young's moduli of the material:

$$E_x = 1.81\,10^{11}$$
$$E_s = 7170000000$$

Shear correction factor:

$$\chi = \frac{5}{6}$$

Cross-sectional properties (width and height of the ribs):

$$b = 0.00666667$$
$$h = 0.02$$

Spacing for each set of ribs:

$$d_0 = 1$$
$$d_{90} = 0.2618$$
$$d_\theta = 0.3023$$

Moments of inertia:

$$I_{90} = \frac{b\,h^3}{12}$$
$$I_\theta = I_{90}$$
$$I_0 = 0$$

Areas of the rib's cross-section:

$$A_{90} = b\,h$$
$$A_\theta = A_{90}$$
$$A_0 = 0$$

Torsional constants for the rectangular cross-section:

$$J_{90} = \frac{h\,b^3}{16}\left(\frac{16}{13} - 3.36\,\frac{h}{b}\left(\frac{b^4}{12\,h^4}\right)\right)$$
$$J_\theta = J_{90}$$
$$J_0 = 0$$

Angle between co-ordinate axes z and an axis of the first family of ribs:

$$\theta\theta = \frac{Pi}{60}$$

$$m = Cos[\theta\theta]$$
$$n = Sin[\theta\theta]$$

Calculation of extensional, extensional-bending coupling, bending and transverse shear stiffness matrices for the ribs:

$$A_{rib} = \left\{\left\{\frac{E_x A_0}{d_0} + 2\,\frac{E_x A_\theta}{d_\theta}\,m^4,\ 2\,\frac{E_x A_\theta}{d_\theta}\,m^2 n^2,\ 0\right\},\right.$$
$$\left.\left\{2\,\frac{E_x A_\theta}{d_\theta}\,m^2 n^2,\ \frac{E_x A_{90}}{d_{90}} + 2\,\frac{E_x A_\theta}{d_\theta}\,n^4,\ 0\right\},\ \left\{0,\ 0,\ 2\,\frac{E_x A_\theta}{d_\theta}\,m^2 n^2\right\}\right\}$$

$$B_{rib} = \{\{0,\ 0,\ 0\},\ \{0,\ 0,\ 0\},\ \{0,\ 0,\ 0\}\}$$

$$D_{rib} = \{\{D_{11},\ D_{12},\ 0\},\ \{D_{21},\ D_{22},\ 0\},\ \{0,\ 0,\ D_{66}\}\}$$

$$D_{11} = \frac{E_x I_0}{d_0} + 2\,\frac{E_x I_\theta}{d_\theta}\,m^4 + 2\,\frac{E_s J_\theta}{d_\theta}\,m^2 n^2$$

$$D_{22} = \frac{E_x I_{90}}{d_{90}} + 2\,\frac{E_x I_\theta}{d_\theta}\,n^4 + 2\,\frac{E_s J_\theta}{d_\theta}\,m^2 n^2$$

$$D_{12} = 2\,\frac{E_x I_\theta}{d_\theta}\,m^2 n^2 - 2\,\frac{E_s J_\theta}{d_\theta}\,m^2 n^2$$

$$D_{21} = D_{12}$$

$$D_{66} = 2\,\frac{E_x I_\theta}{d_\theta}\,m^2 n^2 + \frac{E_s J_0}{4\,d_\theta} + \frac{E_s J_{90}}{4\,d_{90}} + \frac{E_s J_\theta}{2\,d_\theta}\,(m^2 - n^2)^2$$

$$H_{rib} = \left\{\left\{\chi\,\frac{E_s A_0}{d_0} + 2\,\chi\,\frac{E_s A_\theta}{d_\theta}\,m^2,\ 0\right\},\ \left\{0,\ \chi\,\frac{E_s A_{90}}{d_{90}} + 2\,\chi\,\frac{E_s A_\theta}{d_\theta}\,n^2\right\}\right\}$$

```
MatrixForm[A_rib]
MatrixForm[B_rib]
MatrixForm[D_rib]
MatrixForm[H_rib]
```

Stiffness matrix [Q] is calculated for the given lay-up of the skins using PROMAL sofrware for composites:

$$Q_{sk} = \{\{1.81\,10^2,\ 2.897,\ 0\},\ \{2.897,\ 10.35,\ 0\},\ \{0,\ 0,\ 7.17\}\}$$

```
MatrixForm[Q_sk]
```

Calculation of extensional, extensional-bending coupling, bending and transverse shear stiffness matrices for the ribs:

Thickness of the layers:

$$h_{sk} = 0.02$$

```
A_sk = Array[aa, {3, 3}];
B_sk = Array[bb, {3, 3}];
D_sk = Array[dd, {3, 3}];
i = 0;
Label[be2];
i = i + 1; j = 0;
Label[be3];
j = j + 1;
A_sk[[i, j]] = 2 Q_sk[[i, j]] h_sk;
B_sk[[i, j]] = 1/2 Q_sk[[i, j]] h_sk^2;
D_sk[[i, j]] = 1/3 Q_sk[[i, j]] h_sk^3;
If[j < 3, Goto[be3]];
If[i < 3, Goto[be2]];
Print["A_sk = ", MatrixForm[A_sk]];
Print["B_sk = ", MatrixForm[B_sk]];
Print["D_sk = ", MatrixForm[D_sk]];
```

Equivalent Stiffness Matrices of the isogrid structure:

```
A_total = Array[aaa, {3, 3}];
B_total = Array[bbb, {3, 3}];
D_total = Array[ddd, {3, 3}];
i = 0;
Label[be4];
i = i + 1; j = 0;
Label[be5];
j = j + 1;
A_total[[i, j]] = A_rib[[i, j]] + A_sk[[i, j]];
B_total[[i, j]] = B_rib[[i, j]] + B_sk[[i, j]];
D_total[[i, j]] = D_rib[[i, j]] + D_sk[[i, j]];
If[j < 3, Goto[be3]];
If[i < 3, Goto[be2]];
H_total = H_rib
Print["A_total = ", MatrixForm[A_total]];
Print["B_total = ", MatrixForm[B_total]];
Print["D_total = ", MatrixForm[D_total]];
Print["H_total = ", MatrixForm[H_total]];
```

Appendix 2

The symbolic computational routine used for the calculation of the optimum values of geometric parameters for the isogrid cylindrical structure during different design/optimisation runs.

Design/Optimisation of Isogrid Cylinder

■ Shell parameters:

The angle between generator line and axis of rotation of a shell

$$\gamma = 0$$

$$mm = 0$$

Radius of curvature of a median surface

$$R_0 = 5$$

Curvatures of the shell:

$$k_{1d} = 0$$
$$k_{2d} = 1 / R_0$$

$$k_1 = k_{1d} R_0$$
$$k_2 = k_{2d} R_0$$

Equation of the meridian of a shell:

$$r_d = R_0 + z \, \mathrm{Tan}[\gamma]$$

$$r = r_d / R_0$$

Number of intersection points of rib's axes on the paralel of the median surface:

$$m_0 = 60$$

$$c = \sqrt{(1 - s^2)}$$

Parameters of the cross-section of the ribs:

$$b = h / 3$$

$$FF = (b\,h) / R_0 \wedge 2$$

$$F_1 = (b\,h) / R_0 \wedge 2$$
$$F_2 = (b\,h) / R_0 \wedge 2$$
$$F_3 = (b\,h) / R_0 \wedge 2$$
$$F_4 = (b\,h) / R_0 \wedge 2$$

Material properties: Young's and shear module, Pa:

$$E1 = 1.8\ 10 \wedge 11$$

$$E_1 = E1$$
$$E_2 = E1$$
$$E_3 = 0$$
$$E_4 = E1$$

```
G1 = (7.17 10^9) / E1
G3 = 0
G4 = (7.17 10^9) / E1
```

Main central moments of inertia for the ribs: J_1- in the plane normal to the median surface, J_3 – torsional constant of a cross – section :

```
J1 = (b (h)^3) / 12 / R0^4
J13 = (b (h)^3) / 12 / R0^4
J14 = (b (h)^3) / 12 / R0^4
J3 = 1 / R0^4 ((h b^3) / 16 (16 / 13 - 3.36 h / b (b^4 / (12 h^4))))
J33 = 1 / R0^4 ((h b^3) / 16 (16 / 13 - 3.36 h / b (b^4 / (12 h^4))))
J34 = 1 / R0^4 ((h b^3) / 16 (16 / 13 - 3.36 h / b (b^4 / (12 h^4))))
```

Spacing between the axes of adjacent families of ribs:

```
aa = Pi / (s m0)
a1 = aa
a2 = aa
a3 = 2 aa c
a4 = aa c
```

Angle between normal to the median surface and axis of rotation of a shell

```
ψ = ArcSin[√(1 + (∂z r)^2)]
```

```
I1 = (E1 J1) / a1
I3 = (E3 J13) / a3
I4 = (E4 J14) / a4
```

■ Load parameters:

Forces distributed along the surface of a shell:

```
g = 0
```

```
X = g z Sin[γ]
Y = 0
Z = g z Cos[γ]
```

Coefficients of quadratic form

```
A = √(1 + (∂z r)^2)
B0d = r
B1 = ∂z B0
```

```
B0 = B0d / R0
```

```
α11 = (2 FF c^4) / aa + F4 / a4
```

```
α12 = (FF (s2phi)^2) / (2 aa)
```

```
α22 = (2 FF s^4) / aa + F3 / a3
```

```
γ11 = -((2 J1 c^4) / aa + J14 / a4 + (G1 J3 (s2phi)^2) / (2 aa))
```

```
γ12 = -(J1 - G1 J3) (s2phi)^2 / (2 aa)
```

```
γ22 = -((2 J1 s^4) / aa + J13 / a3 + (G1 J3 (s2phi)^2) / (2 aa))
```

$\gamma_{31} = J_1\,(s2phi)\,\hat{}\,2 \,/\, aa + G1\,J_{34} \,/\, a_4 + (2\,G1\,J_3\,c\,\hat{}\,2\;c2phi) \,/\, aa$

$\gamma_{41} = J_1\,(s2phi)\,\hat{}\,2 \,/\, aa + G1\,J_{33} \,/\, a_3 - (2\,G1\,J_3\,s\,\hat{}\,2\;c2phi) \,/\, aa$

$\alpha_{121} = \partial_z \alpha_{12}$

$k_{11} = \partial_z k_1$

$k_{21} = \partial_z k_2$

$B_{11} = \partial_z B_1$

$A_1 = \partial_z A$

$\gamma_{311} = \partial_z \gamma_{31}$

$\gamma_{311} = \partial_z \gamma_{31}$

$\alpha_0 = \alpha_{22} - \alpha_{12}\,\hat{}\,2\;\alpha_{11}\,\hat{}\,(-1)$

$\beta_0 = \gamma_{22} - \gamma_{12}\,\hat{}\,2\;\gamma_{11}\,\hat{}\,(-1)$

$\beta_1 = \gamma_{31} + \gamma_{41}$

$\beta_2 = 1 + \gamma_{12}\,\gamma_{11}\,\hat{}\,(-1)$

$\beta_3 = \gamma_{311}\,B_0 - B_1\,\gamma_{31}$

$\psi_0 = k_{21} - (B_1\,k_1) \,/\, B_0$

$\psi_1 = mm\,\hat{}\,2 \,/\, B_0\,\hat{}\,2 - k_2\,\hat{}\,2$

$\psi_2 = (1 - (k_1 - k_2)\;(k_2\,\gamma_{31}) \,/\, (2\,\alpha_{12}))\,\hat{}\,(-1)$

$\psi_3 = (k_1 - k_2)\;(k_2\,\alpha_{12}\,\gamma_{31}) \,/\, \alpha_{11}$

$p_{11} = -(\alpha_{12}\,B_1) \,/\, (\alpha_{11}\,B_0)$

$p_{12} = -(\alpha_{12}\,mm\,A) \,/\, (\alpha_{11}\,B_0)$

$p_{13} = -A\;(k_1 + \alpha_{12} \,/\, \alpha_{11}\,k_2)$

$p_{14} = 0$

$p_{15} = A \,/\, \alpha_{11}$

$p_{16} = 0$

$p_{21} = (mm\;A) \,/\, B_0$

$p_{22} = B_1 \,/\, B_0$

$p_{23} = 0$

$p_{24} = 0$

$p_{25} = 0$

$p_{26} = A \,/\, \alpha_{12}$

$p_{31} = A\,k_1$

$p_{32} = 0$

$p_{33} = 0$

$p_{34} = A$

$$p_{35} = 0$$

$$p_{36} = 0$$

$$p_{41} = (\gamma_{11}\,\psi_0)/\gamma_{12} + (\alpha_{12}\,k_1\,B_1)/(\alpha_{11}\,B_0)$$

$$p_{42} = (\alpha_{12}\,mm\,k_1\,A)/(\alpha_{11}\,B_0)$$

$$p_{43} = A\,((\gamma_{12}\,\psi_1)/\gamma_{11} + (\alpha_{12}\,k_1\,k_2)/\alpha_{11})$$

$$p_{44} = -(\gamma_{12}\,B_1)/(\gamma_{11}\,B_0)$$

$$p_{45} = -k_1\,A/\alpha_{11}$$

$$p_{46} = 0$$

$$p_{51} = 1/B_0^2\,((\alpha_0\,B_1^2)/A + mm^2\,k_1\,k_2\,\gamma_{31}\,A)$$

$$p_{52} = \alpha_0\,mm\,B_1/B_0^2$$

$$p_{53} = B_1/B_0\,(\alpha_0\,k_2 - \gamma_{31}/B_0^2\,mm^2\,k_1)$$

$$p_{54} = mm^2\,k_1\,\gamma_{31}\,A/B_0^2$$

$$p_{55} = (\alpha_{12}/\alpha_{11} - 1)\,B_1/B_0$$

$$p_{56} = -(mm\,A)/B_0\,(1 + k_1\,\gamma_{31}\,(k_1 - k_2)/(2\,\alpha_{12}))$$

$$p_{61} = (mm\,\psi_2)/B_0^2\,((\alpha_0 - \psi_3 - \beta_1\,k_2^2)\,B_1 - (\beta_0 + \beta_2\,\gamma_{31})\,\psi_0\,k_2\,B_0 - \beta_3\,k_2^2)$$

$$p_{62} = (\alpha_0 - \psi_3)\,(mm^2\,\psi_2\,A)/B_0^2$$

$$p_{63} = (mm\,\psi_2\,k_2\,A)/B_0\,(\alpha_0 + (\beta_1\,B_1^2)/(A^2\,B_0^2) + (\gamma_{31}\,B_{11})/(A^2\,B_0) - \psi_1\,(\beta_0 + (\gamma_{12}\,\gamma_{31})/\gamma_{11}) + k_2\,\gamma_{31}\,(k_1 + (k_2 - k_1)\,\alpha_{12}/\alpha_{11}) + B_1/(A^3\,B_0^3)\,(\gamma_{311}\,A\,B_0^2 - \gamma_{31}\,B_0\,(A_1\,B_0 + 2\,A\,B_1)))$$

$$p_{64} = mm\,\psi_2\,k_2/B_0^2\,((\beta_0 - \beta_1 + \beta_2\,\gamma_{31})\,B_1 - \beta_3)$$

$$p_{65} = mm\,\psi_2\,A/(\alpha_{11}\,B_0)\,(\alpha_{12} + (k_1 - k_2)\,k_2\,\gamma_{31})$$

$$p_{66} = -\psi_2\,((2\,B_1)/B_0 + (k_{21} - k_{11})\,(k_2\,\gamma_{31})/(2\,\alpha_{12}) + ((k_2 - k_1)\,k_2)/(2\,\alpha_{12})\,((\beta_1\,B_1)/B_0 + (\gamma_{311} - \gamma_{31}\,\alpha_{121}/(2\,\alpha_{12}))))$$

```
P = {{p11, p12, p13, p14, p15, p16}, {p21, p22, p23, p24, p25, p26},
  {p31, p32, p33, p34, p35, p36}, {p41, p42, p43, p44, p45, p46},
  {p51, p52, p53, p54, p55, p56}, {p61, p62, p63, p64, p65, p66}}

MatrixForm[P]
```

$$f_1 = 0$$
$$f_2 = 0$$
$$f_3 = 0$$
$$f_4 = -A\,X$$
$$f_5 = 0$$
$$f_6 = -A\,Z$$

```
F1 = {f1, f2, f3, f4, f5, f6}

y = {u[z], w[z], γ1[z], N1[z], M1[z], Q1[z]}

MatrixForm[y]

M = P. y + F1
```

```
MatrixForm[M]
```

Height of a cylinder:

```
z_d = 7.4

z1 = 7.4 / R_0
```

Load in nondimentional form:

```
g0
g = g0 / E1
```

Load scaling factor

```
www = 0.5

m1 = g0 www

m0 = m1 2 Pi R_0 ^ 2

m1 = m0 / (E1 R_0 ^ 2)
```

Solution of a boundary value problem:

```
solution2 = DSolve[ {u'[z] == M[[1]], w'[z] == M[[2]], γ1'[z] == M[[3]], N1'[z]
== M[[4]], M1'[z] == M[[5]], Q1'[z] == M[[6]], u[z1] == 0, w[z1] == 0, γ1[z1] ==
0, N1[0]== -g, M1[0] == m1, Q1[0] == 0}, {u[z], w[z], γ1[z], N1[z], M1[z],
Q1[z]}, z];
```

Notations for calculated homogenised entities:

```
Eu = Evaluate[u[z] /. solution2];
Ew = Evaluate[w[z] /. solution2];
Eγ1 = Evaluate[γ1[z] /. solution2];
EN1 = Evaluate[N1[z] /. solution2];
EN2 = N2;
EQ1 = Evaluate[Q1[z] /. solution2];
EM1 = Evaluate[M1[z] /. solution2];
EM2 = M2;

N2 = (α_22 - α_12 ^ 2 / α_11) (B_1 / (A B_0) Eu + k_2 Ew) + α_12 / α_11 EN1;

M2 =
  (γ_22 - γ_12 ^ 2 / γ_11) ((k_21 - B_1 / B_0 k_1) Eu / A - k_2 ^ 2 Ew - B_1 / (A B_0) Eγ1) + γ_12 / γ_11 EM1;
```

Stress resultants in each family of ribs:

Axial forces in the ribs:

For the case of cylindrical shell with symmetric loading:

```
S = 0;
H1 = 0;
```

```
K1 = (E1 F1) / a1;
K2 = (E2 F2) / a2;
K3 = (E3 F3) / a3;
K4 = (E4 F4) / a4;

KK = K1;

K0 = (2 KK (K3 c^4 + K4 s^4) + K3 K4) ^ (-1)

K3 = 0.0192304220041906894
```

Nondimentional form:

```
NN1 = ((K3 EN1 c^2 + K4 EN2 s^2) K0 + S (K s2phi) ^ (-1)) E1 FF K3;

NN2 = ((K3 EN1 c^2 + K4 EN2 s^2) K0 - S (K s2phi) ^ (-1)) E1 FF K3;

NN3 = ((2 KK c^4 + K4) EN2 - 2 KK EN1 s^2 c^2) K0 E1 FF;

K4 = 29.9439419296801467`;

NN4 = ((2 KK s^4 + K3) EN1 - 2 KK EN2 s^2 c^2) K0 E1 FF K4;
```

Dimentional form:

```
N1 = 10^ (-2) E1 R0 ^2 NN1;
N2 = 10^ (-2) E1 R0 ^2 NN2;
N3 = 10^ (-2) E1 R0 ^2 NN3;
N4 = 10^ (-2) E1 R0 ^2 NN4;
```

Bending and torque moments:

```
C1 = (G1 J3) / a1;

C4 = (G4 J34) / a4;

β31 = I1 s2phi^2 + 2 C1 c^2 c2phi + C4;

I0 = (2 I1 (I3 c^4 + I4 s^4) + I3 I4 + 2 C1 s^2 c^2 (2 I1 + I3 + I4)) ^-1;

K01 = 1.37026407797398370662390761866 10^ (-2);
```

Nondimentional form:

```
MM1 = ((((I3 c^2 + 2 C1 s^2 c^2) EM1 + (I4 s^2 + 2 C1 s^2 c^2) EM2) I0 -
      H1 (I1 s2phi + 2 C1 c^2 cot2phi + C4 (s2phi) ^ (-1)) ^ (-1)) E1 J1 ) K01;

MM2 = ((((I3 c^2 + 2 C1 s^2 c^2) EM1 + (I4 s^2 + 2 C1 s^2 c^2) EM2) I0 +
      H1 (I1 s2phi + 2 C1 c^2 cot2phi + C4 (s2phi) ^ (-1)) ^ (-1)) E1 J1 ) K01;

MM3 = ((2 I1 c^4 + I4 + 2 C1 s^2 c^2) EM2 - 2 EM1 s^2 c^2 (I1 - C1)) I0 E3 J13 ;

K04 = 0.00689623509708214932;

MM4 = (((2 I1 s^4 + I3 + 2 C1 s^2 c^2) EM1 - 2 EM2 s^2 c^2 (I1 - C1)) I0 E4 J14 ) K04;

HH1 = (((2 I1 s^2 + I3) EM1 - (2 I1 c^2 + I4) EM2) I0 + 2 H1 β31 ^ (-1) c2phi) G1 J3;
```

```
HH2 = (-((2 I1 s^2 + I3) EM1 - (2 I1 c^2 + I4) EM2) I0 + 2 H1 β31^(-1) c2phi) G1 J3;

HH3 = -2 G3 J33 H1 β31^(-1);
HH4 = 2 G4 J34 H1 β31^(-1);
```

Dimentional form:

```
M1 = MM1 10^(-4) E1 R0^3;
M2 = MM2 10^(-4) E1 R0^3;
M3 = MM3 10^(-6) E1 R0^3;
M4 = MM4 10^(-4) E1 R0^3;

H1 = HH1 10^(-4) E1 R0^3;
H2 = HH2 10^(-4) E1 R0^3;
H3 = HH3 10^(-4) E1 R0^3;
H4 = HH4 10^(-4) E1 R0^3;
```

Stress calculations

Normal stresses:

```
Nnod = m0 / (2 Pi R0^2) 0.52324850769714106189129751806472;

σ31N = N1 / (b h) + (Nnod c) / (b h);
σ34N = N4 / (b h) ;

x2 = b / 2
x1 = h / 2

G1 = 0
G4 = 0

I2 = (h (b)^3) / 12
```

```
I1 = J1 R0^4
```

```
σ31M = M1 / I2 x2 - G1 / I1 x1;
σ34M = M4 / I2 x2 - G4 / I1 x1;
```

```
σ31 = (σ31N + σ31M);
σ34 = (σ34N + σ34M);
```

Shear stresses:

```
FindMinimum[Pcr4, {h, 0.002}, {φ, 0.001}]
```

```
Q1 = 0
S1 = 0
Q4 = 0
S4 = 0
```

```
τ311 = Q1 / J2 (b / 2 - x1) (b / 4 + x1 / 2)
τ321 = S1 / J1 (h / 2 - x2) (h / 4 + x2 / 2)
```

```
τ314 = Q4 / J2 (b / 2 - x1) (b / 4 + x1 / 2)
τ324 = S4 / J1 (h / 2 - x2) (h / 4 + x2 / 2)
```

Torsion

```
αα = 0.267
```

```
τ121 = H1 / (αα h b^2);
τ124 = H4 / (αα h b^2);
```

Material failure in the ribs

Tensile strength in 3-d direction:

```
X3ten = 1500000000;
```

Compressive strength in 3-d direction:

```
X3comp = 1500000000;
```

Shear strength in 31 and 32 directions:

```
S31 = 68000000;
```

Quadratic failure criterion strength parameters:

```
F33 = 1 / (X3ten X3comp);
F3 = 1 / X3ten - 1 / X3comp;
F44 = 1 / S31^2 ;
F55 = 1 / S31^2 ;
```

```
z = z1;
```

```
rst4 = σ34^2 / (X3ten X3comp) + σ34 (1 / X3ten - 1 / X3comp);
```

```
rst4 = Part[rst4, 1];
```

```
Solution4 = Solve[rst4 == 1, g0];

Solution4 = Part[Solution4, 1];

Solution4 = Part[Solution4, 1];

Pcr4 = g0 /. Solution4;

s = Sin[φ];
```

Surface plot

```
Plot3D[-Pcr4, {h, 0.002, 0.05}, {φ, 0.001, Pi / 1.9999}, PlotPoints → 50,
 Mesh → True, FaceGrids → All, AxesLabel → {"h", "φ", "Pcr4"}]
```

Optimum values of design parameters

```
FindMinimum[Pcr4, {h, 0.002}, {φ, 0.001}]

TimeUsed[]
```